Technical Report

TR-09-17

Permafrost simulations at Forsmark using a numerical 2D thermo-hydro-chemical model

Juha Hartikainen, Reijo Kouhia
Aalto University School of Science and Technology

Thomas Wallroth, Bergab

November 2010

Svensk Kärnbränslehantering AB
Swedish Nuclear Fuel
and Waste Management Co

Box 250, SE-101 24 Stockholm
Phone +46 8 459 84 00

ISSN 1404-0344
SKB TR-09-17

Permafrost simulations at Forsmark using a numerical 2D thermo-hydro-chemical model

Juha Hartikainen, Reijo Kouhia
Aalto University School of Science and Technology

Thomas Wallroth, Bergab

November 2010

Keywords: SKBdoc id 1259252.

Preface

This document contains site-specific information on the development of permafrost and frozen depth in Forsmark. The study constitute a complement to the permafrost modelling study reported in /SKB 2006/. Results from the present study will, together with results from /SKB 2006/, be used in the safety assessment SR-Site.

The report was written by Juha Hartikainen and Reijo Kouhia, Aalto University School of Science and Technology. The collection and management of input data, presented in the appendices, was done by Thomas Wallroth, Bergab. The authors of individual appendices are mentioned in the appendices.

Stockholm, August 2010

Jens-Ove Näslund
Person in charge of the SKB climate programme

Summary

This report provides a 2D numerical estimation of site-specific spatial- and temporal development of permafrost and perennially frozen ground at Forsmark. The study complements the 1D permafrost study that was made for the SR-Can safety assessment /SKB 2006/. When considering environmental conditions (i.e. ice sheets, shore-line displacement and air temperature curve) for the initial 45,000 years of the reconstructed Weichselian glacial cycle, the maximum permafrost depth (the 0°C isotherm) over the repository can vary between 180 and 260 m, and the depth of perennially frozen ground (ground remaining frozen for at least two consecutive years) between 180 and 250 m depending on the surface conditions. Spatially permafrost distribution turns to continuous state (more than 90% coverage) when annual mean air temperature decreases below –6°C and the maximum permafrost depth at the site exceeds a depth of ~50 m. When considering a severe permafrost case consisting of a full 115,000 year long glacial cycle assuming no cover of ice sheet, vegetation, snow, or sea, the maximum permafrost depth over the repository varies between 360 and 390 m and the depth of perennially frozen ground between 330 and 360 m.

Groundwater flow may take place through a perennially frozen ground within a continuous permafrost zone when the unfrozen groundwater content in the perennially frozen ground exceeds 10%, thus allowing for talik formation under lakes at Forsmark. When the unfrozen groundwater content decreases below 10%, groundwater flow is reduced considerably, and taliks are no longer able to form or survive. In the conducted permafrost simulations, through-taliks are formed under specific time periods beneath two future lakes that will form at the Forsmark site along the investigated profile.

Freezing can induce salt exclusion and transport when perennially frozen ground develops deeper than ~200 m at Forsmark. In addition, salinity concentration of groundwater is increased within the perennially frozen ground, if salt transport occurs more slowly than the freezing zone advances.

Contents

1 Introduction 7
1.1 Background 7
1.2 Review of important factors and processes 7
1.3 Purpose and objectives 10
1.4 Settings 10

2 Conceptual model setup 13
2.1 Geometry 13
2.2 Subsurface properties and conditions 15
2.3 Repository and heat production from the spent fuel 20
2.4 Surface conditions 20

3 Mathematical model 31
3.1 Introduction 31
3.2 Mixture concept 31
3.3 State equations 32
3.4 Diffusion laws 36
3.5 Balance laws 37
3.6 Model verification 38
3.6.1 The Elder problem 38
3.6.2 Salt fingering 39
3.6.3 Freezing point of saline water 40
3.6.4 Uniaxial freezing 40

4 Numerical simulations 45
4.1 Numerical method and calculation settings 45
4.2 Description of simulated cases 45
4.2.1 Main simulations 45
4.2.2 Sensitivity analysis 46

5 Results 49
5.1 Main simulations 49
5.2 Sensitivity simulations 83

6 Discussion and conclusions 93

7 References 99

Appendix A Data sets used in the permafrost simulations 103

Appendix B Topography and soil cover 105

Appendix C Rock domains and deformation zones 107

Appendix D Hydraulic properties of soils and bedrock 111

Appendix E Thermal properties 115

Appendix F Ionic composition of groundwater 125

Appendix G Heat generation from the repository 127

Appendix H Reconstructed air temperature curve for the past 120,000 years 131

Appendix I Future lakes developed due to isostatic uplift 133

Appendix J Vegetation/surface cover types for three different climate zones at Forsmark 137

Appendix K Modelling results for the Severe permafrost case 139

1 Introduction

1.1 Background

The presence of permafrost and perennially frozen ground can alter both the surface- and subsurface environment. Climate model simulations show that climate conditions during parts of the Weichselian glacial cycle probably supported development of permafrost and perennially frozen ground at the Forsmark site in Östhammar /Kjellström et al. 2009/. Similar situations are anticipated at the Forsmark site also in the future /SKB 2010a/.

In 2006 SKB presented the SR-Can safety assessment for a deep geological repository for spent nuclear fuel, where important processes and key parameters as well as uncertainties associated with model simplifications and determination of surface and subsurface thermal conditions have been identified /SKB 2006, Section 3.4 and 4.4.1/. The present study constitutes a complement to the SR-Can study, with the aim of further improving the understanding of permafrost and perennially frozen ground at the Forsmark site by demonstrating how permafrost develop and decay influenced by site-specific, spatially variable conditions. The study also includes a full range of sensitivity analyses based on identified and updated uncertainty intervals for model input data. For the SR-Site safety assessment, results from both the present study and from /SKB 2006, Section 3.4 and 4.4.1/ are used.

1.2 Review of important factors and processes

Permafrost is commonly defined as ground which remains at or below the 0°C isotherm for at least two consecutive years /French 2007/. *Perennially frozen ground* is defined as ground that keeps frozen for at least two consecutive years. The definition of permafrost is solely based on temperature, thus disregarding the texture, degree of compaction, water content, and lithologic character of the material, whereas perennially frozen ground is defined on the basis of freezing of water. In general, being influenced by the pressure and composition of the groundwater, and by the adsorptive and capillary properties of the ground matter, water in ground freezes below the 0°C isotherm, and the freezing occurs progressively with decreasing temperature. Consequently, perennially frozen ground is commonly partially frozen containing gradually decreasing amount of unfrozen water and a corresponding progressively increasing amount of ice /Williams and Smith 1989/. Obviously, permafrost is not equal to perennially frozen ground. On the contrary, permafrost encompasses perennially frozen ground, in a partially frozen state, as well as a surrounding unfrozen layer called *cryopeg*, in which water remains completely unfrozen at sub-zero temperatures.

Permafrost and perennially frozen ground originate from the ground surface and grows downwards depending on a complex heat exchange process across the atmosphere/ground boundary layers and on an almost time-invariant geothermal heat flow from the Earth's interior. The heat exchange between the atmosphere and the Earth's surface is governed by solar radiation, longwave terrestrial and atmospheric radiations, sensible and terrestrial heat fluxes, and evaporation and condensation /Lockwood 1979, Washburn 1979, Lunardini 1981, Williams and Smith 1989, Smith and Riseborough 1996, Yershov 1998/.

At present, approximately 25% of the total continental land area of the Earth is occupied by permafrost in continuous- (more than 90% spatial coverage), discontinuous- (between 90 and 50% coverage), sporadic form (less than 50% coverage). About one fifth of this permafrost is estimated to be subglacial in Antarctica and Greenland. Permafrost is abundant in Alaska, the northern parts of Canada and Russia, and in parts of China /French 2007/. Along the coast of southern and south-western Greenland both continuous and discontinuous permafrost is found /Mai and Thomsen 1993/. In the Lupin gold mine area in northern Canada, permafrost depth extends to ~500 to 600 m which is believed to have been developed over the last 5,000 years /Ruskeeniemi et al. 2002, 2004/. The deepest known permafrost occurs in the central part of Siberia in Russia, where thicknesses of up to 1,500 m have been reported /Fotiev 1997/. The extensive region of continuous permafrost in central Siberia corresponds to areas that are believed not to have been covered by Quaternary ice sheets and that have experienced cold subaerial climate conditions for a very long time. Furthermore, permafrost is frequently observed in

mountainous terrain. For example, in the area of Tarfala in the Kebnekaise massif in northern Sweden, discontinuous permafrost has been reported to be 100 to 350 m thick at an altitude above 1,500 m a.s.l. /King 1984, Isaksen et al. 2001/. In the Jotunheimen massif, southern Norway, the permafrost depth is between 100 and 200 m at an altitude of 2,200 m a.s.l.

When perennially frozen ground develops, the freezing of water influences the thermal-, hydraulic-, mechanical-, and chemical behaviour of the ground /Washburn 1979, Williams and Smith 1989, Yershov 1998, Gascoyne 2000, Ahonen 2001, Vidstrand 2003, French 2007/. Freezing of water increases the thermal conductivity and decreases the specific heat capacity of the ground. Ice formation transforms ground to an almost impermeable state, confining groundwater flow through the frozen ground. Freezing can induce frost phenomenon including cryogenic suction, i.e. transport of water from the unfrozen ground to the (partially) frozen ground, and consolidation and heaving of ground. Ice segregation in ground can also lead to rock fracture at shallow depths. Further consequences of freezing are weathering and degradation of the ground surface and formation of patterned ground when freezing occurs cyclically with thawing. In addition, freezing may increase salinity concentration of groundwater when salts are excluded from the ice and transferred into the unfrozen groundwater.

The principal factors controlling the heat exchange between the atmosphere and the Earth's surface are climate, topography, vegetation and snow covers, soil characteristics and water bodies. These factors are mutually dependent and can vary considerably in time and location. The main climatic parameters are solar insolation, air temperature, wind, and precipitation. Insolation is a driving force governing the heat exchange between the atmosphere and the Earth's surface and affecting the other climatic parameters. Air temperature, which is commonly applied to map permafrost distribution, controls the longwave atmospheric radiation, the turbulent heat exchange, and evaporation and condensation. Wind in turn influences mostly the sensible heat exchange, but also latent heat production and loss. Precipitation together with evaporation and condensation determine groundwater recharge affecting the groundwater content and flow and hence the terrestrial heat flux.

Topography has a significant impact on climate conditions. Generally, air temperature decreases as altitude increases being affected by radiation, convection and condensation. The average air temperature lapse rate is ~0.65°C for every 100 metres increase in elevation, e.g. /Danielson et al. 2003/. Furthermore, the slope angle and azimuth of the land surface affect the flux of shortwave radiation, and where topographical differences are large a more patchy distribution of permafrost can be expected.

Vegetation- and snow cover are sensitive to climatic conditions and topography. The characteristic parameters of the surface cover are surface albedo, emissivity, and roughness controlling the incoming shortwave radiation, the longwave terrestrial radiation and the turbulent heat exchange, respectively, as well as the thermal properties and the thickness of the surface cover affecting terrestrial heat transfer. In general, the surface covers moderate the ground temperature and thus the aggradation of permafrost. Vegetation is an insulating cover limiting cooling in winter and warming in summer, hence reducing the annual fluctuation of ground temperature. Vegetation is also important for the creation of snow cover, which protects the ground from heat loss in winter. However, the high albedo of snow can lead to a snow surface temperature almost 2°C lower than the mean winter air temperature /Yershov 1998/. As a rule, for a majority of the surface covers permafrost can build from the ground surface if the annual mean air temperature is lower than a value ranging between –9 and –1°C /Washburn 1979, Williams and Smith 1989, Yershov 1998, French 2007/. One exception is peat layers, which can insulate the ground from warming in summer more effectively than from cooling in winter, resulting in that permafrost may exist when the mean annual air temperature is above 0°C /Williams and Smith 1989/.

The properties and thicknesses of the soil cover affect the terrestrial heat flow. Of importance are the porosity and water content of the soil, influencing the annual fluctuation of ground temperature and the thickness of the active layer, i.e. the seasonally thawing ground layer. The soil cover also acts as an insulating cover, since the thermal conductivity of the soil cover is lower than that of the underlying bedrock.

Water bodies, i.e. sea, lakes, and watercourses, have a considerable influence on permafrost development and distribution since they have a high specific heat content. A talik, i.e. an unfrozen

layer, can exist beneath water bodies that do not freeze to their bottom in winter. Depending on the prevailing climate characteristics, the critical depth of a water body to remain unfrozen in winter is approximately 0.2 to 1.6 metres /Yershov 1998/. In the Lupin gold mine area in northern Canada, lakes deeper than 2 to 3 m are expected to have unfrozen bottoms all year /Ruskeeniemi et al. 2002, 2004/.

Sea water drastically reduces the development of costal permafrost. On the other hand, when the shoreline of a highly saline sea is rising, submerged permafrost and perennially frozen deposits can survive for a long time beneath a cold seabed /Washburn 1979, Yershov 1998/.

The hydrological conditions on the ground surface affect the freezing of groundwater. Especially under glaciated conditions, a warm-based overlying ice sheet can increase the subglacial groundwater pressure around two orders of magnitude, in which case the freezing point can decrease to such a degree that the subglacial ground is kept unfrozen. A similar, but minor, effect can occur when cold ground is submerged and submarine freezing is reduced by the pressure of the sea water. Furthermore, groundwater flow, whether carrying fresh glacial meltwater or saline seawater, can influence the freezing process by altering the groundwater composition.

The ground temperature that defines the presence of permafrost and primarily governs the freezing of water in ground is principally controlled by the ground thermal energy balance in terms of heat transfer, geothermal heat production, the specific heat content and the amount heat generated by phase change processes of water. Heat transfer within the ground can occur through conduction, convection and radiation /Sundberg 1988/. In general, only conduction is viewed as important to permafrost evolution, since radiation is of importance only in unsaturated high-porosity ground at high temperatures, and convection is of importance only when groundwater and gas fluxes are large.

Heat conduction depends on the ground temperature gradient, ambient temperature conditions, and the thermal properties of the ground matter. Thermal conductivity, describing the ability of material to transport thermal energy, and heat capacity characterising the capability of material to store heat, depend on a number of variables such as mineralogy, porosity and groundwater content. Having typically three to four times higher conductivity than other common rock forming minerals, quartz is the most important mineral for determining thermal characteristics in native rock materials.

When the porosity is less than 1%, freezing of water has a minor effect on heat transfer in water-saturated ground. The degree of saturation is of relevance for the thermal properties of the ground due to the very low thermal conductivity and heat capacity of air. The thermal conductivity of 1%-porosity granite can decrease by over 10% with decreasing saturation /Clauser and Huenges 1995/. In rocks, heat capacity is not very dependent on ambient temperature and pressure conditions, whereas thermal conductivity is a rather variable function of both temperature and pressure. The thermal conductivity of granite decreases with increasing temperature by approximately 5 to 20% per 100°C and increases with increasing pressure by about 1 to 2.5% per 100 MPa /Seipold 1995/. The pressure dependence of thermal conductivity is increased when rocks are unsaturated /Sundberg 1988, Clauser and Huenges 1995/. Moreover, /Allen et al. 1988/ reported observations of a strong correlation between lithology and permafrost depth, which could be directly explained by differences in thermal conductivity.

The heat flow from the interior towards the Earth surface varies from place to place and combines effects of mantle heat flow and radioactive decay of elements in the crustal rocks. /Näslund et al. 2005/ made a detailed compilation of heat flow density in the Fennoscandian Shield, which has been used in modelling of ice sheet evolution and ice sheet basal conditions /SKB 2006, Section 3.1/.

In addition to the thermal properties above, the geohydro-chemical and mechanical properties of ground important for freezing of groundwater are permeability, porosity, adsorptive capacity of ground matter, chemical composition of groundwater and deformation properties of the ground.

Also, in the context of assessing the long-term safety of repositories for spent nuclear fuel, the spent nuclear fuel will generate heat with an exponentially decreasing rate for a considerable amount of time. This heat will warm up the surrounding bedrock and can thus act to reduce the thickness of permafrost above and near the repository.

1.3 Purpose and objectives

The 1D modelling work done in SR-Can /SKB 2006, Section 3.4 and 4.4.1/ was conducted to identify the important factors and processes that control development of permafrost and perennially frozen ground at the Forsmark and Laxemar sites. The results showed that the surface conditions were the driving force for the development of permafrost while the subsurface conditions and the heat from the spent fuel acted as either reducing or enhancing factors. The 1D results indicate that if the mean annual ground surface temperature decreases constantly from the present day value to approximately –8°C, permafrost can develop to a depth of 400 m in 80,000 years at Forsmark when heat from the repository is included and in 26,000 years when the heat is excluded. Using surface temperatures based on pessimistically chosen site-specific climate cases, permafrost can develop to a depth of 400 m at Forsmark in a time frame of 100,000 years when the insulating effects of vegetation and snow cover are excluded /SKB 2006, Section 3.4/. Furthermore, permafrost can aggregate from some centimetres to some decimetres in a year whereas its degradation can take place several times faster than that, especially when the surface temperature is increased above 0°C and permafrost degrades simultaneously from the bottom upwards and from the top downwards. To demonstrate the influence of water bodies on permafrost depth and presence of taliks, 2D permafrost simulations were carried out in the vicinity of hypothetical circular lakes with constant positive lake bottom temperatures and constant negative lake bottom level subsurface temperatures. The results indicated that an open talik can survive beneath a circular shallow lake, if its radius is greater than the thickness of surrounding undisturbed permafrost thickness /SKB 2006, Section 3.4/.

The present study is a direct continuation and complement to the 1D modelling work done in SR-Can /SKB 2006, Section 3.4 and 4.4.1/. It provides a numerical estimation of the development of permafrost and perennially frozen ground in a 2D vertical cross-section for site-specific surface and subsurface conditions at Forsmark. The objective is to investigate and demonstrate effects of multidimensional features of surface and subsurface conditions on the occurrence, development and distribution of permafrost and perennially frozen ground. Special emphasis is put on the modelling of surface conditions depending on climate and landscape, including features of water bodies and topography, lateral variations in physical properties and heat generation from the spent fuel. In addition, groundwater flow and salt transport are considered, processes that were neglected in the SR-Can study.

1.4 Settings

2D permafrost simulations based on an improved permafrost model since SR-Can /SKB 2006/ are carried out for a 15 km long and 10 km deep vertical cross-section using site-specific data from Forsmark. Two glacial cycle temperature climate cases denoted i) *Repetition of last glacial cycle* case and ii) *Severe permafrost* case are simulated, accompanied by a number of sensitivity tests. The *Repetition of last glacial cycle* case studied in the present report corresponds to the "Reference glacial cycle" in /SKB 2010a, Section 1.2.3/ while the *Severe permafrost* case corresponds to the climate case "Severe permafrost" in /SKB 2010a, Section 1.2.3/. The same climate developments as used for the last glacial cycle in the SR-Can permafrost simulations /SKB 2006, Section 3.4/ are used, complemented with sensitivity studies on e.g. air temperature uncertainties. However, the *Repetition of last glacial cycle* case now only considers the ice free period from 115,000 to 70,000 years BP, i.e. the period prior to the first phase of ice sheet coverage in the safety assessment reconstruction of the last glacial cycle /SKB 2010a/, since this period ends with the deepest permafrost reconstructed at the site for the entire last glacial cycle /SKB 2006, 2010a/. However, the *Severe permafrost* case simulations are carried out for a full glacial cycle, from 115,000 years BP to present.

Initial conditions are assumed to correspond to present-day conditions regarding bedrock temperature, groundwater salinity and groundwater pressure. Heat generated by the radioactive decay of the spent fuel in the repository is included in all simulations except in one sensitivity study.

Based on the results of the permafrost simulations performed for the SR-Can safety assessment /SKB 2006, Section 3.4 and 4.4.1/, the present 2D analysis focuses on the following issues.

Surface conditions:

- Air temperature and its variation over time.
- Topographical features including slope and relief.
- Water bodies (sea and lakes), including the effect of isostatic uplift.
- Vegetation and snow cover as related to climate and topographical conditions.

Subsurface conditions:

- Spatial variation of bedrock and soil thermal and hydraulic properties.
- Site specific geothermal heat flow.
- Convectional heat transfer due to 2D groundwater flow.
- Heat generation from the repository for spent fuel.
- Salinity exclusion due to freezing and salt transport.

2 Conceptual model setup

2.1 Geometry

The location of the 2D model domain within the Forsmark area is shown in Figure 2-1. For a description of the selection of the profile location, see Appendix A. The model domain encompasses an approximately 15 km long and 10 km deep vertical section consisting of six soil layers, 23 rock domains and 31 deformation zones as shown in Figure 2-2. Figure 2-3 illustrates the thermally different rock mass domains, the deformation zones of the upper 2.1 km of the model domain, as well as the present day Baltic Sea level. The soil layers are shown in Figure 2-4.

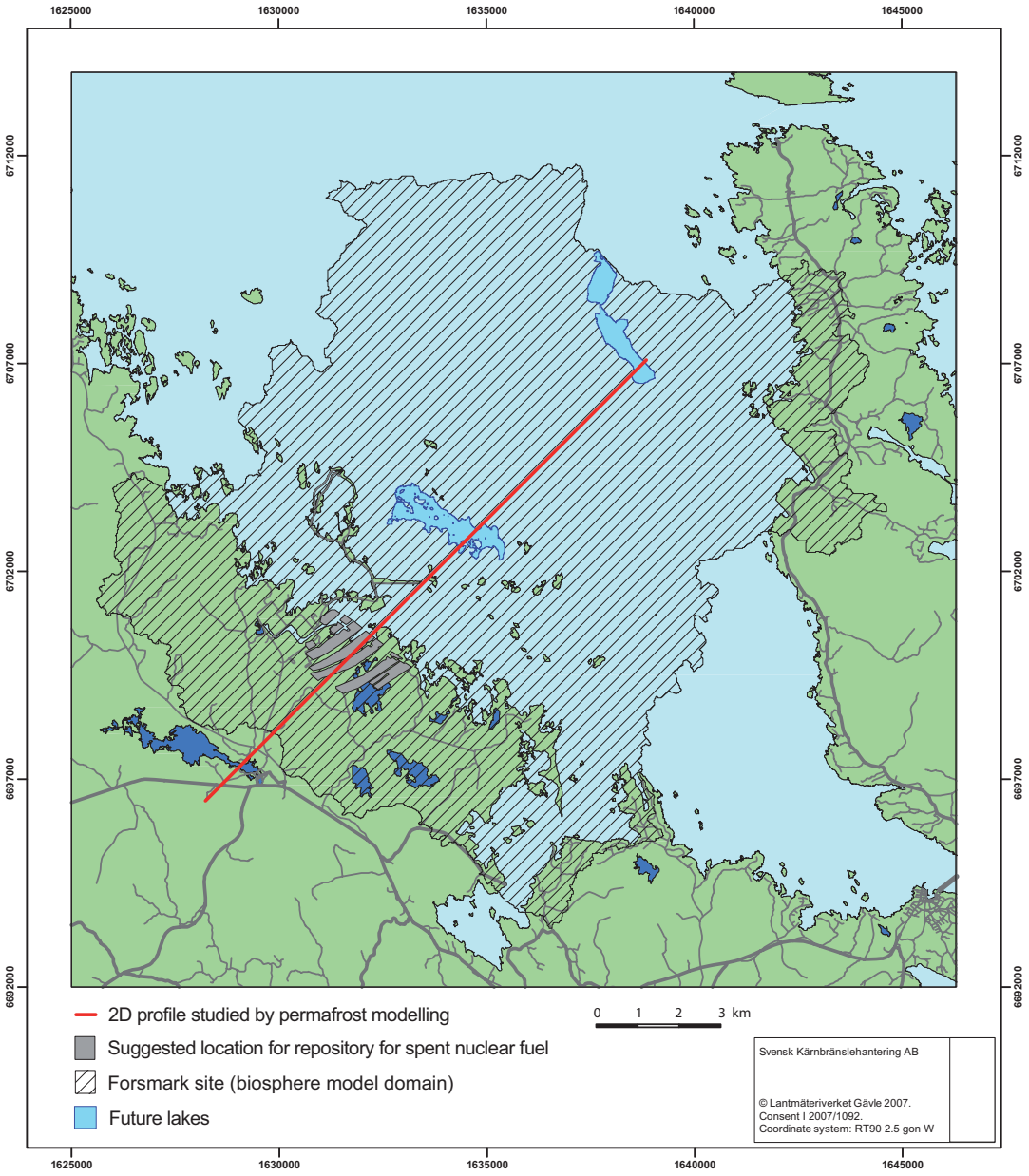

Figure 2-1. *Regional model area and the location of the 2D model domain for the permafrost simulations. The stippled area show the Forsmark site as defined and modelled in the SR-Site biosphere programme /SKB 2010c/. For a description of profile selection, see Appendix A.*

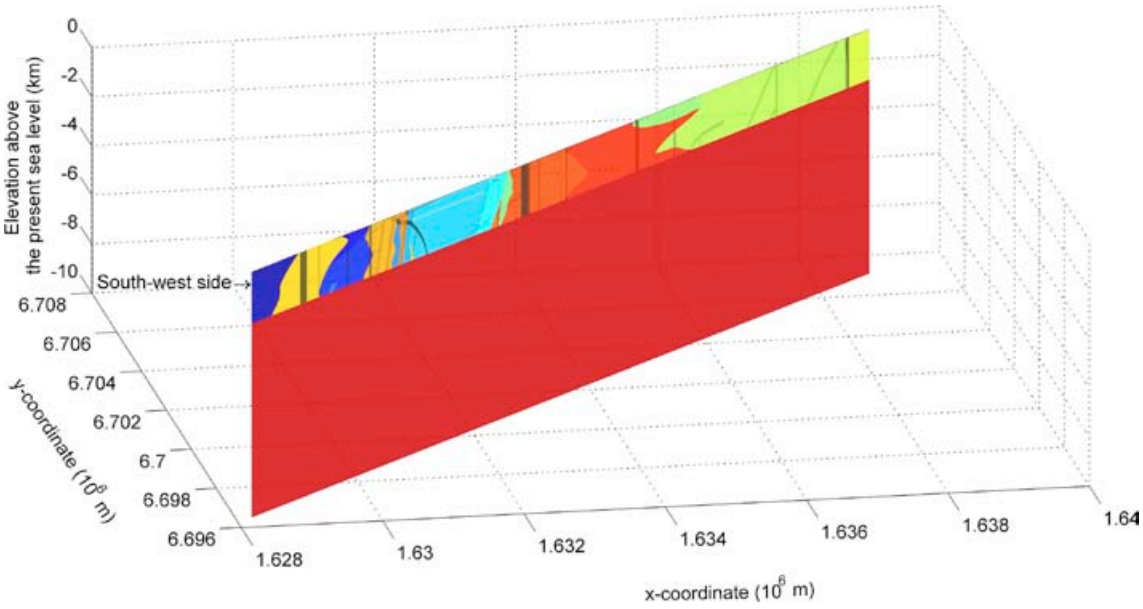

Figure 2-2. *The 2D model domain. Colours from blue to red signify the 23 included rock domains, and gray the 31 included deformation zones. The six soil layers described in Appendix B and Figure 2-4, are too thin to be seen in this figure. The x-axis is directed eastward and y-axis northward. The RT-90 coordinates of the south-west side are x = 1,628,228 m, y = 6,696,472 m.*

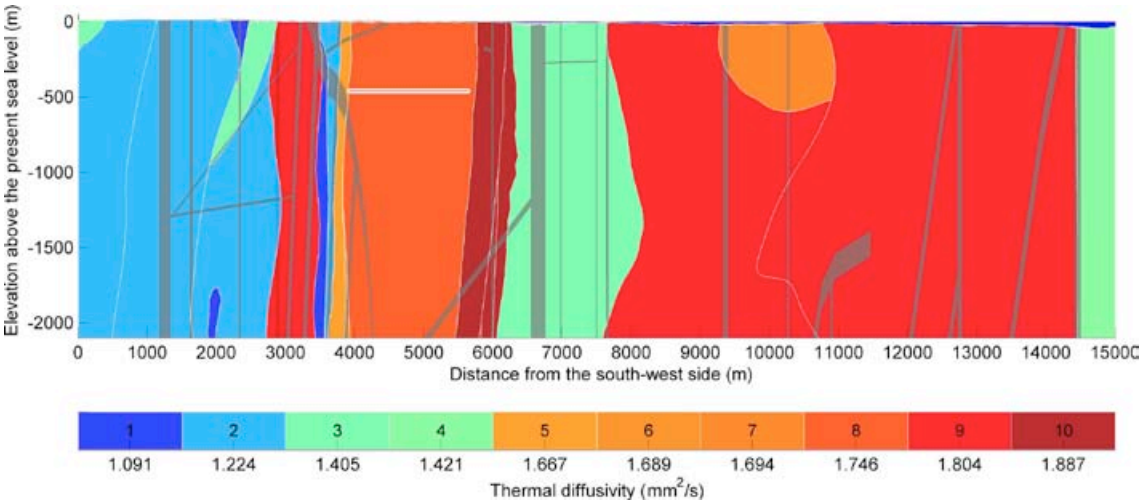

Figure 2-3. *The upper 2.1 km of the 2D model domain. Colours from blue to red signify rock domains with different thermal diffusivity. Numbers from 1 to 10 indicate the rock domains of Table 2-2. The location of deformation zones is illustrated in gray. The repository is shown by a white horizontal line at a depth of 450 m, starting at a distance of about 4,000 m along the profile. The thin blue layer on the top surface represents the present day Baltic Sea level. Further description and references for these data are found in Appendix C.*

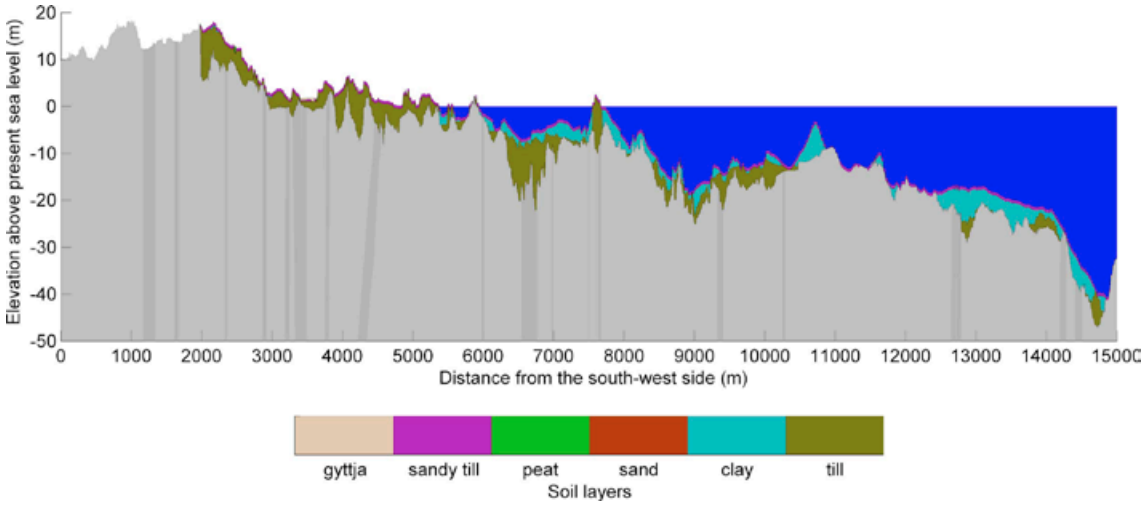

Figure 2-4. *The soil layers of the 2D model domain. Gray colour represents bedrock and blue the present day Baltic Sea. The gyttja, peat and sand layers are too thin to be seen in the figure. Because the first 2,000 metres of the model domain is outside the area of detailed site investigations, no information about the soil cover is used there. Further description and references for these data are found in Appendix B. Note that the vertical axis has a scale which gives a strong vertical exaggeration of topography.*

2.2 Subsurface properties and conditions

The thermal and hydraulic properties of soil layers are presented in Table 2-1. For some of the data, early versions of the site-descriptive data sets were used. However, the effects of discrepancies between the data used and the final values in the site-descriptive model are considered to be negligible on the development of permafrost and perennially frozen ground. Table 2-2 and Table 2-3 present the thermal and hydraulic properties of the rock mass domains. Hydraulic properties of the deformation zones are presented in Appendix D. The thermal properties of deformation zones are assumed to equal the corresponding rock mass domain. The bedrock below a depth of 2.1 km is assumed to have the same thermal and hydraulic properties as the rock domain in which the repository is located. The material properties are described in detail in Appendices D and E. The additional parameters χ_0 and e_s in Table 2-1 that characterize the unfrozen groundwater content function for soils are based on experimental findings on typical soils, see e.g. /Williams and Smith 1989/. The corresponding parameters for rock in Table 2-3 are chosen to be similar to the sand.

Table 2-1. Thermal and hydraulic properties of soil layers. See also Appendix D and E.

Parameter	Unit	Soil layer gyttja	sandy till	peat	sand	clay	till
Thermal properties							
Mean values							
Thermal conductivity	W/(m·K)	0.6	2.14	0.6	2.19	1	2.14
Heat capacity	MJ/(m³·K)	4.2	2.5	4.2	2.7	3.4	2.5
Thermal diffusivity	mm²/s	0.143	0.856	0.143	0.811	0.294	0.856
Range							
Thermal conductivity	W/(m·K)	0.6	1.64–2.45	0.6	1.88–2.54	0.88–1.14	1.64–2.45
Heat capacity	MJ/(m³·K)	4.2	2.3–2.9	4.2	2.5–2.8	3.3–3.6	2.3–2.9
Thermal diffusivity	mm²/s	0.143	0.566–1.065	0.143	0.671–1.016	0.244–0.346	0.566–1.065
Mean hydraulic properties							
Bulk density	kg/m³	46.4	2,000	46.4	1,800	900	2,000
Total and kinematic porosity	%	50	40	40	35	45	25
Hydraulic conductivity	m/s	$3.0 \cdot 10^{-7}$	$2.0 \cdot 10^{-5}$	$3.0 \cdot 10^{-7}$	$1.5 \cdot 10^{-4}$	$1.5 \cdot 10^{-8}$	$1.5 \cdot 10^{-6}$
Parameter χ_0 for unfrozen groundwater content function (Equations 3-11 and 3-12)	–	0.1	0.6	0.1	0.1	0.9	0.6
Parameter e_s for unfrozen groundwater content function (Equations 3-11 and 3-12)	–	0.006	0.002	0.006	0.006	0.004	0.002

Table 2-2. Thermal conductivity, heat capacity, bulk density and total porosity of rock mass domains. See also Appendix E. The rock domains are shown in Figure 2-3.

Rock domain		Thermal conductivity (W/(m·K))		Mean temperature dependency as percentual change for temperature increase of 100°C
No.	Label	Mean	Range	
1	RFM005	2.51	2.42–2.96	–2
	RFM007			
	RFM025			
2	RFM018	2.73	2.71–3.37	–3
	RFM023			
	RFM024			
	RFM030			
3	RFM003	3.02	2.69–3.35	–5
	RFM021			
	RFM031			
4	RFM042	3.04	3.03–3.48	–5
5	RFM012	3.45	3.21–3.59	–8
6	RFM044	3.48	3.26–3.65	–9
7	RFM022	3.49	3.19–3.69	–9
8	RFM029	3.58	3.47–3.68	–9
9	RFM026	3.68	3.34–3.69	–10
	RFM033			
	RFM034			
	RFM040			
10	RFM020	3.83	3.41–3.88	–11
	RFM032			
	RFM043			

Rock domain		Heat capacity (MJ/(m³·K))		Mean temperature dependency as percentual change for temperature increase of 100°C
No.	Label	Mean	Range	
1	RFM005	2.3	2.08–2.48	25
	RFM007			
	RFM025			
2	RFM018	2.23	1.87–2.39	25
	RFM023			
	RFM024			
	RFM030			
3	RFM003	2.15	2.1–2.35	25
	RFM021			
	RFM031			
4	RFM042	2.14	1.95–2.19	25
5	RFM012	2.07	2.02–2.21	25
6	RFM044	2.06	2.03–2.18	25
7	RFM022	2.06	2.01–2.17	25
8	RFM029	2.05	2.02–2.13	25
9	RFM026	2.04	2.02–2.16	25
	RFM033			
	RFM034			
	RFM040			
10	RFM020	2.03	2.02–2.19	25
	RFM032			
	RFM043			

Rock domain		Mean density (kg/m³)	Mean total porosity (%)
No.	Label		
1	RFM005	2,934	0.37
	RFM007		
	RFM025		
2	RFM018	2,737	0.40
	RFM023		
	RFM024		
	RFM030		
3	RFM003	2,732	0.37
	RFM021		
	RFM031		
4	RFM042	2,718	0.45
5	RFM012	2,657	0.43
6	RFM044	2,656	0.37
7	RFM022	2,638	0.50
8	RFM029	2,657	0.43
9	RFM026	2,657	0.43
	RFM033		
	RFM034		
	RFM040		
10	RFM020	2,635	0.40
	RFM032		
	RFM043		

Table 2-3. Additional mean thermal and hydraulic properties of all rock domains /Sundberg et al. 2009/. See also Appendix D.

Parameter	Unit	Mean	Range
Ground-level geothermal heat flow	mW/m^2	61.0	–14% – +12%
Ground-level radiogenic heat production	$\mu W/m^3$	3.00	±0%
Kinematic porosity	%	0.01	±0%
Parameter χ_0 for unfrozen groundwater content function (Equations 3-11 and 3-12)	–	0.1	±0%
Parameter e_s for unfrozen groundwater content function (Equations 3-11 and 3-12)	–	0.006	±0%
Hydraulic conductivity by depth		Horizontal	Vertical
0–100 m	m/s	$1.0 \cdot 10^{-5}$	$1.0 \cdot 10^{-7}$
100–200 m	m/s	$1.0 \cdot 10^{-8}$	$1.0 \cdot 10^{-9}$
200–400 m	m/s	$1.0 \cdot 10^{-9}$	$1.0 \cdot 10^{-10}$
≥ 400 m	m/s	$1.0 \cdot 10^{-11}$	$1.0 \cdot 10^{-11}$

The prevailing geothermal heat flow, crustal radiogenic heat production and ground temperature depth to ~1 km are based on site investigations /Sundberg et al. 2009/; see also Appendices B–F. For depths from ~1 km to 10 km they are modelled as follows.

The crustal radiogenic heat production, A, is assumed to be constant with time and decrease exponentially with depth, z, /Artemieva and Mooney 2001/ as

$$A(z) = A_0 \exp(-z/D) \tag{2-1}$$

where A_0 is the ground-level crustal radiogenic heat production as shown in Table 2-3 and D = 10,000 m the characteristic crustal depth /Balling 1995/. The upward geothermal heat flow, q, is determined considering stationary heat transfer such that $-\mathrm{d}q/\mathrm{d}z = A$. Hence,

$$q(z) = q(0) + A_0 D\,[\exp(-z/D) - 1], \tag{2-2}$$

where $q(0)$ is the geothermal heat flow at the ground-level as presented in Table 2-3. The prevailing ground temperatures for depths from ~1 km to 10 km are then calculated by the equation

$$T(z) = T(0) + \int_0^z \frac{q(s)}{\lambda}\,\mathrm{d}s\,, \tag{2-3}$$

where $T(0)$ is the mean ground surface temperature of a glaciation cycle and λ the thermal conductivity of subsurface. In this study, the value of 0°C for $T(0)$ is based on the modelled ground surface temperature for the *Reference surface conditions* case with vegetation and snow cover as described in /SKB 2006, Section 3.4/. The thermal conductivity of rock domain RFM029 for λ is used. Figure 2-5 shows the initial ground temperature calculated for the mean thermal properties.

The initial salinity concentration of groundwater for depths to ~1.5 km is described in Appendix F, and for depths from ~1.5 km to 10 km it is obtained as a stationary solution of Equation 3-21 and Equation 3-26, using present concentration values on the surface and at the depth of 1.5 km. Figure 2-6 shows that the salinity concentration increases by depth to the value of 30 mass-% at the depth of 10 km.

The present day groundwater pressure is determined as hydrostatic pressure based on the initial conditions of ground temperature and groundwater salinity concentration as well as the hydrostatic pressure at the bottom of Baltic Sea on the ground surface. The results for initial groundwater pressure are shown in Figure 2-7.

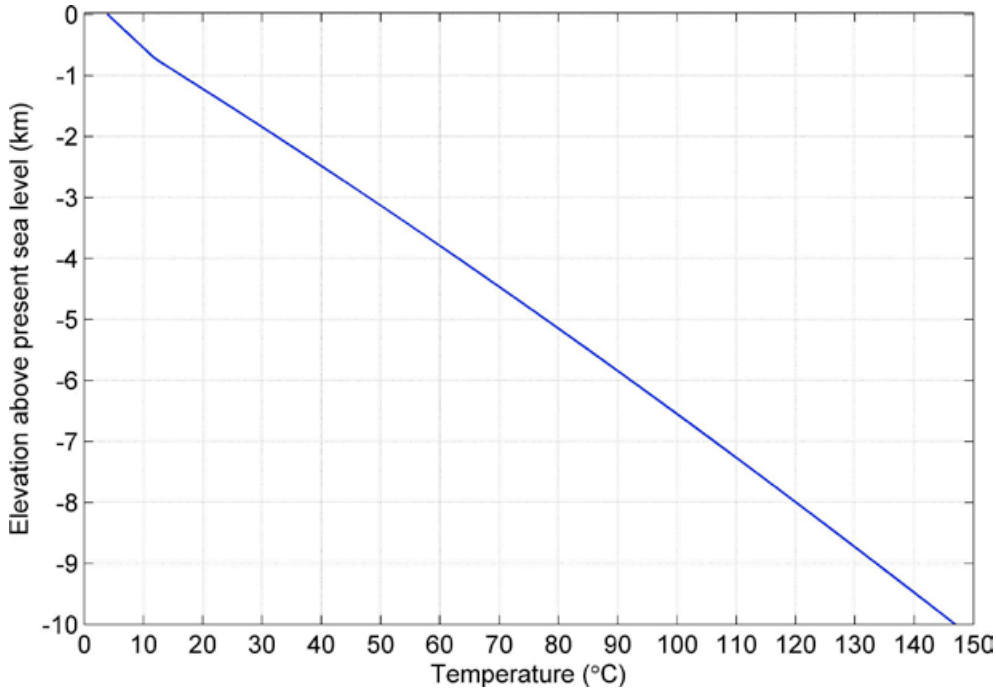

Figure 2-5. *Distribution of initial ground temperature for the mean thermal properties as presented in Table 2-2.*

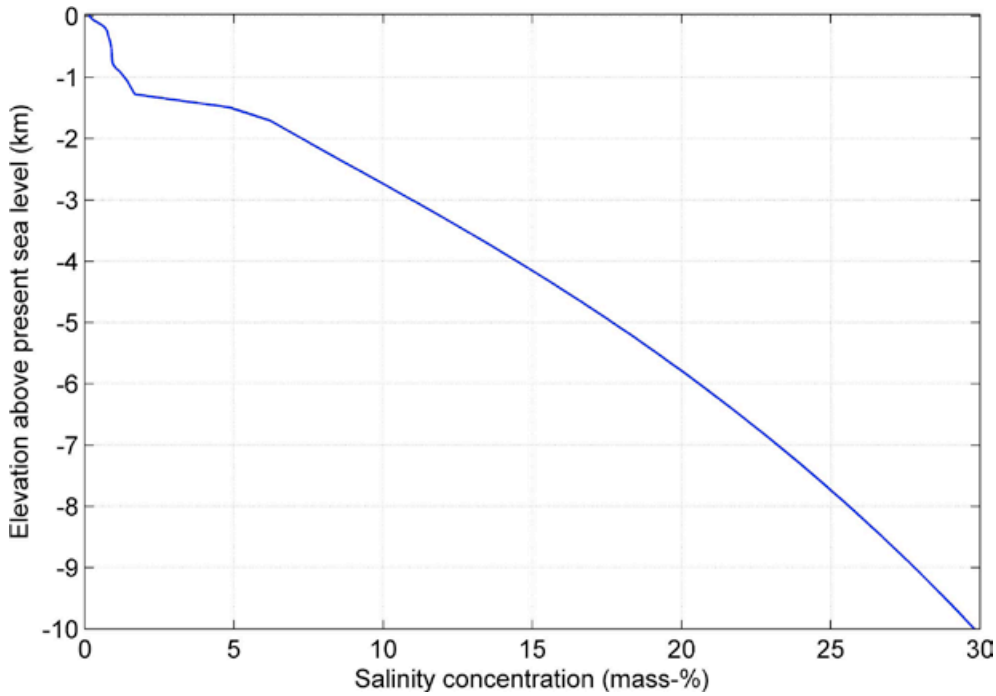

Figure 2-6. *Distribution of initial salinity concentration of groundwater based on data on ionic composition in Appendix F.*

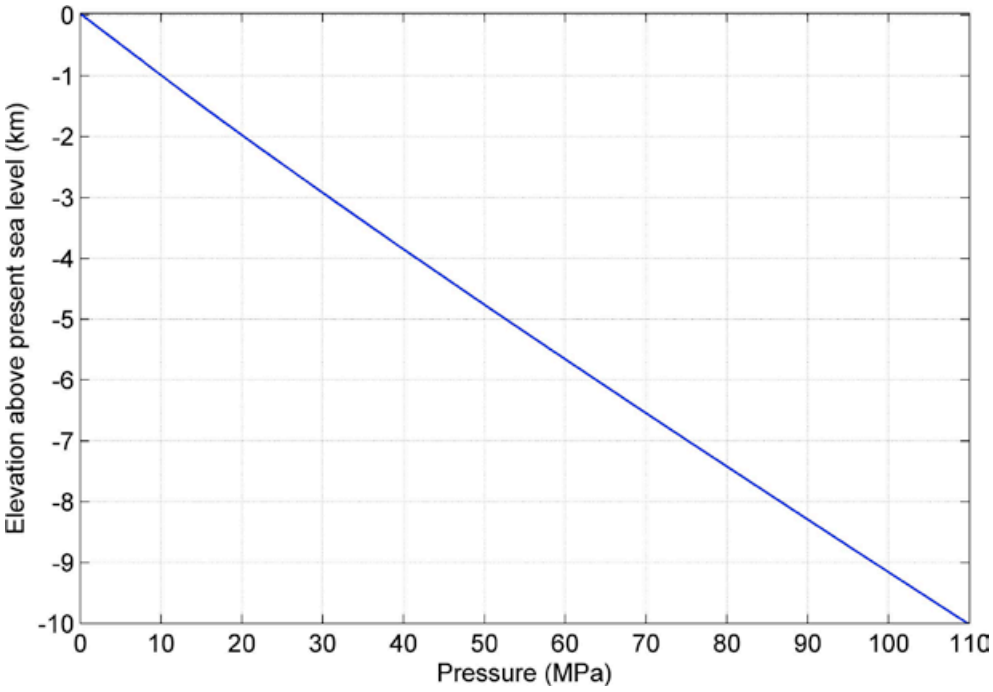

Figure 2-7. *Distribution of initial groundwater pressure associated with the temperature and salinity concentration shown in Figure 2-5 and 2-6.*

2.3 Repository and heat production from the spent fuel

The repository volume is located horizontally along the profile between points x = 1,630,997 m, y = 6,699,230 m and x = 1,632,235 m, y = 6,700,465 m using the RT-90 coordinate system. Vertically the repository is located between the depths of 450 m and 470 m within rock domain RFM029. In the 2D model domain, the 1,749-m wide repository is located at a distance of 3,908 metres from the south-west side.

The canisters will have an initial heat power of around 1,700 W and a normalized time-decaying rate of heat production as shown in Figure 2-8. Based on 3D thermal modelling results the initial heat production power $r = ½(5.4\ \text{W/m} + 6.3\ \text{W/m})/(1\ \text{m} \times 20\ \text{m}) = 0.2925\ \text{W/m}^3$ is distributed evenly over the repository area, see Appendix G.

2.4 Surface conditions

In the modelling of surface conditions, the objective is to define a correlation between air- and ground surface temperatures in consideration of the effects of surface covers. In the following, the simulated climate cases are described first. Then the evolution of water bodies and treatment of vegetation and snow cover along the profile are described. In the end, the empirical *n*-factor concept /Lunardini 1978/ is applied to calculate the ground surface temperature from the air temperature by using statistical relations between the air temperature and ground surface temperature.

Climate cases

The time-dependent surface conditions at Forsmark are associated with the following climate cases /SKB 2010a/:

- *Repetition of last glacial cycle* case (Reference glacial cycle) and
- *Severe permafrost* case.

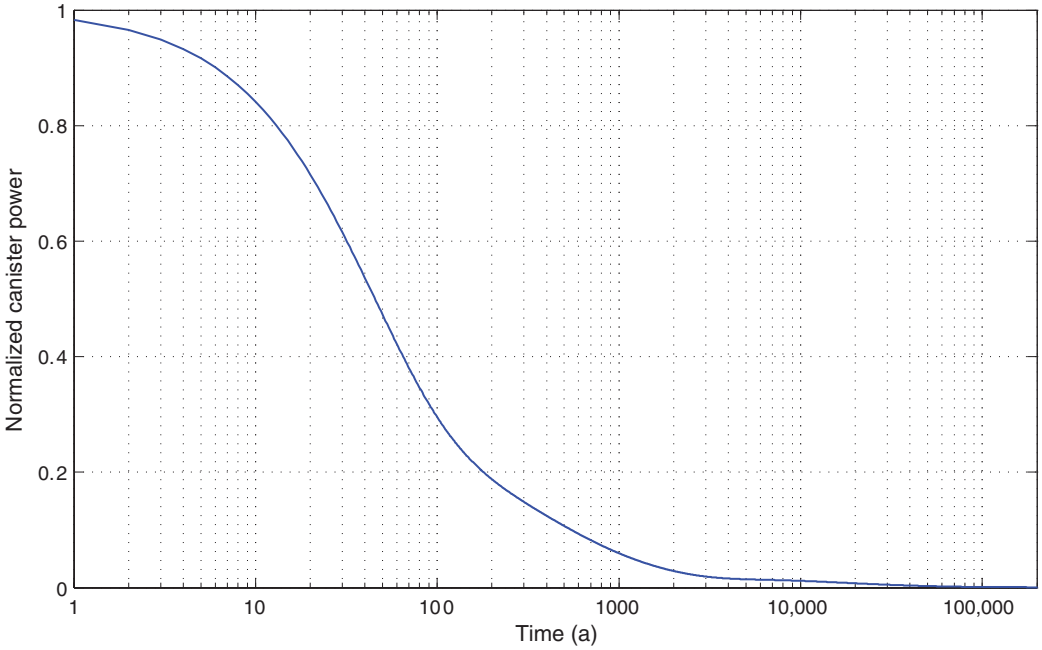

Figure 2-8. *Evolution of normalized heat power from a spent fuel canister. After /Håkansson 2000/.*

The *Repetition of last glacial cycle* case uses environmental conditions (i.e. ice sheets, shore-line displacement and air temperature curve) reconstructed for the Weichselian glacial cycle /SKB 2010a/. However, since permafrost and perennially frozen ground were found to reach their maximum depths around 70,000 years BP for this specific climate development /SKB 2006, 2010a/, only the time period of 115,000–70,000 years BP of this case is simulated.

The *Severe permafrost* case is more favourable for permafrost development than the *Repetition of last glacial cycle* case, since it describes a situation with an extremely dry climate with no ice sheet, vegetation and snow cover formation and the sites remaining above sea level throughout the glacial cycle /SKB 2010a/. The reconstructed mean annual air temperature used for these two cases is described in Appendix H.

Based on the Köppen climate classification /Lohmann et al. 1993/ and long-term observations /Eugster et al. 2000/ both climate cases may be divided into three climate zones: *Boreal*, *Subarctic* and *Arctic*. The climate zones are characterized by the annual mean air temperature, the monthly mean maximum summer air temperature and the monthly mean minimum winter air temperature, and the monthly mean maximum summer and winter precipitations (Table 2-4 and Table 2-5). The large ranges in the monthly mean air temperatures and precipitations are explained by the fact that the description and modelling of surface conditions involve significant data-, conceptual- and model uncertainties /SKB 2010b/.

Table 2-4. Climate information for the Repetition of last glacial cycle case.

Climate zone	Annual mean air temperature (°C)	Monthly mean max. summer air temperature (°C)	Monthly mean min. winter air temperature (°C)	Monthly mean max. summer precipitation (mm/month)	Monthly mean max. winter precipitation (mm/month)
Boreal	> 0	+10 – +20	–15 – +5	10–60	1–50
Subarctic	0 – –6	+5 – +15	–25 – –10	5–60	1–40
Arctic	< –6	< +5 – +10	–35 – –20	5–60	1–40

Table 2-5. Climate information for the Severe permafrost case.

Climate zone	Annual mean air temperature (°C)	Monthly mean max. summer air temperature (°C)	Monthly mean min. winter air temperature (°C)	Monthly mean max. summer precipitation (mm/month)	Monthly mean max. winter precipitation (mm/month)
Boreal	>0	+10 – +20	–15 – +5	5–50	<1
Subarctic	0 – –6	+5 – +15	–25 – –10	5–50	<1
Arctic	<–6	<+5 – +10	–35 – –20	5–50	<1

Water bodies

The evolution of shoreline development and lakes along the profile is based on the future relative shore-level and lake development at the Forsmark site as described in Appendix H and /SKB 2010a/. In other words, the future shore-line and lake development is here envisaged to have occurred also during the first period in the reconstruction of the last glacial cycle conditions. Figure 2-9 shows the water depth contours of the Baltic Sea and two future lakes along the profile and in time. Starting in the Eemian, see Appendix H, the surface of the profile is completely submerged until 114,300 years BP and rises above the water level at 97,500 years BP. The ground surface above the repository starts to emerge at 112,700 years BP and it is completely exposed after 111,700 years BP. One of the lakes (future lake #28), located at a distance of 9 km along the profile, is formed at 109,000 years BP and lives until 105,000 years BP. The other lake (future lake #18), located at a distance of 14.8 km, is formed at 103,000 years BP and lasts till 97,000 years BP.

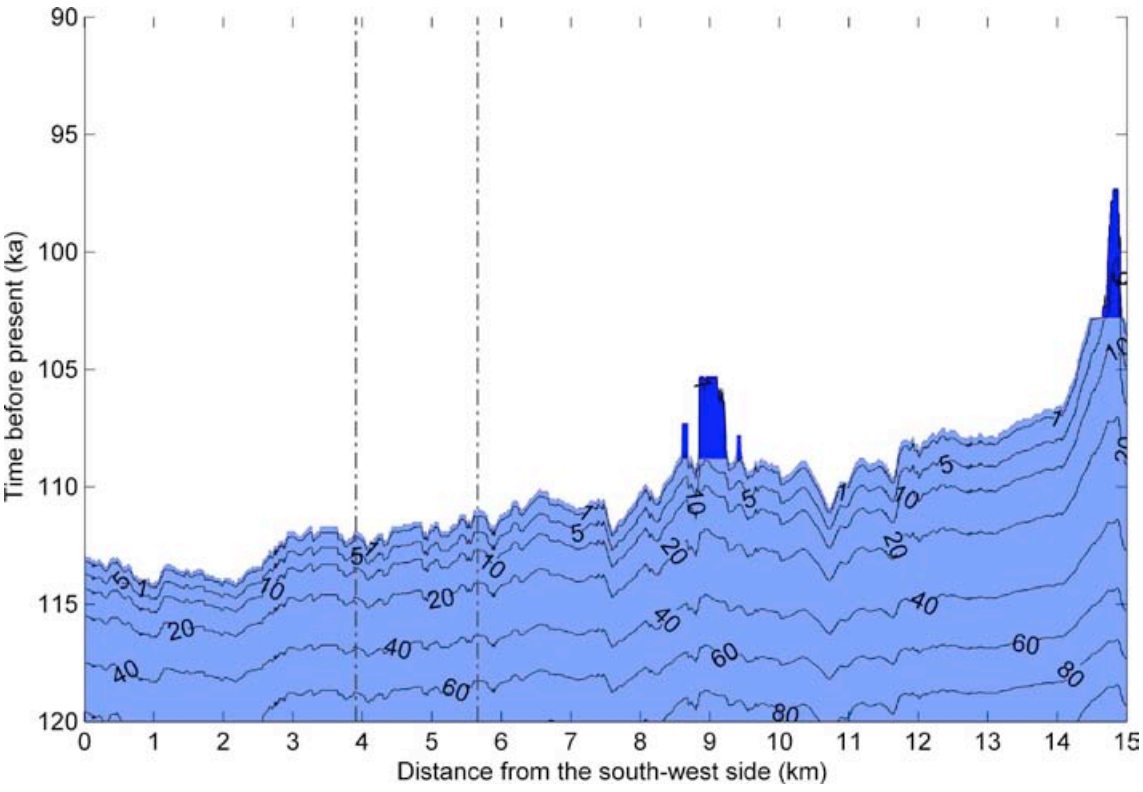

Figure 2-9. *Water depth contours in (m) of Baltic Sea (light blue) and two lakes (blue) along the surface of the profile and in time, see also Appendix I . The repository is located between the dashed vertical lines.*

Vegetation and snow cover

The vegetation and snow cover are closely related to the prevailing climate conditions as well as to other landscape parameters of the site. The presence of different vegetation within different biomes have been described in numerous publication e.g. /Breckle 2002, Archibold 1994/ and the regional response of vegetation types to climate has been modelled /Kjellström et al. 2010/. In the present study, a detailed resolution of the distribution of prevailing major vegetation types for Boreal, Subarctic and Arctic climate zones in the Repetition of last glacial cycle case were described by using local differences in a Topographical Wetness Index (TWI) with the resolution of 20 m × 20 m as described in Appendix J. Figure 2-10 shows the distribution of TWI along the profile used for the permafrost modelling.

A comparison of different TWI values in the landscape of Forsmark today, indicates that the following values, 0–10.9, 10.9–13.2 and 13.2–30 represent dry, fresh-moist and wet surface conditions, respectively, see Appendix J. Table 2-6 presents a matrix how the TWI would affect the vegetation in regard to the dominance of trees, shrubs, grasslands and in accordance with the model settings

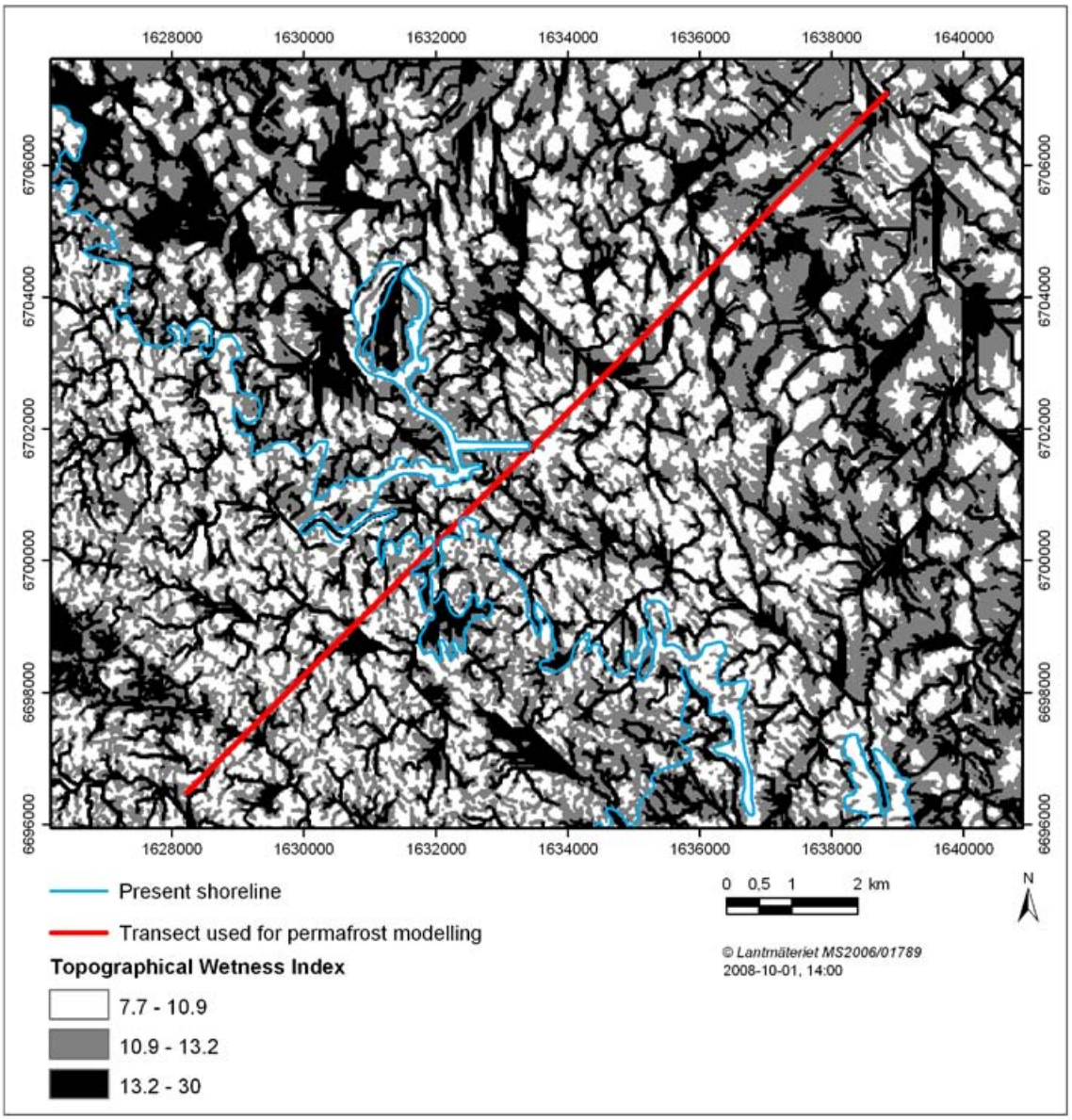

Figure 2-10. *Distribution of Topographic Wetness Index along the profile used for the permafrost modelling with a pixel size of 20 m × 20 m /Strömgren and Brydsten 2008/. Note that the north-east part of the profile today is covered by the Baltic Sea as shown in Figure 2-1. For this area, the figure shows calculated future TWI values, see Appendix J.*

Table 2-6. Main vegetation cover types at Forsmark for three different climate zones and corresponding TWI values. See also Appendix J.

Climate zone	Vegetation cover type and TWI values				
	Forest	Shrubs	Grassland	Barren	Peatland
Boreal	Mixed	–	–	–	Peat
	TWI > 0				TWI > 13.2
Subarctic	Tree line / tundra forest	Moderate / short	Short	–	Peat
	TWI > 13.2	10.9 ≤ TWI ≤ 13.2	TWI < 10.9		TWI > 13.2
Arctic	–	Short	Tussocks	Bare	Peat
		TWI > 13.2	10.9 ≤ TWI ≤ 13.2	TWI < 10.9	TWI > 13.2

under Boreal, Subarctic and Arctic climate zones. It can be seen that, e.g. for the locations along the profile that are associated with TWI values 10.9–13.2 vegetation changes from shrubs to grassland as climate changes from subarctic to arctic. The overall presence of the general vegetation types in each biome follows the description of the /Breckle 2002/. The peatland vegetation type represents the surface cover of the two future lakes along the profile after turning to peat. The snow cover is assumed to follow the TWI values and precipitation such that in the mean winter snow thickness can vary from few centimetres to over 30 cm.

In this attempt to distribute major functional vegetation types and snow cover within different climate zones using TWI, no accounts for factors such as north- and south-facing slopes or prevailing wind directions have been made, which all can be important structuring factors of local subarctic and arctic vegetation patterns. Furthermore, the present landscape of Forsmark is used for TWI during the entire time of investigation excluding changes in topography associated with erosion. The resulting spatial distributions of vegetation have to be regarded as a few snapshots of potential distributions on a continuous scale depending on climate. These snapshots are then used to study the impact of vegetation on the permafrost development.

Ground surface temperature

The implications of vegetation and snow cover and other climate factors on the ground surface temperature and, in turn, on permafrost development is well investigated /Washburn 1979, Williams and Smith 1989, Yershov 1998, French 2007/. In general, an annual mean air temperature ranging between –9 and –1°C is required to build up permafrost for a majority of surface covers, being affected by the radiation, convection, evaporation, condensation, and topography. The surface conditions can be modelled by thermodynamic and hydrodynamic models using surface energy and water balance equations and information of topography and climate conditions such as radiation, precipitation, cloudiness and wind, and their annual and diurnal variation /Riseborough et al. 2008/. However, these sophisticated models are unsuitable for the long time spans associated with glacial cycles, since no climate data besides air temperature can be adequately constructed for site. Therefore, an empirical approach based on *n*-factors /Lunardini 1978/, i.e. statistical correlations between air and ground surface temperature, has been used to construct the ground surface temperature from the reconstructed air temperature, see Appendix H.

The freezing *n*-factors, n_{fr}, are relations between time integrals of ground surface temperature and air temperature below the freezing point while the thawing *n*-factors, n_{th}, are relations between time integrals of ground surface temperature and air temperature above the freezing point defined as follows

$$n_{fr} = \frac{\int_0^{\Delta t_{s-}} T_s \mathrm{d}t}{\int_0^{\Delta t_{a-}} T_a \mathrm{d}t}, \quad n_{th} = \frac{\int_0^{\Delta t_{s+}} T_s \mathrm{d}t}{\int_0^{\Delta t_{a+}} T_a \mathrm{d}t} \tag{2-4}$$

where T_s and T_a are the inter-annual surface and air temperatures, respectively. The time intervals Δt_{s-}, Δt_{a-} , Δt_{s+} and Δt_{a+} denote the periods of a year, Δt_{year}, when the ground surface or air tempera-

ture is below (–) or above (+) the freezing point. Obviously, $\Delta t_{year} = \Delta t_{s-} + \Delta t_{s+} = \Delta t_{a-} + \Delta t_{a+}$. By making use of the *n*-factors, the mean annual surface temperature can be represented as

$$\overline{T}_s = \frac{1}{\Delta t_{year}}\left(\int_0^{\Delta t_{s-}} T_s dt + \int_0^{\Delta t_{s+}} T_s dt\right) = \frac{1}{\Delta t_{year}}\left(n_{fr}\int_0^{\Delta t_{a-}} T_a dt + n_{th}\int_0^{\Delta t_{a+}} T_a dt\right) \quad (2\text{-}5)$$

When the air temperature is approximated by the mean annual value $\overline{T}_a$ and the amplitude A_a using the sinusoid relation

$$T_a = \overline{T}_a + A_a \sin\left(\frac{2\pi t}{\Delta t_{year}}\right) \quad (2\text{-}6)$$

Equation (2-5) can be brought into the form

$$\overline{T}_s = a\overline{T}_a + b \quad (2\text{-}7)$$

where

$$a = \left[\frac{1}{2} - \frac{1}{\pi}\arcsin\left(\frac{\overline{T}_a}{A_a}\right)\right]n_{fr} + \left[\frac{1}{2} + \frac{1}{\pi}\arcsin\left(\frac{\overline{T}_a}{A_a}\right)\right]n_{th} \quad (2\text{-}8)$$

and

$$b = \frac{1}{\pi}\cos\left[\arcsin\left(\frac{\overline{T}_a}{A_a}\right)\right](n_{th} - n_{fr})A_a \quad (2\text{-}9)$$

The *n*-factors for the Forsmark site are estimated by using results of the site investigations for different biophysiographic units in North America /Klene et al. 2001, Karunaratne and Burn 2003, 2004, Kade et al. 2006, Hinkel et al. 2008, Karunaratne et al. 2008, Klene 2008/. The *n*-factors for the *Repetition of last glacial cycle* case and the *Severe permafrost* case are presented in Table 2-7 and Table 2-8, respectively. Knowing that *n*-factors for a certain site, with specific climate and surface conditions, cannot be applied to other sites as such, the *n*-factors for the Forsmark site are determined as mean values of *n*-factors for different sites in North America corresponding to Forsmark's climate and ground surface moisture conditions indicated in Table 2-7 and Table 2-8. In general, the low *n*-factors represent humid conditions with thick vegetation and winter snow cover while high *n*-factors are related to dry conditions with thin vegetation and snow cover.

When the site is submerged by the Baltic Sea or by the two lakes, the ground surface temperature is set to +4°C for water depths greater than 6 metres. For shallower depths the temperature is interpolated between the value of 4°C and the prevailing ground surface temperature.

Figures 2-11, 2-12, 2-13 and 2-14 show the evolution of modelled ground surface temperatures for the *Repetition of last glacial cycle* case at four locations from the south-west side of the profile considering different surface condition types: 3,550 m – wet, 4,783 m – fresh-moist, 11,600 m – dry, 14,600 m – peatland. The corresponding results for the *Severe permafrost* case type are presented in Figure 2-15. Figure 2-16 illustrates the modelled ground surface temperatures along the profile at four different times for the *Repetition of last glacial cycle* case considering different climate conditions: 111,500 years BP – subarctic and partially submerged, 103,500 years BP – *Boreal*, 95,000 years BP – *Subarctic*, 70,000 years BP – *Arctic*. The corresponding results for the *Severe permafrost* case are shown in Figure 2-18. The results concerning the humid variant are obtained by the lowest *n*-factors of Table 2-7 and Table 2-8 while the highest *n*-factors of the same tables yield the results for the dry variant.

The ground surface temperature of +4°C for time periods from 115,000 years to almost 100,000 years BP indicates the time when the profile is submerged by the Baltic Sea or the two lakes. Obviously, the dry surface condition type generates the lowest and the peatland condition type the highest ground surface temperatures in the *Subarctic* and *Arctic* climate zones in *Repetition of last glacial cycle* case. Furthermore, due to thin vegetation and snow cover, the dry variant of *Repetition of last glacial cycle* case results in the lowest ground surface temperatures in the subarctic and arctic climate zones but highest in the *Boreal* climate zone. Contrary to *Repetition of last glacial cycle* case the humid variant of the *Severe permafrost* case results in lower ground surface temperatures than the dry variant of the same case. This is a consequence of the presence of clouds, which is stronger in the humid variant than in the dry variant, is associated with a cooler surface during summers /Groisman et al. 2000/.

Table 2-7. Freezing (winter) and thawing (summer) n-factors for the Repetition of last glacial cycle case.

Climatic zone	Season	Monthly mean max./min.	Monthly mean max.	*n*-factors for specified surface conditions and associated TWI intervals			
		air temperature (°C)	precipitation (mm/month)	Dry (< 10.9)	Fresh-moist (10.9–13.2)	Wet (> 13.2)	Peatland (> 13.2)
Boreal	summer	+10 – +20	10–60	1.2–1.4	1.2–1.4	1.2–1.4	1.0
	winter	–15 – +5	1–50	0.2–0.3	0.2–0.3	0.2–0.3	0.1
Subarctic	summer	+5 – +15	5–60	0.8–1.0	0.7–0.9	0.6–0.8	0.8–1.0
	winter	–25 – –10	1–40	0.5–0.9	0.4–0.8	0.2–0.6	0.1–0.4
Arctic	summer	<+5 – +10	5–60	1.0–1.2	0.5–0.8	0.4–0.7	0.6–0.9
	winter	–35 – –20	1–40	0.7–1.0	0.4–0.8	0.3–0.6	0.2–0.5

Table 2-8, Freezing (winter) and thawing (summer) n-factors for the Severe permafrost case.

Climatic zone	Season	Monthly mean max./min.	Monthly mean max.	*n*-factors for specified surface conditions and associated TWI intervals			
		air temperature (°C)	precipitation (mm/month)	Dry (< 10.9)	Fresh-moist (10.9–13.2)	Wet (> 13.2)	Peatland (> 13.2)
Boreal	summer	+10 – +20	5–50	1.0–1.4	1.0–1.4	1.0–1.4	1.0–1.4
	winter	–15 – +5	<1	1.0	1.0	1.0	1.0
Subarctic	summer	+5 – +15	5–50	1.0–1.4	1.0–1.4	1.0–1.4	1.0–1.4
	winter	–25 – –10	< 1	1.0	1.0	1.0	1.0
Arctic	summer	<+5 – +10	5–50	1.0–1.4	1.0–1.4	1.0–1.4	1.0–1.4
	winter	–35 – –20	< 1	1.0	1.0	1.0	1.0

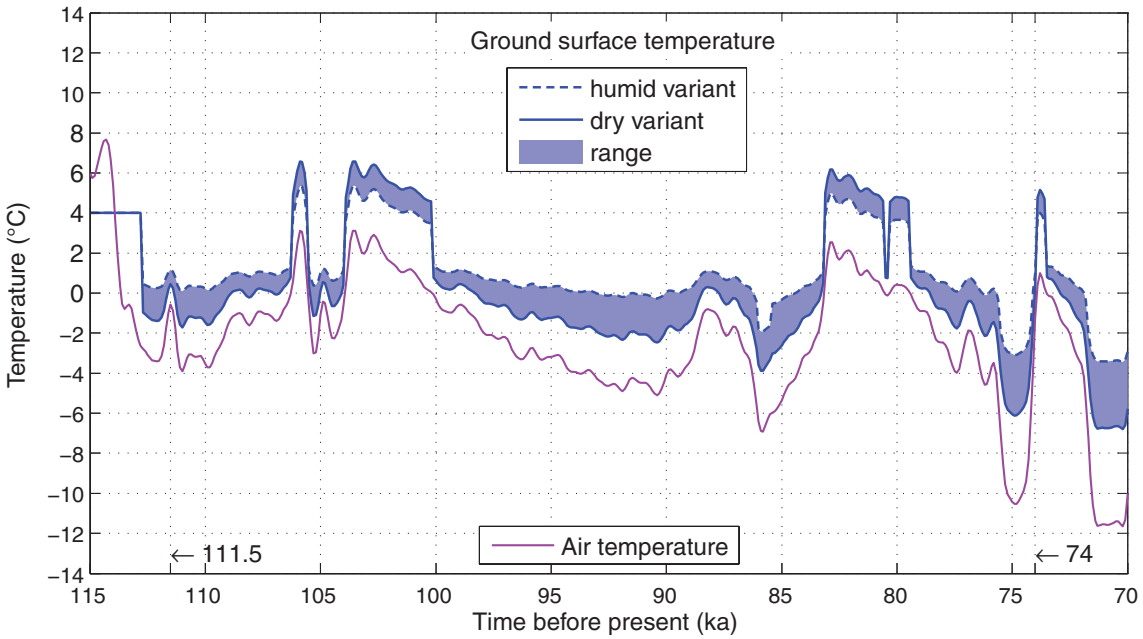

Figure 2-11. *Evolution of air temperature and modelled ground surface temperatures at 3,550 metres from the south-west side of the profile for the Repetition of last glacial cycle case and wet surface condition type.*

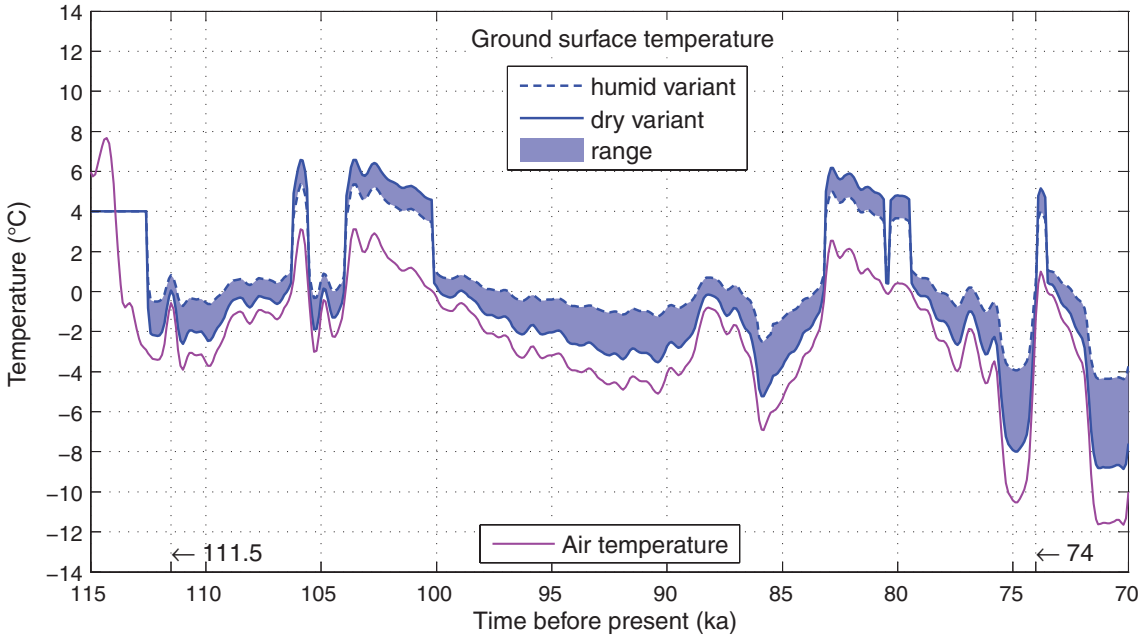

Figure 2-12. *Evolution of air temperature and modelled ground surface temperatures at 4,783 metres from the south-west side of the profile (in the middle of the repository) for the Repetition of last glacial cycle case and fresh-moist surface condition type.*

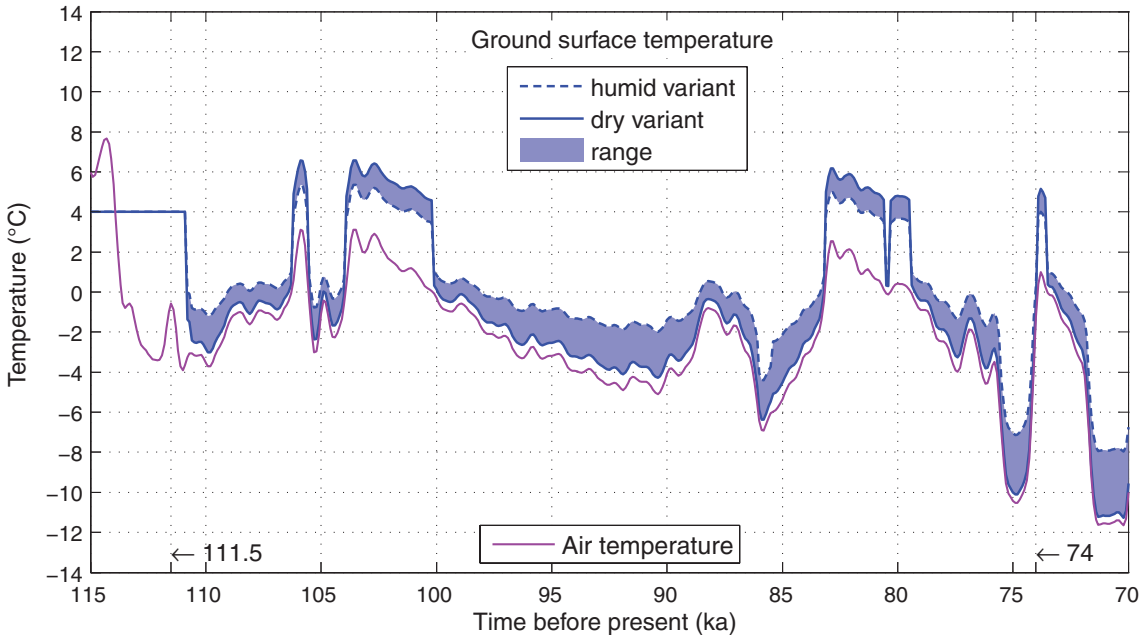

Figure 2-13. *Evolution of air temperature and modelled ground surface temperatures at 11,600 metres from the south-west side of the profile for the Repetition of last glacial cycle case and dry surface condition type.*

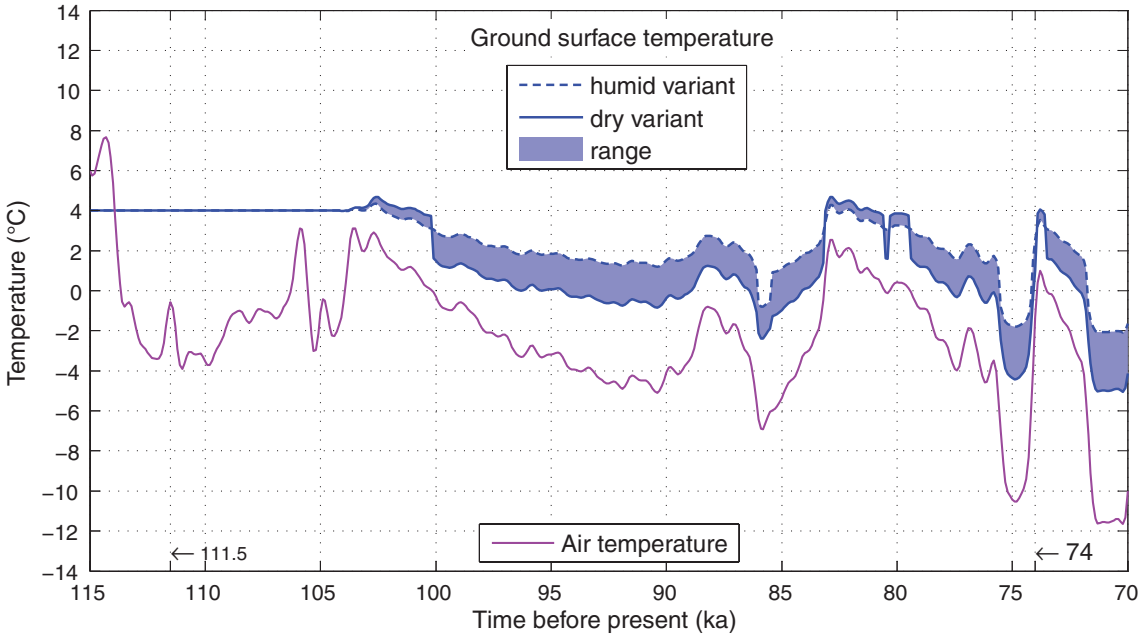

Figure 2-14. *Evolution of air temperature and modelled ground surface temperatures at 14,600 metres from the south-west side of the profile for the Repetition of last glacial cycle case and peatland surface condition type.*

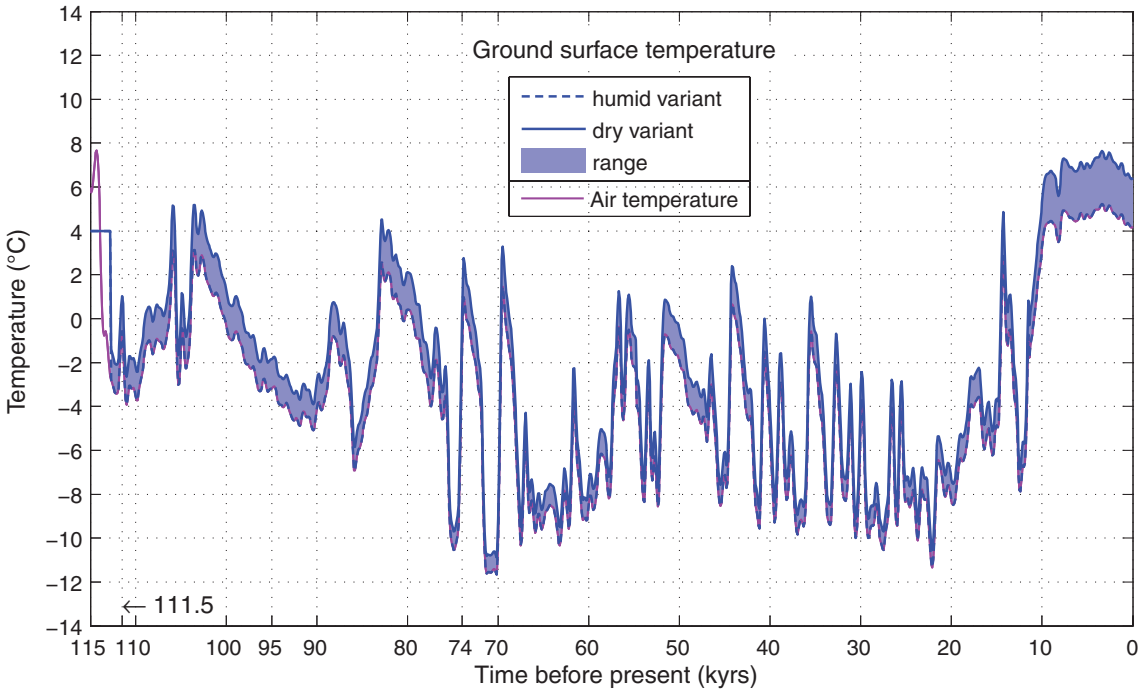

Figure 2-15. *Evolution of air temperature and modelled ground surface temperatures for the Severe permafrost case and dry surface condition type. The air temperature and the ground surface temperature of the humid variant coincide after the profile is exposed beneath the Baltic Sea.*

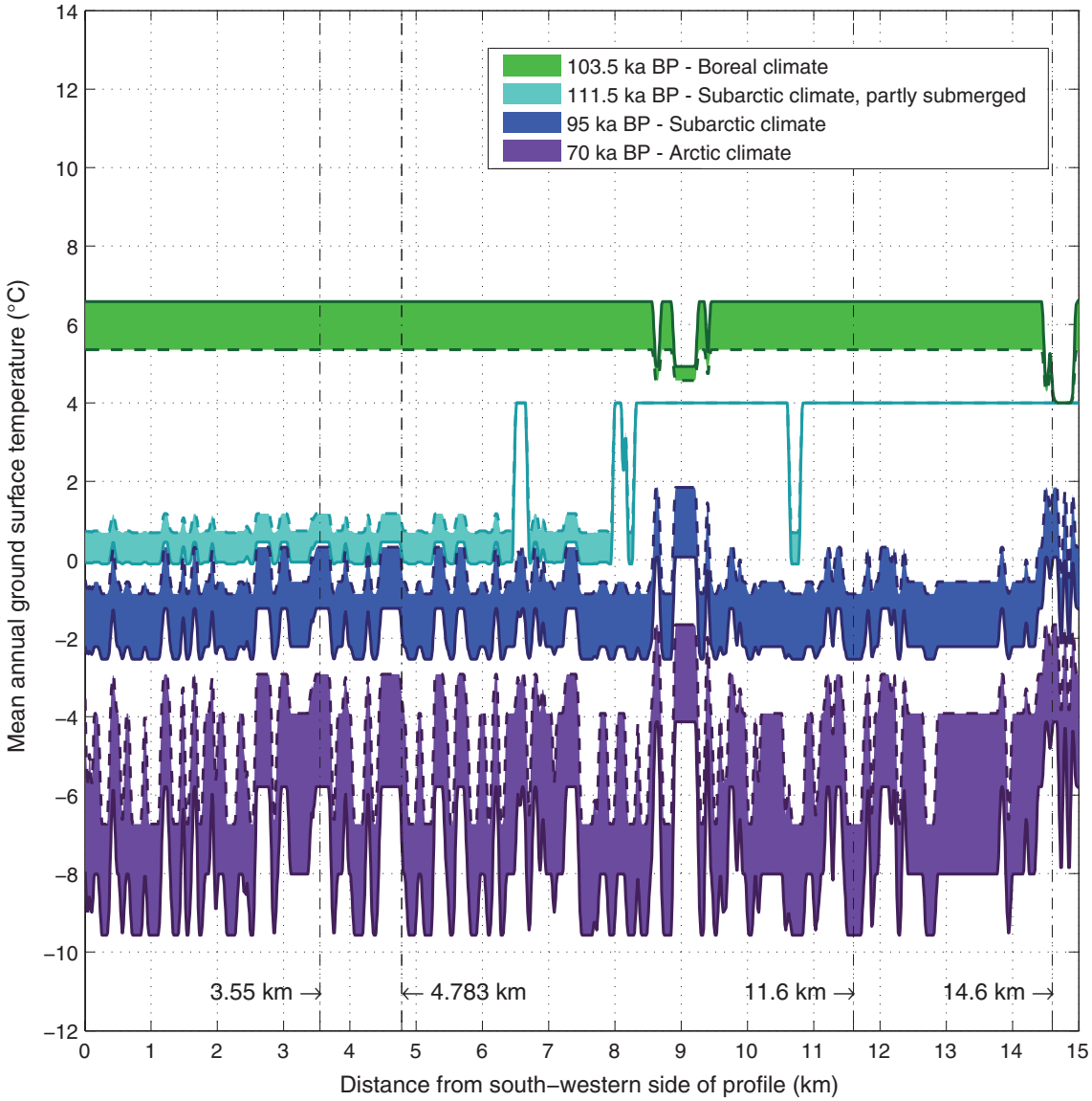

Figure 2-16. *Modelled ground surface temperatures along the profile at four different times for the Repetition of last glacial cycle case considering different climate conditions: Boreal climate at 103.5 ka BP, Subarctic climate and partially submerged conditions at 111.5 ka BP, Subarctic climate at 95 ka BP, Arctic climate at 70 ka BP. The solid border lines of the shadowed areas indicate the dry variant and dashed ones the humid variant of the Repetition of last glacial cycle case. The dashed vertical lines denote the locations of the profile considering different surface condition types: 3.55 km – wet, 4.783 km – fresh-moist, 11.6 km – dry, 14.6 km – peatland.*

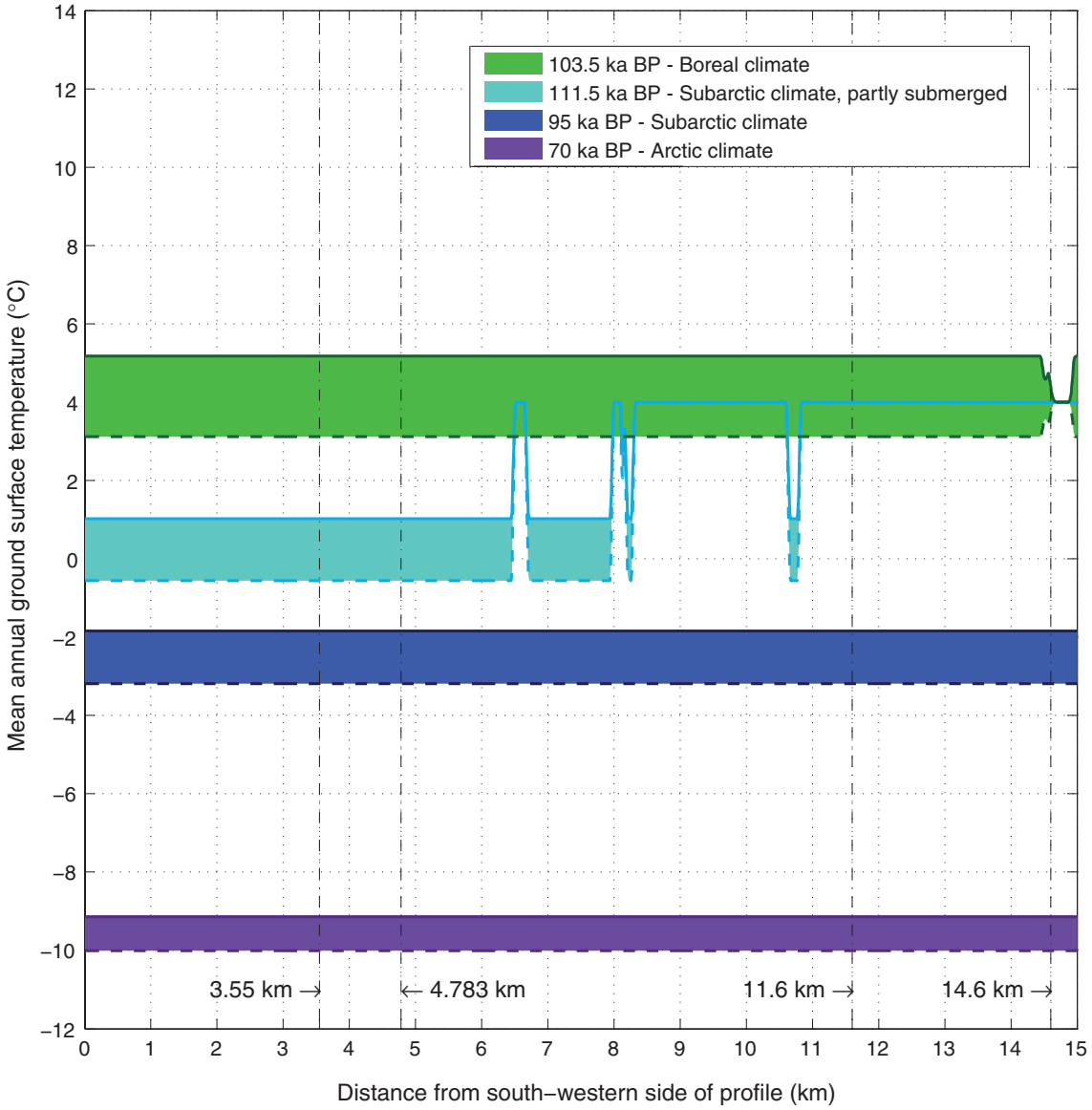

Figure 2-17. *Modelled ground surface temperatures along the profile at four different times for the Severe permafrost case considering different climate conditions: Boreal climate at 103.5 ka BP, Subarctic climate and partially submerged conditions at 111.5 ka BP, Subarctic climate at 95 ka BP, Arctic climate at 70 ka BP. The solid border lines of the shadowed areas indicate the dry variant and dashed ones the humid variant of the Severe permafrost case.*

3 Mathematical model

3.1 Introduction

The mathematical model for freezing and thawing of ground used for the SR-Can safety assessment /SKB 2006, Section 3.4 and 4.4.1/ and in /Hartikainen 2004, 2006/ is based on the theory of mixtures and basic principles of continuum mechanics and thermodynamics considering the freezing ground as an elastic porous medium of soil or rock skeleton saturated by saline groundwater and ice. The model is capable of describing the heat and mass transfer in porous medium, freezing of groundwater being affected by groundwater pressure and salt concentration, and freezing induced groundwater flow. The derivation of the model is described in /Hartikainen and Mikkola 2006/. In the present study, the mathematical model is reformulated in terms of Gibbs free energy functions by taking into account the effects of temperature, pressure and salinity concentration on the properties of groundwater and ice in a more accurate way. The improved model consisting of balance laws of mass, momentum and energy, and the constitutive laws of state and diffusion is capable of describing the exclusion of salt during freezing and the density dependent groundwater flow in unfrozen and partially frozen ground. In addition, the description of effects of pressure and salinity concentration on the freezing temperature of groundwater is also improved. Since ice-sheet development is excluded in the present study, deformations of ground are not considered.

3.2 Mixture concept

The freezing ground is considered as an incompressible porous medium of rock or soil skeleton (s), filled up with groundwater (gw) and ice (i), such that they are found in the volume fractions

$$\beta_P = \frac{\mathrm{d}\, v_P}{\mathrm{d}\, v_\mathrm{s} + \mathrm{d}\, v_\mathrm{gw} + \mathrm{d}\, v_\mathrm{i}} \tag{3-1}$$

where $\mathrm{d}\, v_P$ is the volume element of phase $P \in \{\mathrm{s}, \mathrm{gw}, \mathrm{i}\}$. In addition, groundwater is assumed to be a liquid fluid composed of water (w) and dissolved salts (c) by means of the molar fractions

$$x_S = \frac{n_S}{n_\mathrm{w} + n_\mathrm{c}} \tag{3-2}$$

where n_S is the mole number of substance $\mathrm{S} \in \{\mathrm{w}, \mathrm{c}\}$. Hence, the freezing ground is a mixture of constituents $k \in \{\mathrm{s}, \mathrm{w}, \mathrm{c}, \mathrm{i}\}$, which coexist in the molar volume fractions

$$\{\beta_\mathrm{s}, x_\mathrm{w}\beta_\mathrm{gw}, x_\mathrm{c}\beta_\mathrm{gw}, \beta_\mathrm{i}\} \tag{3-3}$$

such that

$$\beta_\mathrm{s} + \beta_\mathrm{gw} + \beta_\mathrm{i} = 1,\ \beta_P \geq 0,\ P \in \{\mathrm{s}, \mathrm{gw}, \mathrm{i}\}, \quad x_\mathrm{w} + x_\mathrm{c} = 1,\ x_S \geq 0,\ S \in \{\mathrm{w}, \mathrm{c}\} \tag{3-4}$$

Obviously, for the perennially unfrozen ground $\beta_\mathrm{i} = 0$.

The molar volume fractions are related to the porosity, η, the unfrozen groundwater content, χ, and the salinity concentration, C, as

$$\eta = 1 - \beta_\mathrm{s}, \qquad \chi = \frac{\beta_\mathrm{gw}}{\beta_\mathrm{gw} + \beta_\mathrm{i}} = \frac{\beta_\mathrm{gw}}{1 - \beta_\mathrm{s}}, \qquad C = x_\mathrm{c} = 1 - x_\mathrm{w} \tag{3-5}$$

The modelling of salinity is simplified by considering the dissolved salts component as seawater /Feistel 2008/.

3.3 State equations

The state equations for each constituent k are derived from the following expression for the specific Gibbs free energy function

$$g_k = \frac{T}{T_0} g_{k0} - \frac{T - T_0}{T_0} h_{k0} - \int_{T_0}^{T} \int_{T_0}^{T'} \frac{c_k}{T''} dT'' dT' + \frac{1}{\bar{\rho}_{k0}} \int_{p_0}^{p} \exp\left(- \int_{p_0}^{p'} \kappa_k dp'' + \int_{T_0}^{T} \alpha_k dT' - \int_{x_{k0}}^{x_k} \zeta_k dx_k' \right) dp' + \frac{RT}{M_k} f_{\text{sal},k} + \frac{RT}{M_k} f_{\text{add},k} \tag{3-6}$$

where

T is the absolute temperature, [T] = K

p is the absolute pressure, [p] = Pa

h_k is the specific enthalpy, [h_k] = J/kg

c_k is the specific isobaric heat capacity, [c_k] = J/(kg K)

$\bar{\rho}_k$ is the bulk density, [$\bar{\rho}_k$] = kg/m^3

κ_k is the coefficient of isothermal compression, [κ_k] = 1/Pa

α_k is the coefficient of isobaric thermal expansion, [α_k] = 1/K

ζ_k is the coefficient of isothermal haline concentration, [ζ_k] = 1

R is the universal gas constant, R = 8.3145 mol/K

M_k is the molecular weight, [M_k] = kg/mol

$f_{\text{sal},k}$ and $f_{\text{add},k}$ are the interaction function describing the effect of salinity and adsorption, respectively, [$f_{\text{sal},k}$] = 1, [$f_{\text{add},k}$] = 1 .

The subscript 0 refers to the reference state that is defined by the temperature T_0 = 273.15 K, the pressure p_0 = 101,325 Pa and the salinity concentration x_{c0} = 0 (x_{w0} = 1). The specific heat capacity as well as the coefficients of compressibility, thermal expansion and haline concentration of water, dissolved salts and ice are functions of temperature and concentration and expressed by the formula

$$F_k(T, x_k) = F_{k0} \sum_{i=0}^{N_T} a_{k,i} \left(\frac{T - T_0}{T_0} \right)^i \sum_{i=0}^{N_x} b_{k,i} \left(x_k - x_{k0} \right)^i \tag{3-7}$$

where the values of the reference state $F_{k0} = F_k$ (T_0, p_0, x_{k0}) and the values of parameters $a_{k,i}$ and $b_{k,i}$ for water, dissolved salts and ice are given in Table 3-1, Table 3-2 and Table 3-3, respectively. The molecular weight of water and dissolved salts are M_w = 0.0180 kg/mol and M_c = 0.0314 kg/mol /Feistel 2008/.

The specific heat capacity and bulk density of soil, and the bulk density of rock are assumed to be constant. Their reference values are presented in Table 2-1 and Table 2-2. The specific heat capacity of rock depends on the temperature through the following formula

$$c_s(T) = c_{s,20} + \Delta c_s (T - T_0 - T_{20}) \tag{3-8}$$

where $c_{s,20}$ is the specific heat capacity of the rock at the temperature T_{20} = 20°C, and Δc_s its increase for 100°C given in Table 2-2.

The interaction between molecules of water and ions of dissolved salts is expressed through the following functions

$$f_{\text{sal,w}} = -d_{w,1} \left(\frac{x_c}{x_w} \right) - d_{w,2} \left(\frac{x_c}{x_w} \right)^2 \tag{3-9}$$

$$f_{\mathrm{sal,c}} = d_{\mathrm{c},0} \ln\left(\frac{x_{\mathrm{c}}}{x_{\mathrm{w}}}\right) + d_{\mathrm{c},1}\left(\frac{x_{\mathrm{c}}}{x_{\mathrm{w}}}\right) \tag{3-10}$$

where the coefficients $d_{k,j}$ are presented in Table 3-4. It is assumed that salinity is not involved in the Gibbs free energy functions of skeleton and ice, i.e. $f_{\mathrm{sal,s}} = f_{\mathrm{sal,i}} = 0$.

The interaction due to adsorption is described by means of the volume fractions of skeleton and groundwater in the Gibbs free energy functions as follows. Introducing the factor $\phi = (\beta_{\mathrm{s}}/\beta_{\mathrm{s0}})/(\beta_{\mathrm{w}}/\beta_{\mathrm{w0}})$, the interaction functions for adsorption are defined as

$$f_{\mathrm{add,w}} = f_{\mathrm{add,c}} = \begin{cases} e_{\mathrm{gw}}(1-\phi), & \text{if } \phi \geq 1 \\ 0, & \text{if } \phi < 1 \end{cases} \tag{3-11}$$

$$f_{\mathrm{add,s}} = \begin{cases} e_{\mathrm{s}} \ln\phi, & \text{if } \phi \geq 1 \\ 0, & \text{if } \phi < 1 \end{cases} \tag{3-12}$$

In addition, $f_{\mathrm{add,i}} = 0$, and by making use of definitions of Equation 3-5 the factor ϕ can be represented as $\phi = ((1-\eta)/(1-\eta_0))/((\chi\eta)/(\chi_0\eta_0))$. The coefficients $e_{\mathrm{gw}} = e_{\mathrm{s}}$ and the reference values χ_0 are presented in Table 2-1 and Table 2-3. Since no deformations are considered, $\eta_0 = \eta$.

Table 3-1, Values for parameters F_{w0}, $a_{w,i}$ and $b_{w,i}$ of Equation 3-7 for the specific Gibbs free energy function of water (Equation 3-6).

Parameter	Unit	F_{w0}	i	$a_{w,i}$	$b_{w,i}$
Specific Gibbs free energy	J/kg	0			
Specific enthalpy	J/kg	0			
Specific heat capacity	J/(kg · K)	$4.207686 \cdot 10^{3}$	0	1	1
	–		1	$-3.732746 \cdot 10^{-2}$	$-3.020061 \cdot 10^{0}$
	–		2	$1.202990 \cdot 10^{-3}$	$1.476072 \cdot 10^{1}$
Thermal conductivity	W/(m · K)	$5.600000 \cdot 10^{-1}$	0	1	1
Bulk density	kg/m³	$9.998848 \cdot 10^{2}$			
Isothermal compressibility	1/Pa	$4.884986 \cdot 10^{-10}$	0	$9.115172 \cdot 10^{-1}$	1
	–		1	$-1.522016 \cdot 10^{0}$	0
	–		2	$7.358516 \cdot 10^{0}$	0
	–		3	$1.675538 \cdot 10^{1}$	0
	–		4	$2.609616 \cdot 10^{1}$	0
	–		5	$-2.131625 \cdot 10^{1}$	0
	–		6	$7.623942 \cdot 10^{0}$	0
Isobaric thermal expansion	1/K	$-5.335802 \cdot 10^{-5}$	0	1	1
	–		1	$4.222245 \cdot 10^{-3}$	0
	–		2	$-1.107091 \cdot 10^{-2}$	0
	–		3	$2.154741 \cdot 10^{-2}$	0
	–		4	$-2.110495 \cdot 10^{-2}$	0
	–		5	$8.865253 \cdot 10^{-3}$	0
Haline concentration	–	$-6.623695 \cdot 10^{-1}$	0	1	1
	–		1	0	$5.180597 \cdot 10^{0}$

Table 3-2, Values for parameters F_{c0}, $a_{c,i}$ and $b_{c,i}$ of Equation 3-7 for the specific Gibbs free energy function of dissolved salts (Equation 3-6).

Parameter	Unit	F_{c0}	i	$a_{c,i}$	$b_{c,i}$
Specific Gibbs free energy	J/kg	0			
Specific enthalpy	J/kg	0			
Specific heat capacity	J/(kg · K)	$2.413766 \cdot 10^{3}$	0	1	1
	–		1	$-3.732746 \cdot 10^{-2}$	$-3.020061 \cdot 10^{0}$
	–		2	$1.202990 \cdot 10^{-3}$	$1.476072 \cdot 10^{1}$
Thermal conductivity	W/(m · K)	$5.600000 \cdot 10^{-1}$	0	1	1
Bulk density	kg/m³	$1.743003 \cdot 10^{3}$			
Isothermal compressibility	1/Pa	$4.884986 \cdot 10^{-10}$	0	$9.115172 \cdot 10^{-1}$	1
	–		1	$-1.522016 \cdot 10^{0}$	0
	–		2	$7.358516 \cdot 10^{0}$	0
	–		3	$1.675538 \cdot 10^{1}$	0
	–		4	$2.609616 \cdot 10^{1}$	0
	–		5	$-2.131625 \cdot 10^{1}$	0
	–		6	$7.623942 \cdot 10^{0}$	0
Isobaric thermal expansion	1/K	$-5.335802 \cdot 10^{-5}$	0	1	1
	–		1	$4.222245 \cdot 10^{-3}$	0
	–		2	$-1.107091 \cdot 10^{-2}$	0
	–		3	$2.154741 \cdot 10^{-2}$	0
	–		4	$-2.110495 \cdot 10^{-2}$	0
	–		5	$8.865253 \cdot 10^{-3}$	0
Haline concentration	–	$6.623695 \cdot 10^{-1}$	0	1	1
	–		1	0	$-5.180597 \cdot 10^{0}$

Table 3-3, Values for parameters F_{i0}, $a_{i,i}$ and $b_{i,i}$ of Equation 3-7 for the specific Gibbs free energy function of ice (Equation 3-6).

Parameter	Unit	F_{i0}	i	$a_{i,i}$	$b_{i,i}$
Specific Gibbs free energy	J/kg	0			
Specific enthalpy	J/kg	$-3.333618 \cdot 10^{5}$			
Specific heat capacity	J/(kg · K)	$2.088850 \cdot 10^{3}$	0	1	1
	–		1	$1.996378 \cdot 10^{-3}$	0
Thermal conductivity	W/(m · K)	$2.240000 \cdot 10^{0}$	0	1	1
Bulk density	kg/m³	$9.167712 \cdot 10^{2}$			
Isothermal compressibility	1/Pa	$1.144902 \cdot 10^{-10}$	0	$9.970991 \cdot 10^{-1}$	1
	–		1	$4.672083 \cdot 10^{-1}$	0
	–		2	$2.304911 \cdot 10^{-1}$	0
Isobaric thermal expansion	1/K	$1.678074 \cdot 10^{-4}$	0	1	1
	–		1	$2.000831 \cdot 10^{-4}$	0

Table 3-4. Coefficients $d_{w,i}$ and $d_{c,i}$ of the interaction function of salinity for the specific Gibbs free energy function of water and dissolved salts (Equation 3-6).

i	$d_{w,i}$	$d_{c,i}$
0	–	0.87
1	0.87	2.60
2	1.30	–

Specific enthalpy

Specific enthalpies of water, dissolved salts, ice and soil or rock skeleton are derived from the Gibbs free energy function (Equation 3-6) by its temperature derivate as

$$h_k = g_k - T\frac{\partial g_k}{\partial T} = h_{k0} + \int_{T_0}^{T} c_k \, dT' + \int_{p_0}^{p}\left(\overline{\rho}_k^{-1} - T\frac{\partial \overline{\rho}_k^{-1}}{\partial T}\right) dp' \qquad (3\text{-}13)$$

Bulk density

Bulk densities of water, dissolved salts, ice and soil or rock skeleton are obtained by the pressure derivative as

$$\overline{\rho}_k = \left(\frac{\partial g_k}{\partial p} \right)^{-1} = \overline{\rho}_{k0} \exp\left(\int_{p_0}^{p} \kappa_k dp' - \int_{T_0}^{T} \alpha_k dT' + \int_{x_{k0}}^{x_k} \zeta_k dx_k' \right) \tag{3-14}$$

Phase change and unfrozen water content

The state of the phase change between groundwater and ice is defined by the condition that the Gibbs free energies of water and ice are equal in equilibrium:

$$\begin{aligned} g_{\mathrm{w}} - g_{\mathrm{i}} &= -\frac{T - T_0}{T_0}\left(h_{\mathrm{w}0} - h_{\mathrm{i}0}\right) - \int_{T_0}^{T}\int_{T_0}^{T'} \frac{c_{\mathrm{w}} - c_{\mathrm{i}}}{T''} dT'' dT' \\ &+ \int_{p_0}^{p} \left(\overline{\rho}_{\mathrm{w}}^{-1} - \overline{\rho}_{\mathrm{i}}^{-1} \right) dp' + \frac{RT}{M_{\mathrm{w}}} f_{\mathrm{sal,w}} + \frac{RT}{M_{\mathrm{w}}} f_{\mathrm{add,w}} = 0 \end{aligned} \tag{3-15}$$

This equation can be considered as a generalized Clausius-Clapeyron equation for the phase change between water and ice. It can be used to determine the amount of unfrozen groundwater content χ in terms of temperature, pressure and salinity concentration. The associated parameters e_s and χ_0 are evaluated using experimental findings, e.g. /Williams and Smith 1989/. Figure 3-1 shows the calculated unfrozen groundwater content with respect to the temperature for the geological materials of this study in the case with zero salinity and reference water pressure, and in the case with constant salinity concentration of 2 mass-% and water pressure of 5 MPa. It can be seen that due to effects of pressure and salinity concentration a temperature of –1.4°C is required to begin the freezing.

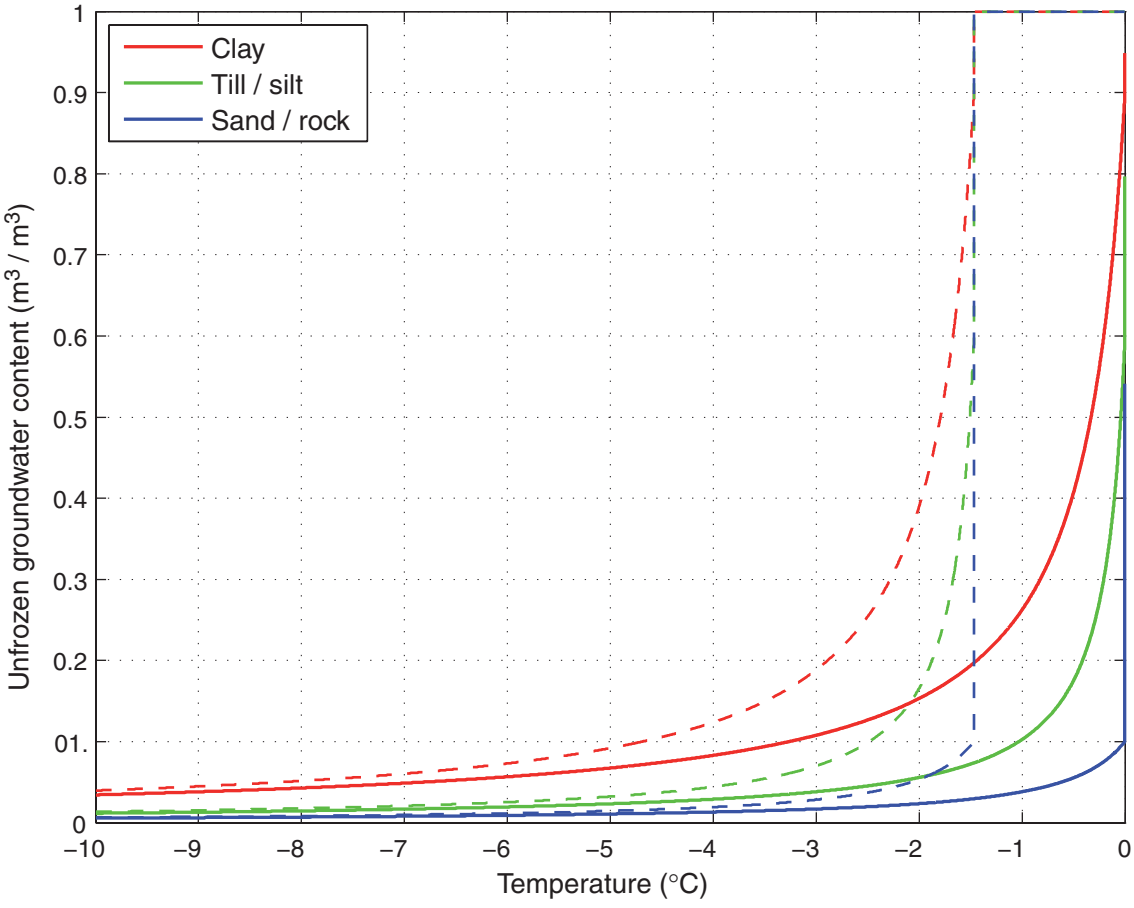

Figure 3-1. *Unfrozen volumetric groundwater content versus temperature in different geological materials for zero salinity and reference water pressure (solid lines), and for constant salinity concentration of 2 mass-% and water pressure of 5 MPa (dashed lines).*

3.4 Diffusion laws

Heat conduction

Heat conduction of the ground is assumed to follow the Fourier's law

$$\mathbf{q} = -\left[\beta_s \lambda_s + x_w \beta_{gw} \lambda_w + x_c \beta_{gw} \lambda_c + \beta_i \lambda_i \right] \mathrm{grad}\, T \tag{3-16}$$

where λ_k is the intrinsic thermal conductivity of constituent $k \in \{s, w, c, i\}$. The temperature dependency of λ_s of the rock is expressed through the following formula

$$\lambda_s(T) = \lambda_{s,20} \frac{1 + b(T_{20} + T_0)}{1 + b(T + T_0)} \tag{3-17}$$

where $\lambda_{s,20}$ is the thermal conductivity of the rock at the temperature $T_{20} = 20°C$. Parameter b is fixed to fit the decrease presented in Table 2-2. The values of λ_w, λ_c and λ_i given in Table 3-1, Table 3-2 and Table 3-3, respectively.

Groundwater flow

Groundwater flow depends on the hydraulic pressure gradient and gravity as follows

$$\mathbf{J}_{gw} = -\frac{\mathbf{k}}{\mu} \cdot \left[\mathrm{grad}\, p - \left(x_w \overline{\rho}_w + x_c \overline{\rho}_c\right) \mathbf{g}\right] \tag{3-18}$$

where $\mathbf{J}_{gw}$ is the Darcian type of volumetric groundwater velocity, $\mathbf{k}$ is the permeability tensor of soil or bedrock, μ the viscosity of groundwater and $\mathbf{g}$ the acceleration of gravity. The reduction of permeability due to freezing /Burt and Williams 1976/ is described by means of the unfrozen groundwater content as

$$\mathbf{k} = \mathbf{k}_0 \chi^q, \tag{3-19}$$

where the exponent q is defined to fix the frozen permeability to the value about $1.83 \cdot 10^{-20}$ m^2, i.e. for the hydraulic conductivity of 10^{-13} m/s, when the unfrozen water content is $\chi = 0.01$. The symbol $\mathbf{k}_0$ indicates the unfrozen state permeability. The viscosity depends on the temperature and salinity concentration according to the exponential function

$$\mu = \mu_0 \exp\left[\gamma(T - T_0) + \omega(x_c - x_{c0})\right] \tag{3-20}$$

where the coefficients $\gamma(T)$ and $\omega(x_c)$ are expressed in terms of F_0, a_i and b_i by Equation 3-7. The values of parameters F_0, a_i and b_i for $\gamma(T)$ and $\omega(x_c)$ based on /Lide 1999/ are presented in Table 3-5.

Table 3-5. Values for parameters F_0, a_i and b_i of Equation 3-7 for the viscosity of groundwater (Equation 3-20).

Parameter	Unit	F_0	i	a_i	b_i
Viscosity	Pa · s	$1.792000 \cdot 10^{-3}$			
Coefficient γ	1/K	$-3.195037 \cdot 10^{-2}$	0	1	1
			1	$5.038917 \cdot 10^{-2}$	
	–		2	$-4.447604 \cdot 10^{-2}$	1
	–		3	$1.528649 \cdot 10^{-2}$	
Coefficient ω	–	$1.039051 \cdot 10^{1}$	0	1	1
	–		1	0	$1.917484 \cdot 10^{0}$

Salt diffusion

The diffusion of dissolved salts is described by the non-Fickian diffusion equation

$$\mathbf{J}_c = -\mathbf{D}\cdot\left[r_1 \operatorname{grad} x_c - r_0 x_c x_w \left(\overline{\rho}_c - \overline{\rho}_w\right)\mathbf{g}\right] \tag{3-21}$$

where $\mathbf{J}_c$ is the molar diffusion velocity and

$$r_1 = \frac{\overline{\rho}_c T}{\overline{\rho}_{c0} T_0}\left[1 + \frac{d_{w,1} + d_{c,1}}{d_{c,0}}\frac{x_c}{x_w} + 2\frac{d_{w,2}}{d_{c,0}}\left(\frac{x_c}{x_w}\right)^2\right]$$

$$r_0 = \left(d_{c,0}\frac{\overline{\rho}_{c0} R T_0}{M_c}\right)^{-1}$$

The diffusion-dispersion tensor, $\mathbf{D}$, is defined as

$$\mathbf{D} = \beta_{gw} D_{m0}\mathbf{I} + \alpha_L \left\|\mathbf{J}_{gw}\right\| \mathbf{e}_L \mathbf{e}_L + \alpha_T \left\|\mathbf{J}_{gw}\right\| \left(\mathbf{I} - \mathbf{e}_L \mathbf{e}_L\right), \quad \mathbf{e}_L = \frac{\mathbf{J}_{gw}}{\left\|\mathbf{J}_{gw}\right\|} \tag{3-22}$$

where $D_{m0} = 10^{-9}$ m^2/s is the molecular diffusion coefficient /Lide 1999/, $\mathbf{I}$ the unit tensor, $\mathbf{e}_L$ the unit vector in the direction of groundwater flow, and $\alpha_L = 40$ m and $\alpha_T = 5$ m are the longitudinal and transverse dispersion lengths /Hoch and Jackson 2004/, respectively.

3.5 Balance laws

Heat transfer

Heat transfer is modelled by the energy balance equation

$$\frac{\partial}{\partial t}(H - p) + \operatorname{div}\left[\left(x_w \overline{\rho}_w h_w + x_c \overline{\rho}_c h_c - p\right)\mathbf{J}_{gw} + \left(\overline{\rho}_c h_c - \overline{\rho}_w h_w\right)\mathbf{J}_c\right] + \operatorname{div}\mathbf{q} = r \tag{3-23}$$

where H is the enthalpy of the ground given by

$$H = \beta_s \overline{\rho}_s h_s + x_w \beta_{gw} \overline{\rho}_w h_w + x_c \beta_{gw} \overline{\rho}_c h_c + \beta_i \overline{\rho}_i h_i \tag{3-24}$$

In addition, r indicates the external heat supply due to radiogenic heat production and heat generated by the spent fuel described in Section 2.3.

Groundwater flow

Groundwater flow is modelled by the mass balance equations of water, dissolved salts and ice. The combination of these equations leads to the equation

$$\begin{aligned}&\frac{\partial \beta_{gw}}{\partial t} + \beta_{gw} x_w \frac{\partial}{\partial t}\left(\ln\frac{\overline{\rho}_w}{\overline{\rho}_{w0}}\right) + \beta_{gw} x_c \frac{\partial}{\partial t}\left(\ln\frac{\overline{\rho}_c}{\overline{\rho}_{c0}}\right)\\ &+ \frac{\overline{\rho}_i}{\overline{\rho}_w}\left[\frac{\partial \beta_i}{\partial t} + \beta_i \frac{\partial}{\partial t}\left(\ln\frac{\overline{\rho}_i}{\overline{\rho}_{i0}}\right)\right]\\ &+ x_w \operatorname{grad}\left(\ln\frac{\overline{\rho}_w}{\overline{\rho}_{w0}}\right)\cdot\mathbf{J}_{gw} + x_c \operatorname{grad}\left(\ln\frac{\overline{\rho}_c}{\overline{\rho}_{c0}}\right)\cdot\mathbf{J}_{gw} + \operatorname{div}\mathbf{J}_{gw} = 0\end{aligned} \tag{3-25}$$

Salt transport

Salt transport is modelled by the mass balance equation of dissolved salts of the form

$$\begin{aligned}&\beta_{gw}\frac{\partial x_c}{\partial t} - x_c \frac{\overline{\rho}_i}{\overline{\rho}_w}\left[\frac{\partial \beta_i}{\partial t} + \beta_i \frac{\partial}{\partial t}\left(\ln\frac{\overline{\rho}_i}{\overline{\rho}_{i0}}\right)\right]\\ &+ \operatorname{grad} x_c \cdot \mathbf{J}_{gw} + \operatorname{grad}\left(\ln\frac{\overline{\rho}_c}{\overline{\rho}_{c0}}\right)\cdot\mathbf{J}_c + \operatorname{div}\mathbf{J}_c = 0\end{aligned} \tag{3-26}$$

3.6 Model verification

The following verification studies, by comparisons with numerical and experimental test, are carried out to evaluate new features of the permafrost model introduced after /Hartikainen 2004, Hartikainen and Mikkola 2006/. First, the density dependent groundwater flow is verified with the Elder problem /Voss and Souza 1987/ and the salt fingering problem /Baker and Osterkamp 1988/. Next, the improvements concerning the effects of pressure and salinity concentration on the freezing temperature of groundwater are verified with experimental evidence on the pressure-temperature curve /Lide 1999/ and salinity concentration-temperature curve /Feistel 2008/. Finally, a laboratory test on freezing of saline soil /Mahar et al. 1982/ is used to verify the exclusion of salt during freezing and salt transport in partially frozen ground.

3.6.1 The Elder problem

The Elder problem is a numerical benchmark test to validate models representing buoyancy flow driven by fluid density differences /Voss and Souza 1987/. The model domain considers a cross section of a closed rectangular box of fresh water in porous media with no subsurface flow occurring. Salt enters the domain from the top boundary increasing the salt concentration in the fresh water until buoyancy flow results and a circulation process begins. The problem is described in Figure 3-2. The top corners are at normal pressure (p_0) and the concentration on the bottom boundary is kept at zero. The domain is initially non-saline and kept at constant temperature. Parameters are presented in Table 3-6.

Since the model domain is symmetric, calculations are carried out for a half of the domain. The results for the relative salt concentration at 1, 4 and 10 years are shown in Figure 3-3. The model produces a little faster evolution for salinity concentration, with steeper concentration gradients, than the model of /Voss and Souza 1987/. This model behaviour is believed to be caused by the nonlinear term r_1 in Equation (3-21) which, describing the behaviour of non-ideal solution, magnifies the diffusion-dispersion tensor with increasing salinity concentration.

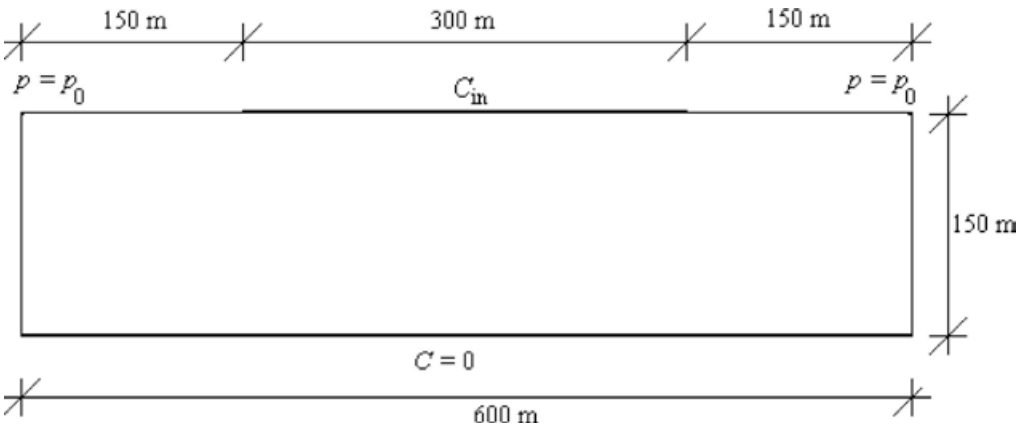

Figure 3-2. *Model domain and boundary conditions for the Elder problem.*

Table 3-6. Parameters used for the Elder problem.

Parameter	Unit	Value
Porosity	–	0.1
Permeability	m^2	$4.845 \cdot 10^{-13}$
Dispersion coefficient	m^2/s	$3.565 \cdot 10^{-6}$
Molar concentration at boundary, C_{in}	–	0.26929118 (corresponds to fluid density of 1,200 kg/ m^3)
Ambient temperature	°C	10

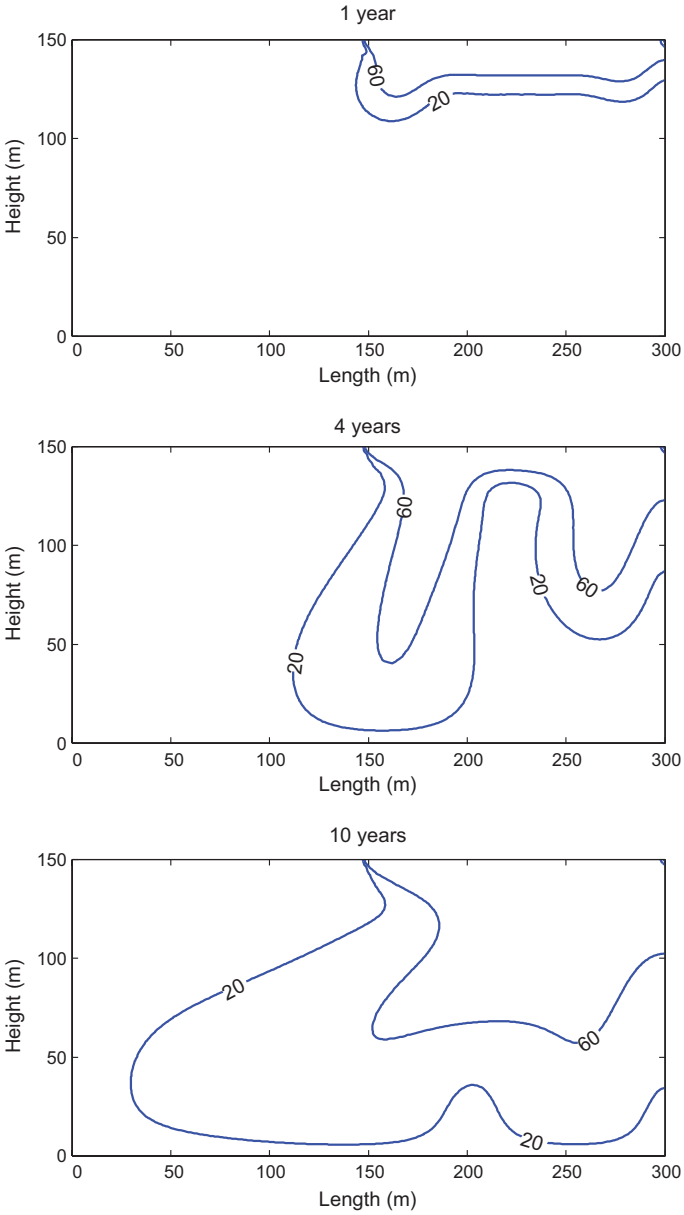

Figure 3-3. *Calculated relative isochors of 20% and 60% with respect of the boundary condition concentration at 1, 4 and 10 years.*

3.6.2 Salt fingering

In order to verify the density dependent groundwater flow further, a laboratory experiment presented by /Baker and Osterkamp 1988/ concerning vertical salt fingers moving downward and fresh water fingers moving upward in sands were simulated. The experiment of /Baker and Osterkamp 1988/ was conducted in a box which was 17 cm wide, 28 cm high, and 5 cm in thickness, and filled with silica sand. The top 10 cm of the sand was initially saturated with 35 ppt sodium chloride solution and the remaining part with distilled water. The parameters for the experiment are presented in Table 3-7.

The results for the modelled relative salt concentration with respect to the initial concentration of 35 ppt at 1, 2 and 3 hours are shown in Figure 3-4. The results compare well with the experimental observations reported in /Baker and Osterkamp 1988/, showing that that modelled gravity driven convection can produce rapid salt movement in sands, in the form of salt fingering, in which salt fingers move downward through non-saline water and fresh water fingers upward through the saline water solution. The modelled salt concentration isochors indicate that the fingers move some centimetres per hour being of the same order as the measured range from 0.24 to 5.6 cm/hour /Baker and Osterkamp 1988/.

Table 3-7. Parameters used for the salt fingering problem.

Parameter	Unit	Value
Porosity	–	0.4
Hydraulic conductivity	m/a	$3.2 \cdot 10^4$
Longitudinal dispersion length	m	0.01
Transverse dispersion length	m	0.002
Diffusion coefficient	m^2/s	10^{-9}
Initial concentration in the top 10 cm of the box	ppt	35
Ambient temperature	°C	20

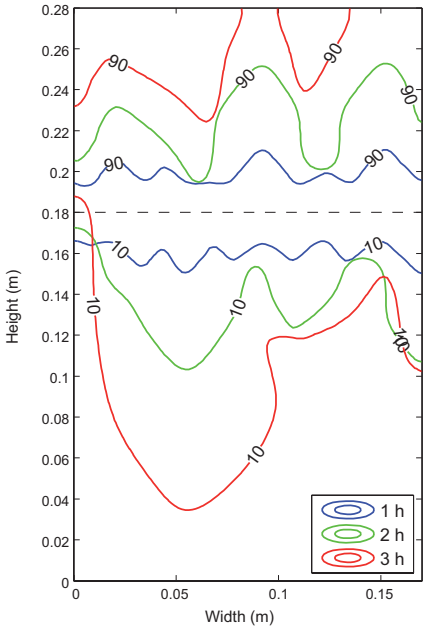

Figure 3-4. *Calculated relative isochors of 10% and 90% with respect to the initial concentration of 35 ppt at 1, 2 and 3 hours. The dashed line at the height of 0.18 m represents the phase boundary between the bottom fresh water and the top saline water solution.*

3.6.3 Freezing point of saline water

The capability of the model to deal with the effects of pressure and salinity concentration on the freezing temperature of water is examined by using Equation (3-15) and experimentally validated reference data presented by /Lide 1999, Feistel 2008/. Figure 3-5 shows the pressure-temperature curve predicted by Equation (3-15) in comparison to the reference data in /Lide 1999/. Figure 3-6 illustrates the salinity concentration-temperature curve given by Equation (3-15) and the reference data presented in /Feistel 2008/. The results indicate that the model accurately describe the effects of pressure and salinity concentration on the phase change of saline groundwater.

3.6.4 Uniaxial freezing

Large-scale laboratory tests have shown the effects of salinity on freezing of seawater saturated gravel /Mahar et al. 1982, 1983, Vinson et al. 1983/. The tests were carried out for 46 cm diameter and 64 cm high soil columns saturated with a seawater solution of known salinities. The columns, with insulated bottom and sides, were frozen uniaxially from the top downward applying various freezing rates.

A test with an initial salinity concentration of 28 ppt is simulated in this work. The parameters for the simulation are presented in Table 3-8. Figure 3-7 shows the measured /Mahar et al. 1982/ and computed /Panday and Corapcioglu 1991/ variation of temperature along the soil column at different times.

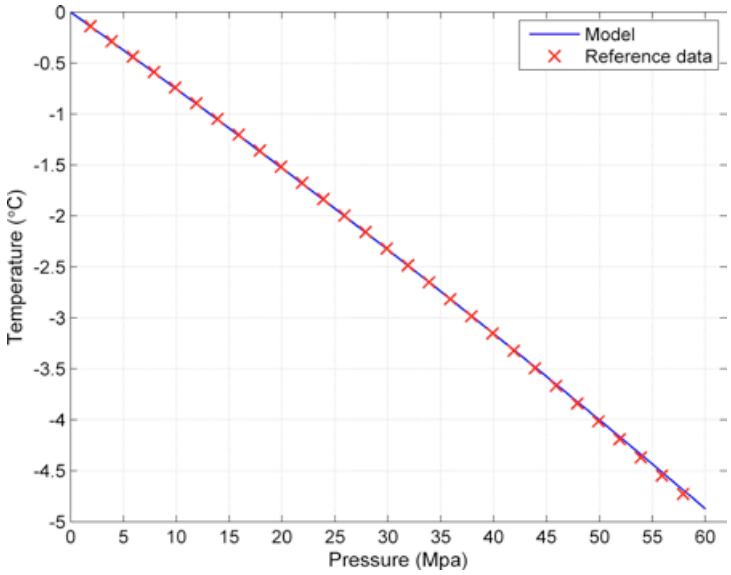

Figure 3-5. *Pressure-temperature curve for non-saline groundwater and $f_{add,w} = 0$. The reference data is obtained from /Lide 1999/.*

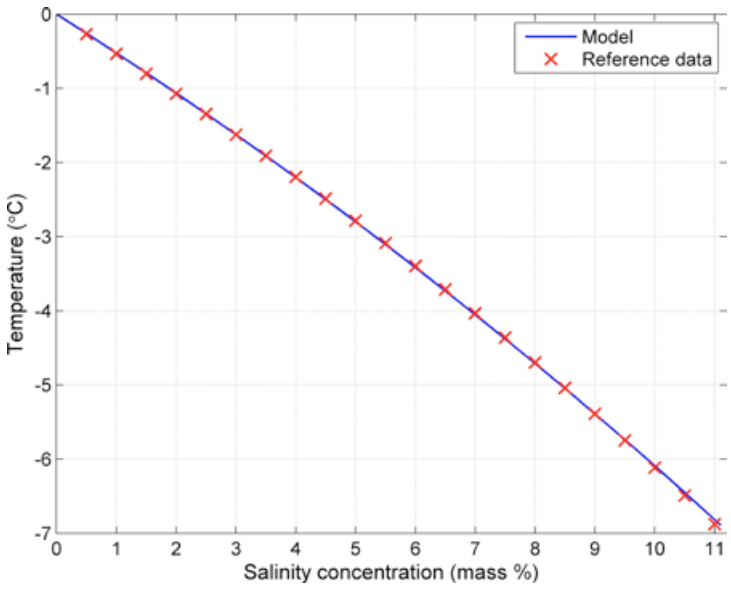

Figure 3-6. *Salinity concentration-temperature curve for saline groundwater at the reference pressure and $f_{add,w} = 0$. The reference data is obtained from /Feistel 2008/.*

Table 3-8. Parameters used for the uniaxial freezing problem.

Parameter	Unit	Value
Thermal conductivity	W/(m·K)	4.1
Heat capacity	MJ/(m³·K)	2.70
Porosity	–	0.283
Hydraulic conductivity	m/a	$6.3 \cdot 10^{3}$
Longitudinal dispersion length	m	0.05
Transverse dispersion length	m	0.01
Diffusion coefficient	m²/s	10^{-9}
Intial pore water concentration	ppt	28
Initial temperature	°C	0.8

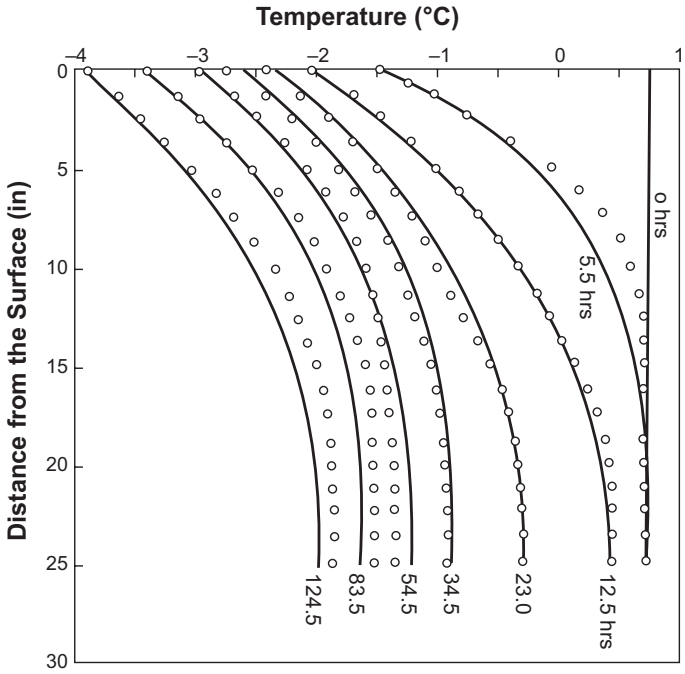

Figure 3-7. *Variation in temperature along the soil column at different times. Solid lines indicate numerical results of /Panday and Corapcioglu 1991/ while discrete points show measured experimental values of /Mahar et al. 1982/.*

Vertical profiles of temperature, unfrozen pore water content, salinity concentration in unfrozen pore water and salinity concentration in total pore water (liquid water and ice) at different times calculated by the permafrost model are shown in Figure 3-8. For comparison, a soil column with fresh water and same initial temperature was also simulated. The results on temperature and unfrozen pore water content are illustrated in Figure 3-9.

The unfrozen pore water content results show that a wide, partially frozen zone with relatively high unfrozen water content and no sharp interface between the unfrozen and frozen saline soil are created. This is in line with the experimental findings of /Vinson et al. 1983/, see also /Arenson and Sego 2006/. The salinity concentration results show that the salinity of unfrozen pore water increases with advancing cooling of soil at sub-zero temperatures, which is in line with the experimental observations /Mahar et al. 1982/, see also /Mahar et al. 1983, Vinson et al. 1983/. Moreover, the decrease in modelled salinity concentration in the total pore water in a narrow section below the soil surface can signify an exclusion of salts during freezing, while the salinity increase in the same profiles can indicate a slow downward movement of salt through the partially frozen zone. The modelled temperature profiles indicate that the soil with saline water cools down more rapidly than the soil with fresh water. This is due to that the phase change with latent heat release takes place to a lesser degree in saline water than in fresh water.

In comparison with the experimental findings shown in Figure 3-7, the modelled results give a similar representation of the thermal evolution of freezing of saline soil, except at the bottom. Discrepancies between the modelled and observed bottom temperatures can be due to differences between the modelled and actual boundary conditions. Oscillations in the unfrozen pore water content and salinity concentration profiles are due to instabilities in the numerical method.

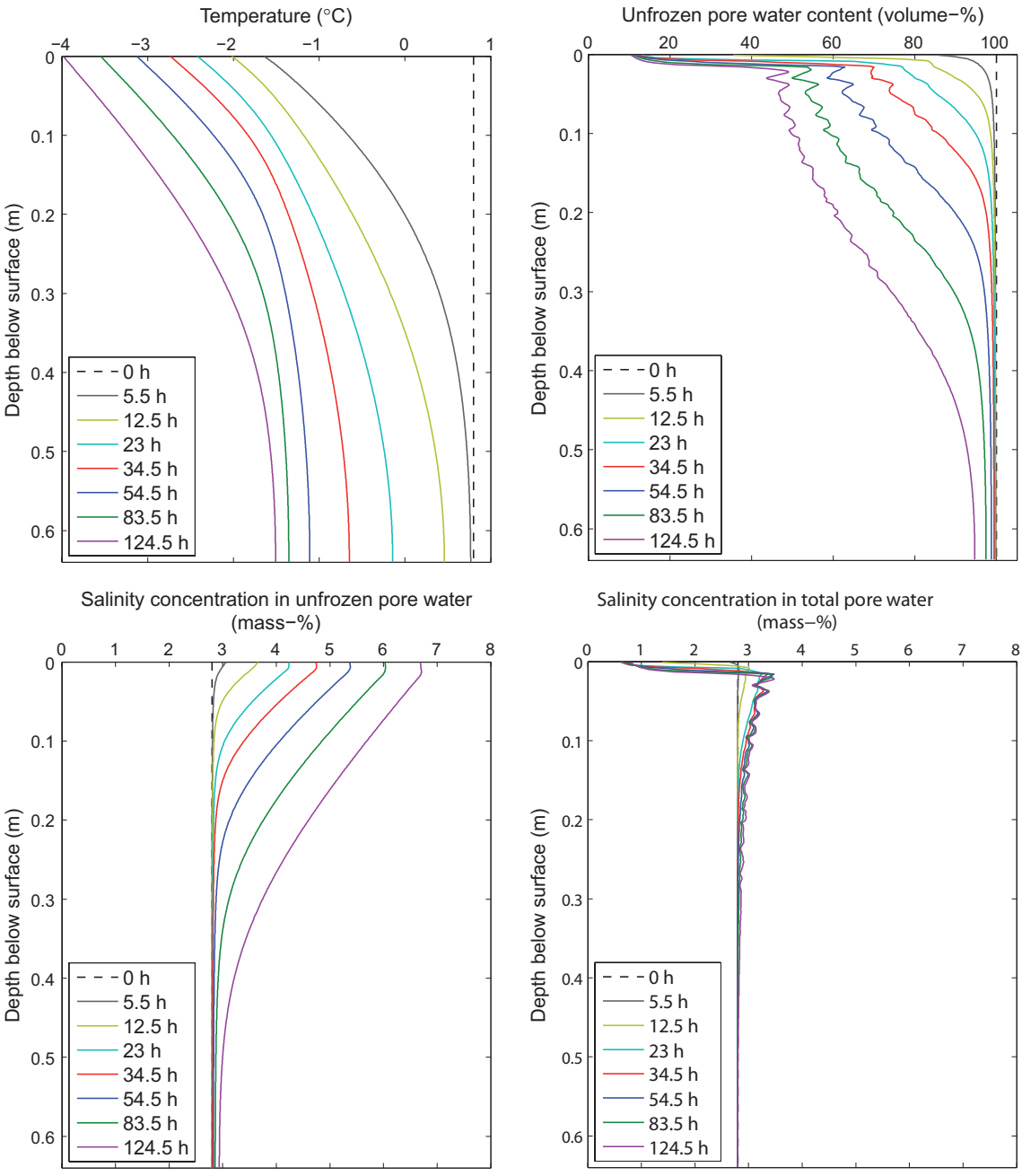

Figure 3-8. *Vertical profiles of temperature, unfrozen pore water content, and salinity concentration in unfrozen pore water and in total pore water (liquid water and ice) along the soil column with saline pore water at different times.*

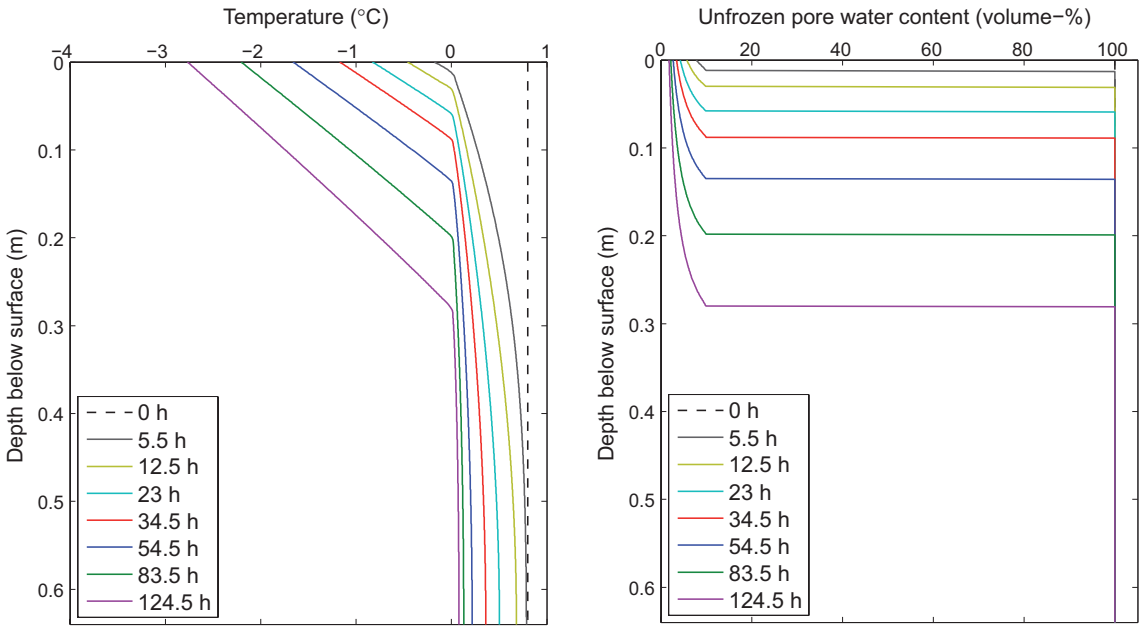

Figure 3-9. *Vertical profiles of temperature and unfrozen pore water content along the soil column with fresh pore water at different times.*

4 Numerical simulations

4.1 Numerical method and calculation settings

Numerical method

The mathematical model has been implemented into a finite element research code, which is based on the methodologies described in /Kouhia 1999, Mikkola and Hartikainen 2001, Mikkola and Hartikainen 2002/, summarised below. The space-time discretisation is based on the finite element method and a fully implicit adaptive time integration scheme. The coupled nonlinear equations are linearized by making use of the Newton-Raphson method. Regarding the permafrost calculations, a new feature of the code is to use the preconditioned stabilized bi-conjugate gradient algorithm /van der Vorst 1992/ to solve the linearized equation system. For the preconditioner, the dual threshold incomplete LU factorization, ILUT, is utilized /Saad 1994/. Prior the solution phase, the equation system is diagonally scaled. The two dropping parameters are chosen to produce preconditioners with approximately the same number of elements as in the coefficient matrix.

Finite element mesh and time stepping

The numerical simulations were carried out using an unstructured finite element mesh of linear triangle elements. The mean grid spacing varied from less than 10 m close to the ground surface to about 300 m at the bottom of the model domain. The maximum time step for the adaptive time integration scheme was limited to 100 years.

Boundary and initial conditions

On the ground surface the following Dirichlet type of boundary conditions are applied:

- Ground temperature is set to the prescribed ground surface temperature $\overline{T}_s$ defined by Equation (2-7): $T = \overline{T}_s$.
- Groundwater pressure equals to the hydrostatic pressure following the water depth, z, of Baltic Sea or the two future lakes (see Figure 2-9): $p = \rho_w g z$; on dry land $p = 0$.
- Groundwater salinity concentration is set to the constant value $\overline{x}_c = 4.03 \cdot 10^{-4}$ corresponding approximately to the value of 0.04 in mass-%: $x_c = \overline{x}_c$.

At the bottom of the model domain at 10-km depth the following Neumann type of boundary conditions are specified:

- The heat flow equals the geothermal heat flow, $\overline{q}$, prescribed by Equation (2-2) at 10-km depth: $\mathbf{q} \cdot \mathbf{n} = \overline{q}$.
- No groundwater flow occurs: $\mathbf{J}_{gw} \cdot \mathbf{n} = 0$.
- A salt diffusion $\overline{J}_c = 9.3 \cdot 10^{-11}$ m/s is assumed to occur, which takes care of the dissolution of soluble salts in the rock matrix $\mathbf{J}_c \cdot \mathbf{n} = \overline{J}_c$.

Both vertical sides of the model domain are insulated, impermeable and no salinity diffusion takes place, i.e. $\mathbf{q} \cdot \mathbf{n} = 0$, $\mathbf{J}_{gw} \cdot \mathbf{n} = 0$, $\mathbf{J}_c \cdot \mathbf{n} = 0$.

The initial conditions for ground temperature, $\overline{T}_0$, groundwater pressure, $\overline{p}_0$, and salinity concentration, $\overline{x}_{c,0}$, are assumed to equal the present conditions described in Section 2.2.

4.2 Description of simulated cases

4.2.1 Main simulations

The objective is to investigate the impact of surface and subsurface conditions on the evolution of permafrost and frozen ground and formation of taliks for the two climate cases, *Repetition of the last glacial cycle* case and *Severe permafrost* case. The exclusion of salts during freezing and salt

transport is also considered. Due to significant uncertainties associated with descriptions of the surface conditions, two variants, one humid and one dry, are considered for both climate cases. This is expected to yield a lower and upper limit for the permafrost and perennially frozen ground development. Thus, the main simulations consist of the following four cases:

1. Humid variant of *Repetition of the last glacial cycle* case.
2. Dry variant of *Repetition of the last glacial cycle* case.
3. Humid variant of *Severe permafrost* case.
4. Dry variant of *Severe permafrost* case.

The minimum values of *n*-factors shown in Table 2-7 and Table 2-8 describe the humid variant while their maximum values yield the dry variant. In addition, mean subsurface properties and conditions are used in all of these cases.

4.2.2 Sensitivity analysis

The uncertainties related to surface conditions including moisture conditions, vegetation and snow cover as well as ground surface temperature are considered in the main simulations by means of the humid and dry variant of the climate cases studied. Variations in hydraulic properties and ionic composition of groundwater are considered to be negligible in regard to permafrost development, and hence not included in the sensitivity analyses. Following this, and results from previous studies /SKB 2006/, the following sensitivity studies were made.

Case 1 – Uncertainty in air temperature

In relation to the uncertainty in air temperature curve used as input, see Appendix H and /SKB 2010b/, the objective is to investigate the impact of the largest estimated uncertainty in air temperature, that is ±6°C, see Figure 4-1. For this purpose the *Repetition of last glacial cycle* case with mean thermal properties of the subsurface is simulated.

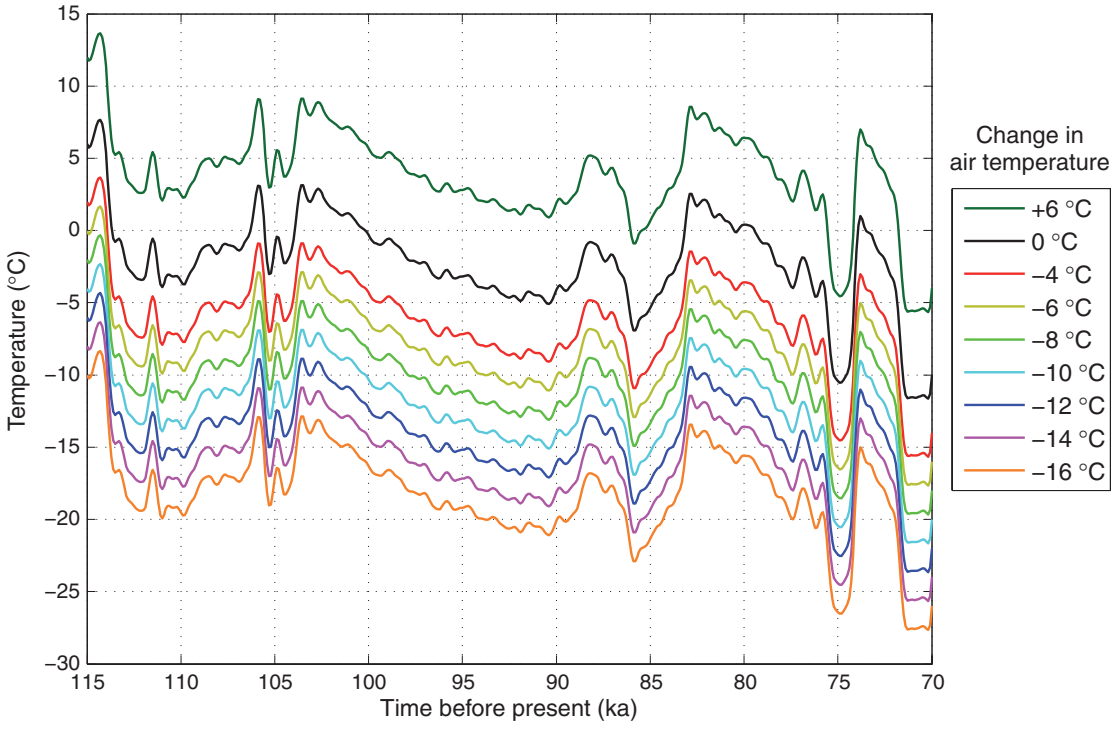

Figure 4-1. *Evolution of air temperature changed by −16, −14, −12, −10, −8, −6, −4, 0 and 6°C for the Repetition of last glacial cycle case.*

In addition, it was also investigated how much the entire air temperature curve is required to be lowered to get the 0°C, −2°C and −4°C isotherms to reach repository depth. The temperature of 0°C corresponds to the freezing point of fresh water at normal pressure. The −2°C temperature constitute the temperature criterion used in the safety assessment for freezing of the back-fill material in the deposition tunnels /SKB 2011/, while the temperature of −4°C constitutes the temperature criterion used for freezing of the buffer clay /SKB 2011/. Based on the SR-Can results /SKB 2006, Section 3.4/, temperature shifts of 4, 6, 8, 10, 12, 14 and 16°C were chosen (Figure 4-1). As a pessimistic selection, the dry variant of the *Repetition of last glacial cycle* case is simulated, since it will result in deeper permafrost than the humid variant. In addition, mean thermal properties of the subsurface were used.

Case 2 – Uncertainty in geothermal heat flow

The objective is to investigate the consequences of the uncertainty in geothermal heat flow on the development of permafrost and perennially frozen ground. The mean surface level value of 61 mW/m^2 and the range from –14% (minimum) to +12% (maximum) are used /Sundberg et al. 2009/. The dry variant of the *Repetition of last glacial cycle* case is simulated.

Case 3 – Uncertainty in thermal conductivity

The objective is to investigate the consequences of uncertainty in thermal conductivity (mean, minimum and maximum) on the development of permafrost and perennially frozen ground. The values for different soil layers and rock domains are presented in Table 2-1 and Table 2-2, respectively. E.g. the rock domain RFM029 has a mean thermal conductivity of 3.58 W/(m · K) and the range of variation of –3.1% to +2.8%, see also Appendix E. The dry variant of the *Repetition of last glacial cycle* case is simulated.

Case 4 – Uncertainty in thermal diffusivity

By definition, the uncertainty in thermal diffusivity results from that of thermal conductivity and heat capacity. The uncertainty is investigated by means of the mean-, minimum- and maximum thermal diffusivities. The associated values of thermal conductivity and heat capacity for different soil layers and rock domains are presented in Table 2-1 and Table 2-2, respectively, e.g. the rock domain RFM029 has the mean thermal diffusivity of 1.69 mm^2/s and the range of variation of −11.5% to +6.4%, see also Appendix E. In addition, the effect of heterogeneity of thermal properties on the development of permafrost and frozen ground is studied by mixed thermal diffusivities, which are obtained by using values of highest difference for adjacent rock domains. The dry variant of the *Repetition of last glacial cycle* case is simulated.

Case 5 – Combination of uncertainties in subsurface thermal conditions

The objective is to investigate the combination of uncertainties in dominant thermal conditions of the subsurface. The limits for the uncertainty interval are obtained by combining the thermal conditions that are assumed to enhance the permafrost development most, i.e. maximum thermal conductivity, minimum heat capacity and minimum geothermal heat flow, as well as the thermal conditions that are expected to diminish the permafrost development most, i.e. minimum thermal conductivity, maximum heat capacity and maximum geothermal heat flow. The properties are declared in the previous cases. The dry variant of the *Repetition of last glacial cycle* case is simulated.

Case 6 – Combination of uncertainties in surface conditions and subsurface thermal conditions

In addition to the previous case, the uncertainties in subsurface thermal conditions are combined with the uncertainties in surface conditions. For the *Repetition of last glacial cycle* case the uncertainty interval is obtained by combining the dry variant of the case with the subsurface thermal conditions enhancing permafrost development most, and the humid variant of the same case with subsurface thermal conditions diminishing permafrost development most. For the *Severe permafrost* case the uncertainty interval results from combining the humid variant of the case with subsurface thermal conditions enhancing permafrost development most, and the dry variant of the case with thermal properties diminishing permafrost development most.

Case 7 – Combination of uncertainties in air temperature, surface conditions and subsurface thermal conditions

This case is conducted in order to illustrate the unlikely case of combining the largest uncertainties in the development of permafrost and perennially frozen ground that result from uncertainties in air temperature, surface conditions and subsurface thermal conditions. For this purpose both variants of the *Repetition of last glacial cycle* case with an air temperature change of ±6°C and thermal properties either enhancing or diminishing permafrost development most are simulated.

Case 8 – Heat from the repository

The effect of heat generated by the spent fuel, see Section 2.3, on the evolution of permafrost and perennially frozen ground is studied. Cases with heat and without heat from the repository for the dry variant of the *Repetition of last glacial cycle* case are simulated.

Case 9 – Convective heat transfer

Finally, the impact of convective heat transfer due to groundwater flow and salt transport on the evolution of permafrost perennially frozen ground is examined. Cases with and without groundwater flow and salinity transport for the dry variant of the *Repetition of last glacial cycle* case are simulated.

5 Results

5.1 Main simulations

Permafrost depth, depth of perennially frozen ground, ground temperature

Resulting ground temperatures and extent of perennially frozen ground at times of 111,500, 95,000, 74,000, 70,000 years BP are illustrated in Figure 5-1 and Figure 5-2 for the humid and dry variant of the *Repetition of last glacial cycle* case. The corresponding results for the humid and dry variant of the *Severe permafrost* case are shown in Figure 5-3 and Figure 5-4. See also the section Unfrozen water content and talik formation below. The selected times represent the four different situations regarding climate zone, shore line development and permafrost conditions:

- at 111,500 years BP subarctic climate prevails, the profile is partially submerged and the exposed ground surface is partially underlain by permafrost, and the ground temperature is at maximum within the repository,
- at 95,000 years BP subarctic climate prevails and discontinuous or continuous permafrost is developing,
- at 74,000 years BP subarctic climate is turning into a boreal climate and permafrost is degrading, changing from continuous to sporadic form,
- at 70,000 years BP arctic climate prevails and continuous permafrost reaches its maximum depth in the *Repetition of last glacial cycle* case.

The evolution of maximum permafrost depth and depth of perennially frozen ground over the repository for the *Repetition of last glacial cycle* case is shown in Figure 5-5 while Figure 5-6 shows the same results over the whole profile as well as the extent of permafrost summarised along the whole profile. Figure 5-7 and Figure 5-8 show the corresponding data for the *Severe permafrost* case. The maximum permafrost depths, maximum depths of perennially frozen ground, and the extent of permafrost distribution have been summarised in Tables 5-1, 5-2, 5-3 and 5-4. In addition, Table 5-5 and Table 5-6 show the evolution of permafrost depth and depth of perennially frozen ground over the repository and whole profile for the time period of 115 to 70 ka BP, respectively. The evolution of permafrost depth and depth of perennially frozen ground over the repository for the entire *Severe permafrost* case are presented in Appendix K.

Vertical profiles of ground temperature at four selected locations corresponding to the four different surface cover types (at 3,550 m – wet, at 4,783 m – fresh-moist, at 11,600 m – dry, at 14,600 m – peat-land) are presented in Figures 5-9, 5-10, 5-11, 5-12 for the humid variant of the *Repetition of last glacial cycle* case. The corresponding results for dry variant one can be seen in Figures 5-13, 5-14, 5-15, 5-16. Figures 5-17, 5-18, 5-19, 5-20 show the vertical temperature profiles of ground temperature for the humid variant of the *Severe permafrost* case, while Figures 5-21, 5-22, 5-23, 5-24 show the corresponding results for the dry variant of the same case. Notice that the vertical profile at 4,783 m is located in the middle of the repository, and in each figure the white colour envelope represents the range of ground temperature fluctuation over the time period of 115,000–70,000 years BP.

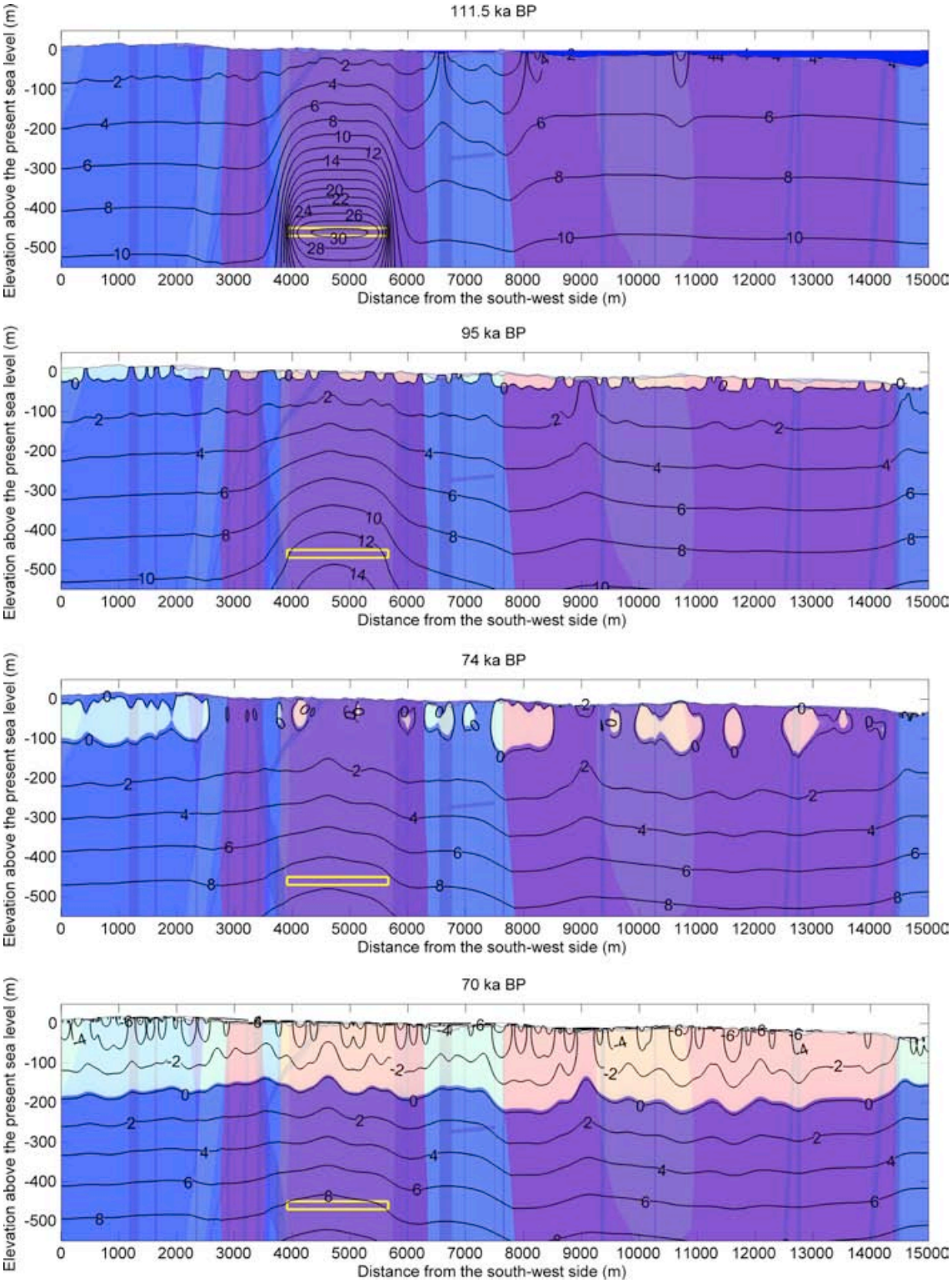

Figure 5-1. *Temperature contours in (°C) and the extent of perennially frozen ground (light colour) within permafrost (0°C isotherm) at times 111.5, 95, 74, 70 ka BP for the humid variant of the Repetition of last glacial cycle. Colour blue on the top of the profile at 111.5 BP ka shows the Baltic Sea. The yellow rectangle indicates the repository.*

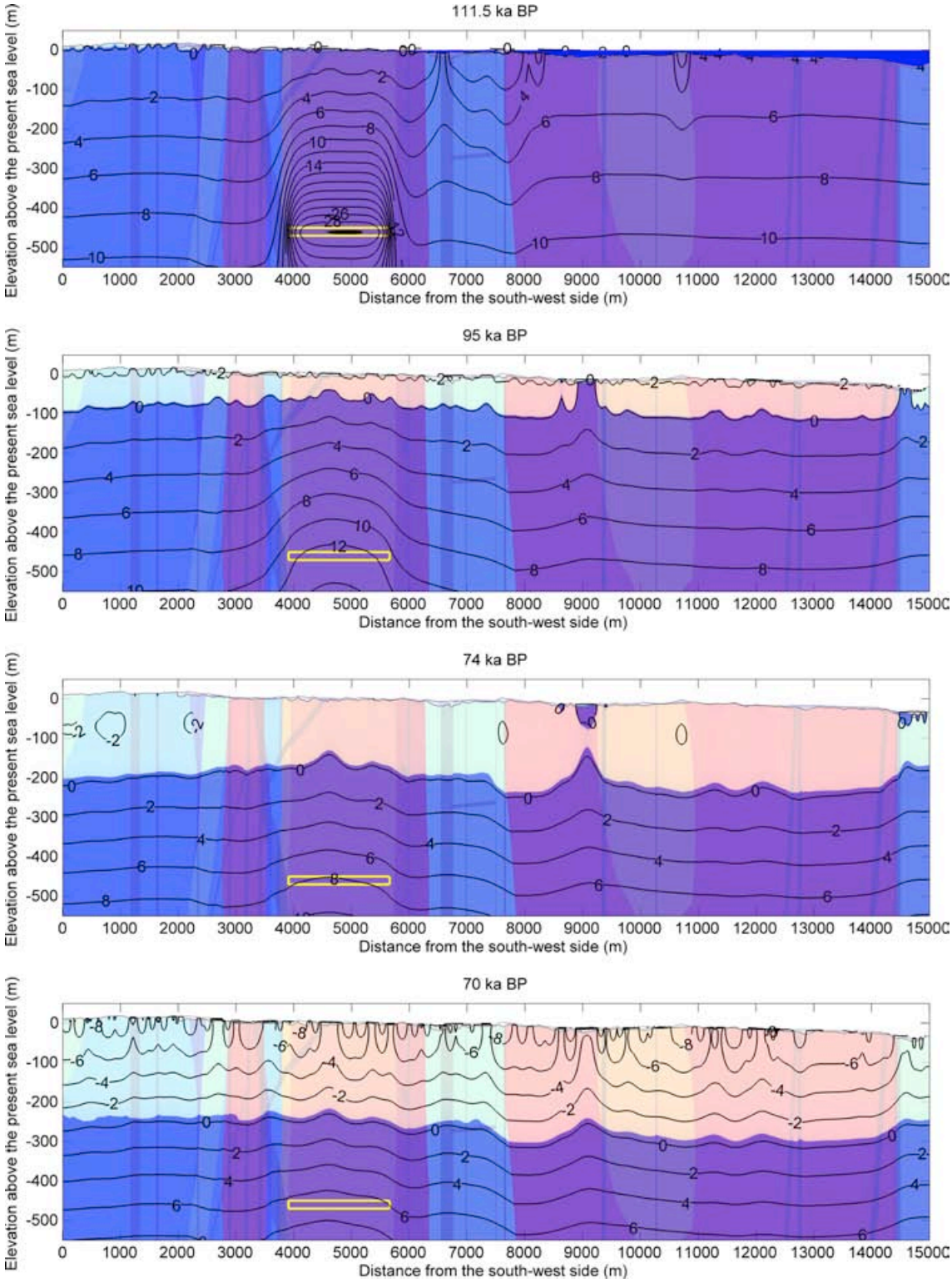

Figure 5-2. *Temperature contours in (°C) and the extent of perennially frozen ground (light colour) within permafrost (0°C isotherm) at times 111.5, 95, 74, 70 ka BP for the dry variant of the Repetition of last glacial cycle. Colour blue on the top of the profile at 111.5 ka BP shows the Baltic Sea. The yellow rectangle indicates the repository.*

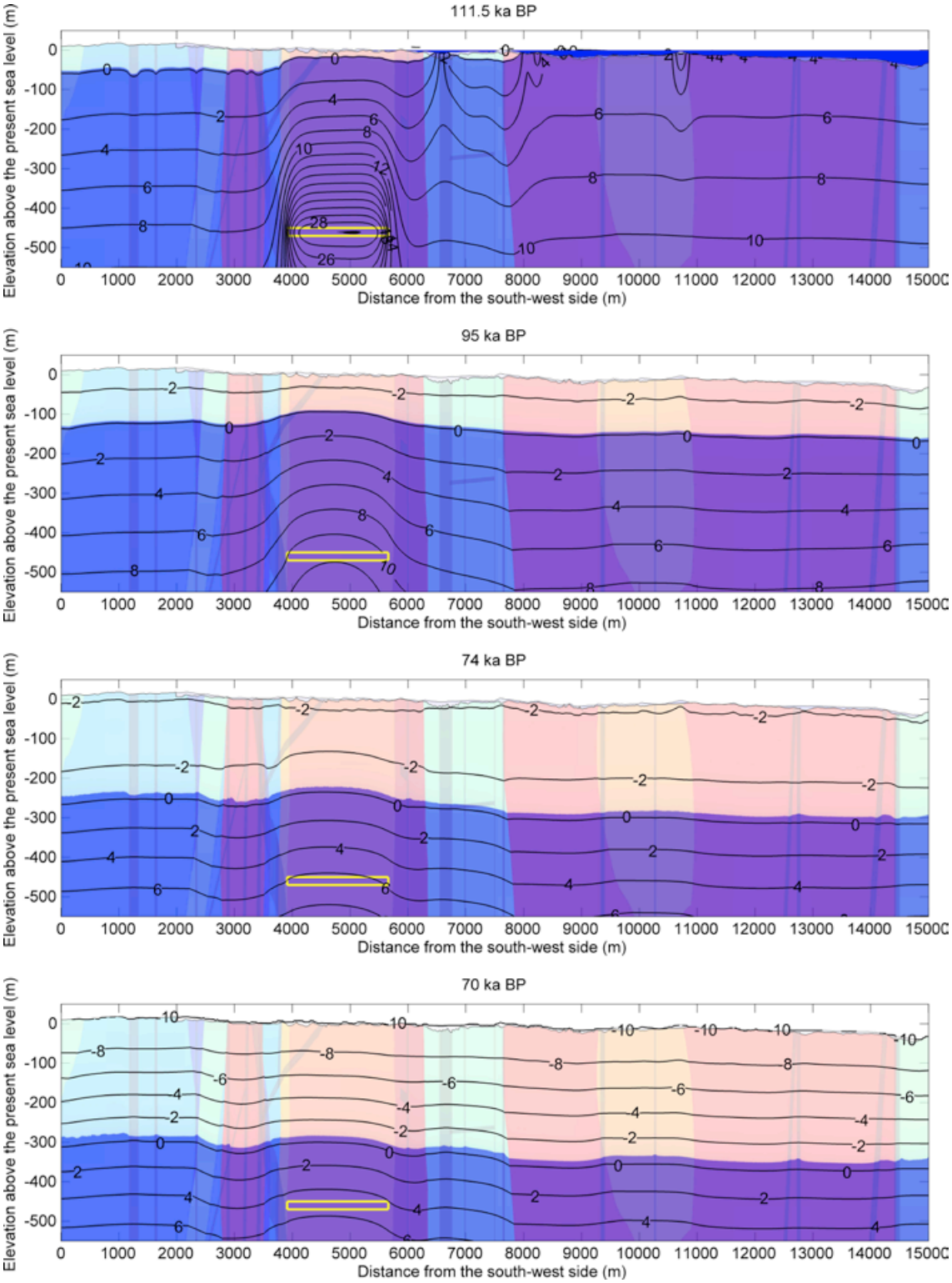

Figure 5-3. *Temperature contours in (°C) and the extent of perennially frozen ground (light colour) within permafrost (0°C isotherm) at times 111.5, 95, 74, 70 ka BP for the humid variant of the Severe permafrost case. Colour blue on the top of the profile at 111.5 BP ka shows the Baltic Sea. The yellow rectangle indicates the repository.*

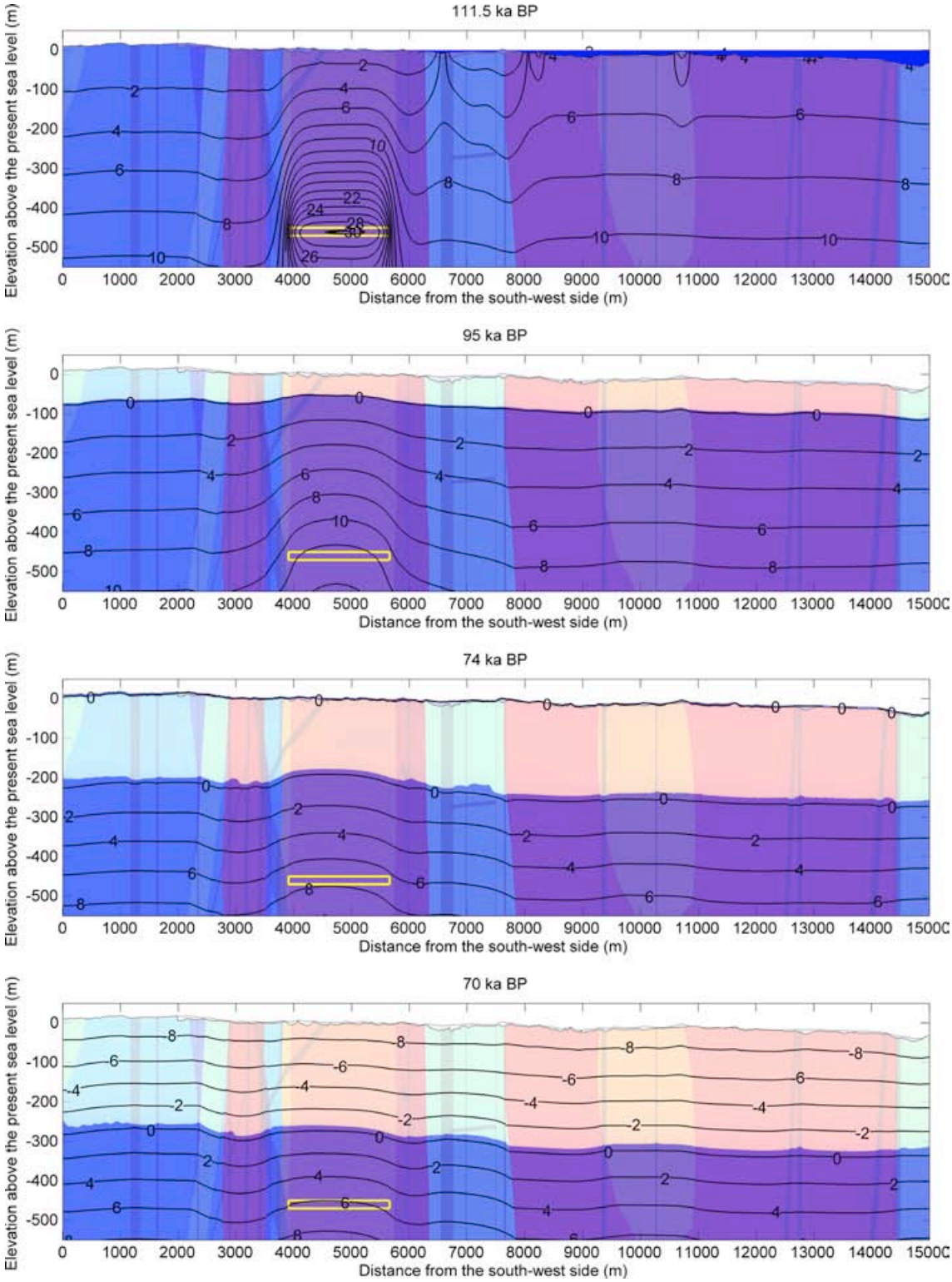

Figure 5-4. *Temperature contours in (°C) and the extent of perennially frozen ground (light colour) within permafrost (0°C isotherm) at times 111.5, 95, 74, 70 ka BP for the dry variant of the Severe permafrost case. Colour blue on the top of the profile at 111.5 BP ka shows the Baltic Sea. The yellow rectangle indicates the repository.*

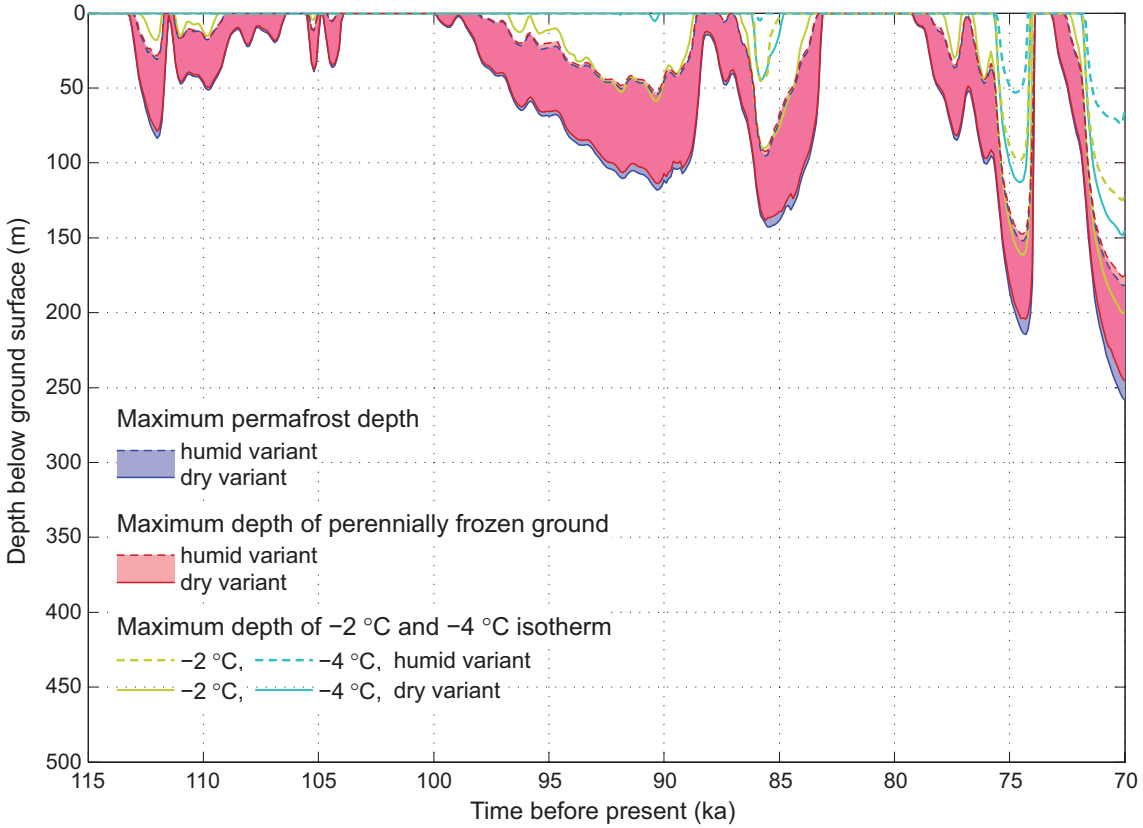

Figure 5-5. *Evolution of maximum permafrost depth, maximum depth of perennially frozen ground and maximum depth of −2 and −4°C isotherms over the repository for the Repetition of last glacial cycle case. The upper permafrost surface, for periods of degradation from above, is not shown. The shaded area in blue and red represents the range within which a result is expected to lie when considering surface conditions between the dry and humid climate variants of the Repetition of last glacial cycle case. The lilac colour indicates that the results for permafrost and perennially frozen ground overlap.*

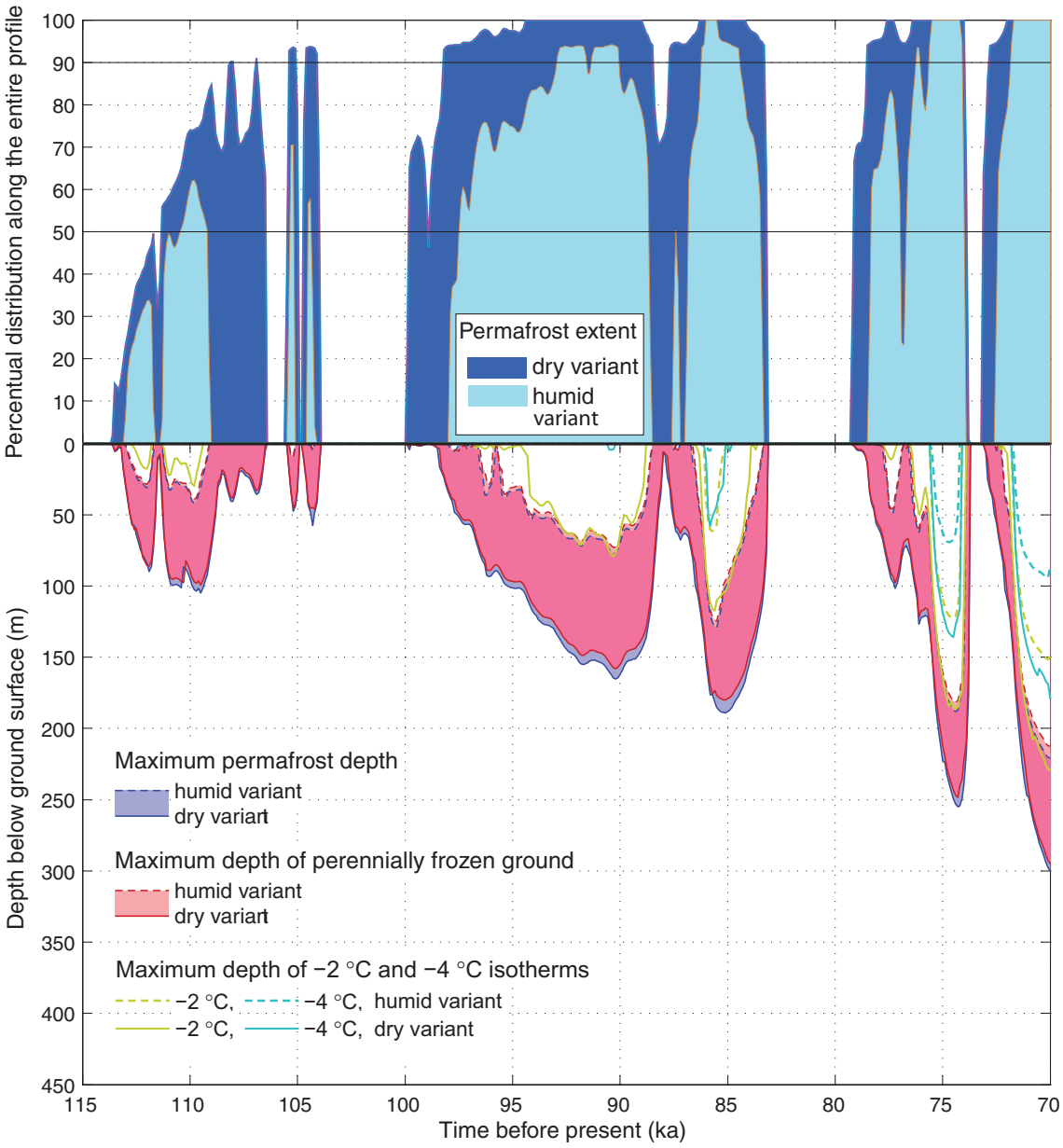

Figure 5-6. *Evolution of maximum permafrost depth, maximum depth of perennially frozen ground and maximum depth of −2 and −4°C isotherms over the whole profile for the Repetition of last glacial cycle case. The figure also shows the percentual permafrost distribution along the profile. The transition from sporadic to discontinuous permafrost occurs at 50-% coverage and from discontinuous to continuous permafrost at 90-% coverage. The upper permafrost surface, for periods of degradation from above, is not shown. The shaded area in blue and red represents the range within which a result is expected to lie when considering surface conditions between the dry and humid climate variants of the Repetition of last glacial cycle case. The lilac colour indicates that the results for permafrost and perennially frozen ground overlap.*

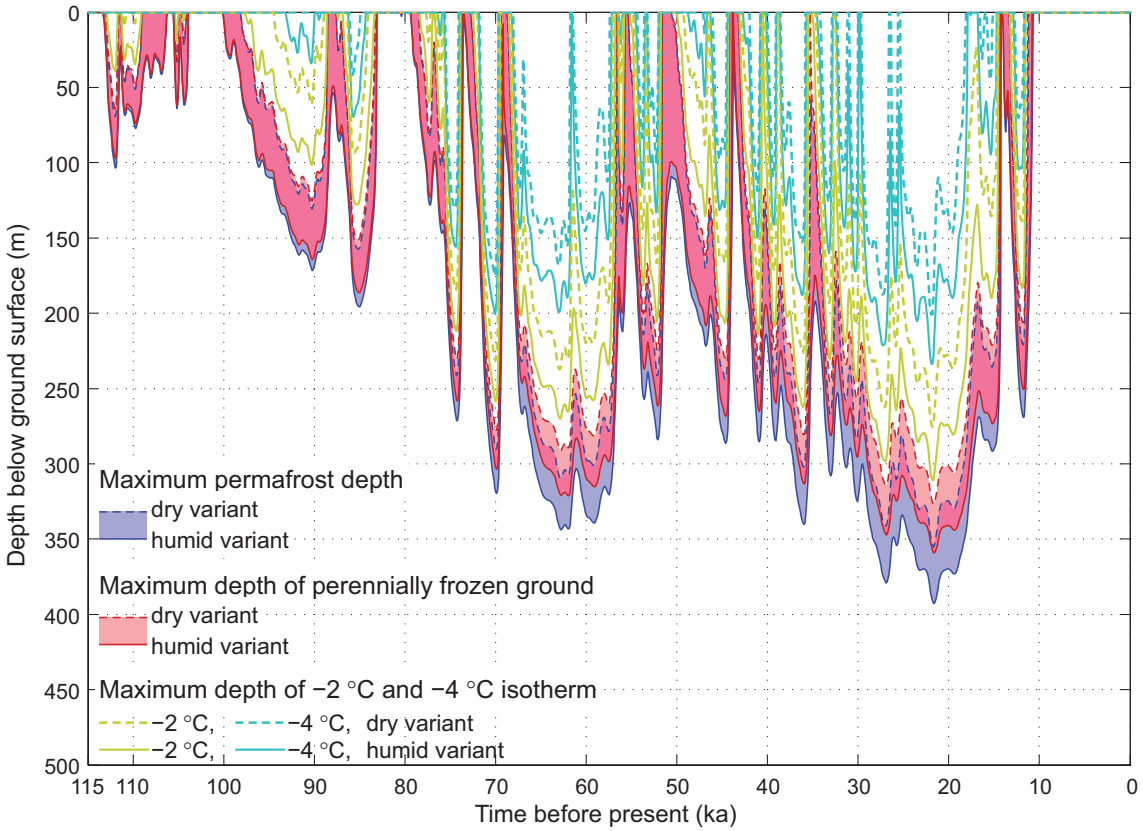

Figure 5-7. *Evolution of maximum permafrost depth, maximum depth of perennially frozen ground and maximum depths of the −2 and −4°C isotherms over the repository for the Severe permafrost case. The upper permafrost surface, for periods of degradation from above, is not shown. The shaded area in blue and red represents the range within which a result is expected to lie when considering surface conditions between the dry and humid climate variants of the Severe permafrost case. The lilac colour indicates that the results for permafrost and perennially frozen ground overlap.*

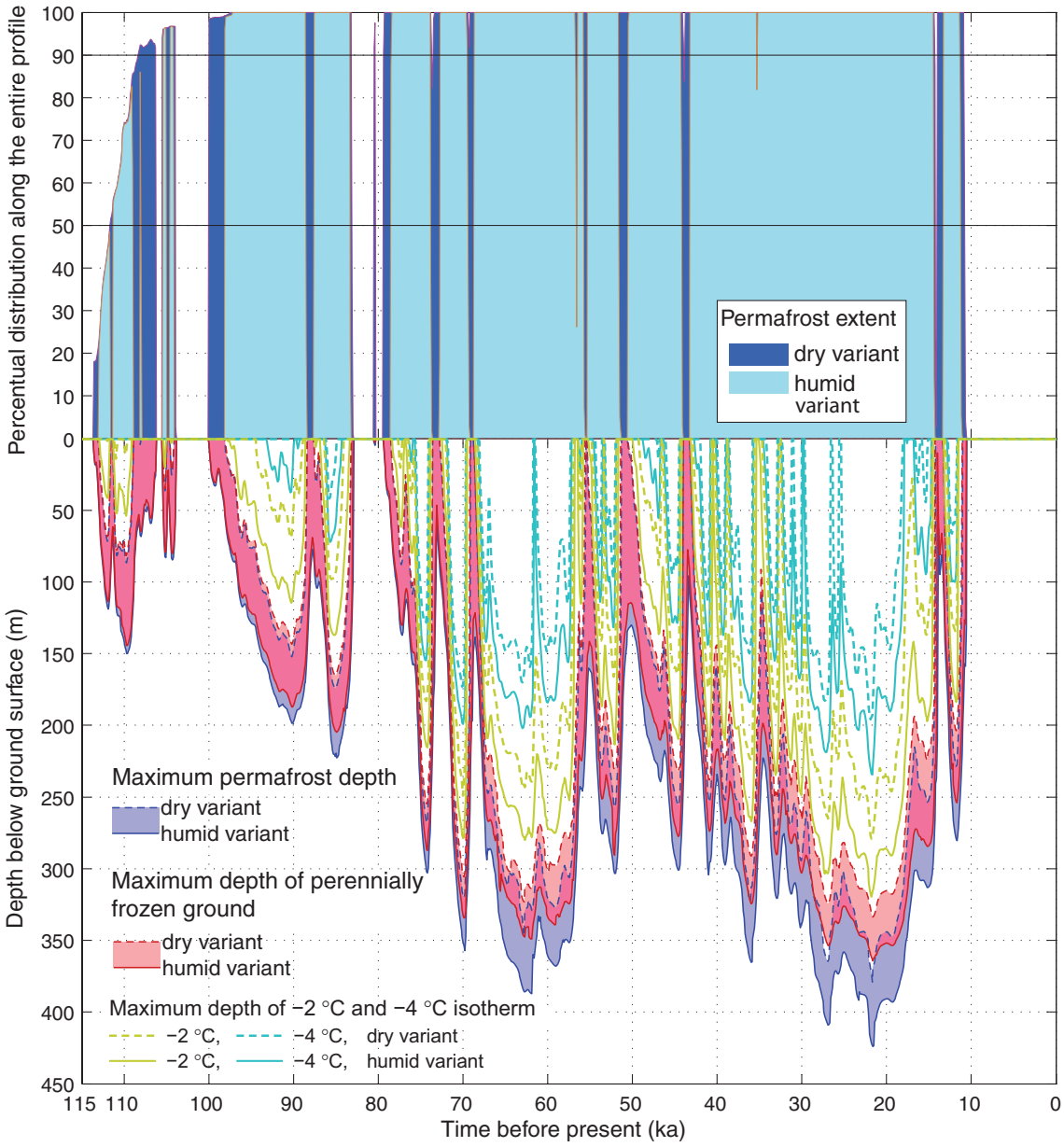

Figure 5-8. *Evolution of maximum permafrost depth, maximum depth of perennially frozen ground and maximum depth of −2 and −4°C isotherms over the whole profile for the Severe permafrost case. The figure also shows the percentual permafrost distribution along the profile. The transition from sporadic to discontinuous permafrost occurs at 50-% coverage and from discontinuous to continuous permafrost at 90-% coverage. The upper permafrost surface, for periods of degradation from above, is not shown. The shaded area in blue and red represents the range within which a result is expected to lie when considering surface conditions between the dry and humid climate variants of the Severe permafrost case. The lilac colour indicates that the results for permafrost and perennially frozen ground overlap.*

Table 5-1. Times of permafrost occurrence and associated maximum permafrost depth and maximum depth of perennially frozen ground over the whole profile and over the repository modelled for the humid variant of Repetition of last glacial cycle case. The table also gives the time and horizontal location of maximum permafrost depth and the percentual extent of permafrost distribution.

Time periods of permafrost occurrence (ka BP)		Over the whole site					Over the repository			
		Maximum permafrost depth (m)	Time of occurrence of maximum permafrost depth (ka BP)	Distance from the south-west side (m)	Maximum depth of perennially frozen ground (m)	Percentual extent of permafrost distribution (%)	Maximum permafrost depth (m)	Time of occurrence of maximum permafrost depth (ka BP)	Distance from the south-west side (m)	Maximum depth of perennially frozen ground (m)
113 …	111.7	31	112	4,960	29	34	31	112	4,960	29
111.3 …	109.1	42	109.8	7,960	39	62	18	111	5,540	17
105.4 …	105.1	10	105.2	14,290	9	71	12	105.2	5,540	11
104.6 …	104.2	2	104.4	14,320	1	58	6	104.4	5,540	5
98 …	88.6	77	90.3	12,750	73	94	55	90.3	4,970	52
87.5 …	87.2	1	87.4	14,320	4	50	6	87.4	5,540	5
86.9 …	83.4	129	85.5	11,620	125	100	95	85.6	5,160	92
78.4 …	74	188	74.4	11,630	182	100	152	74.4	5,120	148
72.6 …	70	221	70	11,630	212	100	182	70.1	5,110	176

Table 5-2. Times of permafrost occurrence and associated maximum permafrost depth and maximum depth of perennially frozen ground over the whole profile and over the repository modelled for the dry variant of Repetition of last glacial cycle case. The table also gives the time and horizontal location of maximum permafrost depth and the percentual extent of permafrost distribution.

Time periods of permafrost occurrence (ka BP)		Over the whole site					Over the repository			
		Maximum permafrost depth (m)	Time of occurrence of maximum permafrost depth (ka BP)	Distance from the south-west side (m)	Maximum depth of perennially frozen ground (m)	Percentual extent of permafrost distribution (%)	Maximum permafrost depth (m)	Time of occurrence of maximum permafrost depth (ka BP)	Distance from the south-west side (m)	Maximum depth of perennially frozen ground (m)
113.6 …	106.4	104	109.7	7,950	98	74	84	112	4,100	79
105.5 …	104	48	104.4	13,970	46	94	39	105.2	5,540	38
99.9 …	83.2	189	85.1	12,770	180	100	143	85.5	5,652	137
79.2 …	73.8	255	74.3	12,810	249	100	215	74.3	5,650	204
73.1 …	70	301	70	12,820	295	100	259	70	5,650	246

Table 5-3. Times of permafrost occurrence and associated maximum permafrost depth and maximum depth of perennially frozen ground over the whole profile and over the repository modelled for the humid variant of the Severe permafrost case. The table also gives the time and horizontal location of maximum permafrost depth and the percentual extent of permafrost distribution.

Time periods of permafrost occurrence (ka BP)		Over the whole site					Over the repository			
		Maximum permafrost depth (m)	Time of occurrence of maximum permafrost depth (ka BP)	Distance from the south-west side (m)	Maximum depth of perennially frozen ground (m)	Percentual extent of permafrost distribution (%)	Maximum permafrost depth (m)	Time of occurrence of maximum permafrost depth (ka BP)	Distance from the south-west side (m)	Maximum depth of perennially frozen ground (m)
113.6 …	106.3	150	109.7	100	144	75	104	112	3,950	97
105.5 …	103.9	85	104.3	12,280	80	97	64	105.2	5,650	62
100.1 …	83	223	84.9	14,910	205	100	196	85.1	5,650	186
80.5 …	80.4	5	80.4	14,870	3	95	3	80.4	5,610	1
79.4 …	10.6	424	21.6	12,240	364	100	393	21.6	5,650	359

Table 5-4. Times of permafrost occurrence and associated maximum permafrost depth and maximum depth of perennially frozen ground over the whole profile and over the repository modelled for the dry variant of the Severe permafrost case. The table also gives the time and horizontal location of maximum permafrost depth and the percentual extent of permafrost distribution.

Time periods of permafrost occurrence (ka BP)		Over the whole site					Over the repository			
		Maximum permafrost depth (m)	Time of occurrence of maximum permafrost depth (ka BP)	Distance from the south-west side (m)	Maximum depth of perennially frozen ground (m)	Percentual extent of permafrost distribution (%)	Maximum permafrost depth (m)	Time of occurrence of maximum permafrost depth (ka BP)	Distance from the south-west side (m)	Maximum depth of perennially frozen ground (m)
113 …	111.7	72	112	3,020	68	44	69	112	3,950	64
111.3 …	109	87	109.7	7,990	81	74	52	109.8	5,650	50
108.2 …	108	4	108.1	12,360	1	79	2	108.1	5,620	0
105.4 …	105	36	105.2	14,280	35	96	33	105.2	5,650	32
104.6 …	104.2	25	104.4	14,280	22	97	21	104.4	5,650	20
98.1 …	88.5	152	90.2	14,840	143	100	131	90.3	5,650	125
87.6 …	83.3	174	85.1	14,880	165	100	157	85.2	5,650	151
78.5 …	73.7	268	74.3	13,890	255	100	242	74.3	5,650	231
72.8 …	69.2	320	69.9	13,790	306	100	290	70	5,650	277
68.7 …	55.6	326	62	14,890	314	100	310	62.8	5,650	291
55.3 …	51.4	257	52.1	14,980	231	100	241	52.2	5,650	224
50.5 …	44.1	256	44.6	14,980	232	100	244	44.6	5,650	230
43.2 …	14.3	379	21.7	13,940	333	100	355	21.7	5,650	327
13.3 …	11.1	229	11.8	14,980	204	100	221	11.8	5,650	206

Table 5-5. Evolution of maximum permafrost depth and maximum depth of perennially frozen ground over the repository modelled for the Repetition of last glacial cycle case and the Severe permafrost case. The table also shows the prevailing mean annual air temperatures.

Time before present (ka)	Mean annual air temperature (°C)	Maximum permafrost depth (m)				Maximum depth of perennially frozen ground (m)			
		Humid variant of the Repetition of last glacial cycle case	Dry variant of the Repetition of last glacial cycle case	Humid variant of the Severe permafrost case with	Dry variant of the Severe permafrost case with	Humid variant of the Repetition of last glacial cycle case	Dry variant of the Repetition of last glacial cycle case	Humid variant of the Severe permafrost case with	Dry variant of the Severe permafrost case with
112	–3.4	31	84	104	69	29	79	97	64
111.5	–0.6	0	3	30	0	0	1	27	0
110	–3.5	15	47	71	46	15	46	68	44
108	–1.5	0	22	44	0	0	21	42	0
106	2.5	0	0	0	0	0	0	0	0
104	–0.6	0	6	33	0	0	5	30	0
102	1.6	0	0	0	0	0	0	0	0
100	–0.3	0	0	7	0	0	0	5	0
98	–1.9	2	30	55	9	0	28	52	8
96	–2.9	18	62	102	56	16	60	97	53
95	–3.2	23	69	110	64	20	66	105	61
94	–3.9	35	84	127	86	33	81	122	82
92	–4.8	49	108	158	117	47	103	151	113
90	–4.1	45	112	168	123	43	107	161	118
88	–0.9	0	15	54	0	0	13	49	0
86	–6.4	73	116	155	120	71	113	149	115
84	–3.1	31	108	164	105	29	104	156	98
82	2.1	0	0	0	0	0	0	0	0
80	0.4	0	0	0	0	0	0	0	0
78	–2.5	12	52	88	37	10	50	84	35
76	–4.2	45	101	147	102	43	97	140	98
75	–10.4	135	186	232	204	131	179	219	194
74	–1.3	85	180	256	211	77	168	241	198
72	–3.6	33	86	130	78	31	82	124	74
70	–10	181	259	319	290	175	246	303	277

Table 5-6. Evolution of maximum permafrost depth and maximum depth of perennially frozen ground over the whole profile modelled for the Repetition of last glacial cycle case and the Severe permafrost case. The table also shows the prevailing mean annual air temperatures.

Time before present (ka)	Mean annual air temperature (°C)	Maximum permafrost depth (m)				Maximum depth of perennially frozen ground (m)			
		Humid variant of the Repetition of last glacial cycle case	Dry variant of the Repetition of last glacial cycle case	Humid variant of the Severe permafrost case with	Dry variant of the Severe permafrost case with	Humid variant of the Repetition of last glacial cycle case	Dry variant of the Repetition of last glacial cycle case	Humid variant of the Severe permafrost case with	Dry variant of the Severe permafrost case with
112	–3.4	31	84	117	72	29	86	112	64
111.5	–0.6	0	12	79	0	0	10	73	0
110	–3.5	37	95	142	77	34	89	136	44
108	–1.5	0	41	69	0	0	38	65	0
106	2.5	0	0	0	0	0	0	0	0
104	–0.6	0	23	60	0	0	20	54	0
102	1.6	0	0	0	0	0	0	0	0
100	–0.3	0	0	3	0	0	0	3	0
98	–1.9	0	34	60	12	0	32	57	8
96	–2.9	29	93	117	66	26	89	111	53
95	–3.2	34	101	129	76	31	97	122	61
94	–3.9	49	119	147	99	46	114	139	82
92	–4.8	70	151	182	136	66	145	172	113
90	–4.1	70	162	197	147	65	155	186	118
88	–0.9	0	7	92	0	0	6	82	0
86	–6.4	96	153	169	128	93	147	158	115
84	–3.1	50	155	196	140	46	147	190	98
82	2.1	0	0	0	0	0	0	0	0
80	0.4	0	0	0	0	0	0	0	0
78	–2.5	1	59	95	39	1	56	90	35
76	–4.2	55	122	157	108	52	117	149	98
75	–10.4	165	222	256	217	160	212	243	194
74	–1.3	150	239	283	242	140	222	269	198
72	–3.6	44	110	143	84	41	105	133	74
70	–10	221	301	351	319	212	295	332	277

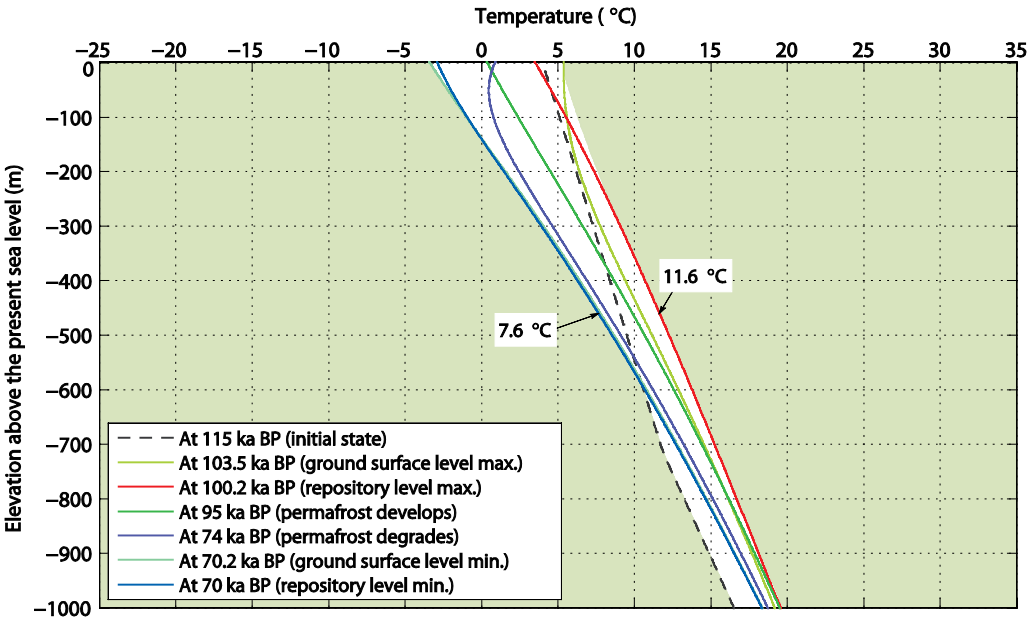

Figure 5-9. *Ground temperature along a vertical profile located at 3,550 m from the south-western side of the profile for the humid variant of the Repetition of last glacial cycle case and wet surface cover type. White envelope represents the range of temperature fluctuation over the time period of 115 to 70 ka BP.*

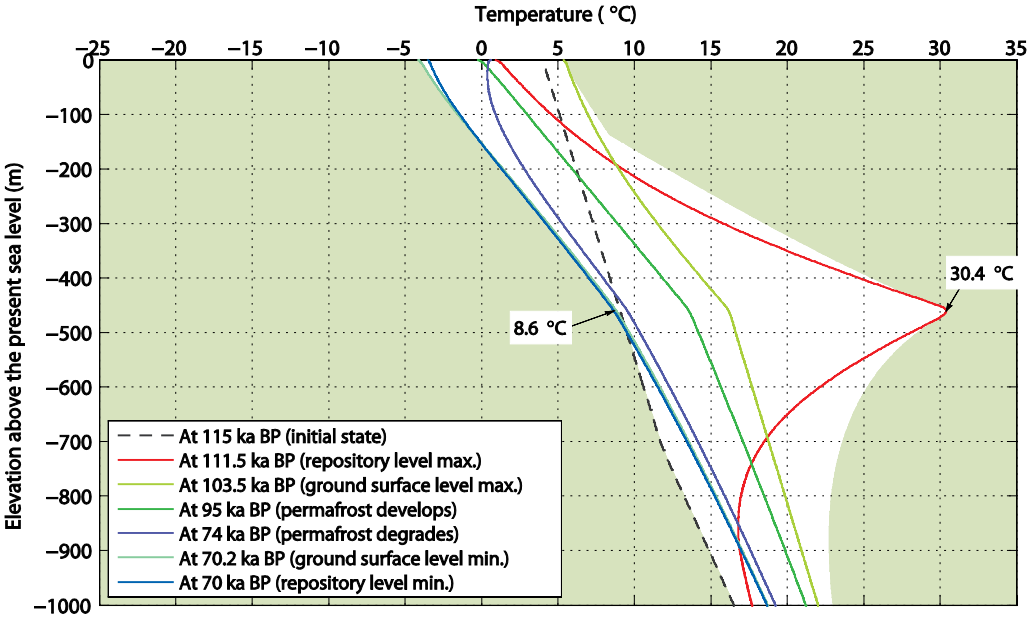

Figure 5-10. *Ground temperature along a vertical profile located in the middle of the repository at 4,783 m from the south-western side of the for the humid variant of the Repetition of last glacial cycle case and fresh-moist surface cover type. White envelope represents the range of temperature fluctuation over the time period of 115 to 70 ka BP.*

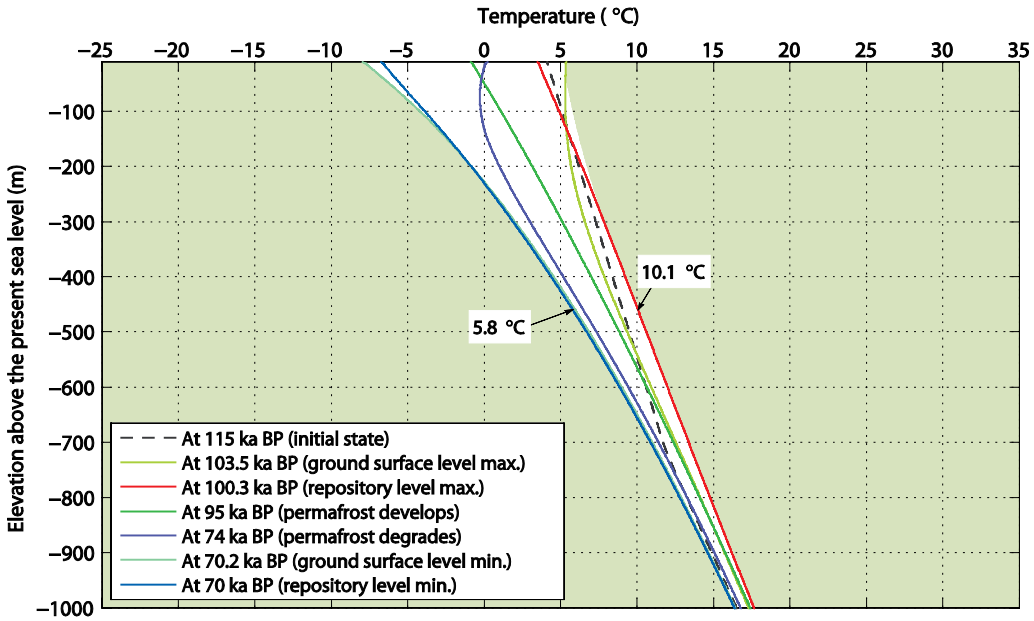

Figure 5-11. *Ground temperature along a vertical profile located at 11,600 m from the south-western side of the profile for the humid variant of the Repetition of last glacial cycle case and dry surface cover type. White envelope represents the range of temperature fluctuation over the time period of 115 to 70 ka BP.*

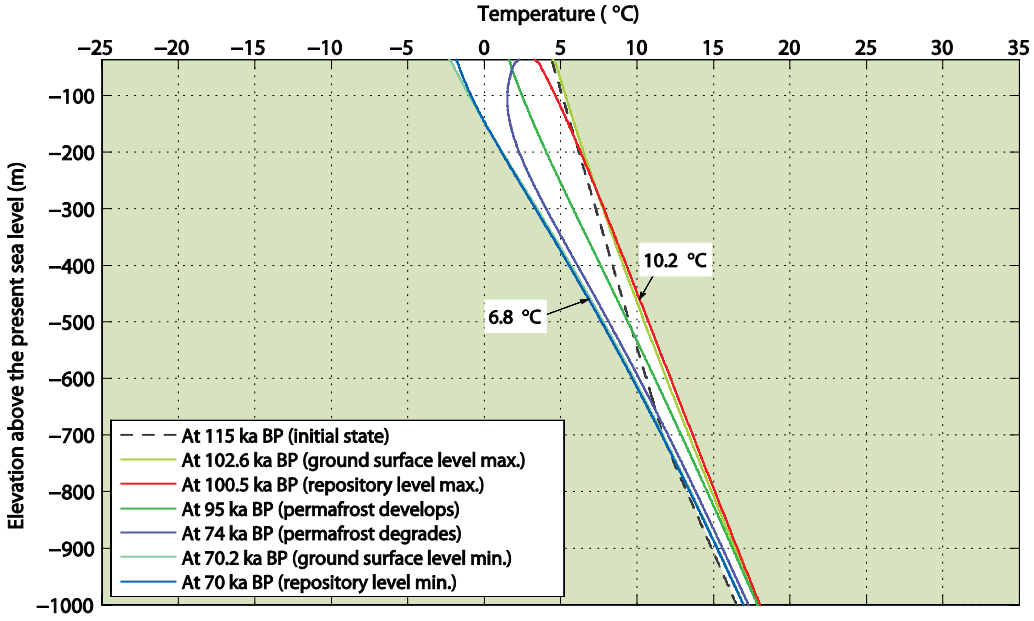

Figure 5-12. *Ground temperature along a vertical profile located at 14,600 m from the south-western side of the profile for the humid variant of the Repetition of last glacial cycle case and peatland surface cover type. White envelope represents the range of temperature fluctuation over the time period of 115 to 70 ka BP.*

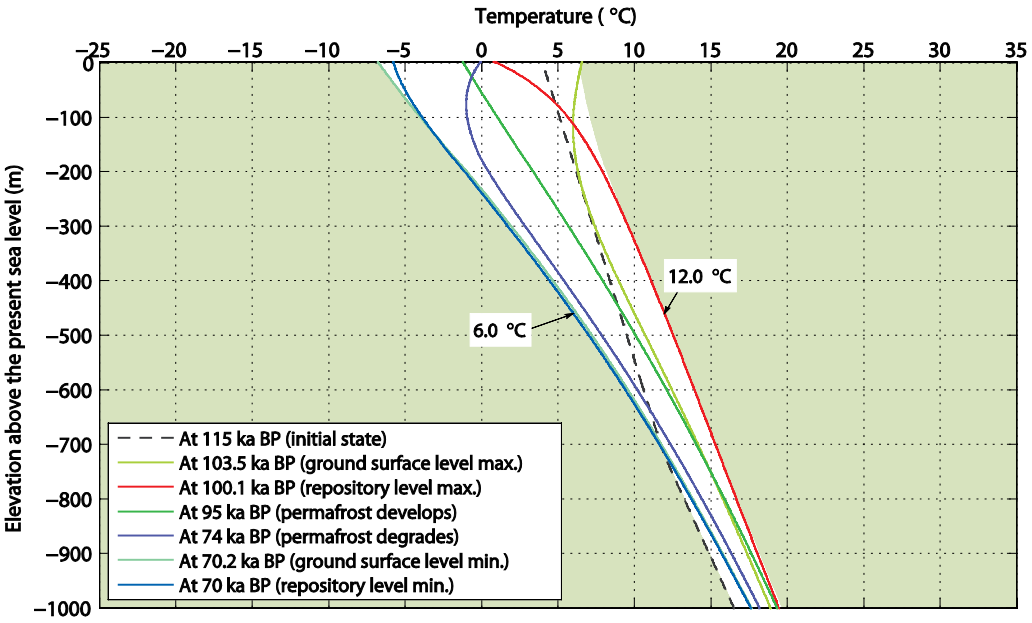

Figure 5-13. *Ground temperature along a vertical profile located at 3,550 m from the south-western side of the profile for the dry variant of the Repetition of last glacial cycle case and wet surface cover type. White envelope represents the range of temperature fluctuation over the time period of 115 to 70 ka BP.*

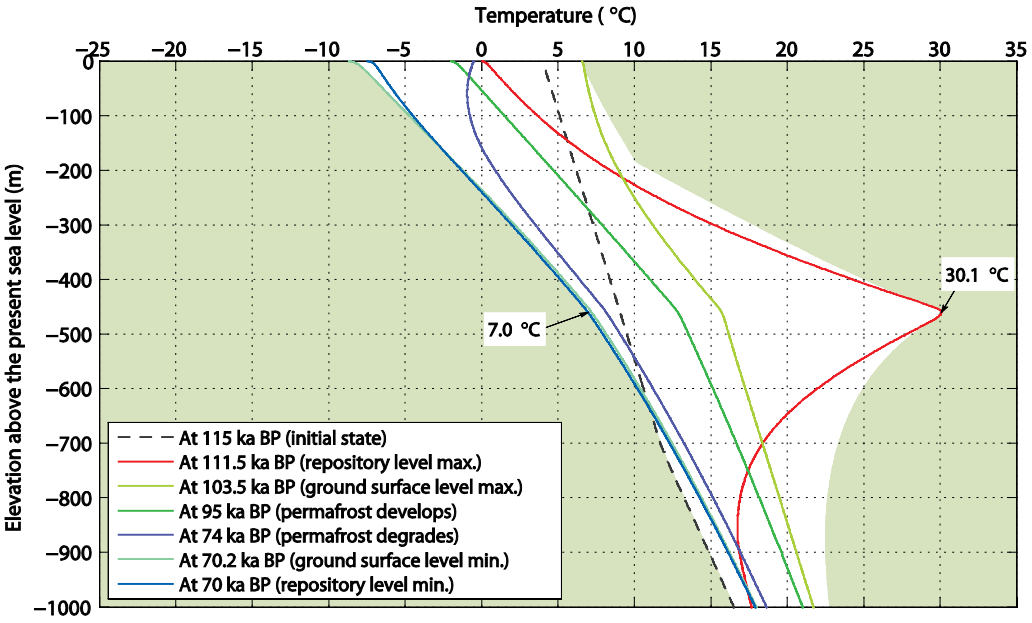

Figure 5-14. *Ground temperature along a vertical profile located in the middle of the repository at 4,783 m from the south-western side of the profile for the dry variant of the Repetition of last glacial cycle case and fresh-moist surface cover type. White envelope represents the range of temperature fluctuation over the time period of 115 to 70 ka BP.*

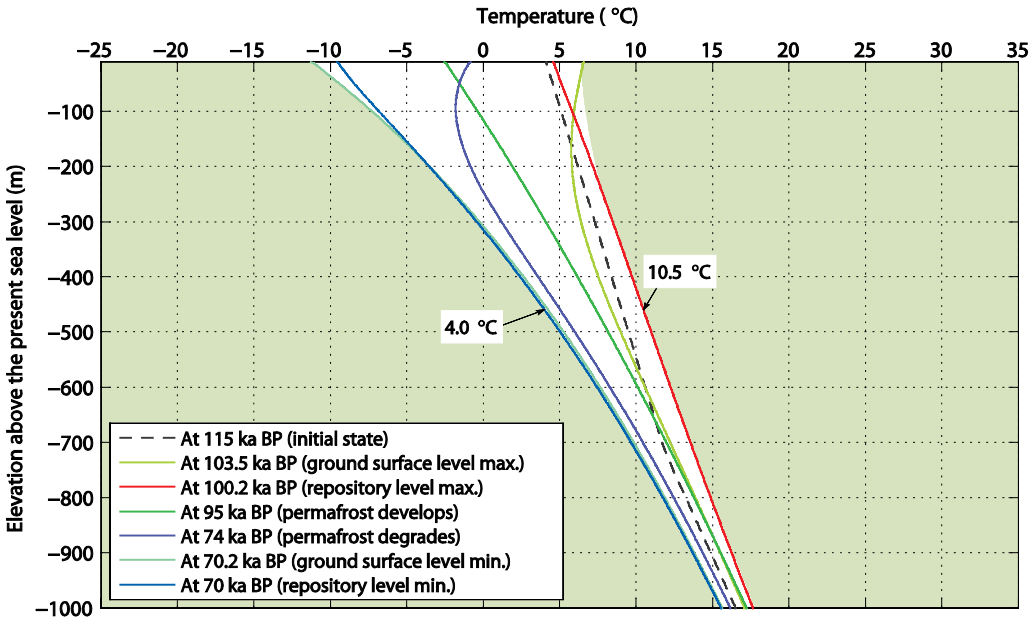

Figure 5-15. *Ground temperature along a vertical profile located at 11,600 m from the south-western side of the profile for the dry variant of the Repetition of last glacial cycle case and dry surface cover type. White envelope represents the range of temperature fluctuation over the time period of 115 to 70 ka BP.*

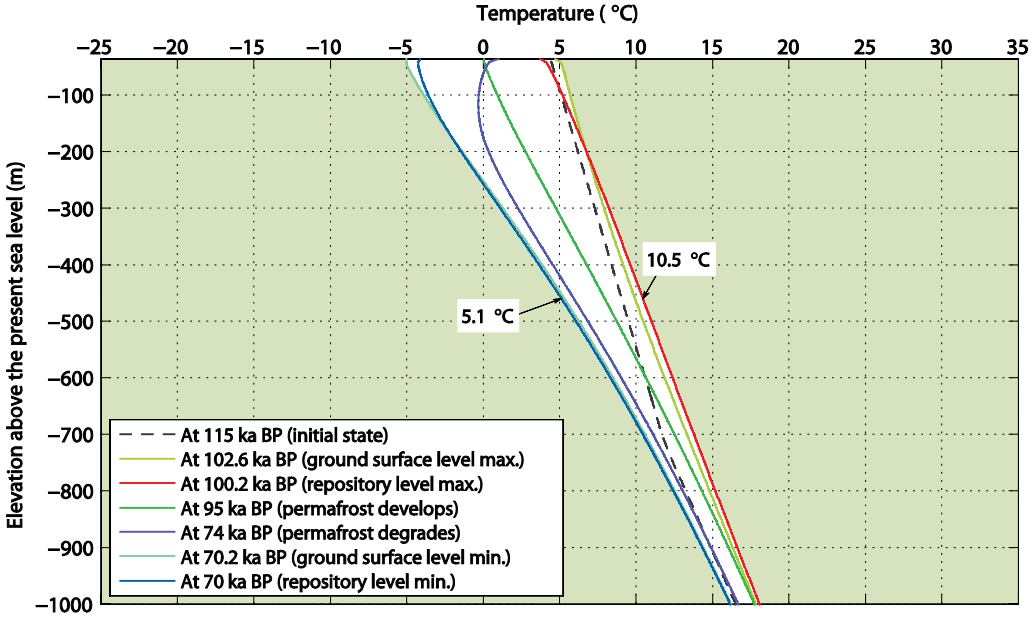

Figure 5-16. *Ground temperature along a vertical profile located at 14,600 m from the south-western side of the profile for the dry variant of the Repetition of last glacial cycle case and peatland surface cover type. White envelope represents the range of temperature fluctuation over the time period of 115 to 70 ka BP.*

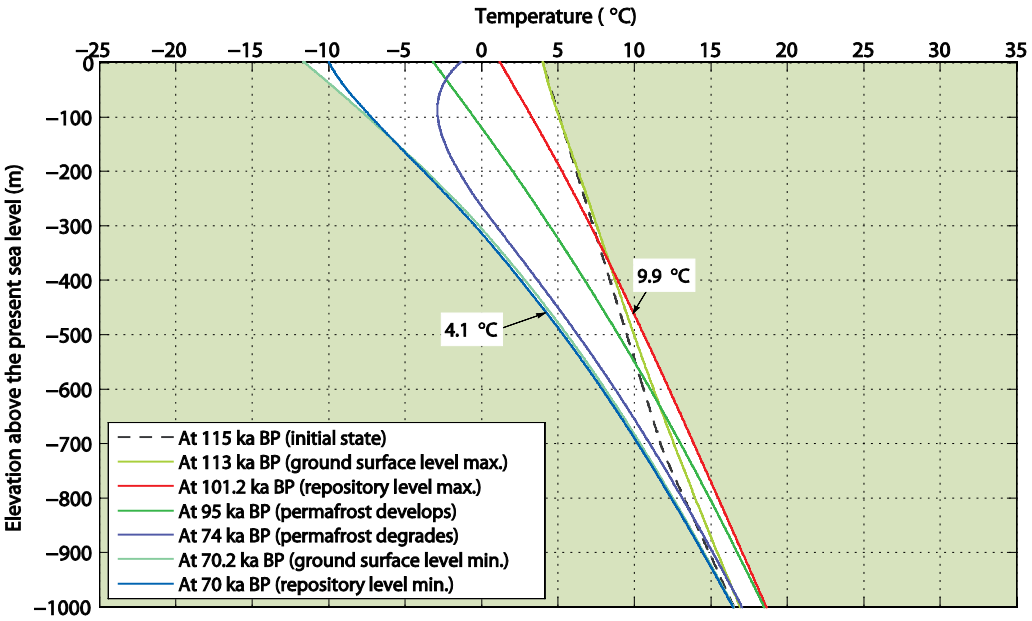

Figure 5-17. *Ground temperature along a vertical profile located at 3,550 m from the south-western side of the profile for the humid variant of Severe permafrost case and dry surface condition type. White envelope represents the range of temperature fluctuation over the time period of 115 to 70 ka BP.*

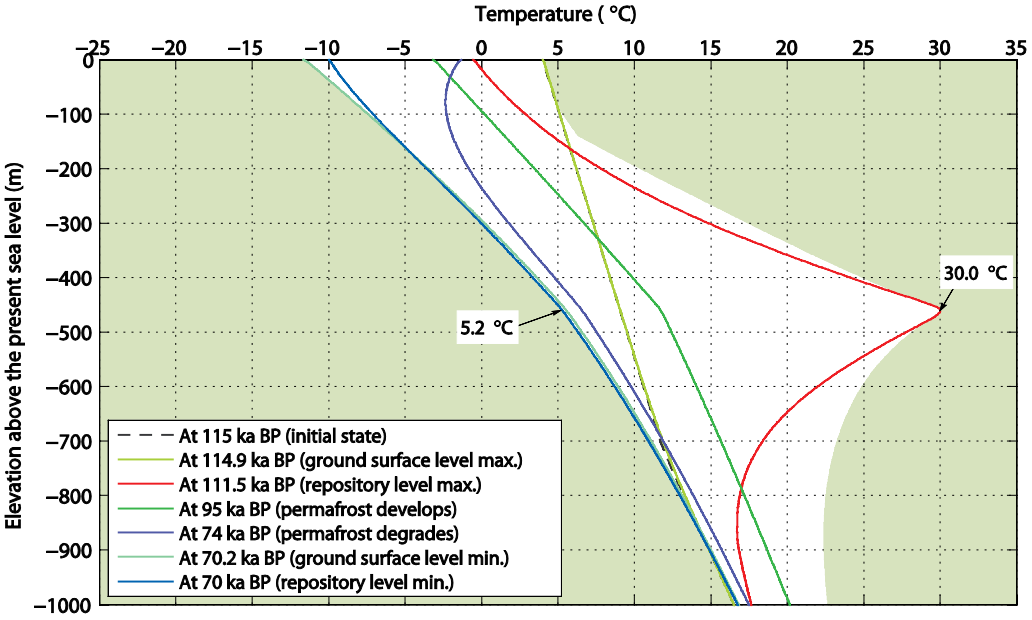

Figure 5-18. *Ground temperature along a vertical profile located in the middle of the repository at 4,783 m from the south-western side of the profile for the humid variant of the Severe permafrost case and dry surface condition type. White envelope represents the range of temperature fluctuation over the time period of 115 to 70 ka BP.*

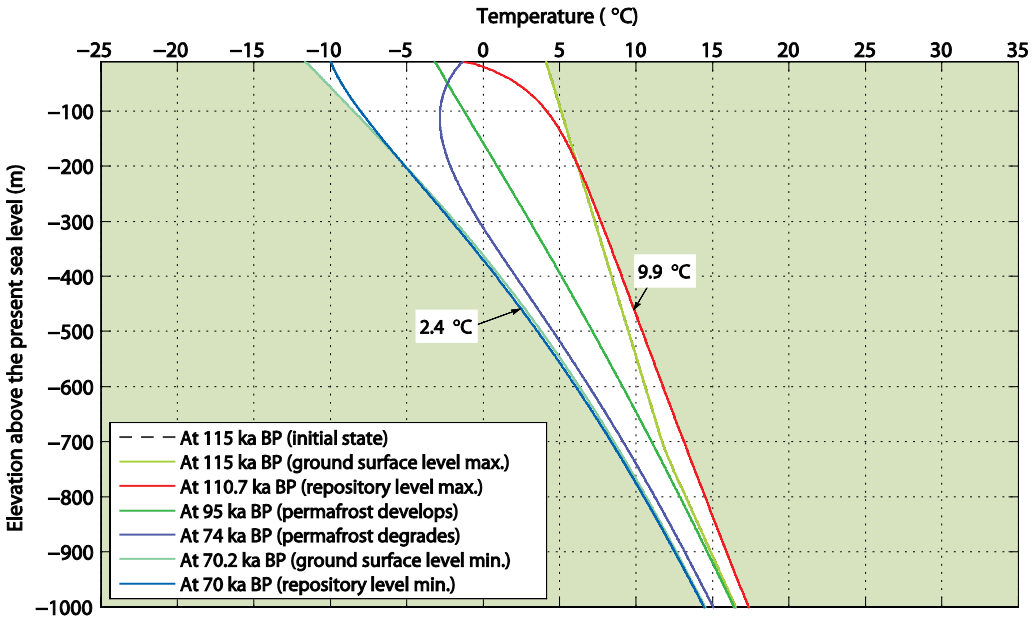

Figure 5-19. *Ground temperature along a vertical profile located at 11,600 m from the south-western side of the profile for the humid variant of the Severe permafrost case and dry surface condition type. White envelope represents the range of temperature fluctuation over the time period of 115 to 70 ka BP.*

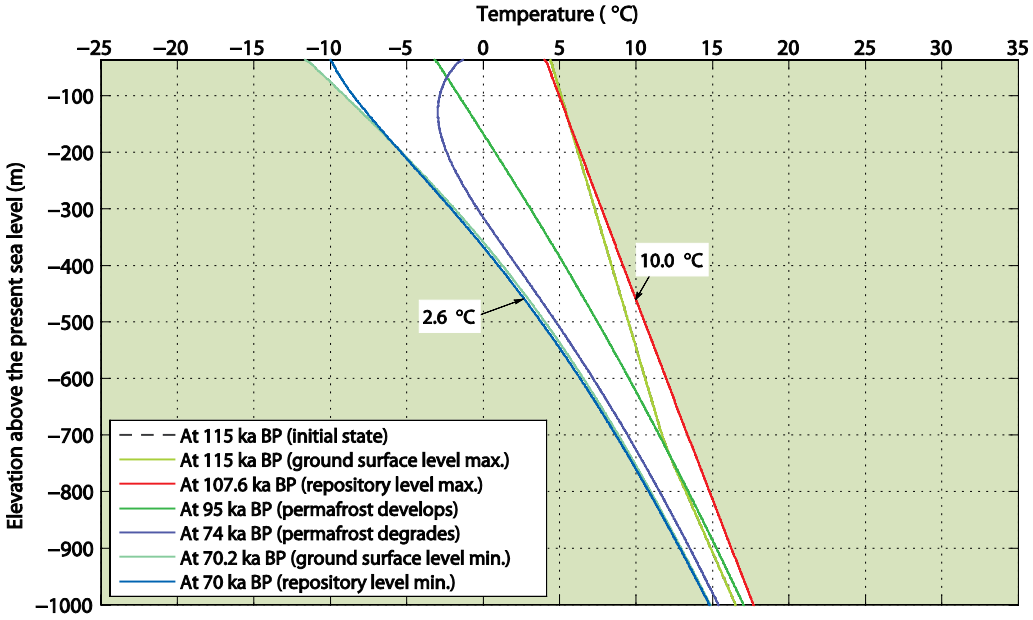

Figure 5-20. *Ground temperature along a vertical profile located at 14,600 m from the south-western side of the profile for the humid variant of the Severe permafrost case and dry surface condition type. White envelope represents the range of temperature fluctuation over the time period of 115 to 70 ka BP.*

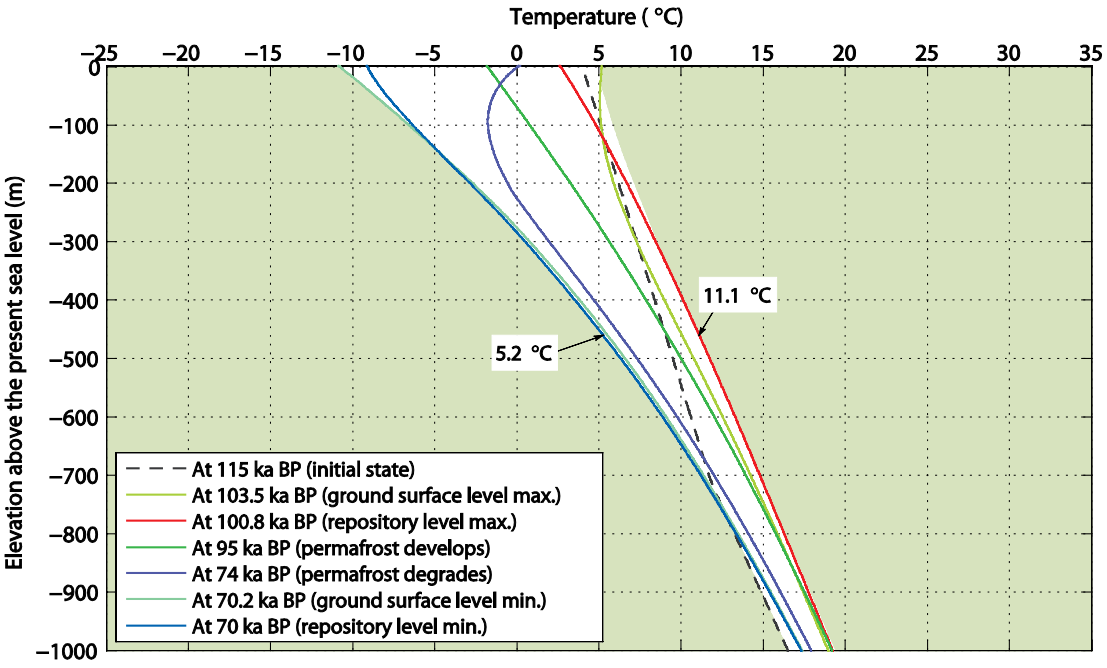

Figure 5-21. *Ground temperature along a vertical profile located at 3,550 m from the south-western side of the profile for the dry variant of the Severe permafrost case and dry surface condition type. White envelope represents the range of temperature fluctuation over the time period of 115 to 70 ka BP.*

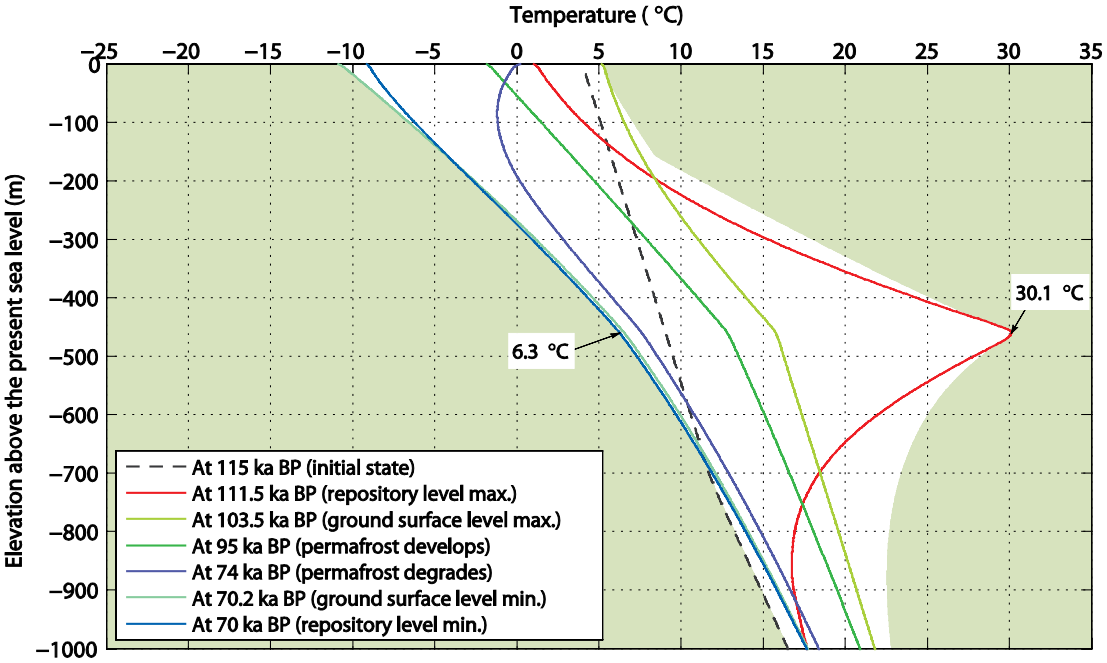

Figure 5-22. *Ground temperature along a vertical profile located in the middle of the repository at 4,783 m from the south-western side of the profile for the dry variant of the Severe permafrost case and dry surface condition type. White envelope represents the range of temperature fluctuation over the time period of 115 to 70 ka BP.*

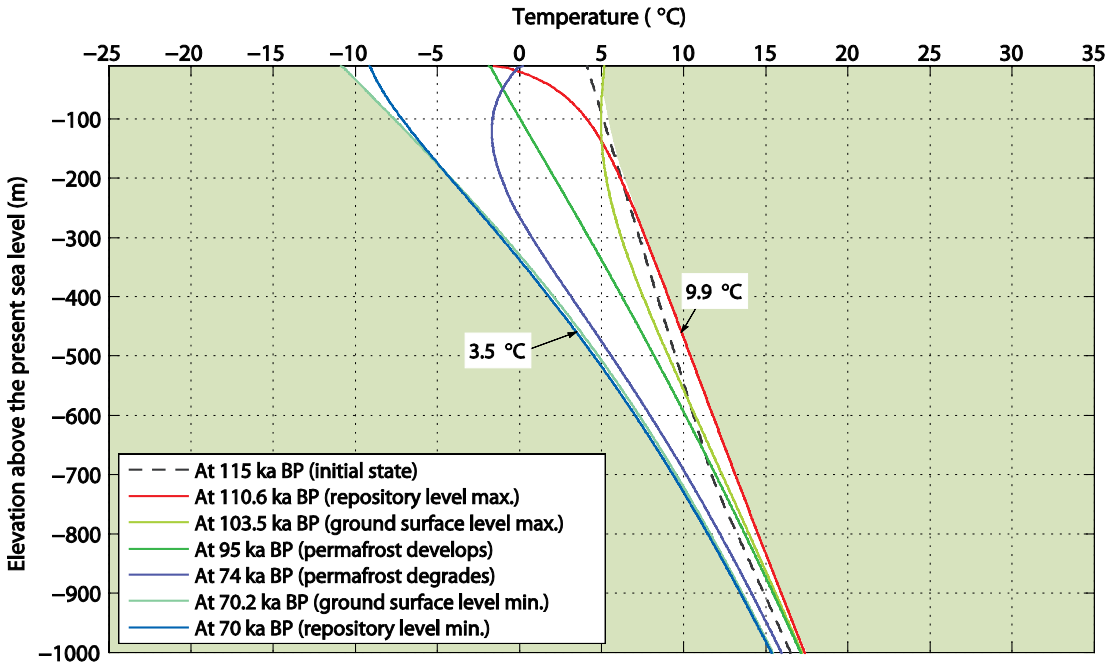

Figure 5-23. *Ground temperature along a vertical profile located at 11,600 m from the south-western side of the profile for the dry variant of the Severe permafrost case and dry surface condition type. White envelope represents the range of temperature fluctuation over the time period of 115 to 70 ka BP.*

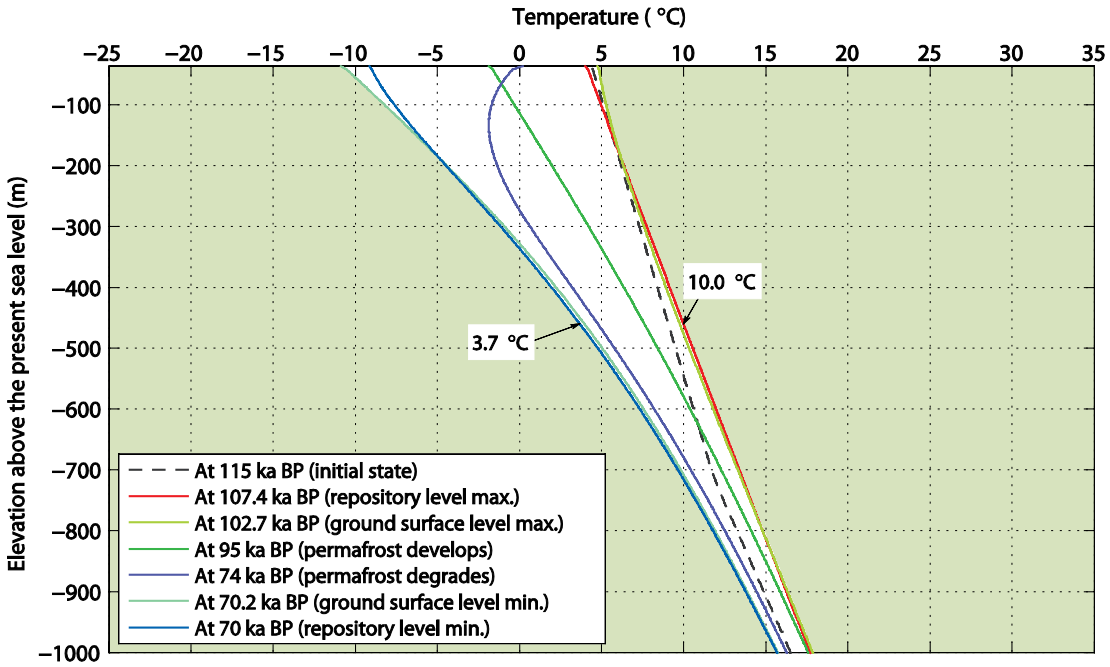

Figure 5-24. *Ground temperature along a vertical profile located at 14,600 m from the south-western side of the profile for the dry variant of the Severe permafrost case and dry surface condition type. White envelope represents the range of temperature fluctuation over the time period of 115 to 70 ka BP.*

Unfrozen water content and talik formation

The unfrozen water content and the groundwater flow (Darcy velocity) directions at a time of 90,400 years BP for the humid and dry variants of the *Repetition of last glacial cycle* case considering mean subsurface conditions are shown in Figure 5-25 and Figure 5-26, respectively. The figures show the whole profile, and the close-ups of the highly conductive deformation zone ZFMA2 at a distance of 4,000 m, and the near-by area of the two future lakes at the distances of 9,000 m and 14,600 m. The results show that during phases of the simulated time period, taliks form at these lake locations. The corresponding results at the times of 85,800 and 70,000 years BP are shown in Figures 5-27, 5-28, 5-29, 5-30. The results for groundwater flow showed maximum flow velocity of ~50 m/a when no permafrost occurred and some metres per year beneath the perennially frozen ground. In the perennially frozen ground the flow velocities were much smaller.

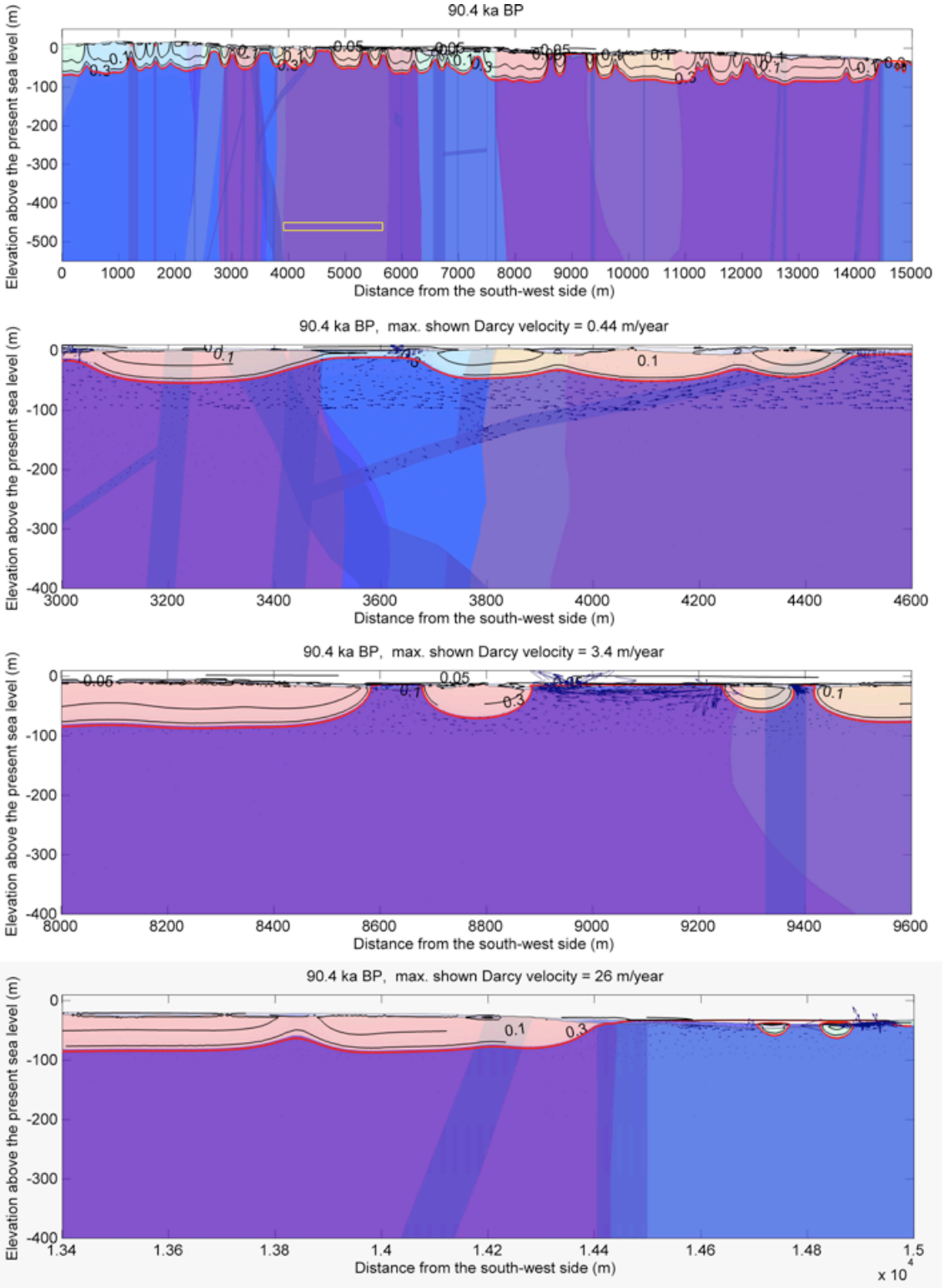

Figure 5-25. *Unfrozen volumetric (m^3/m^3) groundwater content contours and Darcy flow directions at 90.4 ka BP for the humid variant of the Repetition of last glacial cycle case shown for the whole profile and the close-ups of the deformation zone ZFMA2 at ~4,000 m, and the near-by area of the lakes at the distances 9,000 m and 14,600 m from the south-west side of the profile. Light colour shows the extent of perennially frozen ground, the red line shows the 0°C isotherm, and the yellow box in the upper panel shows the repository.*

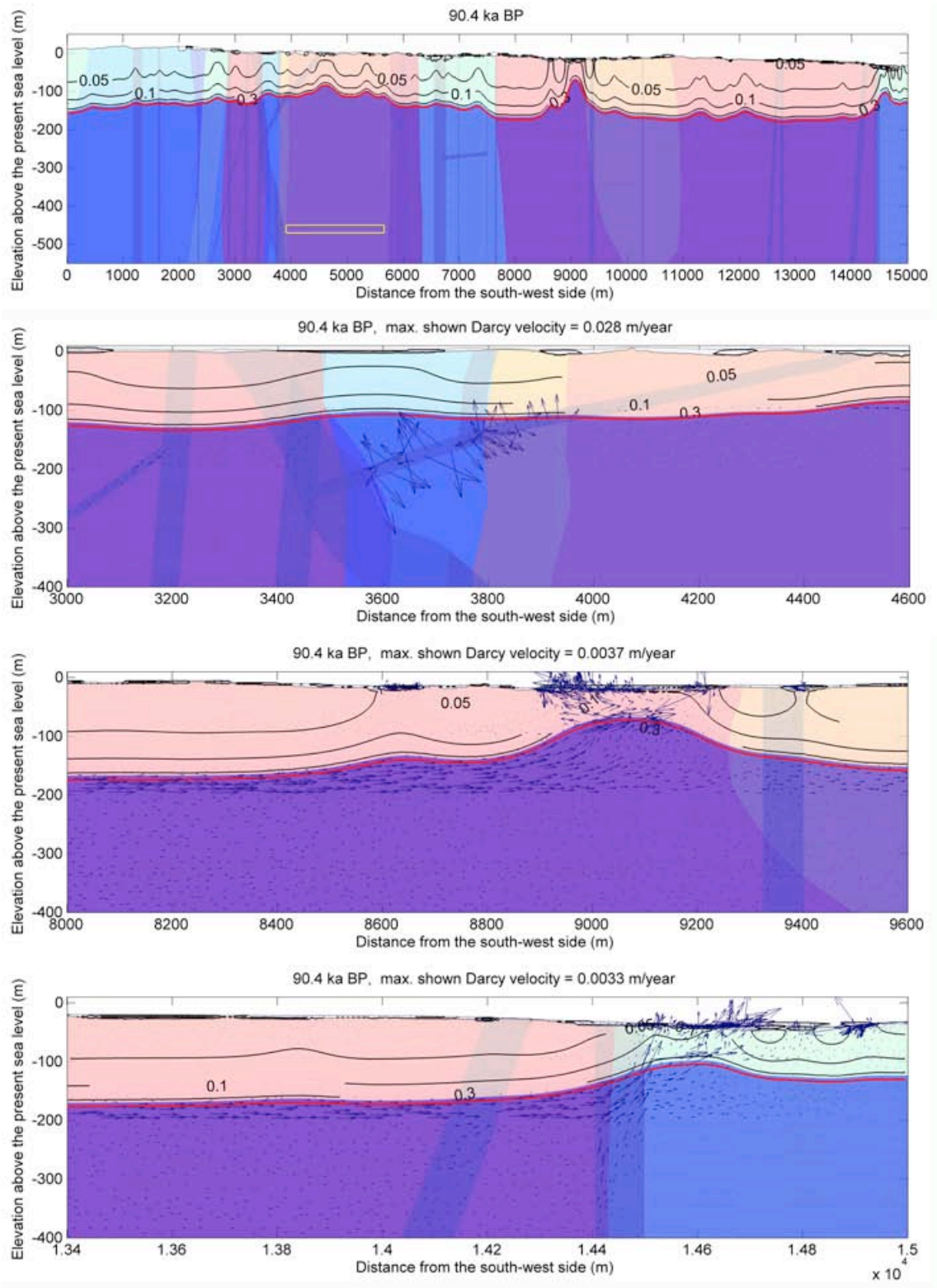

Figure 5-26. *Unfrozen volumetric (m^3/m^3) groundwater content contours and Darcy flow directions at 90.4 ka BP for the dry variant of the Repetition of last glacial cycle case shown for the whole profile and the close-ups of the deformation zone ZFMA2 at ~4,000 m, and the near-by area of the lakes at the distances 9,000 m and 14,600 m from the south-west side of the profile. Light colour shows the extent of perennially frozen ground, the red line shows the 0°C isotherm (i.e. permafrost depth), and the yellow box in the upper panel shows the repository.*

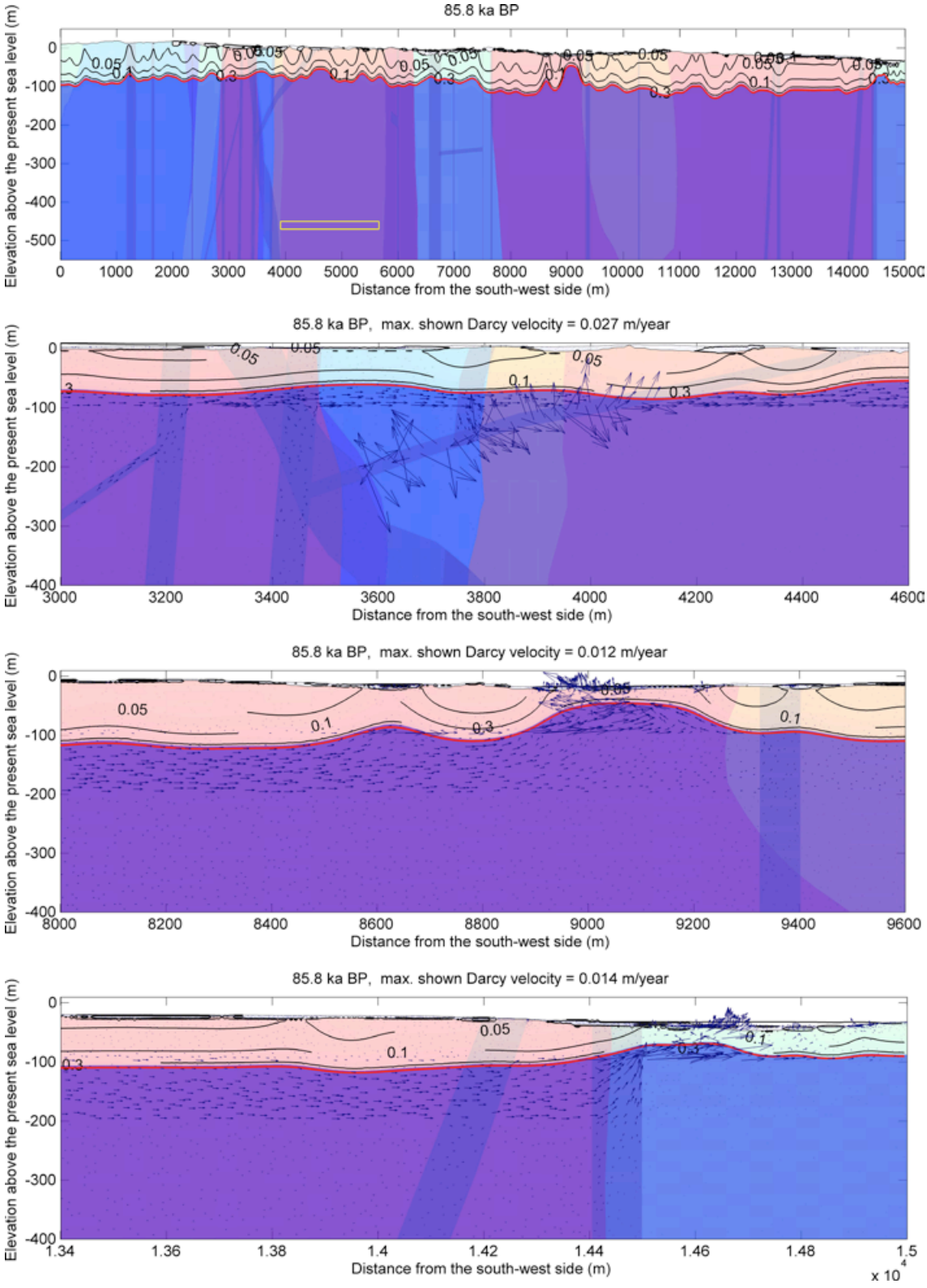

Figure 5-27. *Unfrozen volumetric (m^3/m^3) groundwater content contours and Darcy flow directions at 85.8 ka BP for the humid variant of the Repetition of last glacial cycle case shown for the whole profile and the close-ups of the deformation zone ZFMA2 at ~4,000 m, and the near-by area of the lakes at the distances 9,000 m and 14,600 m from the south-west side of the profile. Light colour shows the extent of perennially frozen ground, the red line shows the 0°C isotherm (i.e. permafrost depth), and the yellow box in the upper panel shows the repository.*

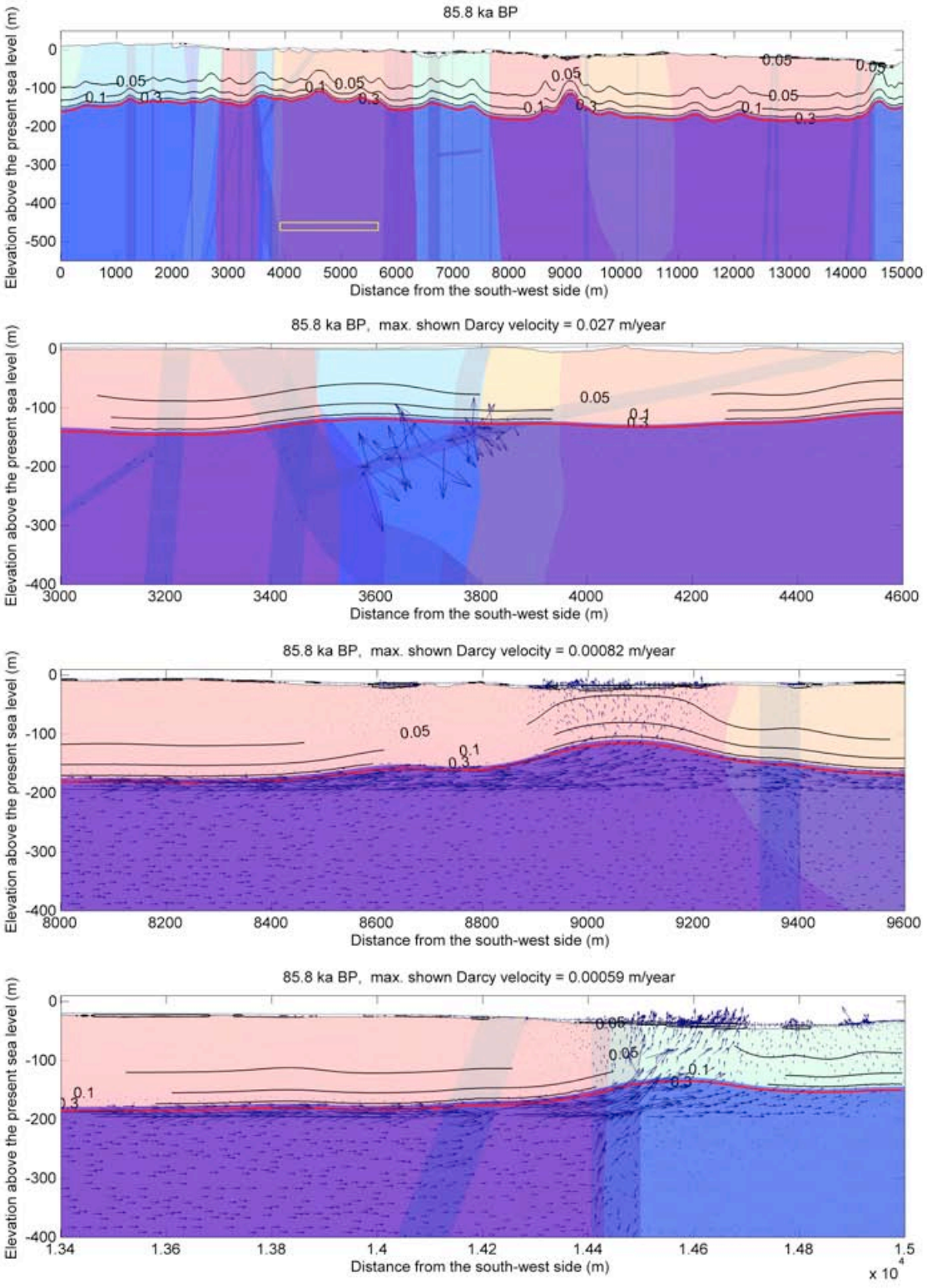

Figure 5-28. *Unfrozen volumetric (m^3/m^3) groundwater content contours and Darcy flow directions at 85.8 ka BP for the dry variant of the Repetition of last glacial cycle case shown for the whole profile and the close-ups of the deformation zone ZFMA2 at ~4,000 m, and the near-by area of the lakes at the distances 9,000 m and 14,600 m from the south-west side of the profile. Light colour shows the extent of perennially frozen ground, the red line shows the 0°C isotherm (i.e. permafrost depth), and the yellow box in the upper panel shows the repository.*

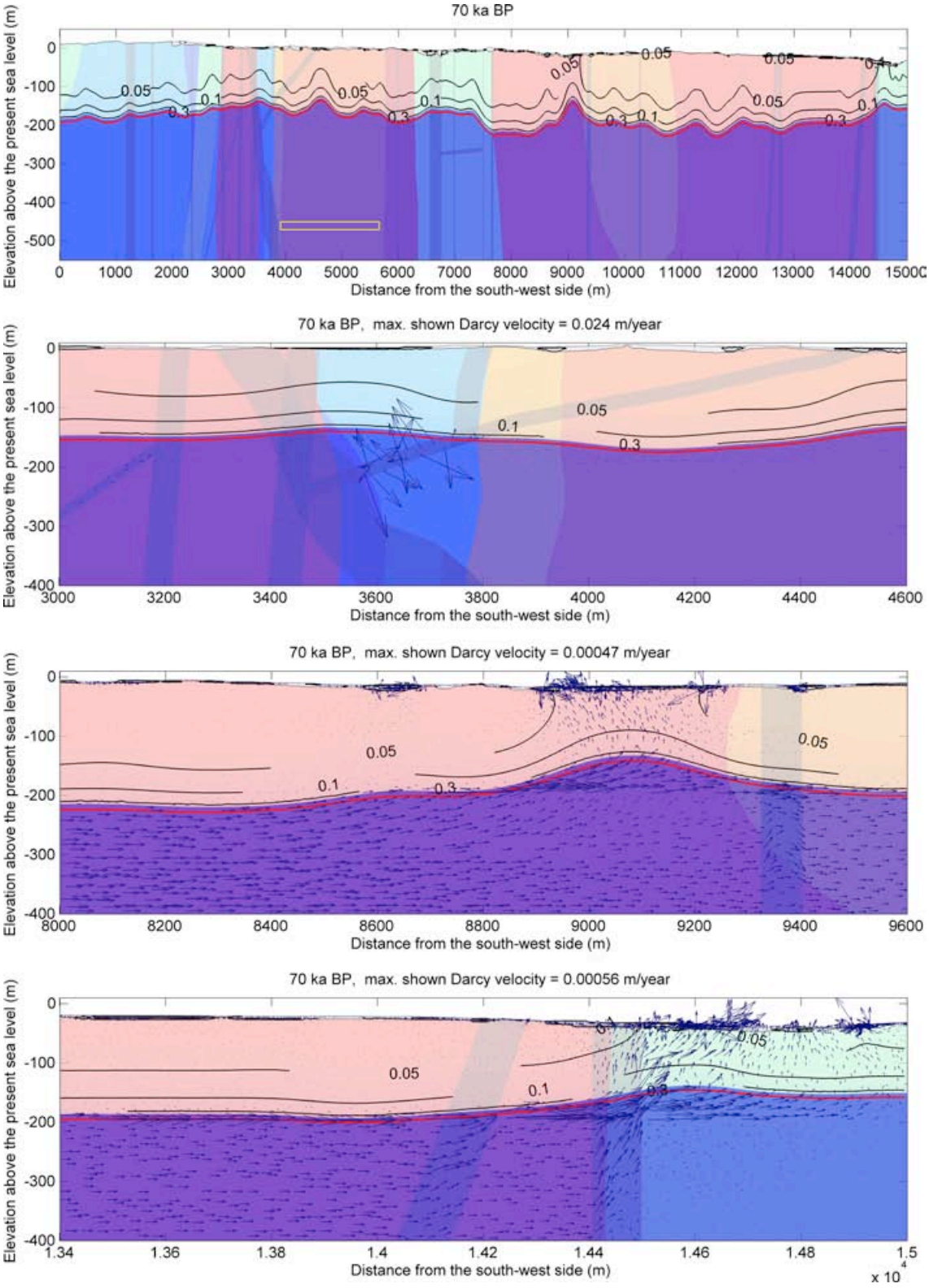

Figure 5-29. *Unfrozen volumetric (m^3/m^3) groundwater content contours and Darcy flow directions at 70 ka BP for the humid variant of the Repetition of last glacial cycle case shown for the whole profile and the close-ups of the deformation zone ZFMA2 at ~4,000 m, and the near-by area of the lakes at the distances 9,000 m and 14,600 m from the south-west side of the profile. Light colour shows the extent of perennially frozen ground, the red line shows the 0°C isotherm (i.e. permafrost depth), and the yellow box in the upper panel shows the repository.*

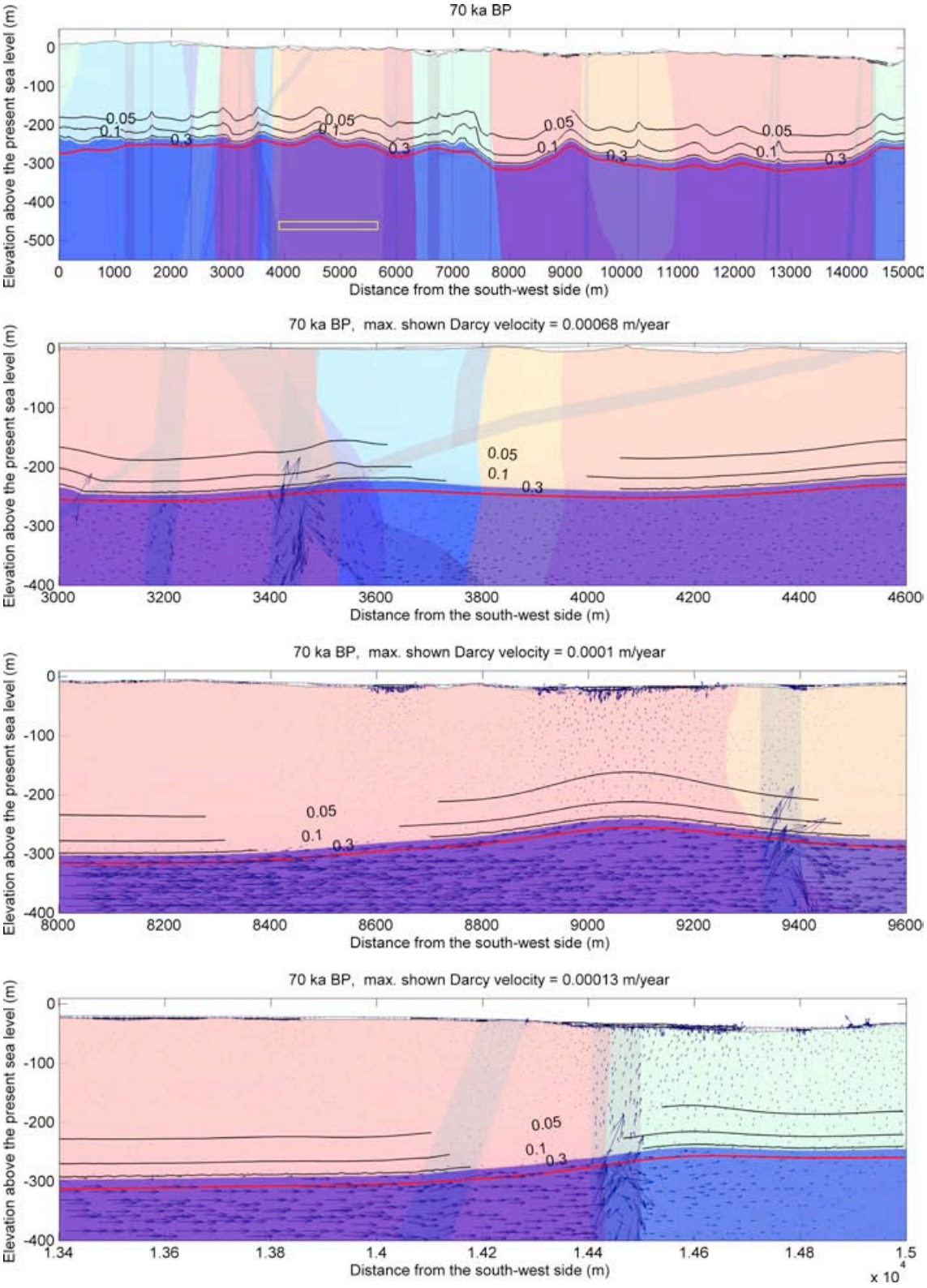

Figure 5-30. *Unfrozen volumetric (m^3/m^3) groundwater content contours and Darcy flow directions at 70 ka BP for the dry variant of the Repetition of last glacial cycle case shown for the whole profile and the close-ups of the deformation zone ZFMA2 at ~4,000 m, and the near-by area of the lakes at the distances 9,000 m and 14,600 m from the south-west side of the profile. Light colour shows the extent of perennially frozen ground, the red line shows the 0°C isotherm (i.e. permafrost depth), and the yellow box in the upper panel shows the repository.*

Salinity concentration

Given the permafrost and freezing results presented above for the *Repetition of last glacial cycle* case and the *Severe permafrost* case, the associated results on salinity concentration at times of 111,500, 95,000, 74,000, 70,000 years BP are illustrated in Figures 5-31 to 5-34.

Due to low salinity concentrations at shallow depths, the impacts of freezing on salinity exclusion and redistribution are difficult to see from the results. However, under more severe conditions when the air temperature is decreased very much, i.e. by 8°C, in the dry variant of *Repetition of last glacial cycle* case, the freezing occurs more intensively and an increase in salinity concentration due to the exclusion can be seen in Figure 5-35.

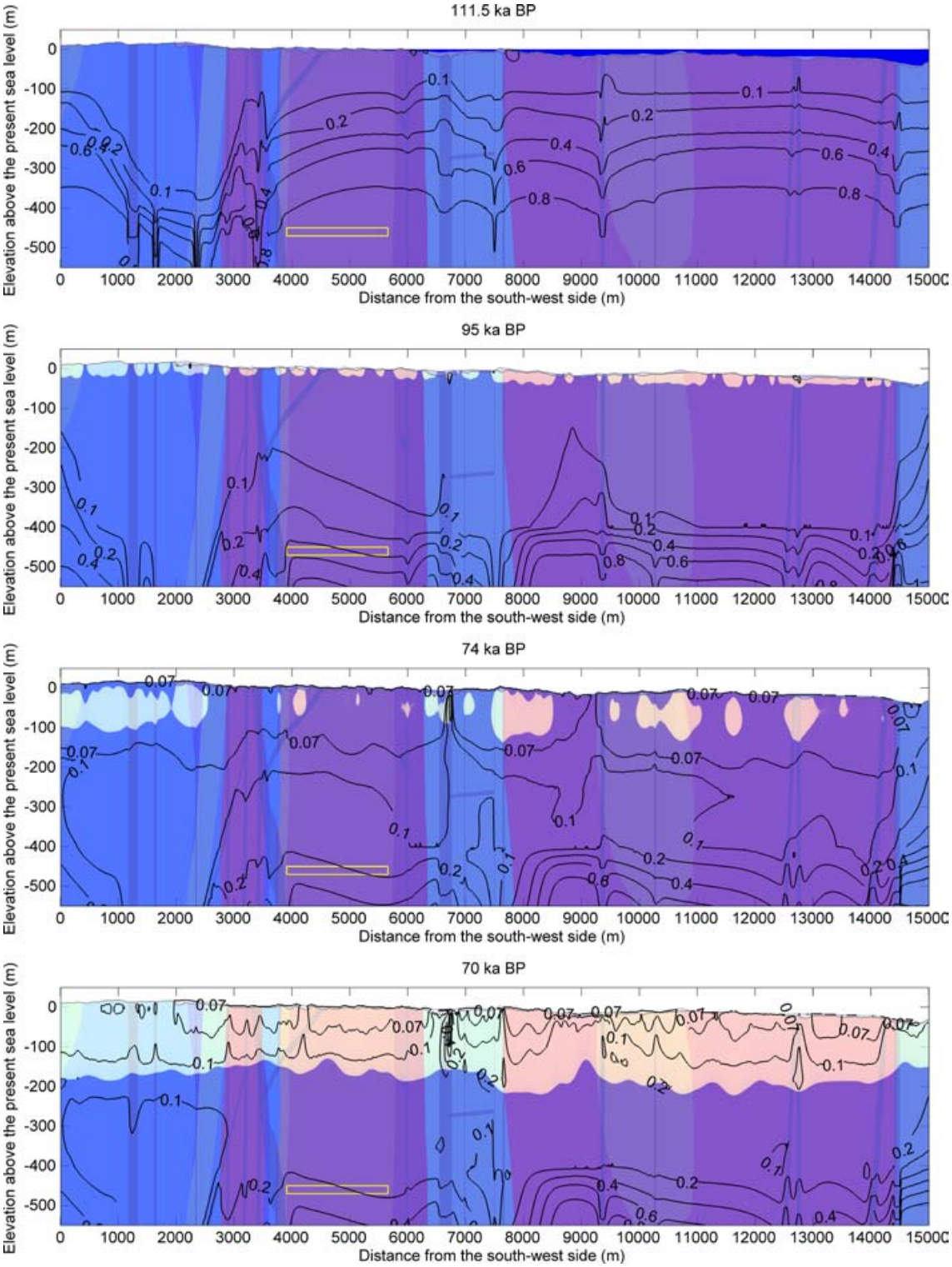

Figure 5-31. *Salinity concentration isochors 0.07, 0.1, 0.2, 0.4, 0.6, 0.8, 1, 1.2, 1.5, 2, 3, 4, 5 mass-% at times 111.5, 95, 74, 70 ka BP for the humid variant of the Repetition of last glacial cycle case. The light colour shows the extent of perennially frozen ground, and colour blue on the top of the profile at 111.5 ka BP illustrates the Baltic Sea.*

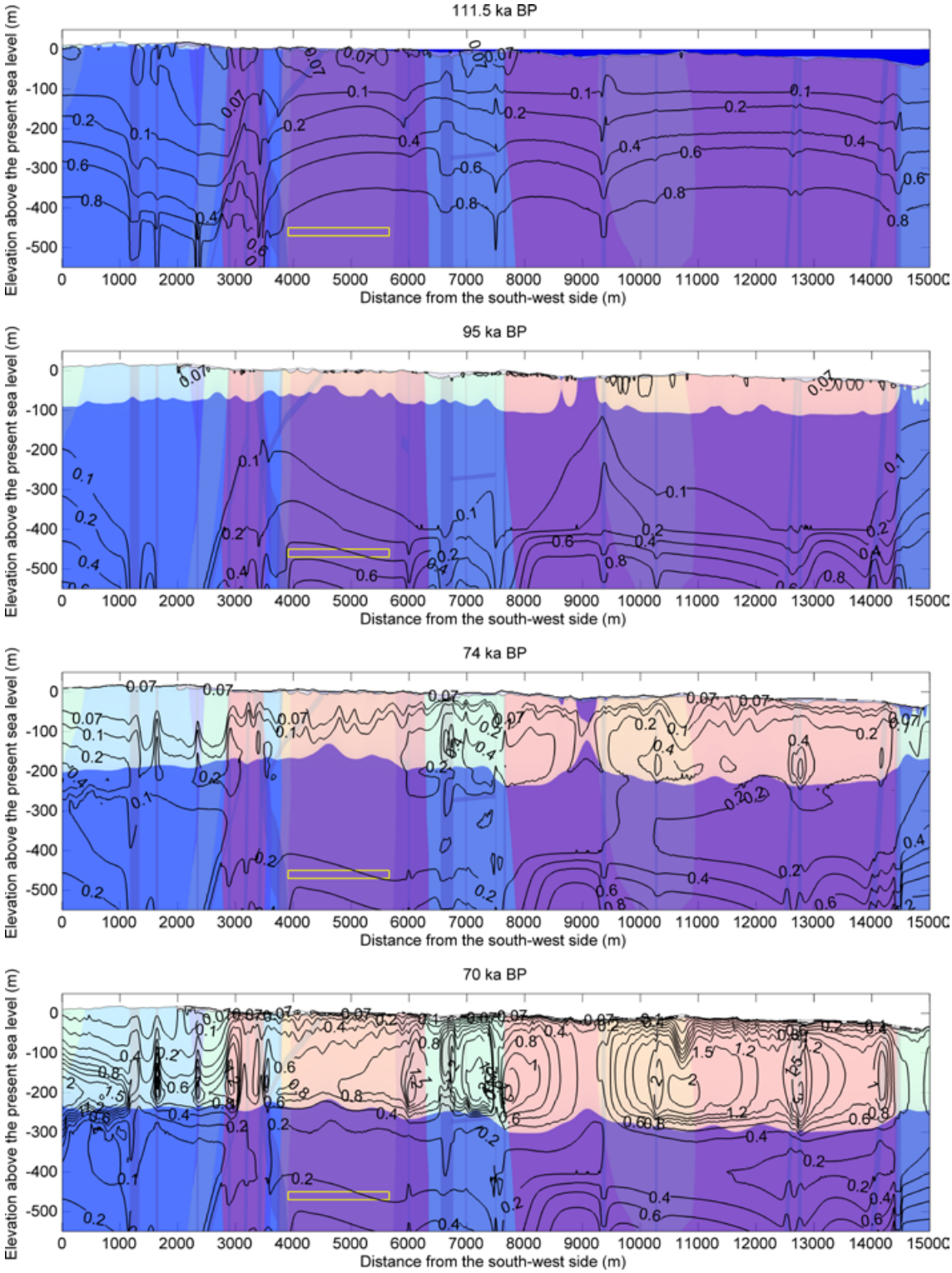

Figure 5-32. *Salinity concentration isochors 0.07, 0.1, 0.2, 0.4, 0.6, 0.8, 1, 1.2, 1.5, 2, 3, 4, 5 mass-% at times 111.5, 95, 74, 70 ka BP for the dry variant of the Repetition of last glacial cycle case. The light colour shows the extent of perennially frozen ground, and colour blue on the top of the profile at 111.5 ka BP illustrates the Baltic Sea.*

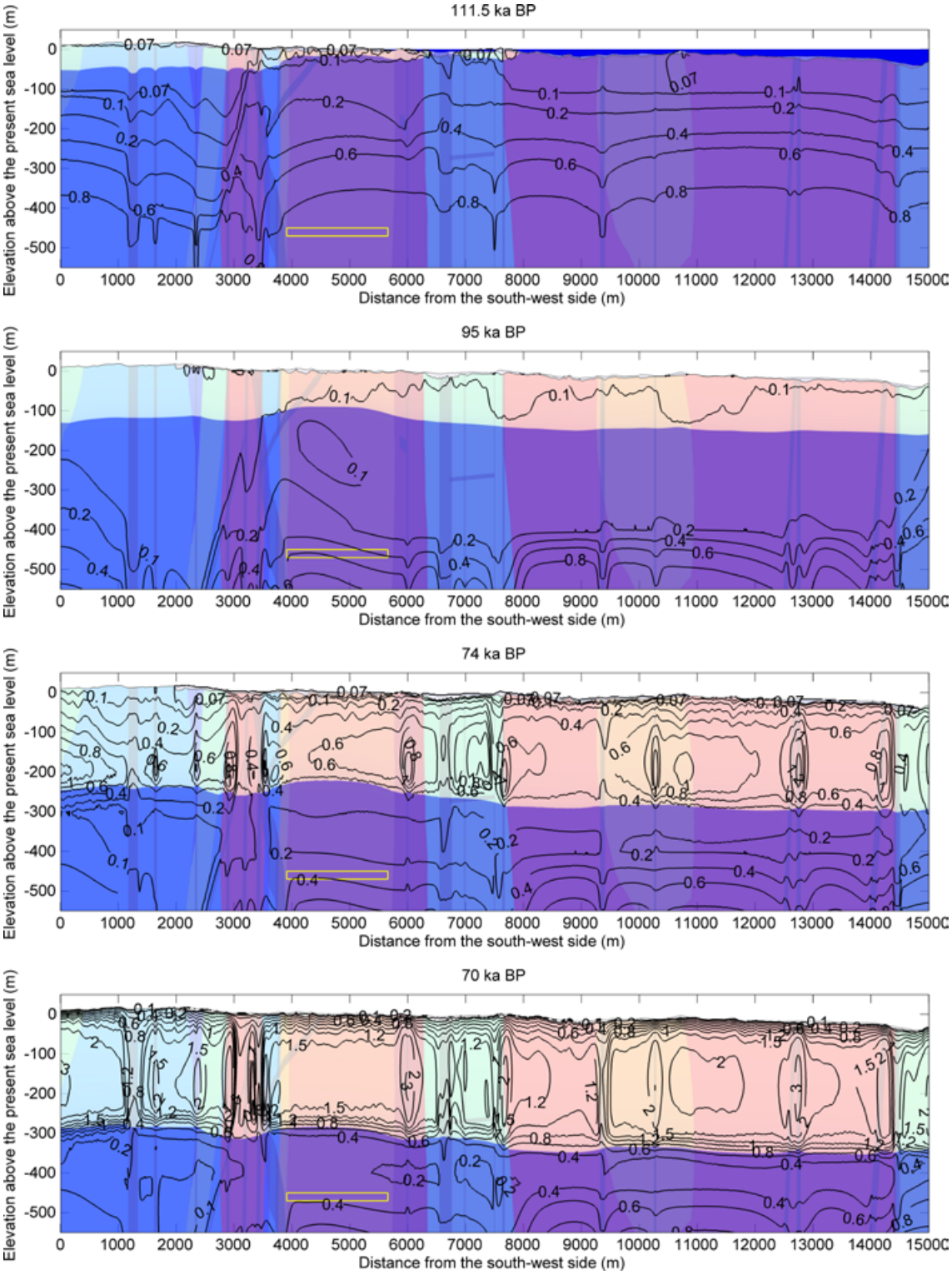

Figure 5-33. *Salinity concentration isochors 0.07, 0.1, 0.2, 0.4, 0.6, 0.8, 1, 1.2, 1.5, 2, 3, 4, 5 mass-% at times 111.5, 95, 74, 70 ka BP for the humid variant of the Severe permafrost case. The light colour shows the extent of perennially frozen ground, and colour blue on the top of the profile at 111.5 ka BP illustrates the Baltic Sea.*

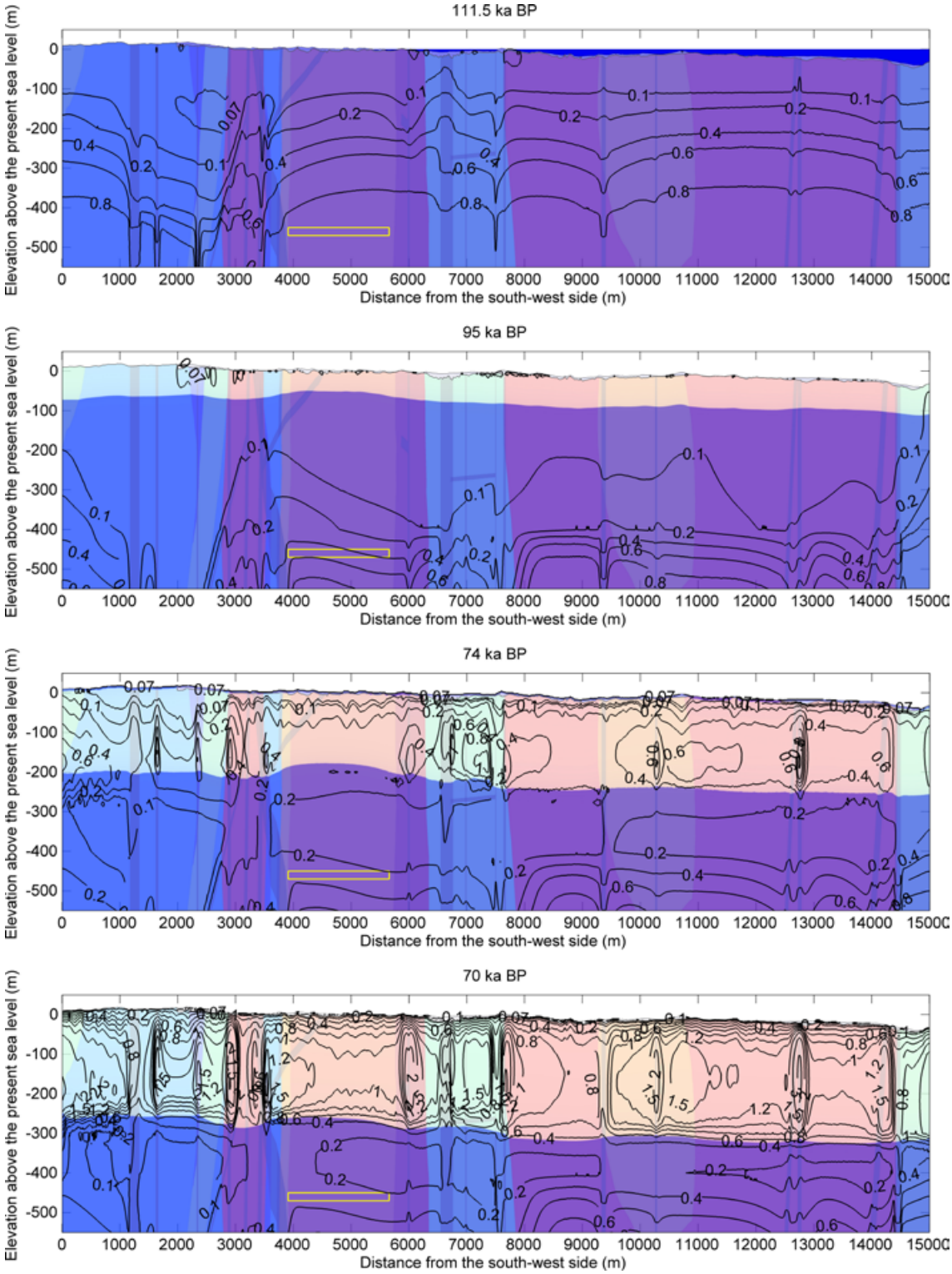

Figure 5-34. *Salinity concentration isochors 0.07, 0.1, 0.2, 0.4, 0.6, 0.8, 1, 1.2, 1.5, 2, 3, 4, 5 mass-% at times 111.5, 95, 74, 70 ka BP for the dry variant of the Severe permafrost case. The light colour shows the extent of perennially frozen ground, and colour blue on the top of the profile at 111.5 ka BP illustrates the Baltic Sea.*

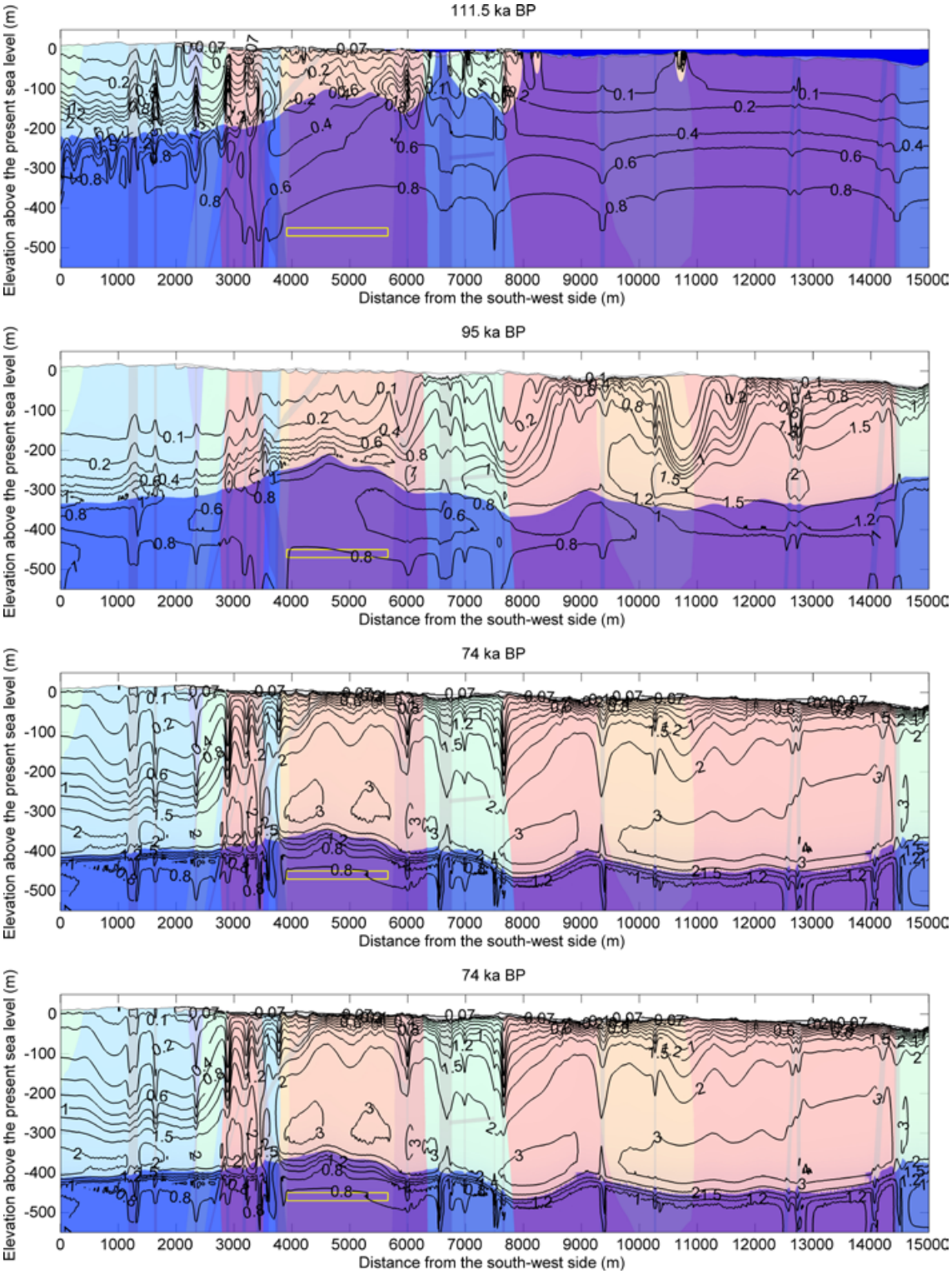

Figure 5-35. *Salinity concentration isochors 0.07, 0.1, 0.2, 0.4, 0.6, 0.8, 1, 1.2, 1.5, 2, 3, 4, 5 mass-% at times 111.5, 95, 74, 70 ka BP for the dry variant of Repetition of last glacial cycle case and air temperature decreased by 8°C. The light colour shows the extent of perennially frozen ground, and colour blue on the top of the profile at 111.5 ka BP illustrates the Baltic Sea.*

5.2 Sensitivity simulations

Case 1 – Uncertainty in air temperature

The evolution of maximum permafrost depth and maximum depth of perennially frozen ground over the repository for the *Repetition of last glacial cycle* case considering mean subsurface thermal conditions and the air temperature changed by −6, 0 and +6°C are shown in Figure 5-36.

The evolution of maximum 0°C isotherm depth, i.e. maximum permafrost depth, and maximum depth of perennially frozen ground over the repository and the whole profile for the dry variant of the *Repetition of last glacial cycle* case considering mean subsurface thermal conditions and the air temperature changed by −4, −6, −8, −10, −12, −14 and −16°C are shown in Figure 5-37 and Figure 5-38, respectively. The evolution of maximum −2°C and −4°C isotherm depth over the repository are shown in Figure 5-39 and Figure 5-40, respectively. It can be seen that temperature shifts of ~8, ~10 and ~14°C are needed to get the 0°C, −2°C and −4°C isotherms to reach the repository at the time with deepest permafrost at 70,000 years BP.

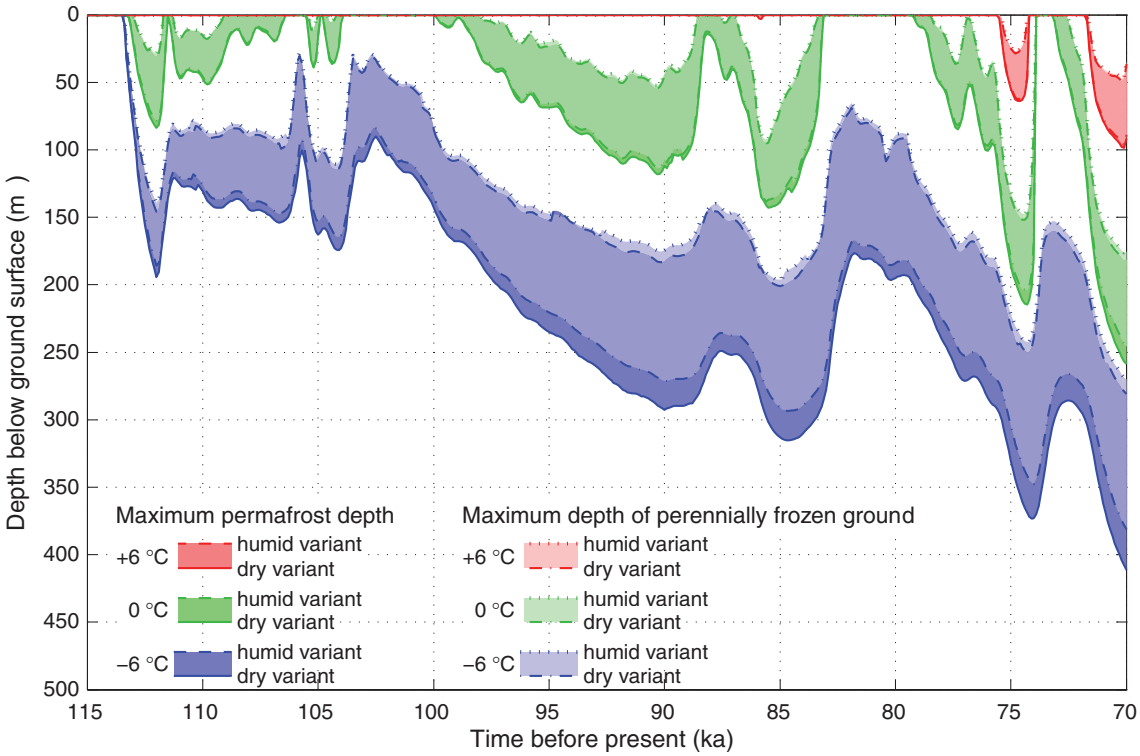

Figure 5-36. *Evolution of maximum permafrost depth (solid lines) and maximum depth of perennially frozen ground (dashed lines) over the repository for the Repetition of last glacial cycle case considering mean subsurface thermal conditions and the air temperature curve shifted by −6, 0 and +6°C. The shaded area in blue and red represents the range within which a result is expected to lie when considering surface conditions between the dry and humid variants of the Repetition of last glacial cycle case. The results for permafrost and perennially frozen ground overlap to a large degree.*

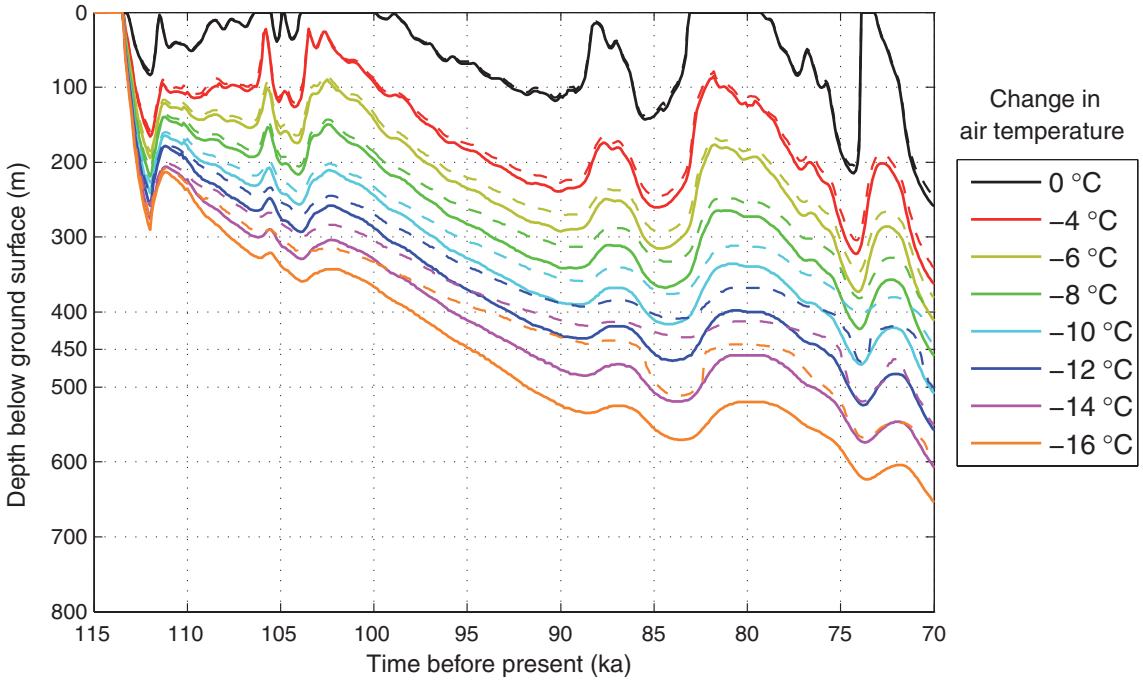

Figure 5-37. *Evolution of maximum permafrost depth (solid lines) and maximum depth of perennially frozen ground (dashed lines) over the repository for the dry variant of the Repetition of last glacial cycle case and the air temperature curve shifted by −4, −6, −8, −10, −12, −14 and −16°C.*

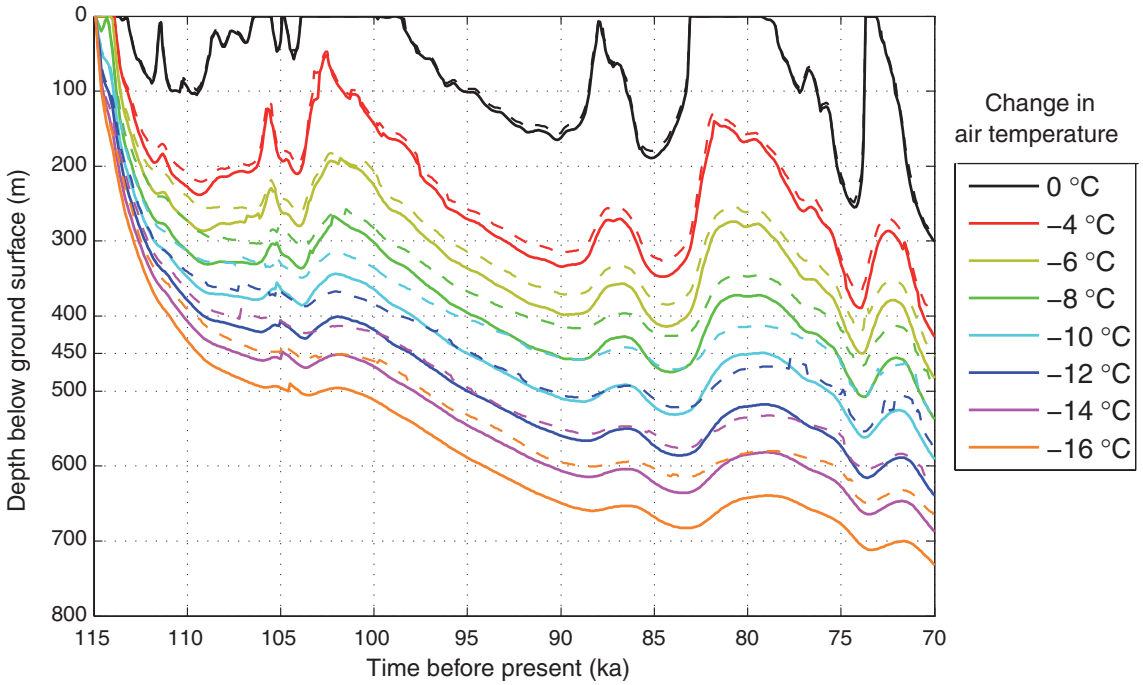

Figure 5-38. *Evolution of maximum permafrost depth (solid lines) and maximum depth of perennially frozen ground (dashed lines) over the whole profile for the dry variant of the Repetition of last glacial cycle case and the air temperature curve shifted −4, −6, −8, −10, −12, −14 and −16°C.*

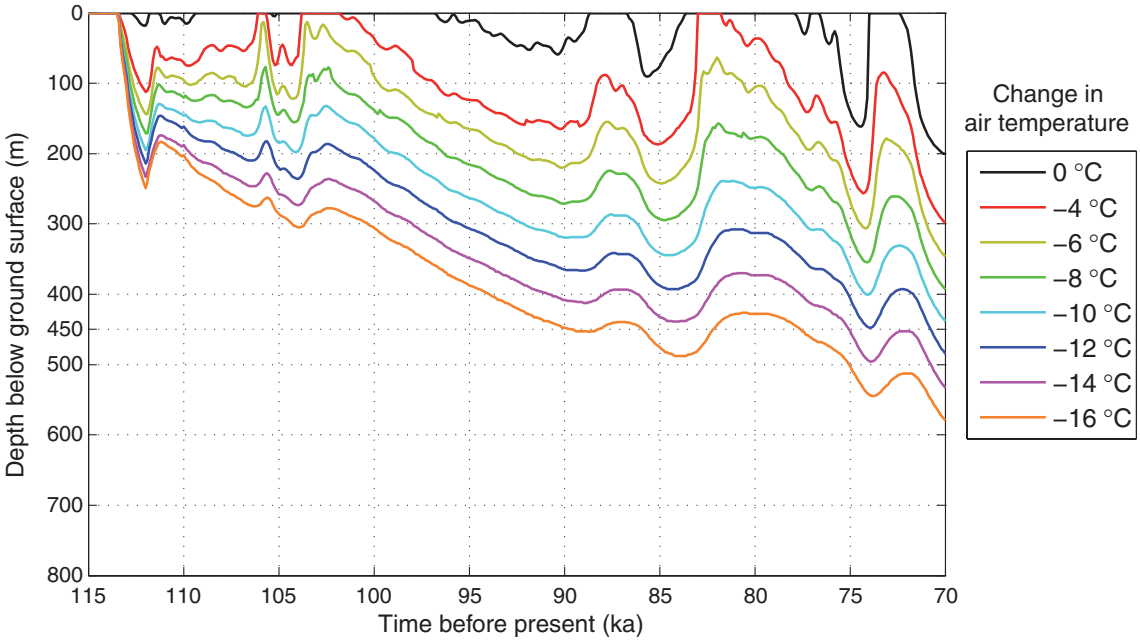

Figure 5-39. *Evolution of maximum −2°C -isotherm depth over the repository for the dry variant of the Repetition of last glacial cycle case and the air temperature curve shifted by −4, −6, −8, −10, −12, −14 and −16°C.*

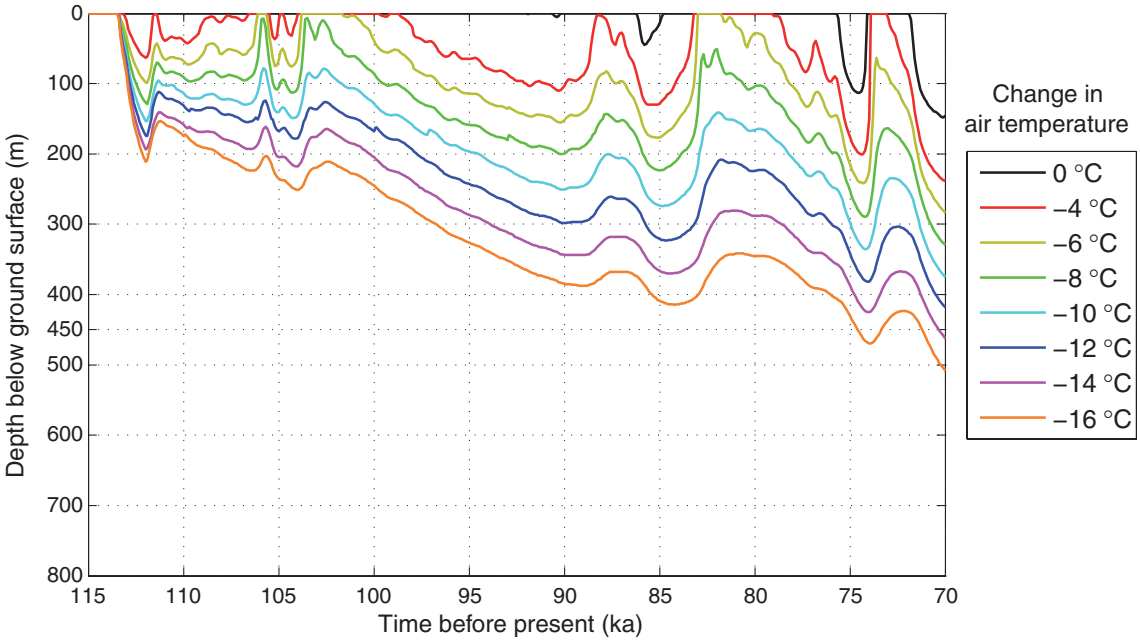

Figure 5-40. *Evolution of maximum −4°C -isotherm depth over the repository for the dry variant of the Repetition of last glacial cycle case and the air temperature curve shifted by −4, −6, −8, −10, −12, −14 and −16°C.*

Case 2 – Uncertainty in geothermal heat flow

The evolution of maximum permafrost depth and maximum depth of perennially frozen ground over the repository for the dry variant of the *Repetition of last glacial cycle* case considering variable geothermal heat flow as described in Table 2-3, Section 2.2, see also /Sundberg et al. 2009/, are illustrated in Figure 5-41. The calculated range for the maximum permafrost depth at 70,000 years BP is 243–280 m and 232–265 m for the maximum depth of perennially frozen ground.

Case 3 – Uncertainty in thermal conductivity

The evolution of maximum permafrost depth and maximum depth of perennially frozen ground over the repository for the dry variant of the *Repetition of last glacial cycle* case considering variable thermal conductivity as described in Table 2-1 and Table 2-2, Section 2.2, see also Appendix E, are shown in Figure 5-42. The uncertainty range for the maximum permafrost depth at 70,000 years BP is 247–266 m and 236–253 m for the maximum depth of perennially frozen ground.

Case 4 – Uncertainty in thermal diffusivity

The evolution of maximum permafrost depth and maximum depth of perennially frozen ground over the repository for the dry variant of the *Repetition of last glacial cycle* case considering variable thermal diffusivity as described in Table 2-1 and Table 2-2, Section 2.2, see also Appendix E, are shown in Figure 5-43. The calculated range for the maximum permafrost depth at 70,000 years BP is 243–268 m and 232–254 m for the maximum depth of perennially frozen ground.

The evolution of maximum permafrost depth and maximum depth of perennially frozen ground over the repository for the dry variant of the *Repetition of last glacial cycle* case considering mixed thermal diffusivities with highest difference for adjacent rock domains is shown in Figure 5-44. The results keep in the range for absolute minimum and maximum thermal diffusivities.

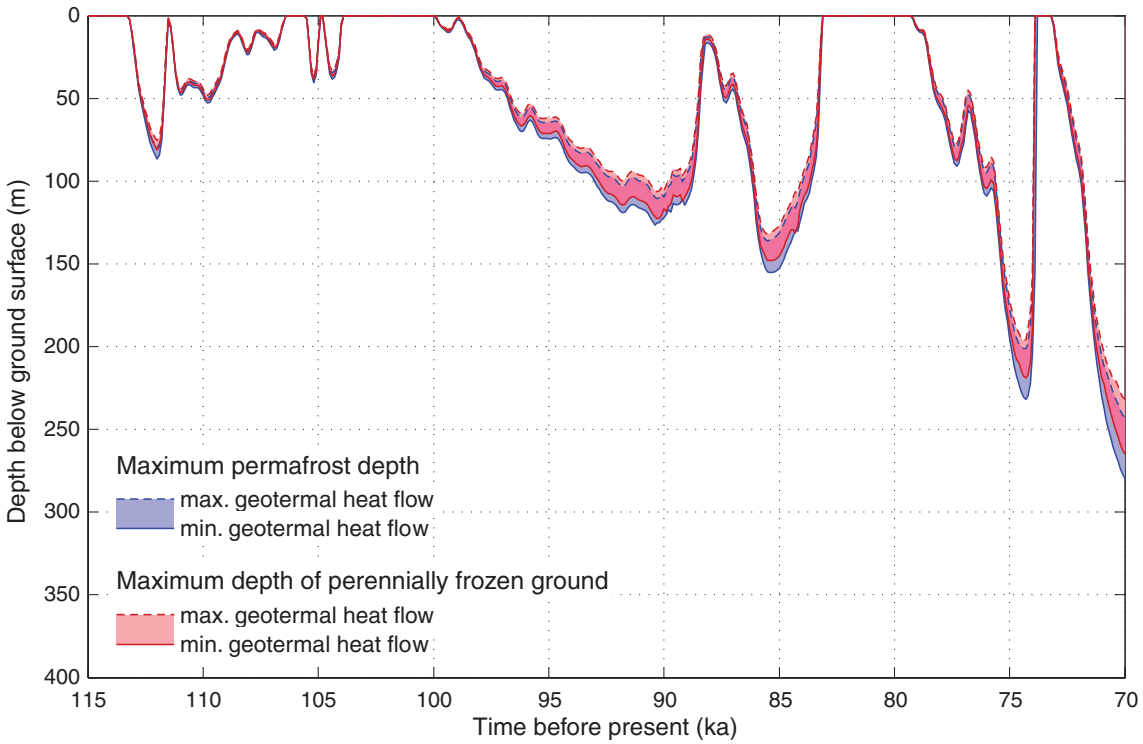

Figure 5-41. *Evolution of maximum permafrost depth and maximum depth of perennially frozen ground over the repository for the dry variant of the Repetition of last glacial cycle case considering uncertainty in geothermal heat flow. The shaded area in blue and red represents the range within which a result is expected to lie when considering geothermal heat flow between the minimum and maximum values. The lilac colour indicates that the results for permafrost and perennially frozen ground overlap to a large degree.*

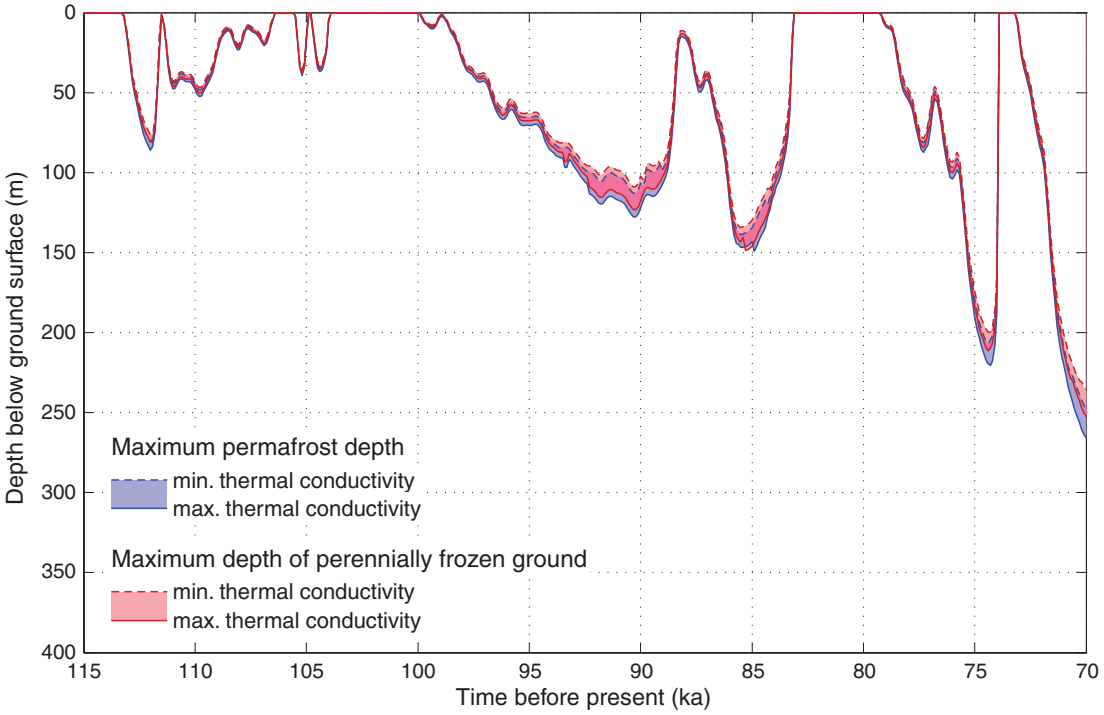

Figure 5-42. *Evolution of maximum permafrost depth and maximum depth of perennially frozen ground over the repository for the dry variant of the Repetition of last glacial cycle case considering uncertainty in thermal conductivity. The shaded area in blue and red represents the range within which a result is expected to lie when considering thermal conductivities between the minimum and maximum values. The lilac colour indicates that the results for permafrost and perennially frozen ground overlap to.*

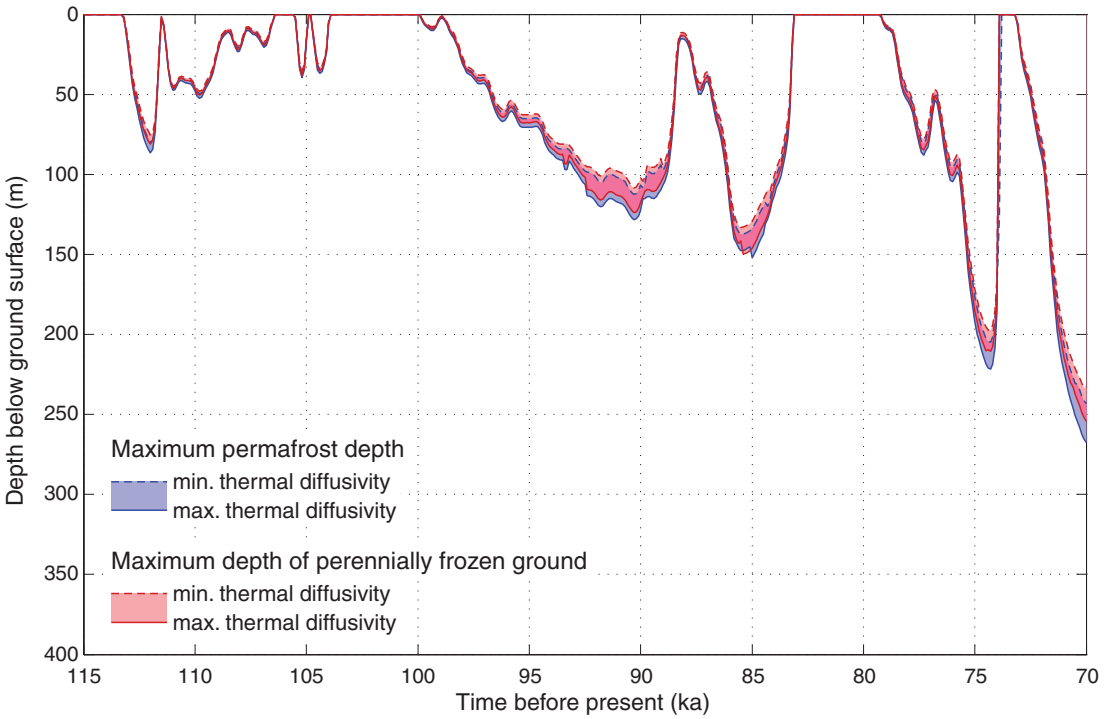

Figure 5-43. *Evolution of maximum permafrost depth and maximum depth of perennially frozen ground over the repository for the dry variant of the Repetition of last glacial cycle case considering uncertainty in thermal diffusivity. The shaded area in blue and red represents the range within which a result is expected to lie when considering thermal diffusivities between the minimum and maximum values. The lilac colour indicates that the results for permafrost and perennially frozen ground overlap.*

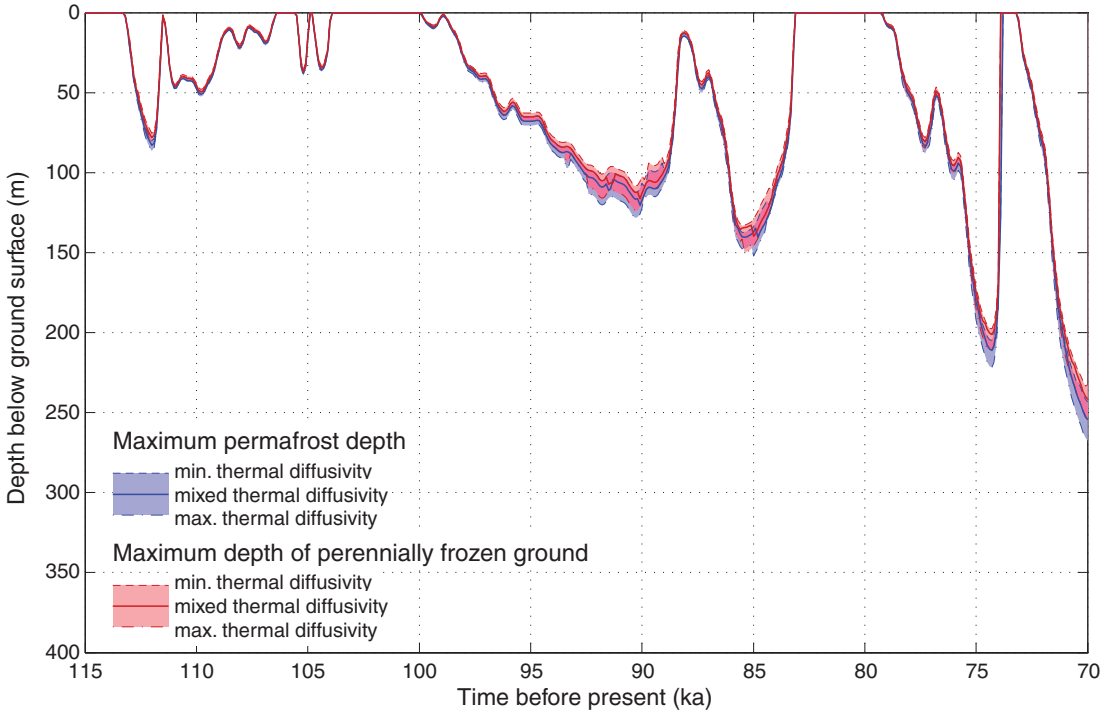

Figure 5-44. *Evolution of maximum permafrost depth and maximum depth of perennially frozen ground over the repository for the dry variant of the Repetition of last glacial cycle case considering mixed thermal diffusivities with highest difference for adjacent rock domains. The shaded area in blue and red represents the range within which a result is expected to lie when considering thermal diffusivities between the minimum and maximum values. The lilac colour indicates that the results for permafrost and perennially frozen ground overlap.*

Case 5 – Combination of uncertainties in subsurface thermal conditions

The evolution of maximum permafrost depth and maximum depth of perennially frozen ground over the repository for the dry variant of the *Repetition of last glacial cycle* case considering variable geothermal heat flow and thermal diffusivity as described in Case 5, Section 4.2.2 are shown in Figure 5-45. The calculated range for the maximum permafrost depth at 70,000 years BP is 231–289 m and 223–274 m for the maximum depth of perennially frozen ground.

Case 6 – Combination of uncertainties in surface conditions and subsurface thermal conditions

Figure 5-46 shows the evolution of maximum permafrost depth, maximum depth of perennially frozen ground and maximum depth of –2 and −4°C isotherms over the repository for the *Repetition of last glacial cycle* case considering combined uncertainties in surface conditions and subsurface thermal conditions as described in Section 2.2 and Section 2.4, see also Appendix E, I and J. The calculated range for the maximum permafrost depth at 70,000 years BP is 163–289 m and 159–274 m for the maximum depth of perennially frozen ground.

The results for the evolution of maximum permafrost depth, maximum depth of perennially frozen ground and maximum depth of –2 and −4°C isotherms over the repository for the Severe permafrost case are shown in Figure 5-47. The calculated range for the maximum permafrost depth at 21,500 years BP is 309–456 m and 279–408 m for the maximum depth of perennially frozen ground at 21,600 years BP.

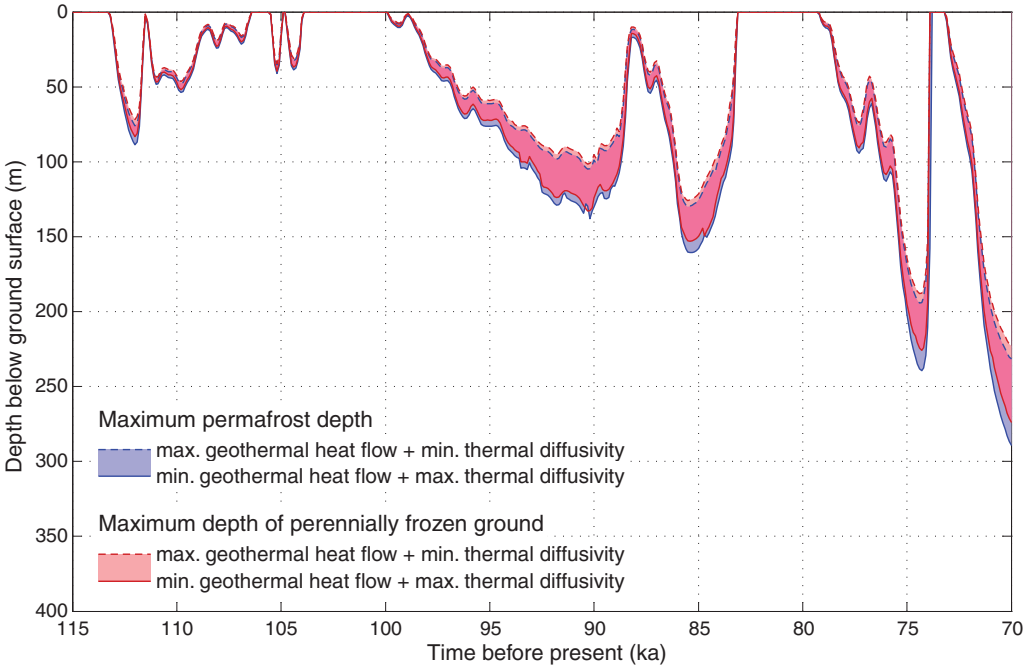

Figure 5-45. *Evolution of maximum permafrost depth and maximum depth of perennially frozen ground over the repository for the dry variant of the Repetition of last glacial cycle case considering combined uncertainty in thermal conditions. The shaded area in blue and red represents the range within which a result is expected to lie when considering thermal conditions between the values enhancing and diminishing permafrost development most. The lilac colour indicates that the results for permafrost and perennially frozen ground overlap.*

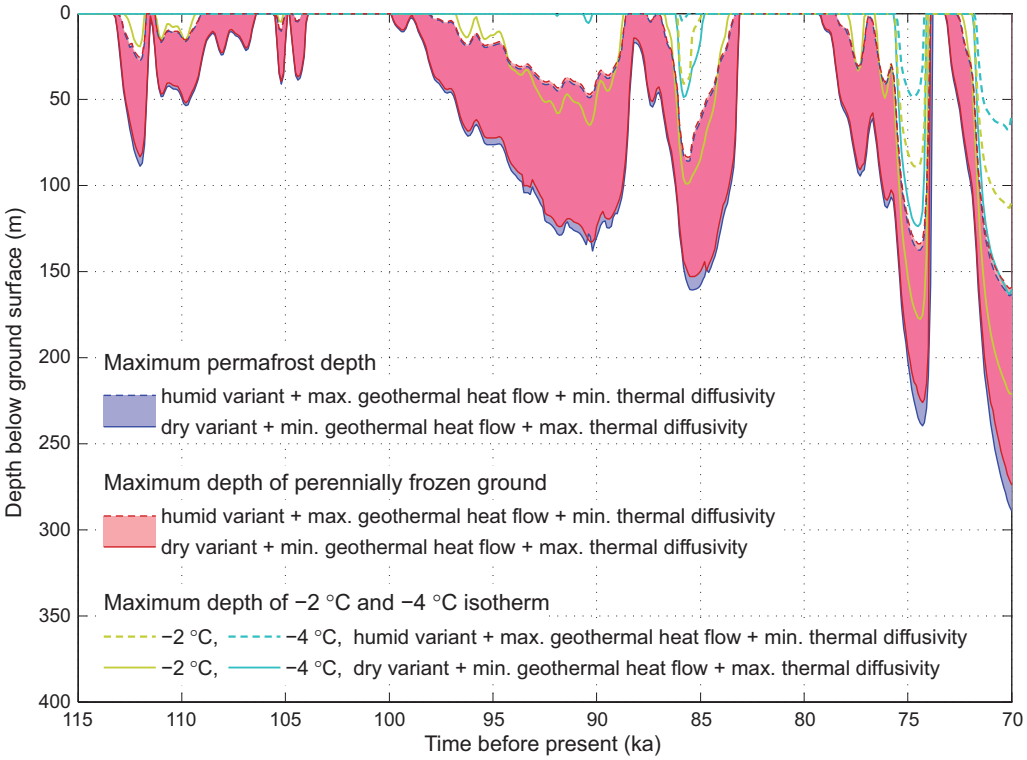

Figure 5-46. *Evolution of maximum permafrost depth, maximum depth of perennially frozen ground and maximum depth of −2 and −4°C isotherms over the repository for the Repetition of last glacial cycle case considering combined uncertainties in surface conditions and subsurface thermal conditions. The shaded area in blue and red represents the range within which a result is expected to lie when considering surface conditions and subsurface thermal conditions between the values enhancing and diminishing permafrost development most. The lilac colour indicates that the results for permafrost and perennially frozen ground overlap.*

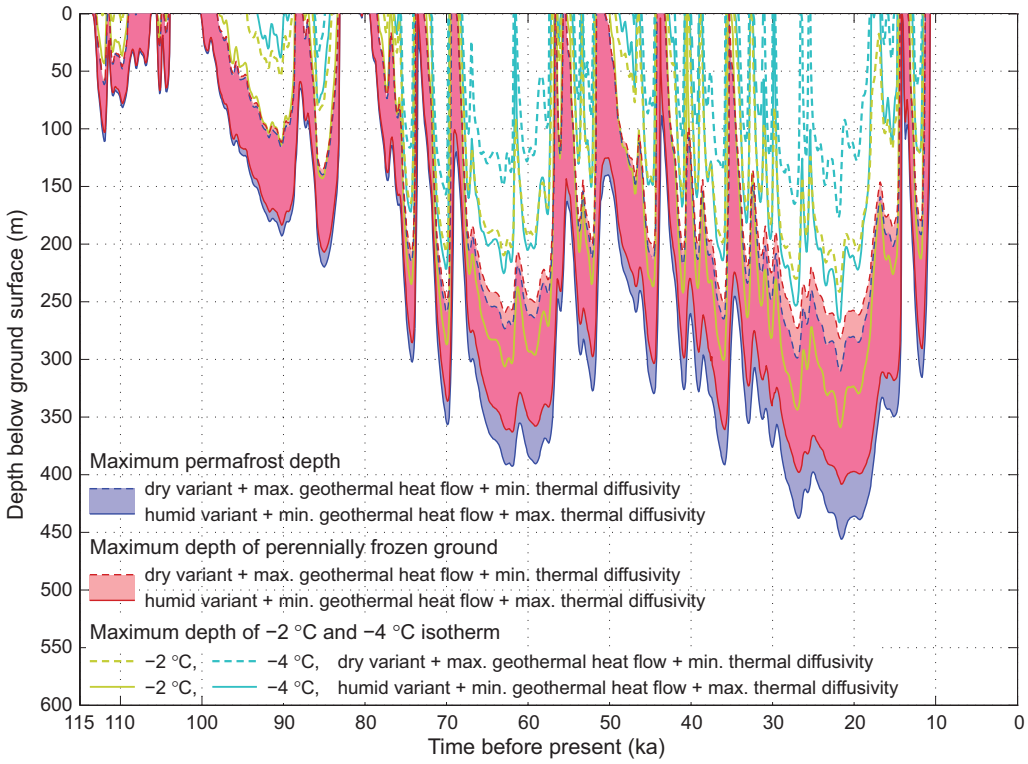

Figure 5-47. *Evolution of maximum permafrost depth, maximum depth of perennially frozen ground and maximum depth of −2 and −4°C isotherms over the repository for the Severe permafrost case considering combined uncertainties in surface conditions and subsurface thermal conditions. The shaded area in blue and red represents the range within which a result is expected to lie when considering surface conditions and subsurface thermal conditions between the values enhancing and diminishing permafrost development most. The lilac colour indicates that the results for permafrost and perennially frozen ground overlap.*

Case 7 – Combination of uncertainties in air temperature, surface conditions and subsurface thermal conditions

Figure 5-48 shows the evolution of maximum permafrost depth, maximum depth of perennially frozen ground and maximum depth of –2 and −4°C isotherms over the repository for the *Repetition of last glacial cycle* case considering combined uncertainties in air temperature, surface conditions and subsurface thermal conditions as described in Section 2.2 and Section 2.4, see also Appendix E, H, I and J. The calculated overall range for the maximum permafrost depth at 70,000 years BP is 32–463 m, while the maximum depth of perennially frozen ground at the same time reaches 30–422 m.

Case 8 – Heat from the repository

The evolution of maximum permafrost depth and maximum depth of perennially frozen ground over the repository for the dry variant of the *Repetition of last glacial cycle* case considering variable heat production from the repository from zero to the reference value as described in Section 2.3, see also Appendix G, are illustrated in Figure 5-49. The calculated range for the maximum permafrost depth at 70,000 years BP is 259–295 m and 246–280 m for the maximum depth of perennially frozen ground.

Case 9 – Convective heat transfer

The evolution of maximum permafrost depth and maximum depth of perennially frozen ground over the repository for the dry variant of the *Repetition of last glacial cycle* case considering mean subsurface thermal conditions, and with and without groundwater flow and salinity transport are illustrated in Figure 5-50. The results for the permafrost depth are considerably close to each other. The deviation in the maximum permafrost depth at 70,000 years BP is negligible small (~0.1 m) – the maximum value is ~260 m, while the deviation in the maximum depth of perennially frozen ground at the same time is little larger, i.e. 240–246 m.

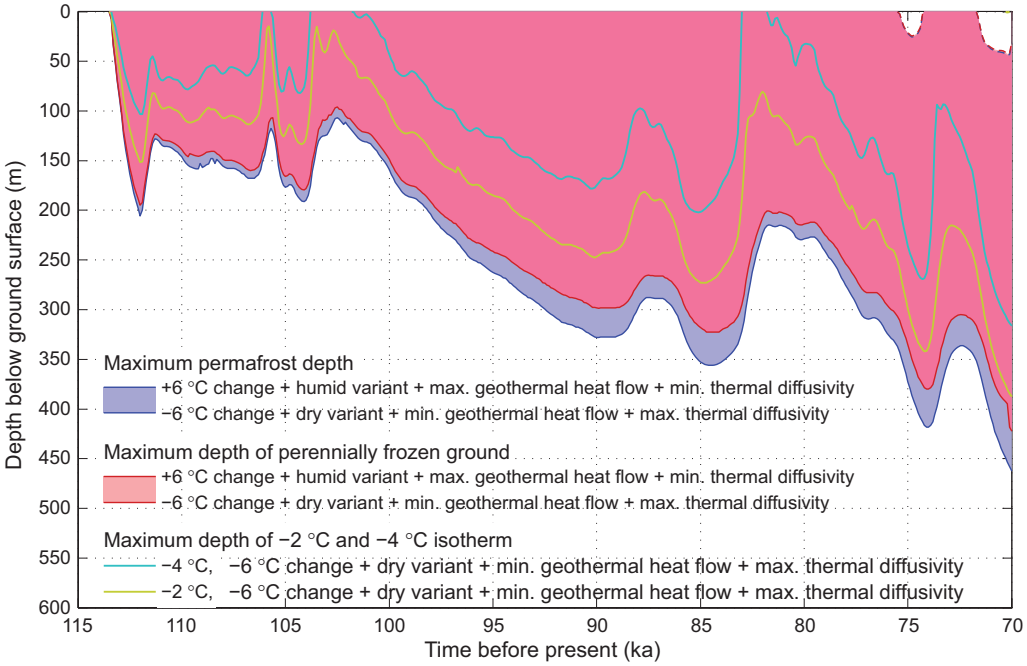

Figure 5-48. *Evolution of maximum permafrost depth, maximum depth of perennially frozen ground and maximum depth of –2 and −4°C isotherms over the repository for the Repetition of last glacial cycle case considering the unlikely case of combined largest uncertainties in air temperature, surface conditions and subsurface thermal conditions enhancing and diminishing permafrost growth most. The shaded area in blue and red represents the range within which a result is expected to lie. The lilac colour indicates that the results for permafrost and perennially frozen ground overlap.*

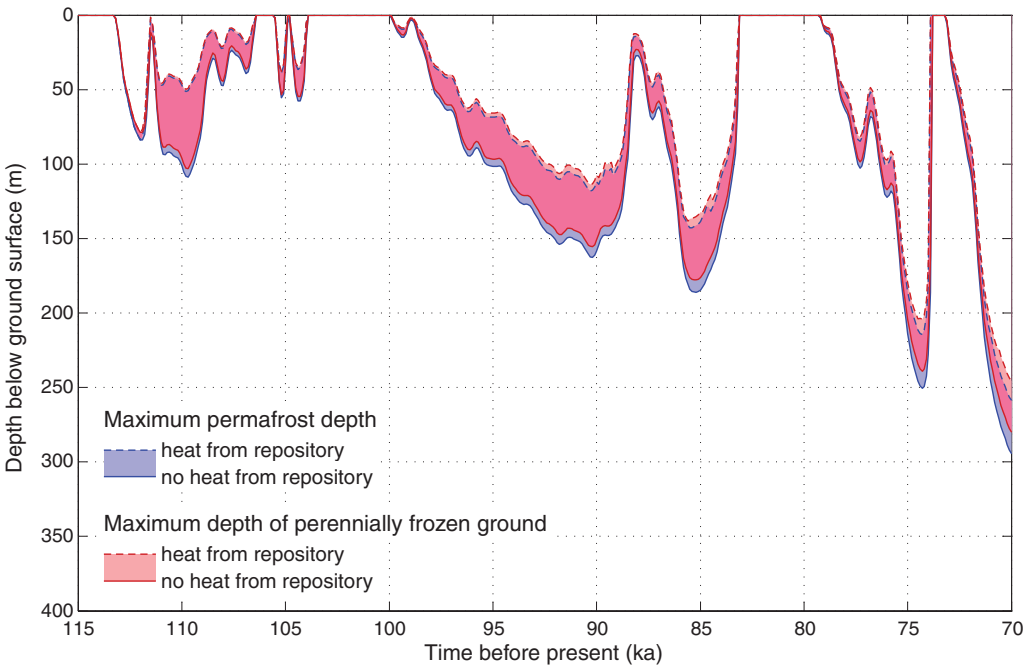

Figure 5-49. *Evolution of maximum permafrost depth and maximum depth of perennially frozen ground over the repository for the dry variant of the Repetition of last glacial cycle case considering mean thermal properties and variable heat production from the repository from zero to the reference value. The shaded area in blue and red represents the range within which a result is expected to lie when considering heat production from the repository between the zero and reference amounts. The lilac colour indicates that the results for permafrost and perennially frozen ground overlap.*

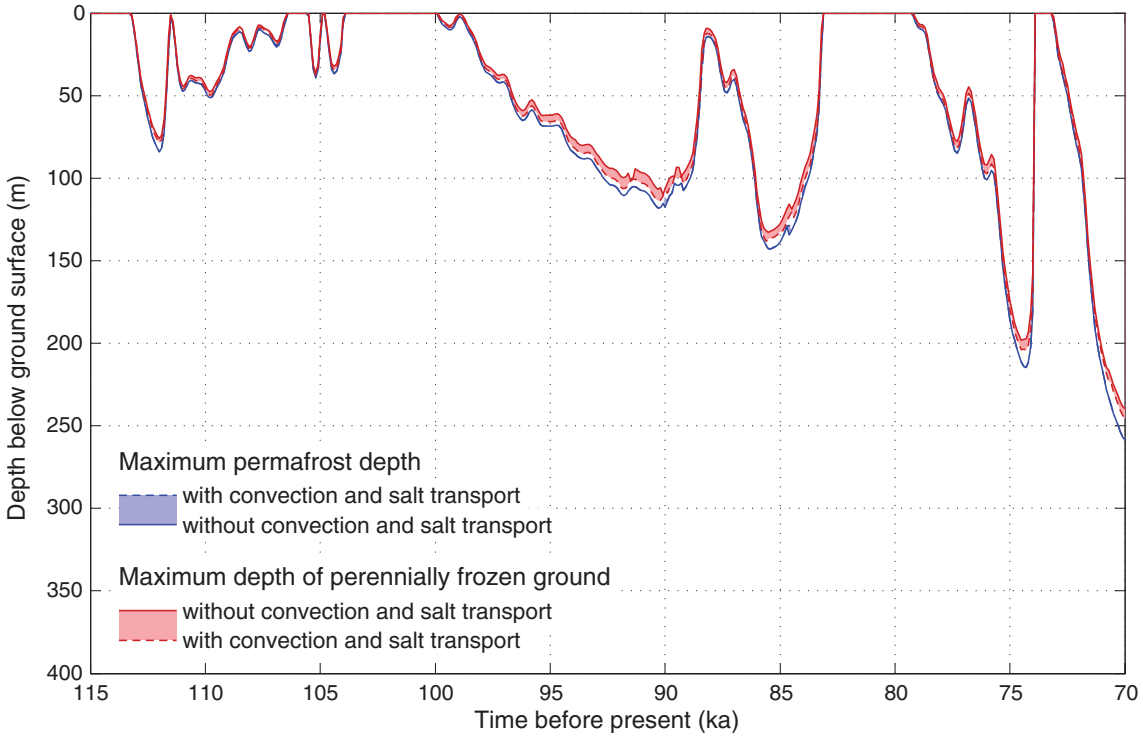

Figure 5-50. *Evolution of maximum permafrost depth and maximum depth of perennially frozen ground over the repository for the dry variant of the Repetition of last glacial cycle case considering mean subsurface thermal conditions, and with and without groundwater flow and salinity transport. The shaded area in blue and red represents the range within which a result is expected to lie when considering groundwater flow and salt transport between the reference case and case without groundwater flow and salt transport. The lilac colour indicates that the results for permafrost and perennially frozen ground overlap.*

6 Discussion and conclusions

Main simulations

The main objective of the present study was to investigate impacts of surface and subsurface conditions on the development of permafrost and perennially frozen ground at Forsmark using site specific information on climate and landscape including features of water bodies and topography, as a complement to the previous 1D permafrost studies made for Forsmark (SKB 2006, Section 3.4 and 4.4.1). An approach based on the Topographical Wetness Index (TWI) to describe the vegetation and snow cover in relation to the prevailing climate and surface moisture conditions was introduced. TWI was used to locate four relevant surface condition types, dry, moist-humid, wet and peatland, that could be expected to occur on the profile in *Boreal*, *Subarctic* and *Arctic* climate zones. Thereafter, the ground surface temperatures were deduced from the air temperature by making use of *n*-factors that yield a statistical relation between the air and ground surface temperatures in consideration of climate and surface moisture conditions. Due to considerable uncertainties related in description of surface conditions by TWI and modelling of ground surface temperatures by means of *n*-factors, two variants, a humid one and a dry one, for the climate cases *Repetition of last glacial cycle* and *Severe permafrost* were considered. Moreover, in order to describe the site specific spatial variation of surface conditions that controls the areal distribution of permafrost and perennially frozen ground, the modelling was carried out in 2D.

The modelling results for the *Repetition of last glacial cycle* case show that annual mean ground surface temperature can vary considerably in time and location depending on the climate zone and surface moisture condition type (Figures 2-11 to 2-14, Figure 2-16). In the time frame of consideration, the dry surface condition resulted in ground surface temperatures below −11°C at lowest in the *Arctic* climate zone and over +6°C at highest in the *Boreal* climate zone (Figure 2-13). The wet surface condition yielded milder ground surface temperatures in both the *Arctic* and *Boreal* climate zones ranging from under −3°C to over +5°C over the same time period (Figure 2-11). Further, the peatland condition, having the moistest surface conditions, resulted in even milder ground surface temperatures ranging approximately between −2°C and +4°C (Figure 2-14). In addition, the difference in ground surface temperature could be several degrees from place to place along the profile (Figure 2-16). The spatial fluctuation in ground surface temperature is largest in the *Arctic* climate zone when the air temperature is lowest, and lowest in the boreal climate zone when air temperature is close to 0°C.

The simulation results (Figures 5-1 to 5-4, Figure 5-6, Figure 5-8) demonstrate that discontinuous permafrost development is characteristic for the humid variant of the *Repetition of the last glacial cycle* case while continuous permafrost development prevails for the dry variant, as well as for the dry and humid variants of the *Severe permafrost* case. In all cases permafrost turned to continuous spatial distribution when annual mean air temperature decreases below −6°C and the maximum permafrost depth exceeds a depth of ~50 m. In addition, sporadic permafrost distribution was detected at around 74,000 years BP when the deep permafrost quickly degraded in ~1,000 years.

The variation in ground surface temperature has the strongest effect on ground temperature fluctuation within the upper part of the vertical profile (Figures 5-9 to 5-24). The fluctuation is largest at the surface and reduces considerably with depth except where the heat from the repository influences (Figure 5-10, 5-14, 5-18 and 5-22).

Regarding the evolution of permafrost depth and depth of perennially frozen ground, the results for the *Repetition of the last glacial cycle* case considering variations in surface moisture conditions and mean thermal properties for the subsurface indicated that permafrost (defined by the 0°C isotherm) can reach a depth between ~180 m and ~260 m over the repository (Figure 5-5) and a depth between ~220 m and ~300 m outside the repository (Figure 5-6) in a time frame of 45,000 years. The maximum depth of perennially frozen ground can range between ~180 m and ~250 m over the repository and between ~210 m and ~300 m over the whole site at the same time.

For the *Severe permafrost* case, considering no vegetation and snow cover, no ice sheet formation and that the site remains above sea level throughout the glacial cycle, permafrost (the 0°C isotherm)

can reach a depth between ~360 m and ~390 m over the repository and between ~380 m and ~420 m outside the repository, in a time frame of 100,000 years. Meanwhile, the maximum depth of perennially frozen ground can vary between ~330 m and ~360 m over both the repository and the rest of the profile (Figure 5-7 and 5-8).

A comparison between results from the present 2D modelling for the *Repetition of the last glacial cycle* case and the corresponding 1D modelling simulation performed for SR-Can /SKB 2006, Section 3.4/ (Reference surface conditions of the base variant) shows a good agreement regarding the maximum permafrost depth at 70,000 years BP (Figure 6-1).

The formation of taliks was studied by means of the unfrozen amount of groundwater and groundwater flow. The results (Figures 5-25 to 5-30) show that under continuous permafrost conditions both the local and regional groundwater flow are reduced considerably in the perennially frozen ground but also in the unfrozen ground beneath permafrost. On the other hand, the results demonstrate that when the unfrozen groundwater content is greater than 10%, groundwater flow can occur through a continuous partially frozen permafrost zone, though the flow velocity is only some millimetres per year (Figure 5-26 and 5-27). This can indicate that under continuous permafrost conditions taliks are able to form under lakes through perennially frozen ground down to ~50 m depth, if favourable groundwater flow conditions with open flow paths prevail. When the freezing of ground is advanced to a degree with unfrozen water content under 10%, groundwater flow is reduced considerably, and thus a talik is not able to form or survive. The results also show that when a groundwater path is closed as deformation zone ZFMA2, mainly local groundwater circulation occurs. It is also quite evident that a 2D model is unsuitable for modelling talik formation properly, since the important 3D groundwater flow network is not included.

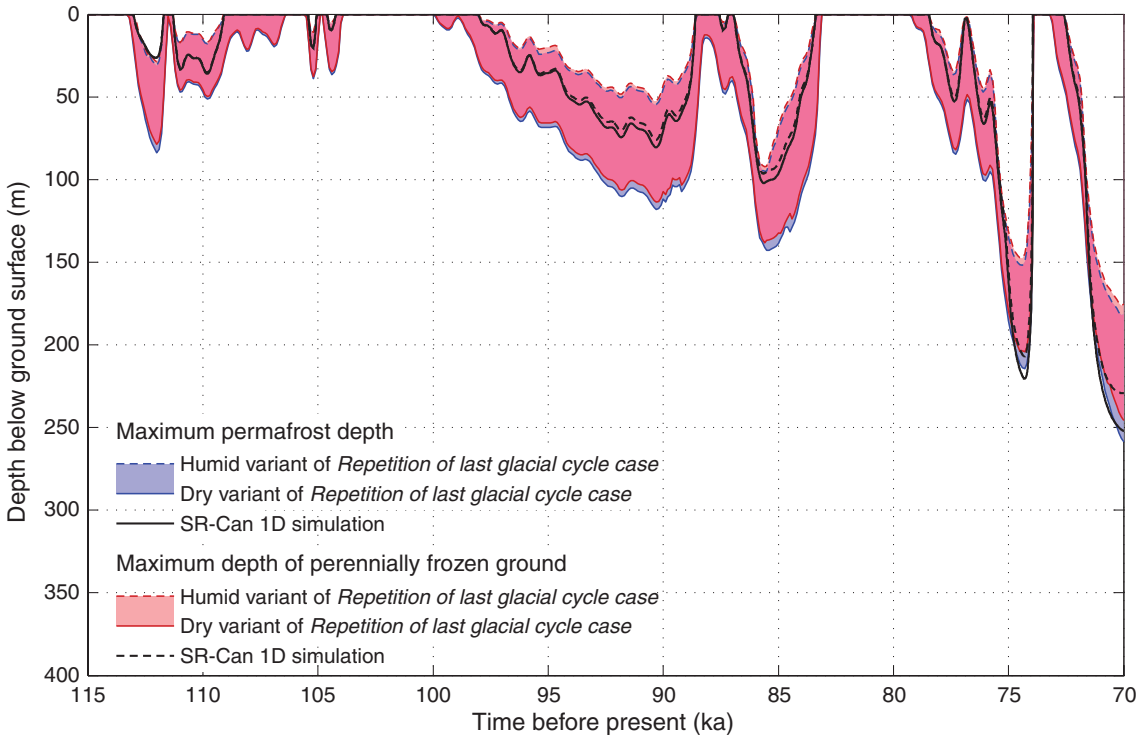

Figure 6-1. *Evolution of permafrost and frozen ground depth over the repository for the Repetition of last glacial cycle case of the present study, and for the reference surface conditions of the base variant of the preceding one for SR-Can /SKB 2006/. The shaded area in blue and red represents the range within which a result is expected to lie when considering surface conditions between the humid and dry climate variants of the Repetition of last glacial cycle case. The lilac colour indicates that the results for permafrost and perennially frozen ground overlap.*

Groundwater flow is an integral part of salinity transport modelling, which hence suffers from the same restrictions as the 2D groundwater flow modelling. However, the results for salinity concentration (Figures 5-32 to 5-35) show that freezing can induce salt exclusion and transport when perennially frozen ground development exceeds 200 m depth. This can be seen as increased salinity concentration extending downwards in front of the partially frozen bedrock. At shallow depths the impacts of freezing cannot be seen since the salinity concentration of groundwater has been diluted prior to the development of perennially frozen ground. The increased salinity concentration within the perennially frozen ground is mainly due to that salt transport occurs more slowly than the freezing zone advances.

Sensitivity analysis

In Case 1, uncertainties in air temperature were investigated for the *Repetition of the last glacial cycle* case by making constant changes in the air temperature. According to the results, the constant temperature change of −6°C in the air temperature can increase permafrost depth by 55 to 60% from the range of ~180–260 m to ~280–410 m while the constant temperature change of +6°C can reduce permafrost depth by 65 to 80% to range of ~40–90 m (Figure 5-36). A similar effect can be seen in the depth of perennially frozen ground, i.e. the temperature curve shift of −6°C results in a change from the range ~180–250 m to ~270–380 m, while a +6°C temperature shift reduces the range to ~30–90 m.

In addition, the results for the dry variant of the *Repetition of the last glacial cycle* case indicate that almost a 8°C colder climate is required to make permafrost reach the repository depth in 45,000 years (Figure 5-37), and that temperature shifts of ~10°C and ~14°C are needed to get the −2°C and −4°C isotherms to reach the repository at the same time (Figure 5-39 and 5-40). The large difference of up to more than 100 m between cases “over the repository” and “over the whole profile” (Figure 5-37 and 5-38) is mainly due to the heat from repository. The effect of topography is minor and further reduced with depth. A less important factor is that some rock domains (RFM026, RFM033, RFM034, RFM040) outside the repository have higher thermal conductivity (2.8%) than the one (RFM029) where the repository is located.

Regarding uncertainties in geothermal heat flow, the sensitivity analyses for the dry variant of the *Repetition of the last glacial cycle* case in Case 2 showed that a variation of –14% to +12% in geothermal heat flow can cause an approximate fluctuation of +8.0% to –6.3% (~280 m to ~240 m) in permafrost depth, and correspondingly an approximate fluctuation of +7.7% to –5.7% (~260 m to ~230 m) in the depth of perennially frozen ground (Figure 5-41).

In Case 3, the uncertainties in thermal properties of the subsurface were investigated by means of thermal conductivity and thermal diffusivity. The results for thermal conductivity indicated that the mean variation of –6.1% to +8.6% in thermal conductivity can cause an approximate fluctuation of –4.6% to +2.7% (~250 m to ~270 m) in permafrost depth, and correspondingly an approximate fluctuation of –4.1% to +2.7% (~240 m to ~250 m) in perennially frozen ground depth (Figure 5-42).

The uncertainty in thermal diffusivity causes a slightly larger variation in permafrost depth than solely the uncertainty in thermal conductivity. The results for Case 4 (Figure 5-43) demonstrate that the mean variation of –11.5% to +14.6% in thermal diffusivity can cause an approximate fluctuation of –6.0% to +3.4% (~240 m to ~270 m) in permafrost depth, and correspondingly an approximate fluctuation of –5.5% to +3.4% (~230 m to ~250 m) in perennially frozen ground depth. In addition, the variation in thermal properties between adjacent rock domains has a minor effect on the development of permafrost and perennially frozen ground (Figure 5-44). The reason for this is probably the flat topography of the site, due to which heat transfer takes place mainly vertically. This is also supported by the results for the ground temperature and perennially frozen ground (Figures 5-1 to 5-4) which show a rather uniform permafrost development with depth when it occurs in continuous format.

In Case 5, combinations of uncertainties related to subsurface thermal conditions were studied. The combination of the uncertainties regarding thermal conductivity, heat capacity and geothermal heat flow was investigated by means of values that gave the largest increase or decrease of permafrost. Based on e.g. the results from SR-Can /SKB 2006/, maximum thermal conductivity, minimum heat capacity and minimum geothermal heat flow were expected to be the most favourable parameters for permafrost development while minimum thermal conductivity, maximum heat capacity and maximum geothermal heat flow were assumed to act as the most unfavourable parameters. The results

(Figure 5-46) show that the combined uncertainties can cause a variation of –10.5% to +11.8% (~230 m to ~290 m) in the permafrost depth and a variation of –9.3% to +11.5% (~220 m to ~270 m) in the depth of perennially frozen ground.

Subsequently, the combination of uncertainties related to subsurface thermal properties and conditions and surface moisture conditions were studied in Case 6 in terms of the parameters of the previous case and humid and dry variants of the *Repetition of the last glacial cycle* case and *Severe permafrost case.* The results for the *Repetition of the last glacial cycle* case (Figure 5-46) show that the combined uncertainties can produce a fluctuation of ~160 m to ~290 m in the maximum permafrost depth and a fluctuation of ~160 m to ~270 m in the maximum depth of perennially frozen ground. The corresponding results for the *Severe permafrost case* (Figure 5-47) show that maximum permafrost depth can vary between ~310 m and ~460 m and the maximum depth of perennially frozen ground between ~280 m and ~410 m.

In order to investigate the combination of all relevant factors favourable and unfavourable for permafrost development a sensitivity case based on the *Repetition of the last glacial cycle* case with constant air temperature changes of −6°C and +6°C and considering the most favourable and unfavourable subsurface thermal conditions as described above was conducted in Case 7. The results (Figure 5-48) show, as expected, a very large fluctuation in both permafrost depth (~30 m to ~460 m) and perennially frozen ground depth (~30 m to ~420 m). These two cases indicate that if setting all uncertainties in their most pessimistic settings, which is a quite unrealistic case, permafrost is able to reach the repository depth of 450 m in the *Repetition of the last glacial cycle* case in 45,000 years. The perennially frozen depth does not reach repository at this time. For these unrealistic assumptions, permafrost is able to reach the repository depth of 450 m in 95,000 years in the *Severe permafrost* case.

Finally, the studies on the heat from the repository in Case 8 gave the expected result that the heat from the repository reduces the permafrost and perennially frozen ground depths, e.g. permafrost depth is reduced by ~38% at 109,700 years BP and by ~14% at 70,000 years BP (Figure 5-49). In addition, the effect of convective heat transfer due to groundwater flow and salinity transport on the development of permafrost and perennially frozen ground was found to be very weak in Case 9 (Figure 5-50). The permafrost depths in consideration of groundwater flow and salinity transport are less than a metre greater than those without it. A somewhat larger difference in frozen depth (~5 metres) is possibly a consequence of reduced salinity concentration due to salt transport. It should again be emphasised that the results on groundwater flow and salinity are strongly affected by the 2D modelling approach.

Main conclusions

The conclusion drawn within the preceding permafrost investigations for SR-Can /SKB 2006/ that the surface conditions can be seen as the driving force for the development of permafrost has been strengthened by the present studies. In addition, the conclusion that the subsurface conditions and the heat from the spent fuel act as either reducing or enhancing factors for the permafrost and perennially frozen ground development is also supported. In summary, the following main conclusions can be made from the study:

- Given the climate development as described in SR-Site, the study demonstrates how the site-specific spatial and temporal development of permafrost and perennially frozen ground takes place at the Forsmark site, important information that was not available for SR-Can.
- The study provides a full range of sensitivity analyses of relevant sub-surface and surface conditions, including air temperature variations.
- For the *Repetition of last glacial cycle* case, the simulated maximum permafrost (the 0°C isotherm) depth over the repository varies between 180 and 260 m depending on the surface conditions. The corresponding range for the entire investigated profile is from 220 to 300 m.
- For the *Repetition of last glacial cycle* case, the simulated maximum depth of perennially frozen ground over the repository fluctuates between 180 and 250 m depending on the surface conditions. The corresponding range for the entire investigated profile is from 210 to 300 m.

- For the *Severe permafrost* case, assuming a complete 115,000 years long last glacial cycle but without any cover of ice sheet, vegetation, snow or sea, the range for the maximum permafrost depth (the 0°C isotherm) over the repository is 360 to 390 m depending on the surface conditions. The corresponding range for the entire investigated profile is from 380 to 420 m.
- For the *Severe permafrost* case, assuming a complete 115,000 year long last glacial cycle but without any cover of ice sheet, vegetation, snow or sea, the maximum depth of perennially frozen ground over the repository and the entire profile ranges between 330 and 360 m depending on the surface conditions.
- The prevailing surface conditions, such as air- and ground surface temperatures and surface moisture conditions, are the main driving force for the spatial and temporal development of permafrost and perennially frozen ground at Forsmark.
- Subsurface conditions, such as bedrock thermal properties and groundwater salinity, modify the spatial and temporal development of permafrost and perennially frozen ground, but are of secondary importance compared to surface conditions.
- The longitudinal variation in thermal properties seems to have only a slight influence on permafrost (the 0°C isotherm) development. Therefore the uncertainties introduced by excluding lateral variations in subsurface thermal properties in the SR-Can 1D model /SKB 2006/ are considered insignificant.
- Although groundwater flow and salt transport seem to have a small influence on permafrost and perennially frozen ground, the significance of uncertainties introduced by excluding convective heat transfer and salt transport in the SR-Can 1D model /SKB 2006/ remains unclear, since the present 2D model is not able to describe the groundwater flow realistically.
- If making the very pessimistic combination of setting all known uncertainties (e.g. in air temperature, surface vegetation and snow conditions, bedrock thermal conductivity and heat capacity, and geothermal heat flow) in the position most favourable for permafrost growth, permafrost (i.e. the 0°C isotherm) may reach 450 m depth in 45,000 years in the *Repetition of last glacial cycle* case. However, the perennially frozen ground does not reach repository depth. Likewise, if combining the *Severe permafrost* case (which assumes no ice sheet, winter snow, vegetation or sea coverage during the entire glacial cycle), with maximum thermal conductivity and minimum heat capacity for the subsurface, as well as using the minimum geothermal heat flow value, the simulated maximum permafrost depth over the repository may extend the 450 m in 95,000 years. It should be noted though that the combination of assumptions in both these cases are quite unrealistic.
- Under continuous permafrost conditions, the unfrozen groundwater content in the perennially frozen ground under lakes can exceed 10% down to a ~50 m depth. This indicates that taliks are able to form under lakes through perennially frozen ground if favourable groundwater flow conditions with open flow paths prevail. When unfrozen groundwater content decreases below 10%, groundwater flow is reduced considerably, and taliks are no longer able to form or survive.
- Freezing can induce salt exclusion and transport when perennially frozen ground develops deeper than ~200 m. At more shallow depths the impacts of freezing are difficult to see since the salinity of groundwater has been diluted prior to the development of perennially frozen ground. When salt transport occurs more slowly than the freezing zone advances, salinity concentration is increased within the perennially frozen ground.
- The uncertainty dealing with groundwater flow remains, since the 3D flow network is omitted in the 2D model. However, the topography of the site is rather flat to generate significant hydraulic gradients, suggesting that this would only have a minor impact on the results.
- The model uncertainty regarding the neglect of salinity transport in the 1D model /SKB 2006/ seems to be insignificant mainly due to the low rock porosity, although the present 2D model is not able to describe the groundwater flow realistically.
- Based on the results and the investigations on ground temperature modelling by /Sundberg et al. 2009/ the uncertainty associated with determination of the ground surface temperature from the air temperature as well as with estimation of the in situ temperature and geothermal heat flow for the 1,000–10,000 m-depth for the thermal boundary and initial conditions of the model is reduced considerably.

7 References

SKB's (Svensk Kärnbränslehantering AB) publications can be found at www.skb.se/publications.

Ahonen L, 2001. Permafrost: occurrence and physicochemical processes. Posiva 2001-05, Posiva Oy.

Allen D, Michel F, Judge A, 1988. Paleoclimate and permafrost in the Mackenzie delta. In: Proceedings of 5th international conference on permafrost. Trondheim, 2–5 August 1988. Tapir publishers, vol. 1, pp 33–38.

Archibold O W, 1994. Ecology of world vegetation. New York: Springer.

Arenson L U, Sego S C, 2006. The effect of salinity on the freezing of coarse-grained sands. Canadian Geotechnical Journal, Vol. 43, pp 325–337.

Artemieva I M, Mooney W D, 2001. Thermal thickness and evolution of Precambrian lithosphere: a global study. Journal of Geophysical Research, 106, pp 16387–16414.

Baker G C, Osterkamp T E, 1988. Implications of salt fingering processes for salt movement in thawed coarse-grained subsea permafrost. Cold Regions Science and Technology, Vol. 15, pp 45–52.

Balling N, 1995. Heat flow and thermal structure of lithosphere across the Baltic Shield and northern Tornquist Zone. Tectonophysics, 244, pp 13–50.

Breckle S-W, 2002. Walter's vegetation of the earth: the ecological systems of the geo-biosphere. Berlin: Springer.

Burt T P, Williams P J, 1976. Hydraulic conductivity in frozen soils. Earth Surface Processes, 1, pp 349–360.

Clauser C, Huenges E, 1995. Thermal conductivity of rocks and minerals. In: Ahrens T J (ed). Rock physics and phase relations: a handbook of physical constants. Washington, DC: American Geophysical Union. (AGU Reference Shelf 3), pp 105–126.

Danielson E W, Levin J, Abrams E, 2003. Meteorology. 2nd ed. New York: McGraw-Hill.

Eugster W, Rouse W R, Pielke Sr, Roger A, Mcfadden J P, Baldocchi D D, Kittel T G F, Chapin F S, Liston G E, Vidale, P L, Vaganov E, Chambers S, 2000. Land-atmosphere energy exchange in Arctic tundra and boreal forest: available data and feedbacks to climate. Global Change Biology, 6 (Supplement 1), pp 84–115.

Feistel R, 2008. A Gibbs function for seawater thermodynamics for –6 to 80°C and salinity up to 120 g kg^{-1}. Deep-Sea Research I, 55, pp 1639–1671.

Fotiev S M, 1997. Permafrost groundwater: Russian literature review. In: Haldorsen S, Liebman M, Nelson G, van Everdingen R O, Boike J, 1997. State-of-the-art report on saturated water movement in permafrost areas. Report 4/97 (54), Agricultural University of Norway.

French H M, 2007. The periglacial environment. 3rd ed. Chichester: Wiley.

Gascoyne M, 2000. A review of published literature on the effects of permafrost on the hydrogeochemistry of bedrock. SKB R-01-56, Svensk Kärnbränslehantering AB.

Groisman P Y, Bradley R S, Sun B, 2000. The relationship of cloud cover to near-surface temperature and humidity: comparison of GCM simulations with empirical data. Journal of Climate, 13, pp 1858–1878.

Hartikainen J, 2004. Permafrost modelling in DECOVALEX III for BMT3. In: Eloranta E (ed). DECOVALEX III, 1999–2003. An international project for the modelling of coupled Thermo-Hydro-Mechanical processes for spent fuel disposal. Finnish national contributions. Helsinki: Radiation and Nuclear Safety Authority (STUK). Report STUK-YTO-TR 209, Appendix IV.

Hartikainen J, 2006. Numerical simulation of permafrost depth at Olkiluoto. Posiva 2006-52, Posiva Oy.

Hartikainen J, Mikkola M, 2006. Thermomechanical modelling for freezing of solute saturated soil. In: Gladwell G M L, Huyghe J M, Raats P A C, Cowin S C (eds). IUTAM Symposium on the mechanics of physicochemical and electromechanical interactions in porous media, pp 335–341.

Hinkel K M, Klene A E, Nelson F E, 2008. Spatial and interannual patterns of winter N-factors near Barrow, Alaska. In: Proceedings of the 9th International Conference on Permafrost. University of Alaska Fairbanks, 29 June–3 July 2008, pp 705–709.

Hoch A R, Jackson C P, 2004. Rock-matrix diffusion in transport of salinity: implementation in CONNECTFLOW. SKB R-04-78, Svensk Kärnbränslehantering AB.

Håkansson R, 2000. Beräkning av nuklidinnehåll, resteffekt, aktivitet samt doshastighet för utbränt kärnbränsle. SKB R 99-74, Svensk Kärnbränslehantering AB.

Isaksen K, Holmlund P, Sollid J L, Harris C, 2001. Three deep alpine-permafrost boreholes in Svalbard and Scandinavia. Permafrost and Periglacial Processes, 12, pp 13–26.

Kade A, Romanovsky V E, Walker D A, 2006. The n-factor of nonsorted circles along a climate gradient in Arctic Alaska. Permafrost and Periglacial Processes, 17, pp 279–289.

Karunaratne K C, Burn C R, 2003. Freezing n-factors in discontinuous permafrost terrain near Mayo, Yukon Territory. In: Proceedings of the 8th International Conference on Permafrost. Zurich: University of Zurich-Irche, pp 519–524.

Karunaratne K C, Burn C R, 2004. Relations between air and surface temperature in discontinuous permafrost terrain near Mayo, Yukon Territory. Canadian Journal of Earth Sciences, 41, pp 1437–1451.

Karunaratne K C, Kokelj C R, Burn C R, 2008. Near-surface permafrost conditions near Yellowknife, Northwest Territories, Canada. In: Proceedings of the 9th International Conference on Permafrost. University of Alaska Fairbanks, 29 June–3 July 2008, pp 907–912.

King L, 1984. Permafrost in Skandinavien: Untersuchungsergebnisse aus Lappland, Jotunheimen und Dovre/Rondane. Heidelberg: Geographisches Institut der Universität. (Heidelberger geographische Arbeiten 76)

Kjellström E, Strandberg G, Brandefelt J, Näslund J-O, Smith B, Wohlfart B, 2009. Climate conditions in Sweden in a 100,000 year time perspective. SKB TR-09-04, Svensk Kärnbränslehantering AB.

Kjellström E, Brandefelt J, Näslund J-O, Smith B, Strandberg G, Voelker A H L, Wohlfart B, 2010. Simulated climate conditions in Europe during the Marine Isotope Stage 3 stadial. Boreas, 39, pp 436–456.

Klene A E, Nelson F E, Shiklomanov N I, Hinkel K M, 2001. The N-factor in natural landscapes: variability of air and soil-surface temperatures, Kuparuk River Basin, Alaska. Arctic, Antarctic, and Alpine Research, 33, pp 140–148.

Klene A E, 2008. Interannual variability of winter n-factors in the Kuparuk river basin, Alaska. In: Proceedings of the 9th International Conference on Permafrost. University of Alaska Fairbanks, 29 June–3 July 2008, pp 953–958.

Kouhia R, 1999. Techniques for the analysis of non-linear systems: with applications to solid and structural mechanics. Espoo: Finnish Academy of Technology. (Acta polytechnica Scandinavica, civil engineering and building construction series 116)

Lide D R (ed), 1999. CRC handbook of chemistry and physics. Boca Raton: CRC Press.

Lockwood J G, 1979. Causes of climate. London: Arnold.

Lohmann U, Sausen R, Bengtsson L, Cubasch U, Perlwitz J, Roeckner E, 1993. The Köppen climate classification as a diagnostic tool for general circulation models. Climate Research, 3, pp 177–193.

Lunardini V J, 1978. Theory of n-factors and correlation of data. In: Proceedings of the 3rd International Conference on Permafrost. Edmonton, Alta 10–13 July 1978. Ottawa: National Research Council of Canada, pp 40–46.

Lunardini V J, 1981. Heat transfer in cold climates. New York: Van Nostrand Reinhold.

Mahar L J, Vinson T S, Wilson R M, 1982. Effects of salinity on freezing of granular soils. In Proceedings of the Third International Symposium on Ground Freezing Vol. 2, Special Report 82-16, Cold Regions Research and Engineering Laboratory, Hanover N H, 1982, pp 77–82.

Mahar L J, Wilson R M, Vinson T S, 1983. Physical and numerical modeling of uniaxial freezing in a saline gravel. In Proceedings of the Fourth International Conference on Permafrost, National Academy of Sciences, Washington, DC, 1983, pp 773–778.

Mai H, Thomsen T, 1993. Permafrost studies in Greenland. In: Proceedings of the 6th international conference on permafrost. Beijing, 5–9 July 1993. South China University of Technology Press, vol. 2.

Mikkola M, Hartikainen J, 2001. Mathematical model of soil freezing and its numerical implementation. International Journal for Numerical Methods in Engineering, 52, pp 543–557.

Mikkola M, Hartikainen J, 2002. Computational aspects of soil freezing problem. In: Proceedings of the 5th World Congress on Computational Mechanics. Vienna, 7–12 July 2002. (CD-ROM)

Näslund J-O, Jansson P, Fastook J L, Johnson J, Andersson L, 2005. Detailed spatially distributed geothermal heat flow data for modelling of basal temperatures and melt water production beneath the Fennoscandian ice sheet. Annals of Glaciology, 40, pp 95–101.

Panday S, Corapcioglu M Y, 1991. Solute rejection in freezing soils. Water Resources Research, Vol. 27, pp 99–108.

Riseborough D W, Shiklomanov N, Etzelmüller B, Gruber S, Marchenko S, 2008. Recent advances in permafrost modelling. Permafrost and Periglacial Processes, 19, pp 137–156.

Ruskeeniemi T, Paananen M, Ahonen L, Kaija J, Kuivamäki A, Frape S, Moren L, Degnan P, 2002. Permafrost at Lupin: report of phase I. Report YST-112, Geological Survey of Finland, Nuclear Waste Disposal Research.

Ruskeeniemi T, Ahonen L, Paananen M, Frape S, Stotler R, Hobbs M, Kaija J, Degnan P, Blomqvist R, Jensen M, Lehto K, Moren L, Puigdomenech I, Snellman M, 2004. Permafrost at Lupin: report of phase II. Report YST-119, Geological Survey of Finland, Nuclear Waste Disposal Research.

Saad Y, 1994. A dual threshold incomplete LU factorization. Numerical Linear Algebra with Applications, 1, pp 387–402.

Seipold U, 1995. The variation of thermal transport properties in Earth's crust. Journal of Geodynamics, 20, pp 145–154.

SKB, 2006. Climate and climate-related issues for the safety assessment SR-Can. SKB TR-06-23, Svensk Kärnbränslehantering AB.

SKB, 2010a. Climate and climate related issues for the safety assessment SR-Site. SKB TR-10-49, Svensk Kärnbränslehantering AB.

SKB, 2010b. Data report for the safety assessment SR-Site. SKB TR-10-52, Svensk Kärnbränslehantering AB.

SKB, 2010c. Landscape Forsmark, SR-Site Biosphere. SKB TR-10-05, Svensk Kärnbränslehantering AB.

SKB, 2011. Long-term safety for the final repository for spent nuclear fuel at Forsmark. Main report of the SR-Site project. SKB TR-11-01, Svensk Kärnbränslehantering AB.

Smith M W, Riseborough D W, 1996. Permafrost monitoring and detection of climate change, Permafrost and Periglacial Processes, 7, pp 301–309.

Strömgren M, Brydsten L, 2008. Digital elevation models of Forsmark, Site-descriptive modeling. SDM-Site Forsmark. SKB R-08-62, Svensk Kärnbränslehantering AB.

Sundberg J, 1988. Thermal properties of soils and rocks. Ph. D. thesis. Chalmers Tekniska Högskola, Göteborg. (Geologiska institutionen, A 57)

Sundberg J, Back P-E, Ländell M, Sundberg A, 2009. Modelling of temperature in deep boreholes and evaluation of geothermal heat flow at Forsmark and Laxemar. SKB TR-09-14, Svensk Kärnbränslehantering AB.

van der Vorst H A, 1992. Bi-CGSTAB: a fast and smoothly convergent variant of Bi-CG for the solution of nonsymmetric linear systems. SIAM Journal on Scientific and Statistical Computing, 13, pp 631–644.

Vidstrand P, 2003. Surface and subsurface conditions in permafrost areas: a literature review. SKB TR 03-06, Svensk Kärnbränslehantering AB.

Vinson T S, Mahar L J, Wilson R M, 1983. Model study of freezing front penetration in offshore granular fill structures. In Proceedings of the Fourth International Conference on Permafrost, National Academy of Sciences, Washington, DC, 1983, pp 1025–1034.

Voss C I, Souza W R, 1987. Variable density flow and solute transport simulation of regional aquifers containing a narrow freshwater-saltwater transition zone. Water Resources Research, Vol. 23, pp 1851–1866.

Washburn A L, 1979. Geocryology. London: Arnold.

Williams P J, Smith M W, 1989. The frozen earth: fundamentals of geocryology. Cambridge: Cambridge University Press.

Yershov E D, 1998. General geocryology. Cambridge: Cambridge University Press.

Appendix A

Data sets used in the permafrost simulations

Thomas Wallroth, Bergab

Background

Appendices A–J comprise the data delivered to Helsinki University of Technology, to be used in the 2D permafrost modelling for the Forsmark site. When necessary, data to be used in the 2D permafrost model has been simplified in relation to the original site-descriptive data. Depending on the data type and characteristics, different choices have been made how to simplify the geometrical descriptions, as well as which specific input to be used.

In several cases, early versions of the site-descriptive data sets have been necessary to use. The references to the data sets are found in the respective appendices below. Given the large and unavoidable uncertainties for other parameters not emanating from the site investigation programme, such as the air temperature curve, it is considered that the consequences of using early and simplified data sets for some parameters from the site investigations are of secondary importance. In general, the uncertainties in input data, such as air temperature, surface conditions and thermal properties of bedrock, are taken care of by the dedicated sensitivity experiments.

Model input data

The following site-specific data sets have been used in the 2D permafrost model:

- Topography and soil cover, Appendix B.
- Rock domains and deformation zones, Appendix C.
- Hydraulic properties of soils and bedrock, Appendix D.
- Thermal properties for different rock domains and soil types, Appendix E.
- Ionic composition of groundwater, Appendix F.
- Heat generation from the repository, Appendix G.
- Reconstructed air temperature curve for the past 120,000 years, Appendix H.
- Future lakes developed due to isostatic uplift, Appendix I.
- Vegetation/surface cover types for three different climate zones at Forsmark, Appendix J.

Selection of profile

As a first consideration, the orientation of the profile was decided with respect to the present topography in order to follow the direction of the regional hydraulic gradient in the area. Five parallel profiles were studied and compared (Figure A-1). Besides from the criteria that the profile preferably should cross the repository layout, the profiles were evaluated and compared based on the following criteria:

- Positions of future lakes outside the present-day coast line, as described in studies of future landscape development.
- Topographic relief and differences in elevation.
- Possible ground water recharge and discharge areas according to ground water modelling studies.
- Present-day lakes.
- Soil cover variations as described from the site investigations.
- Variations in rock types and deformation zones as described from the site investigations.

Weighing all the above parameters together, it was decided to choose the fourth profile from the top in Figure A-1.

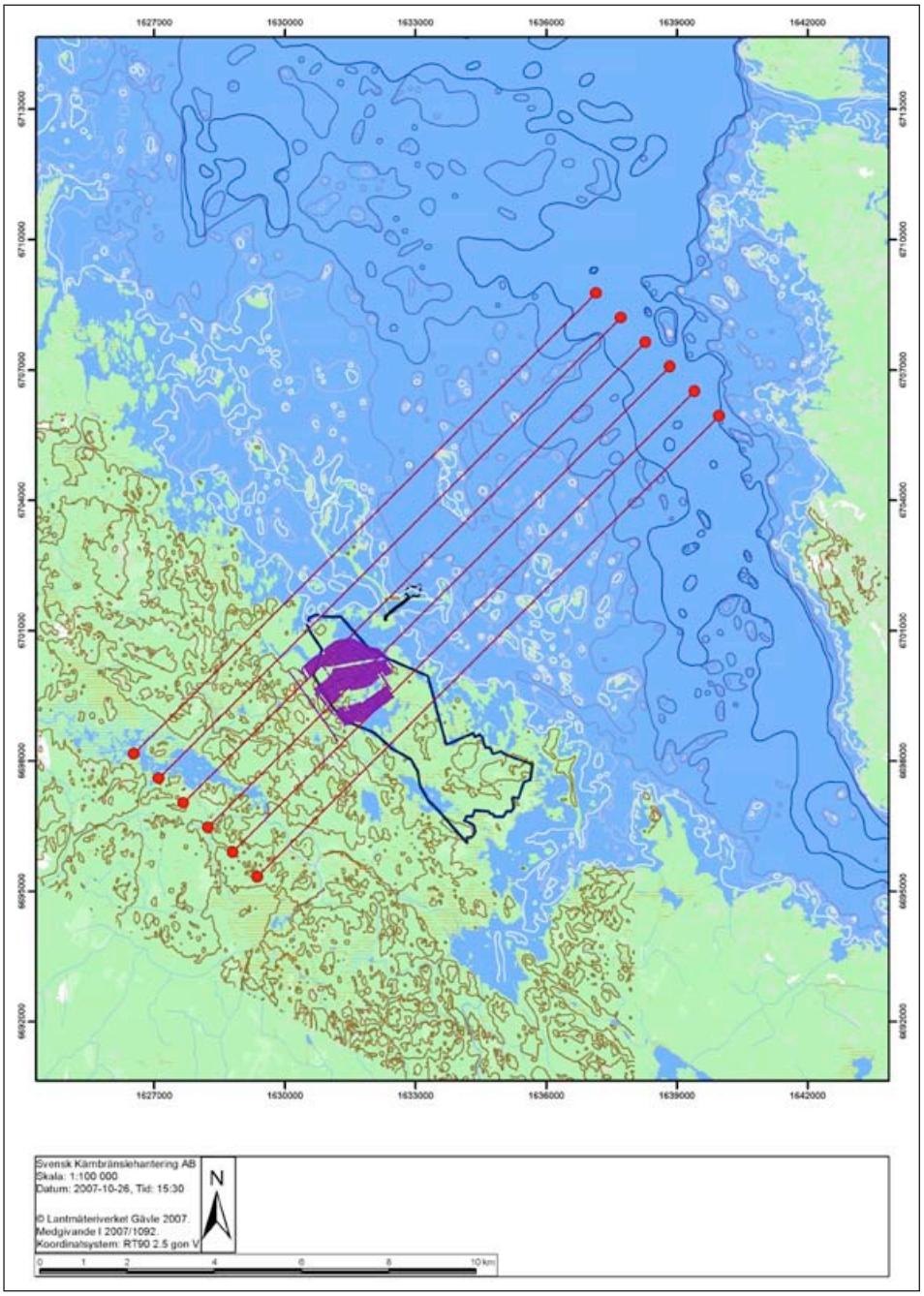

Figure A-1. *Evaluated profiles across the Forsmark area. The purple area marks the layout of the planned repository.*

Appendix B

Topography and soil cover

Thomas Wallroth, Bergab

The topography included in the permafrost simulations is based on a 20 m grid Digital Elevation Model (DEM) for the area. In Figure B-1 the topographical variation along the profile is illustrated together with layers in the regolith geometry, including the depth to the bedrock surface.

The description of soil cover along the profile has been provided from the regolith depth model in the Site Descriptive Model, version 2.2 /Hedenström et al. 2008/. The model describes the total regolith depth subdivided into a number of layers. These layers described are only geometrical and have no specified properties. Properties (e.g. hydraulic and thermal) are assigned by the user of the model. For the present study the assigned properties are presented in Appendices D–E.

The model has a spatial resolution of 20 × 20 m and presents the geometry of the lower boundary of each layer. Z5 represents the bedrock surface. The conceptual regolith model is shown in Figure B-2. Descriptions of each soil layer are given in Table B-1.

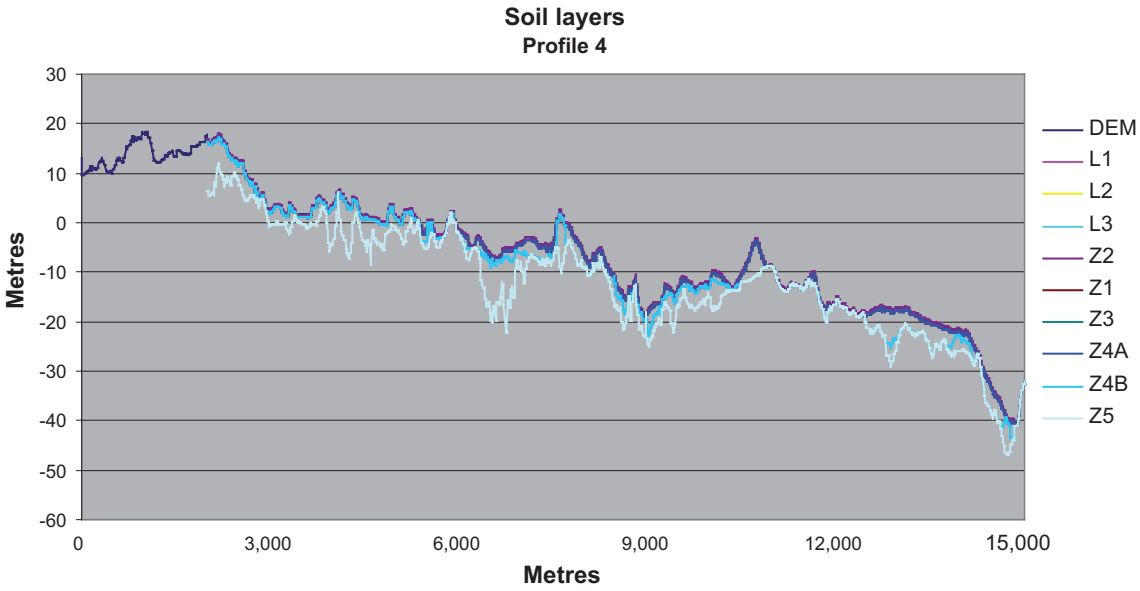

Figure B-1. *Topographic relief (height system RH70) and thickness of soil layers (lower boundary of each layer) along the chosen profile which goes from SW (0 m) to NE (15,000 m).*

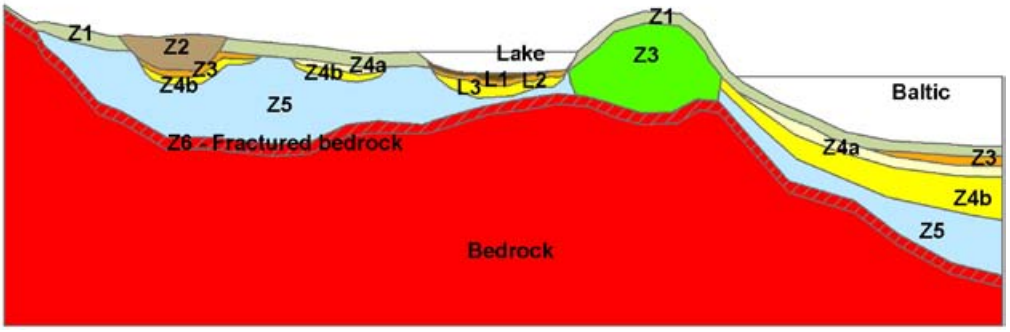

Figure B-2. *Conceptual model used for the regolith depth model /Hedenström et al. 2008/.*

Table B-1. Description of different layers used in the regolith model /Hedenström et al. 2008/.

Description of layer/lens	Simplified code	Description/occurrence
Gyttja (algal gyttja, calcareous gyttja, clay gyttja-gyttja clay), Peat	L1	Present inside the boundary of the lakes. When peat is present as surface layer within the lake area, this is included in the L1 lens. The sediment in L1 and Z4a partly consist of the same geological units.
Postglacial sand and/or gravel	L2	Present inside the boundary of the lakes. The sediments in L2 and Z3 consist of the same geological unit.
Clay (glacial and postglacial)	L3	Present inside the boundary of the lakes. The sediments in L3 and Z4a and Z4b consist of the same geological unit.
Surface layer	Z1	The layer is affected by surface processes, e.g soil forming processes in the terrestrial parts or sedimentation/transport/ersion in the limnic/marine parts. This layer is present within the entire modelled area, except where the surface is covered by peat or where the model has a lens (under lakes). On bedrock outcrops, the layer is 0.1 m and 0.6 m in other areas. If the total modelled regolith depth is less than 0.6 m, Z1 will be the only layer. The layer can be connected to a GIS application such as the map of Quaternary deposits or soiltype map and assigned properties in accordance to the properties of the deposits.
Peat	Z2	This layer is only present where peat is presented in the QD map. Calculated average depths are used for the layer since too few observations are available for interpolating. The average depth is used for peat above and below the 5 m.a.s.l. contour line ,1.4 m and 0.4 m respectively. Postglacial sand (Z3) always underlie Z2. If peat is intersecting glacial clay or sand on the QD map, Z4b underlie Z3.
Postglacial sand/gravel, glaciofluvial sediment and artificial fill	Z3	The layer is only present where the surface layer consists of postglacial sand/gravel, glaciofluvial sediment or artificial fill. The layer geometry is interpolated from input data and average values. This may result in a discrepancy between the modelled Z3 a and the marine geological map. In the the terrestrial parts, Z3 is assigned average depth values for postglacial sand and artificial fill and glaciofluvial sediment. The glaciofluvial sediment and artificial fill are modelled to always be situated directly on bedrock. Z3 as sand is always present under peat (Z2).
Postglacial clay including gyttja clay	Z4a	Z4a is present in the marine area where postglacial clay is the surface layer. In the marine areas, the layer geometry is interpolated from input data and average values. This may result in a discrepancy between the modelled Z4a and the marine geological map. When average values are used, Z4a is always underlain by Z4b.
Glacial clay	Z4b	Z4b is present where glacial clay is the surface layer. Additionally, Z4b is present under Z3 when peat is located next to sand or glacial clay and when sand is located next to glacial clay. In the marine area, the layer geometry is based on interpolation from input data and average values. In the terrestrial area, the layers are assigned calculated average depth values. In the marine are, interpolated Z4b values > 0.5 m are rejected in areas where the geological map shows till or glaciofluvial sediment. This may result in a discrepancy between the modelled Z4b and the marine geological map.
Till	Z5	This layer is present in a major part of the model area. The thickness of the layer is based on interpolation from input data and average values. Z5 is 0 at bedrock outcrops, if the total QD depth is < 0.6 m or if the layers/lenses are located directly on the bedrock surface. The lower limitation of Z5 represents the bedrock surface, i.e. Z5 represents a Digital Elevation Model for the bedrock surface.
Fractured bedrock	Z6	This layer has a constant depth of 0.6 m and represents the bedrock upper part, calculated from the interpolated Z5.The layer represents a high conductive zone that have been observed in many of the hydraulic tests within Forsmark.

References

Hedenström A, Sohlenius G, Strömgren M, Brydsten L, Nyman H, 2008. Depth and stratigraphy of regolith at Forsmark. Site descriptive modelling SDM Site Forsmark. SKB R-08-07, Svensk Kärnbränslehantering AB.

Appendix C

Rock domains and deformation zones

Thomas Wallroth, Bergab

Data on rock domains and deformation zones are taken from SDM 2.2 /Stephens et al. 2007/.

A *rock domain* refers to a rock volume in which rock units that show specifically similar composition, grain size, degree of bedrock homogeneity, and degree and style of ductile deformation have been combined and distinguished from each other. The term rock domain is used in the 3D geometric modelling work and different rock domains at Forsmark are referred to as RFMxxx.

A *deformation zone* is a general term that refers to an essentially 2D structure along which there is a concentration of brittle, ductile or combined brittle and ductile deformation. Deformation zones that are longer than 1,000 m are modelled deterministically and are included in the deformation zone block models for Forsmark. The zones are referred to as ZFM followed by two to 8 letters or digits, which depend on their dip and strike.

The used model of rock domains is the RVS model RD_PFM_REG_v22.rvs. The used deformation zone model is the RVS model DZ_PFM_REG_v22.rvs.

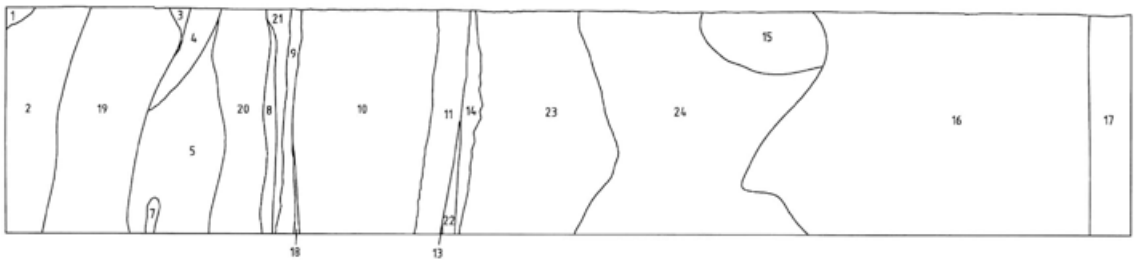

Figure C-1. *Rock domains cut by the chosen profile from southwest to northeast. The length of the profile is 15 km.*

Table C-1. Rock domains.

Number	Rock domain
1	RMF 003
2	RMF 024
3	RMF 005
4	RMF 031
5	RMF 023
7	RMF 007
8	RMF 025
9	RMF 012
10	RMF 029
11	RMF 032
13	RMF 034
14	RMF 043
15	RMF 022
16	RMF 040
17	RMF 042
18	RFM 044
19	RFM 030
20	RFM 026
21	RFM 018
22	RFM 020
23	RFM 021
24	RFM 033

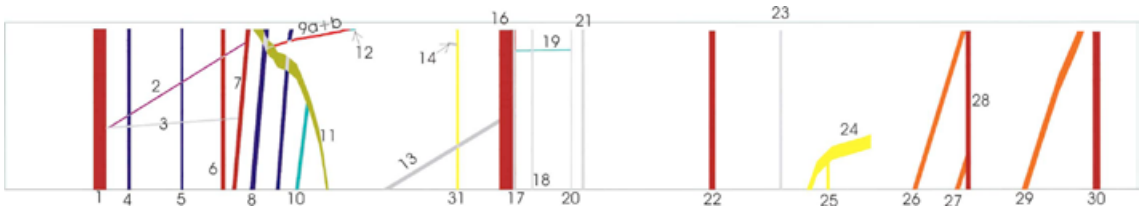

Figure C-2. *Deformation zones cut by the chosen profile from southwest to northeast.*

Table C-2. Deformation zones.

Number	Deformation zone
1	ZFMWNW0004
2	ZFMJ2
3	ZFMK1
4	ZFMWNW0024
5	ZFMWNW0035
6	ZFMWNW0036
7	ZFMNW0003
8	ZFMNW0017
9a	ZFMNW1200
9b	ZFMNW1200
10	ZFMWNW0123
11	ZFMENE0060A
12	ZFMA2
13	ZFMA1
14	ZFMB7
15	ZFMWNW0809A
16	ZFMWNW0001
17	ZFMWNW1127
18	ZFMWNW0835B
19	ZFM871
20	ZFMNW0805
21	ZFMWNW0836
22	ZFMNW0806
23	ZFMWNW0974
24	ZFMNE0808A
25	ZFMEW1156
26	ZFMNNE1132
27	ZFMNNE0929
28	ZFMWNW0853
29	ZFMNNE1133
30	ZFMNW0854
31	ZFM1203

References

Stephens M B, Fox A, La Pointe P, Simeonov A, Isaksson H, Hermanson J, Öhman J, 2007. Geology Forsmark. Site descriptive modelling Forsmark stage 2.2. SKB R-07-45, Svensk Kärnbränslehantering AB.

Appendix D

Hydraulic properties of soils and bedrock

Thomas Wallroth, Bergab

Data on hydraulic properties of the Quaternary deposits and the bedrock have been extracted from the work concerning hydrogeological modelling of the Forsmark site /Follin 2008/.

The Quaternary deposits consist of different layers, described in Appendix B. Hydraulic properties of these layers are presented in Table D-1.

In the site descriptive modelling at Forsmark, a methodology has been adopted where the deformation zones have been described deterministically and hydraulically referred to as Hydraulic Conductor Domains (HCD). Data are presented in Table D-2. The less fractured bedrock outside these zones is referred to as Hydraulic Rock Domains (HRD). These domains are not geometrically described in the 2D profile studied in the permafrost modelling work. Therefore, the hydraulic properties of the rock domains described in Appendix C have been assigned as generalized ranges of values for different depth intervals, as presented in Table D-3.

Table D-1. Hydraulic properties of different soil layers (based on data in /Follin et al. 2007a/. The layers referred to are described in Appendix B.

Layer	Hydraulic conductivity (m/s)	Total porosity
L1	Gyttja: $3\ 10^{-7}$	0.5
	Peat: z<0.6 m: $1\ 10^{-6}$	0.6
	Peat: z>0.6 m: $3\ 10^{-7}$	0.4
L2	$1.5\ 10^{-4}$	0.35
L3	z<0.6 m: $1\ 10^{-6}$	0.55
	z>0.6 m: $1.5\ 10^{-8}$	0.45
Z1	Till: $3\ 10^{-5}$	0.35
	Clay: $1\ 10^{-6}$	0.55
	Sand: $1.5\ 10^{-4}$	0.35
Z2	$3\ 10^{-7}$	0.40
Z3	$1.5\ 10^{-4}$	0.35
Z4	$1.5\ 10^{-8}$	0.45
Z5	$1.5\ 10^{-6}$	0.25

Table D-2. Hydraulic conductivity for deformation zones (data from /Follin et al. 2007b/. Deformation zones are described in Appendix C.

	0–100 m	100–200 m	200–300 m	300–400 m	400–500 m	500–600 m	600–700 m	700–800 m	800–900 m	900– m
ZFM871	$2.5\ 10^{-5}$	$9.5\ 10^{-6}$	$3.5\ 10^{-6}$	$1.3\ 10^{-6}$	$4.8\ 10^{-7}$	$1.8\ 10^{-7}$	$6.7\ 10^{-8}$	$2.5\ 10^{-8}$	$9.2\ 10^{-9}$	$3.4\ 10^{-9}$
ZFM1203	$1.8\ 10^{-5}$	$6.6\ 10^{-6}$	$2.5\ 10^{-6}$	$9.1\ 10^{-7}$	$3.4\ 10^{-7}$	$1.3\ 10^{-7}$	$4.7\ 10^{-8}$	$1.7\ 10^{-8}$	6.410^{-9}	$2.4\ 10^{-9}$
ZFMA1	$4.0\ 10^{-7}$	$1.5\ 10^{-7}$	$5.5\ 10^{-8}$	$2.0\ 10^{-8}$	$7.6\ 10^{-9}$	$2.8\ 10^{-9}$	$1.1\ 10^{-9}$	$1.0\ 10^{-9}$	$1.0\ 10^{-9}$	$1.0\ 10^{-9}$
ZFMA2	$5.7\ 10^{-5}$	$5.7\ 10^{-5}$	$5.7\ 10^{-5}$	$5.7\ 10^{-5}$	$1.1\ 10^{-6}$	$4.0\ 10^{-7}$	$1.5\ 10^{-7}$	$5.5\ 10^{-8}$	$2.1\ 10^{-8}$	$7.6\ 10^{-9}$
ZFMB7	$9.9\ 10^{-7}$	$3.7\ 10^{-7}$	$1.4\ 10^{-7}$	$5.1\ 10^{-8}$	$1.9\ 10^{-8}$	$7.0\ 10^{-9}$	$2.6\ 10^{-9}$	$1.0\ 10^{-9}$	$1.0\ 10^{-9}$	$1.0\ 10^{-9}$
ZFMENE0060A	$3.5\ 10^{-7}$	$1.3\ 10^{-9}$	$4.8\ 10^{-9}$	$1.8\ 10^{-8}$	$6.6\ 10^{-9}$	$2.4\ 10^{-9}$	$1.0\ 10^{-9}$	$1.0\ 10^{-9}$	$1.0\ 10^{-9}$	$1.0\ 10^{-9}$
ZFMEW1156	$1.5\ 10^{-9}$	$1.0\ 10^{-9}$	$1.0\ 10^{-9}$	$1.0\ 10^{-9}$	$1.0\ 10^{-9}$	$1.0\ 10^{-9}$	$1.0\ 10^{-9}$	$1.0\ 10^{-9}$	$1.0\ 10^{-9}$	$1.0\ 10^{-9}$
ZFMJ2	$6.2\ 10^{-6}$	$2.3\ 10^{-6}$	$8.6\ 10^{-7}$	$3.2\ 10^{-7}$	$1.2\ 10^{-7}$	$4.4\ 10^{-8}$	$1.6\ 10^{-8}$	$6.1\ 10^{-9}$	$2.3\ 10^{-9}$	$8.4\ 10^{-10}$
ZFMK1	$6.2\ 10^{-6}$	$2.3\ 10^{-6}$	$8.6\ 10^{-7}$	$3.2\ 10^{-7}$	$1.2\ 10^{-7}$	$4.4\ 10^{-8}$	$1.6\ 10^{-8}$	$6.1\ 10^{-9}$	$2.3\ 10^{-9}$	$8.4\ 10^{-10}$
ZFMNE0808A	$1.3\ 10^{-9}$	$1.0\ 10^{-9}$	$1.0\ 10^{-9}$	$1.0\ 10^{-9}$	$1.0\ 10^{-9}$	$1.0\ 10^{-9}$	$1.0\ 10^{-9}$	$1.0\ 10^{-9}$	$1.0\ 10^{-9}$	$1.0\ 10^{-9}$
ZFMNNE0929	$2.4\ 10^{-8}$	$8.8\ 10^{-9}$	$3.3\ 10^{-9}$	$1.2\ 10^{-9}$	$1.0\ 10^{-9}$	$1.0\ 10^{-9}$	$1.0\ 10^{-9}$	$1.0\ 10^{-9}$	$1.0\ 10^{-9}$	$1.0\ 10^{-9}$
ZFMNNE1132	$2.4\ 10^{-8}$	$8.8\ 10^{-9}$	$3.3\ 10^{-9}$	$1.2\ 10^{-9}$	$1.0\ 10^{-9}$	$1.0\ 10^{-9}$	$1.0\ 10^{-9}$	$1.0\ 10^{-9}$	$1.0\ 10^{-9}$	$1.0\ 10^{-9}$
ZFMNNE1133	$2.1\ 10^{-8}$	$7.7\ 10^{-9}$	$2.9\ 10^{-9}$	$1.1\ 10^{-9}$	$1.0\ 10^{-9}$	$1.0\ 10^{-9}$	$1.0\ 10^{-9}$	$1.0\ 10^{-9}$	$1.0\ 10^{-9}$	$1.0\ 10^{-9}$
ZFMNW0003	$3.9\ 10^{-7}$	$1.5\ 10^{-7}$	$5.4\ 10^{-8}$	$2.0\ 10^{-8}$	$7.5\ 10^{-9}$	$2.8\ 10^{-9}$	$1.0\ 10^{-9}$	$1.0\ 10^{-9}$	$1.0\ 10^{-9}$	$1.0\ 10^{-9}$
ZFMNW0017	$3.9\ 10^{-6}$	$1.4\ 10^{-6}$	$5.3\ 10^{-7}$	$2.0\ 10^{-7}$	$7.4\ 10^{-8}$	$2.7\ 10^{-8}$	$1.0\ 10^{-8}$	$3.8\ 10^{-9}$	$1.4\ 10^{-9}$	$1.0\ 10^{-9}$
ZFMNW0805	$2.5\ 10^{-6}$	$9.1\ 10^{-7}$	$3.4\ 10^{-7}$	$1.3\ 10^{-7}$	$4.7\ 10^{-8}$	$1.7\ 10^{-8}$	$6.5\ 10^{-9}$	$2.4\ 10^{-9}$	$1.0\ 10^{-9}$	$1.0\ 10^{-9}$
ZFMNW0806	$3.1\ 10^{-7}$	$1.1\ 10^{-7}$	$4.2\ 10^{-8}$	$1.6\ 10^{-8}$	$5.8\ 10^{-9}$	$2.2\ 10^{-9}$	$1.0\ 10^{-9}$	$1.0\ 10^{-9}$	$1.0\ 10^{-9}$	$1.0\ 10^{-9}$
ZFMWNW0835B	$5.3\ 10^{-9}$	$2.0\ 10^{-9}$	$1.0\ 10^{-9}$	$1.0\ 10^{-9}$	$1.0\ 10^{-9}$	$1.0\ 10^{-9}$	$1.0\ 10^{-9}$	$1.0\ 10^{-9}$	$1.0\ 10^{-9}$	$1.0\ 10^{-9}$
ZFMWNW0836	$2.6\ 10^{-9}$	$1.0\ 10^{-9}$	$1.0\ 10^{-9}$	$1.0\ 10^{-9}$	$1.0\ 10^{-9}$	$1.0\ 10^{-9}$	$1.0\ 10^{-9}$	$1.0\ 10^{-9}$	$1.0\ 10^{-9}$	$1.0\ 10^{-9}$
ZFMNW0854	$2.6\ 10^{-7}$	$9.6\ 10^{-8}$	$3.6\ 10^{-8}$	$1.3\ 10^{-8}$	$4.9\ 10^{-9}$	$1.8\ 10^{-9}$	$1.0\ 10^{-9}$	$1.0\ 10^{-9}$	$1.0\ 10^{-9}$	$1.0\ 10^{-9}$
ZFMNW1200	$2.7\ 10^{-7}$	$1.0\ 10^{-7}$	$3.7\ 10^{-8}$	$1.4\ 10^{-8}$	$5.2\ 10^{-9}$	$6.0\ 10^{-11}$	$1.0\ 10^{-9}$	$1.0\ 10^{-9}$	$1.0\ 10^{-9}$	$1.0\ 10^{-9}$
ZFMWNW0001	$1.5\ 10^{-7}$	$5.5\ 10^{-9}$	$1.0\ 10^{-7}$	$7.6\ 10^{-9}$	$2.8\ 10^{-9}$	$1.1\ 10^{-9}$	$1.0\ 10^{-9}$	$1.0\ 10^{-9}$	$1.0\ 10^{-9}$	$1.0\ 10^{-9}$
ZFMWNW0004	$1.5\ 10^{-7}$	$5.7\ 10^{-8}$	$2.1\ 10^{-8}$	$7.9\ 10^{-9}$	$2.9\ 10^{-9}$	$1.1\ 10^{-9}$	$1.0\ 10^{-9}$	$1.0\ 10^{-9}$	$1.0\ 10^{-9}$	$1.0\ 10^{-9}$
ZFMWNW0024	1.810^{-9}	$1.0\ 10^{-9}$	$1.0\ 10^{-9}$	$1.0\ 10^{-9}$	$1.0\ 10^{-9}$	$1.0\ 10^{-9}$	$1.0\ 10^{-9}$	$1.0\ 10^{-9}$	$1.0\ 10^{-9}$	$1.0\ 10^{-9}$
ZFMWNW0035	$2.3\ 10^{-9}$	$1.0\ 10^{-9}$	$1.0\ 10^{-9}$	$1.0\ 10^{-9}$	$1.0\ 10^{-9}$	$1.0\ 10^{-9}$	$1.0\ 10^{-9}$	$1.0\ 10^{-9}$	$1.0\ 10^{-9}$	$1.0\ 10^{-9}$
ZFMWNW0036	$1.4\ 10^{-9}$	$1.0\ 10^{-9}$	$1.0\ 10^{-9}$	$1.0\ 10^{-9}$	$1.0\ 10^{-9}$	$1.0\ 10^{-9}$	$1.0\ 10^{-9}$	$1.0\ 10^{-9}$	$1.0\ 10^{-9}$	$1.0\ 10^{-9}$
ZFMWNW0123	$1.0\ 10^{-9}$	$1.0\ 10^{-9}$	$1.0\ 10^{-9}$	$1.0\ 10^{-9}$	$1.0\ 10^{-9}$	$3.8\ 10^{-11}$	$1.0\ 10^{-9}$	$1.0\ 10^{-9}$	$1.0\ 10^{-9}$	$1.0\ 10^{-9}$
ZFMWNW0809A	$3.2\ 10^{-9}$	$1.2\ 10^{-9}$	$1.0\ 10^{-9}$	$1.0\ 10^{-9}$	$1.0\ 10^{-9}$	$1.0\ 10^{-9}$	$1.0\ 10^{-9}$	$1.0\ 10^{-9}$	$1.0\ 10^{-9}$	$1.0\ 10^{-9}$
ZFMWNW0853	$1.3\ 10^{-9}$	$1.0\ 10^{-9}$	$1.0\ 10^{-9}$	$1.0\ 10^{-9}$	$1.0\ 10^{-9}$	$1.0\ 10^{-9}$	$1.0\ 10^{-9}$	$1.0\ 10^{-9}$	$1.0\ 10^{-9}$	$1.0\ 10^{-9}$
ZFMWNW0974	$2.6\ 10^{-9}$	$1.0\ 10^{-9}$	$1.0\ 10^{-9}$	$1.0\ 10^{-9}$	$1.0\ 10^{-9}$	$1.0\ 10^{-9}$	$1.0\ 10^{-9}$	$1.0\ 10^{-9}$	$1.0\ 10^{-9}$	$1.0\ 10^{-9}$
ZFMWNW1127	$2.3\ 10^{-9}$	$1.0\ 10^{-9}$	$1.0\ 10^{-9}$	$1.0\ 10^{-9}$	$1.0\ 10^{-9}$	$1.0\ 10^{-9}$	$1.0\ 10^{-9}$	$1.0\ 10^{-9}$	$1.0\ 10^{-9}$	$1.0\ 10^{-9}$

Table D-3. Hydraulic conductivity for the rock mass between deformation zones (based on data in /Follin et al. 2007a, b/).

Rock mass Depth	Hydraulic conductivity K (m/s) Vertical	Hydraulic conductivity K (m/s) Horizontal
0–100 m	$1\ 10^{-7}$ to $1\ 10^{-8}$	$1\ 10^{-5}$ to $1\ 10^{-7}$
100–200 m	$1\ 10^{-9}$ to $1\ 10^{-11}$	$1\ 10^{-8}$ to $1\ 10^{-10}$
200–400 m	$1\ 10^{-10}$ to $1\ 10^{-11}$	$1\ 10^{-9}$ to $1\ 10^{-10}$
400–	$1.0\ 10^{-11}$	$1\ 10^{-11}$

Table D-4. Porosity of rock mass and deformation zones (based on data in /Follin et al. 2007a, b/).

Porosity	Total	Kinematic
Rock mass	$4.0\ 10^{-3}$	$1.0\ 10^{-4}$
Def zone	$2.0\ 10^{-2}$	$5.0\ 10^{-4}$

References

Follin S, 2008. Bedrock hydrogeology Forsmark. Site descriptive modelling. SDM Site Forsmark. SKB-R-08-95, Svensk Kärnbränslehantering AB.

Follin S, Johansson P-O, Hartley L, Jackson P, Roberts D, Marsic N, 2007a. Hydrogeological conceptual model development and numerical modelling using CONNECTFLOW, Forsmark modelling stage 2.2. SKB R-07-49, Svensk Kärnbränslehantering AB.

Follin S, Levén J, Hartley L, Jackson P, Joyce S, Roberts D, Swift B, 2007b. Hydrogeological characterisation and modelling of deformation zones and fracture domains, Forsmark modelling stage 2.2. SKB R-07-48, Svensk Kärnbränslehantering AB.

Appendix E

Thermal properties

Jan Sundberg, John Wrafter, Märta Ländell, Geo Innova

Thermal conductivity and heat capacity for rock domains

Method

Data on thermal properties of rock domains are required for use in permafrost modelling of the Forsmark site. Since permafrost simulations are conducted for a very large scale, it is reasonable to assume that it is the large-scale variations (100–1,000 m) in thermal properties that are relevant. The approach adopted here aims to deal with the rather large uncertainties that exist with regard to quantifying large-scale thermal properties. With this purpose in mind certain assumptions have been made. At the scale in question (100–1,000 m), small-scale variations in thermal conductivity within a rock type are assumed to be evened out. What remains are the variations resulting from any large-scale heterogeneity within a rock type, as well as variation between different rock types. Even larger-scale variation within a rock type is judged to be of little importance at this scale and may be ignored.

It is assumed that the large-scale heterogeneity in rock type composition is described by the rock domains which have been defined for the Forsmark area. However, there are large uncertainties in the composition of most rock domains intersected by the profile studied. It is, nonetheless, important to place reasonable limits on these uncertainties. Since for most rock domains no "hard" data is available, expert judgements are required to estimate the possible ranges in rock composition for each domain.

The range of uncertainty for the mean thermal conductivity of a rock domain is dependent on three main factors:

1. uncertainties in rock composition,
2. uncertainties in the mean thermal conductivity for each rock type,
3. the model used for estimating the effective thermal conductivity of the rock mass. Since thermal conductivity is a transport property, the upper and lower limits of thermal conductivity for a rock domain may be defined respectively as the arithmetic and harmonic means of its constituents, i.e. its rock composition.

These uncertainties are dealt with separately below.

The equivalent uncertainty intervals for heat capacity are determined by factors 1 and 2 above. Averaging is performed using the arithmetic mean only.

Uncertainties in rock type composition of domains

Most rock domains in Forsmark are comprised of several different rock types. To simplify the problem, rock types having similar thermal properties were grouped together. Three groups were defined as presented in Table E-1. This classification is a further simplification of the thermal rock class system developed in the thermal site descriptive modelling /Back et al. 2007/.

Table E-1. Classification of rock types and description of rock groups.

Rock Group	Overall composition	Rock types (rock code)	Range of mean thermal conductivities for different rock types /Back et al. 2007/
F	felsic + ultra-mafic rock	Granite to granodiorite, metamorphic, medium-grained (101057) Granite, metamorphic, aplitic (101058) Pegmatite, pegmatitic granite (101061) Granite, fine- to medium-grained (111058) Ultramafic rock (101004)	ca. 3.46–3.83 W/(m·K)
F-I	felsic to intermediate	Tonalite to granodiorite, metamorphic (101054) Granodiorite, metamorphic (101056) Granite, granodiorite and tonalite, metamorphic, fine- to medium-grained (101051) Felsic to intermediate volcanic rock, metamorphic (103076)	ca. 2.97–3.12 W/(m·K)
M	mafic	Amphibolite (102017) Diorite, quartz diorite and gabbro, metamorphic (101033)	ca. 2.37–2.51 W/(m·K)

Ultramafic rock, which is present in a couple of rock domains, was classified with the felsic group. Despite the contrast in composition, ultramafic rock is considered to have similar thermal conductivity to granite rocks. Typical minerals in these metamorphic ultramafic rocks are olivine, pyroxenes and serpentinite, all of which have thermal conductivities between 3 and 5 W/(m·K). From a thermal properties perspective, the main difference between the rocks in the felsic (F) group and the more felsic rocks in the felsic-intermediate (F-I) group is the lower quartz and higher plagioclase content of the latter.

For rock domains in Forsmark that will incorporate a future repository, namely RFM029 and RFM045, the uncertainties in rock composition are relatively small, and have been obtained from /Sundberg et al. 2008/. For the remaining rock domains, the uncertainties are much larger. The following references have been inspected for the purpose of approximating the possible ranges in rock composition:

1. The property tables in the regional rock domain model published in Appendix 1 in /SKB 2005/ for rock domains RFM003, RFM005, RFM007, RFM022, RFM023, RFM024, RFM030, RFM031, RFM033, RFM040 and RFM042.
2. The property tables in the local rock domain model published in Appendix 14 in /Stephens et al. 2007/ for rock domains RFM012, RFM018, RFM020, RFM021, RFM025, RFM026, RFM032, RFM043 and RFM044.

In the above tables, quantitative data on rock type percentages are available for domains RFM007, RFM012 and RFM044 only, whereas for the majority of domains the dominant rock type and subordinate rock types are simply listed. In other words, no quantitative information is available for these domains.

In collaboration with Forsmark geologist Michael Stephens, we have estimated possible ranges in the proportions of each rock group for each domain of interest. It is important to point out that this exercise was performed with thermal properties in mind. Furthermore, it should be remembered that estimates of ranges for domains for which no quantitative data exist are little more than qualified guesswork based on impressions gained in the field during the surface bedrock mapping activities (Michael Stephens, pers. comm.). The estimates are presented in Appendix AE.

While the stated ranges place limits on the uncertainties in the mean composition of a rock domain, they also reflect some of the inherent large-scale heterogeneity present.

Confidence limits for mean thermal conductivity

Uncertainties in the mean thermal conductivity for each rock group are required. These estimates are based on the confidence intervals for individual rock types. In /Back et al. 2007/, thermal conductivity data, from both measurements and calculations from mineral composition, were presented for each rock type. Using these data, 95% upper and lower confidence limits (UCL and LCL respectively) for the mean thermal conductivity for individual rock types were calculated (see Table E-2). From these estimates, values were assigned to the rock groups in each domain. The dominant rock group in a domain was assigned the value for the dominant rock type. A different approach was used for the other rock groups in a rock domain, since in most cases the relative proportions of each rock type was not known. For example, the lowest LCL value of all rock types within a rock group was selected when estimating the lower bound of thermal conductivity. For calculating the upper bound of thermal conductivity, the highest UCL value of all rock types within a rock group was selected. By adopting this approach we have bounded the mean thermal conductivity for a rock group with a high degree of certainty. The ranges may also reflect some of the large-scale variability in thermal conductivity within a rock type.

Model for calculating the bulk thermal conductivity

To calculate an effective thermal conductivity for an entire rock domain according to the proportions and thermal conductivity of its components, an appropriate mixing model must be selected. The harmonic mean is used to define the lower limit of thermal conductivity. Such a model is appropriate when heat flow is parallel with the rock contacts. The arithmetic mean is used for the upper limit of thermal conductivity which is an appropriate model when heat flow is perpendicular to the rock contacts.

Heat capacity

Uncertainty ranges of heat capacity have been calculated in much the same way as for thermal conductivity, with the exception for the last step. To calculate a bulk heat capacity that is representative for a whole domain only the arithmetic mean was required. Confidence intervals for the mean heat capacity for individual rock types are presented in Table E-3. These ranges are based on data reported in /Sundberg et al. 2008/, and are estimated either as 95% upper and lower confidence limits, or for rock types with five data values or less, using the min and max values.

Table E-2. 95% lower confidence limits (LCL) and upper confidence limits (UCL) for mean thermal conductivities for different rock types. Based on data in /Back et al. 2007/ and assuming normal distributions. The lowest LCL and highest UCL values in each rock group are in bold.

Rock group	Rock type (code)	95% LCL	95% UCL
F	101057	3.64	3.72
	101058	3.73	3.92
	101061	3.3	3.63
	111058	3.27	3.71
F-I	103076	2.8	3.24
	101051	2.98	3.19
	101054	2.83	3.11
	101056	3.01	3.24
M	102017	2.3	2.41
	101033	2.37	2.65

Table E-3. Upper and lower confidence limits for mean heat capacities for different rock types. Based on data in /Sundberg et al. 2008/. The lowest lower confidence limit and highest upper confidence limit in each rock group are in bold.

Rock group	Rock type (code)	Lower confidence limit	Upper confidence limit	Comment
F	101057	2.02	2.09	95% LCL and UCL
	101058	2.01	2.14	95% LCL and UCL
	101061	1.73	2.07	min and max values
	111058	2.01	2.13	min and max values
F-I	103076	2.19	2.33	min and max values
	101051	2.1	2.2	95% LCL and UCL
	101054	1.93	2.39	min and max values
	101056	2.16	2.34	min and max values
M	102017	2.32	2.5	95% LCL and UCL
	101033	2.2	2.5	guesstimate

Results

Data for thermal and physical properties of rock domains used in permafrost modelling of the Forsmark site are presented in Table E-4. The sources of these data for each domain are given in the footnotes of the table. For most rock domains the mean property values are based on the dominant rock type in each domain. Modelled thermal properties which take consideration of the rock type proportions comprising a domain are available for a only a couple of rock domains, e.g. domain RFM029.

For each rock domain along profile studied, the ranges of possible thermal conductivities and heat capacities have been estimated as described in detail in this appendix. These are also presented in Table E-4. It should be pointed out that for each rock domain, the minimum thermal conductivity value is linked to the maximum heat capacity value, while the maximum thermal conductivity value is coupled to the minimum heat capacity value.

Data for domain RFM034, which is small and occurs at depth, have not been calculated. Investigation of the domain properties described in /SKB 2005/ and /Stephens et al. 2007/ indicates that RFM034 has a similar rock composition to domain RFM033. Therefore, the data given for RFM033 in Table E-4 can also be used too represent RFM034.

Some data have been revised after delivery to the permafrost modelling project. For completion, these data are also given in Table E-4 and referenced in the footnotes. The discrepancies can be explained by the fact that, at a later date, some changes were made to the assumptions on which the data are based.

Table E-4. Data for thermal and physical properties of rock domains used in permafrost modelling. The data values in bold italics refer to data that have been revised after the delivery of thermal data for permafrost modelling and thus have not been used in this modelling.

Rock domain	Rock code	Dominant rock type (SKB 2005, Stephens et al. 2007)	Density (kg/m³)[12]	Porosity (%)[10]	Thermal conductivity (W/(m·K))				Heat capacity (MJ/(m³·K))				Temperature dependence for thermal conductivity (%)		Temperature dependence for heat capacity (%)	
	(dominant)		mean	mean	mean	revised mean[7]	range		mean[8]	revised mean[9]	range		mean	revised mean[10]	mean	revised mean[11]
RFM003[1]	103076	felsic to intermediate volcanic rock, metamorphic	2,732	0.37	3.02	3.02	2.69	3.35	2.15	2.26	2.1	2.35	–5	–5	25	25
RFM005[1]	101033	diorite, quartz diorite and gabbro, metamorphic	2,934	0.37	2.51	2.51	2.42	3.06	2.30	2.33	2.04	2.48	–2	–1	25	10
RFM007[1]	101033	diorite, quartz diorite and gabbro, metamorphic	2,934	0.37	2.51	2.51	2.40	2.84	2.30	2.33	2.13	2.48	–2	–1	25	10
RFM012[2]	101057	granite to granodiorite, metamorphic	2,657	0.43	3.45	3.45	3.21	3.59	2.07	2.17	2.02	2.21	–8	–8	25	28
RFM018[1]	101054	tonalite to granodiorite, metamorphic	2,737	0.40	2.73	2.73	2.71	3.37	2.23	2.12	1.87	2.39	–3	–3	25	25
RFM020[1]	101058	granite, metamorphic, aplitic	2,635	0.40	3.83	3.83	3.41	3.88	2.03	2.08	2.02	2.19	–11	–11	25	25
RFM021[1]	103076	felsic to intermediate volcanic rock, metamorphic	2,732	0.37	3.02	3.02	2.69	3.45	2.15	2.26	2.03	2.35	–5	–5	25	25
RFM022[1]	111058	granite, fine- to medium grained	2,638	0.50	3.49	3.49	3.19	3.69	2.06	2.06	2.01	2.17	–9	–9	25	25
RFM023[1]	101054	tonalite to granodiorite, metamorphic	2,737	0.40	2.73	2.73	2.71	3.37	2.23	2.12	1.87	2.39	–3	–3	25	25
RFM024[1]	101054	tonalite to granodiorite, metamorphic	2,737	0.40	2.73	2.73	2.71	3.37	2.23	2.12	1.87	2.39	–3	–3	25	25
RFM025[1]	101033	diorite, quartz diorite and gabbro, metamorphic	2,934	0.37	2.51	2.51	2.42	2.96	2.30	2.33	2.08	2.48	–2	–1	25	10
RFM026[1]	101057	granite to granodiorite, metamorphic	2,657	0.43	3.68	3.68	3.34	3.69	2.04	2.06	2.02	2.16	–10	–10	25	28
RFM029[3]	101057	granite to granodiorite, metamorphic	2,657	0.43	3.58	3.58	3.47	3.68	2.05	2.06	2.02	2.13	–9	–9	25	28
RFM030[1]	101054	tonalite to granodiorite, metamorphic	2,737	0.40	2.73	2.73	2.71	3.37	2.23	2.12	1.87	2.39	–3	–3	25	25
RFM031[1]	103076	felsic to intermediate volcanic rock, metamorphic	2,732	0.37	3.02	3.02	2.69	3.35	2.15	2.26	2.1	2.35	–5	–5	25	25
RFM032[1]	101058	granite, metamorphic, aplitic	2,635	0.40	3.83	3.83	3.31	3.85	2.03	2.08	2.01	2.22	–11	–11	25	25
RFM033[1]	101057	granite to granodiorite, metamorphic	2,657	0.43	3.68	3.68	3.26	3.69	2.04	2.06	2.02	2.18	–10	–10	25	28
RFM040[1]	111057[6]	granite to granodiorite, metamorphic, veined to migmatitic	2,657	0.43	3.68	3.68	3.26	3.69	2.04	2.06	2.02	2.18	–10	–10	25	28
RFM042[1]	111051[5]	granitoid, metamorphic	2,718	0.45	3.04	3.12	3.03	3.48	2.14	2.15	1.95	2.19	–5	–5	25	25
RFM043[1]	101058	granite, metamorphic, aplitic	2,639	0.38	3.83	3.83	3.41	3.88	2.03	2.08	2.02	2.19	–11	–11	25	25
RFM044[4]	101057	granite to granodiorite, metamorphic	2,656	0.37	3.48	3.48	3.26	3.65	2.06	2.07	2.03	2.18	–9	–9	25	28

[1] Rock type proportions not known. Mean thermal conductivity for dominating rock type /Back et al. 2007, Sundberg et al. 2008/

[2] Rock type proportions known. Mean thermal conductivity has been modelled /Sundberg et al. 2005/

[3] Rock type proportions known. Mean thermal conductivity has been modelled /Back et al. 2007/

Footnootes continues on next page.

[4] Mean thermal conductivity calculated from rock type proportions /Stephens et al. 2007/ and thermal properties data for rock types /Back et al. 2007, Sundberg et al. 2008/

[5] Rock type 111051 not investigated. Originally assumed similar to 101056 as regards density, porosity, mean thermal conductivity. Later equated with 101051 for determination of ranges of thermal conductivity and heat capacity.

[6] Not investigated; similar to 101057 /Stephens et al. 2007/.

[7] Revised thermal conductivity from /SKB 2010b/. Rock type 111051 not investigated, but assumed similar to 101051.

[8] Heat capacity calculated from relationship with thermal conductivity described in /Back et al. 2007/.

[9] Revised heat capacity from /SKB 2010b/.

[10] Revised temperature dependence for thermal conductivity from /SKB 2010b/.

[11] Revised temperature dependence for heat capacity from /SKB 2010b/.

[12, 13]/SKB 2005, Stephens et al. 2007/

For the purpose of permafrost modelling, a further simplification was made. Domains with the same mean values of thermal conductivity and heat capacity were grouped together. However, in most cases the quoted ranges of thermal conductivity and heat capacity for the domains within each group differ slightly. Therefore, one domain was chosen to represent the property ranges for a group. An implication of this approach is that the full range of uncertainty in thermal properties of a domain may not have been accounted for. This uncertainty applies even to thermal diffusivity which is calculated from thermal conductivity and heat capacity. These uncertainties in the ranges are considered to be small compared to other uncertainties.

Temperature dependence

The thermal conductivity is influenced by the temperature. The estimated temperature dependence for the different rock domains are presented in Table E-4.

Also the heat capacity is influenced by the temperature, but the variation between different rock types is much smaller, see Table E-4.

Heat generation

The heat generation based on mean proportions of different rock types and contents of U, Th and K has been calculated to be 3.16 and 3.11 $\mu W/m^3$, for domains RFM029 and RFM045, respectively. /Sundberg et al. 2009/.

Thermal properties of soil

Data for density, thermal conductivity, specific heat capacity and latent heat are presented in Table E-5. No measured data of the thermal properties are available for Forsmark. Theoretical calculations with methods presented in /Sundberg 1988/ have been made.

All estimates and calculations are based on the assumption of fully saturated conditions.

The data of thermal conductivity and specific heat capacity for a frozen state as well as the latent heat are valid for a completely frozen material.

Table E-5. Thermal properties of soil.

								Unfrozen state					
Soil type	**Dry density (kg/m³)**			**Porosity (%)**			**No of samples**	**Thermal conductivity (W/(m·K))**			**Heat capacity (MJ/m³·K))**		
	mean	**min**	**max**	**mean**	**min**	**max**		**mean**	**min**	**max**	**mean**	**min**	**max**
peat/mud[1, 2, 3]	46.4	23.4	83.2				4	0.6			4.2		
sand[1, 2]	1,800	1,600	2,000	32.2	26.4	37.9	2	2.19	1.88	2.54	2.7	2.5	2.8
clay[4]	900	700	1,100	66.7	59.3	75.1		1.0	0.88	1.14	3.4	3.3	3.6
sandy till[1, 2]	2,000	1,600	2,300	24	14	42	14	2.14	1.64	2.45	2.5	2.3	2.9

	Latent heat (MJ/m³)			**Completety frozen state**			
Soil type				**Thermal conductivity (W/(m·K))**			**Heat capacity (MJ/(m³·K))**
	mean	**min**	**max**	**mean**	**min**	**max**	**mean**
peat/mud[3]	325			1.9			2.1
sand	110	85	125	3.1	3.0	3.3	2.0
clay[4]	230	200	250	2.2	2.1	2.3	2.1
sandy till	80	45	140	2.5	2.3	2.6	2.0

Thermal properties have been calculated based on diagrams in /Sundberg 1988/
[1] Density values for peat, sand and till from SICADA
[2] Porosity of sand and till from SICADA. The porosity of peat has been calculated ($n=1-(\rho_d/\rho_s)$, where ρ_s= 1,700 kg/m³)
[3] The variation of thermal conductivity with density is small for peat
[4] Typical values of the density of clay are from /Sundberg 1988/. Porosity has been calculated ($n=1-(\rho_d/\rho_s)$, where ρ_s= 2,700 kg/m³)

References

Back P-E, Wrafter J, Sundberg J, Rosén L, 2007. Thermal properties, Site descriptive modelling Forsmark – stage 2.2. SKB R-07-47, Svensk Kärnbränslehantering AB.

SKB 2005. Preliminary site description Forsmark area – version 1.2. SKB R-05-18, Svensk Kärnbränslehantering AB.

SKB 2006. Site descriptive modelling Forsmark stage 2.1. Feedback for completion of the site investigation including input from safety assessment and repository engineering. SKB R-06-38, Svensk Kärnbränslehantering AB.

SKB 2010b. Data Report for the safety assessment SR-Site. SKB TR-10-52, Svensk Kärnbränslehantering AB.

Stephens M B, Fox A, La Pointe P, Simeonov A, Isaksson H, Hermanson J, Öhman J, 2007. Geology Forsmark: Site descriptive modelling, Forsmark stage 2.2. SKB R-07-45, Svensk Kärnbränslehantering AB.

Sundberg J, 1988. Thermal properties of soils and rocks. Publ A 57, PhD thesis, Department of Geology, Chalmers University of Technology and University of Göteborg.

Sundberg J, Back P-E, Bengtsson A, Ländell M, 2005. Thermal modelling. Preliminary site description Forsmark area – version 1.2. SKB R-05-31, Svensk Kärnbränslehantering AB.

Sundberg J, Wrafter J, Back P-E, Ländell M, Rosén L, 2008. Thermal properties, Forsmark – Modelling stage 2.3. Complementary analysis and verification of the thermal bedrock model, stage 2.2. SKB R-08-65, Svensk Kärnbränslehantering AB.

Sundeberg J, Back P-E, Ländell M, Sundberg A, 2009. Modelling of temperature in deep boreholes and evaluation of geothermal heat flow at Forsmark and Laxemar. SKB TR-09-14, Svensk Kärnbränslehantering AB.

Appendix AE

Table AE-1. Possible ranges of proportions of different rock groups in selected rock domains. Unless otherwise stated, the proportions are not based on hard data, but are rather approximations based on geological knowledge of the Forsmark area.

Rock domain	Dominant rock type (code) /SKB 2005, SKB 2006/	Rock composition – low thermal conductivity			Rock composition – high thermal conductivity			Comments
		F	F-I	M	F	F-I	M	
RFM003	felsic to intermediate volcanic rock, metamorphic (103076)	10.0	65.0	25.0	20.0	75.0	5.0	F-I group dominant, F group characterised by pegmatite only. Based on /SKB 2005/.
RFM005	diorite, quartz diorite and gabbro, metamorphic (101033)	5.0	5.0	90.0	25.0	15.0	60.0	M group dominant, Ultramafics also present. Based on /SKB 2005/.
RFM007	diorite, quartz diorite and gabbro, metamorphic (101033)	5.0	–	95.0	15.0	–	85.0	Based on estimate given in SDM 1.2 Forsmark /SKB 2005/: M = 90%, F = 10%.
RFM012	granite to granodiorite, metamorphic (101057)	65.0	25.0	10.0	80.0	15.0	5.0	F group dominant. Based on estimate given in geology SDM 2.2 Forsmark /Stephens et al. 2007/: F = 72%, F-I = 19%, M = 6%.
RFM018	tonalite to granodiorite, metamorphic (101054)	10.0	65.0	25.0	35.0	60.0	5.0	F-I group dominant. Based on /Stephens et al. 2007/.
RFM020	granite, metamorphic, aplitic (101058)	85.0	–	15.0	97.0	–	3.0	F group dominant, M group characterised by amphibolite only. Based on /Stephens et al. 2007/
RFM021	felsic to intermediate volcanic rock, metamorphic (103076)	10.0	65.0	25.0	35.0	60.0	5.0	F-I group dominant. Based on /Stephens et al. 2007/.
RFM022	granite, fine- to medium grained (111058)	85.0	15.0	–	95.0	5.0	–	F group dominant, no M group rocks. Based on /SKB 2005/.
RFM023	tonalite to granodiorite, metamorphic (101054)	10.0	65.0	25.0	35.0	60.0	5.0	F-I group dominant. Based on /SKB 2005/.
RFM024	tonalite to granodiorite, metamorphic (101054)	10.0	65.0	25.0	35.0	60.0	5.0	F-I group dominant. Based on /SKB 2005/.
RFM025	diorite, quartz diorite and gabbro, metamorphic (101033)	5.0	5.0	90.0	20.0	10.0	70.0	M group dominant, F group characterised by pegmatite only. Based on /Stephens et al. 2007/.
RFM026	granite to granodiorite, metamorphic (101057)	80.0	10.0	10.0	96.0	2.0	2.0	F group dominant. Rock domain RFM026 is compositionally similar to rock domain RFM029. Based on /Stephens et al. 2007/.
RFM029	granite to granodiorite, metamorphic (101057)	89.0	5.0	6.0	87.0	1.0	3.0	Based on 95% confidence intervals estimated in /Sundberg et al. 2008/.
RFM030	tonalite to granodiorite, metamorphic (101054)	10.0	65.0	25.0	35.0	60.0	5.0	F-I group dominant. Based on /SKB 2005/.
RFM031	felsic to intermediate volcanic rock, metamorphic (103076)	10.0	65.0	25.0	20.0	75.0	5.0	F-I group dominant, F group characterised by pegmatite only. Based on /SKB 2005/.

Rock domain	Dominant rock type (code) /SKB 2005, SKB 2006/	Rock composition – low thermal conductivity			Rock composition – high thermal conductivity			Comments
		F	F-I	M	F	F-I	M	
RFM032	granite, metamorphic, aplitic (101058)	75.0	10.0	15.0	92.0	5.0	3.0	F group dominant, M group characterised by amphibolite only. Based on /Stephens et al. 2007/.
RFM033	granite to granodiorite, metamorphic (101057)	75.0	10.0	15.0	96.0	2.0	2.0	F group dominant, M group characterised by amphibolite only. Based on /SKB 2005/.
RFM040	granite to granodiorite, metamorphic, veined to migmatitic (111057[1])	75.0	10.0	15.0	96.0	2.0	2.0	F group dominant, M group characterised by amphibolite only. Based on /SKB 2005/.
RFM042	granitoid, metamorphic (111051[2])	20.0	80.0	–	40.0	60.0	–	F-I group dominant, no M group rocks. Based on /SKB 2005/.
RFM043	granite, metamorphic, aplitic (101058)	85.0	–	15.0	97.0	–	3.0	F group dominant, M group characterised by amphibolite only. Based on /Stephens et al. 2007/.
RFM044	granite to granodiorite, metamorphic (101057)	75.0	10.0	15.0	92.0	3.0	5.0	F group dominant. Based on estimate given in /Stephens et al. 2007/: F = 84%, F-I = 4%, M = 9%.
RFM045	granite, metamorphic, aplitic (101058)	78.0	13.0	9.0	93.0	5.0	2.0	Based on 95% confidence intervals estimated in /Sundberg et al. 2008/.

[1] No thermal data available. Similar to 101057 /Stephens et al. 2007/.

[2] No thermal data available. Assumed to be similar to 101051.

Appendix F

Ionic composition of groundwater

Thomas Wallroth, Bergab

The data presented in this appendix are based on the hydrogeochemical site description work carried out at Forsmark /Laaksoharju et al. 2008/. Several groundwater types present in the bedrock can be associated with past climatic events. The present groundwaters are a result of mixing and reactions over a long period of geological time. The interfaces between different water types are not sharp but reflect the variability in the structural-hydraulic properties. In Table F-1, a generalised description of the various water types present at the site is given. The ionic composition within different depth intervals represent average values assigned on the basis of ranges of compositions from different investigation boreholes.

The total molar concentration, x_c, is determined by the formulas presented in Table F-2 by making use of the volume concentrations C_k of different salt or ion pieces and volume concentration of water $C_{H2O} = 999.8848 \cdot 10^3$ mg/l. The molecular weights M_k of salt or ion pieces and water can be found in /Lide 1999/. The molecular weight of seawater is $M_{sea} = 31.4038$ g/mol. The total concentration in mass-% can be defined by

$$c = \frac{x_c}{x_c + (1 - x_c)\dfrac{M_{H_2O}}{M_{sea}}}. \qquad \text{(F-1)}$$

Table F-1. Ionic composition (mg/l) (John Smellie, Conterra AB, pers. comm.).

Depth	Type	Na	Ca	Cl	SO_4	K	Mg	Br	HCO_3
0–100	Fresh	200	20	60	100	10	10	0.1	450
100–400	Brackish marine	1,800	900	4,600	300	30	140	20	60
400–900	Brackish non-marine	1,800	1,800	6,000	30	10	10	50	20
900–1,400	Saline	2,000	4,000	10,000	50	10	10	100	10
>1,400	Highly saline	8,000	19,000	45,000	800	30	3	300	10

Table F-2. Formulas for definition of total molar concentration.

depth									
0-100	Salt/Ion	NaCl	$CaCl_2$	Na_2SO_4	$MgSO_4$	K	Br	HCO_3	
	Concentration *C* (mg/l)	40	60	270	20	10	0.1	450	
	Formula for total molar concentration x_c	$x_{c1} = \left(\frac{2C_{NaCl}}{M_{NaCl}} + \frac{3C_{CaCl_2}}{M_{CaCl_2}} + \frac{3C_{Na_2SO_4}}{M_{Na_2SO_4}} + \frac{2C_{MgSO_4}}{M_{MgSO_4}} + \frac{C_K}{M_K} + \frac{C_{Br}}{M_{Br}} + \frac{C_{HCO_3}}{M_{HCO_3}} \right) \Big/ \frac{C_{H_2O}}{M_{H_2O}}$								
100-400	Salt/Ion	Na	Ca	Cl	SO4	K	Mg	Br	HCO3
	Concentration *C* (mg/l)	1800	900	4600	300	30	140	20	60
	Formula for total molar concentration x_c	$x_{c2} = \left(\frac{C_{Na} + C_{Ca} + C_{Cl} + C_{SO_4} + C_K + C_{Mg} + C_{Br} + C_{HCO_3}}{M_{sea}} \right) \Big/ \frac{C_{H_2O}}{M_{H_2O}}$							
400-900	Salt/Ion	NaCl	$CaCl_2$	Na	SO_4	K	Mg	Br	HCO_3
	Concentration *C* (mg/l)	3600	5400	600	30	10	10	50	20
	Formula for total molar concentration x_c	$x_{c3} = \left(\frac{2C_{NaCl}}{M_{NaCl}} + \frac{3C_{CaCl_2}}{M_{CaCl_2}} + \frac{C_{Na}}{M_{Na}} + \frac{C_{SO_4}}{M_{SO_4}} + \frac{C_K}{M_K} + \frac{C_{Mg}}{M_{Mg}} + \frac{C_{Br}}{M_{Br}} + \frac{C_{HCO_3}}{M_{HCO_3}} \right) \Big/ \frac{C_{H_2O}}{M_{H_2O}}$							
900-1400	Salt/Ion	NaCl	$CaCl_2$		SO_4	K	Mg	Br	HCO_3
	Concentration *C* (mg/l)	4000	12000		50	10	10	100	10
	Formula for total molar concentration x_c	$x_{c4} = \left(\frac{2C_{NaCl}}{M_{NaCl}} + \frac{3C_{CaCl_2}}{M_{CaCl_2}} + \frac{C_{SO_4}}{M_{SO_4}} + \frac{C_K}{M_K} + \frac{C_{Mg}}{M_{Mg}} + \frac{C_{Br}}{M_{Br}} + \frac{C_{HCO_3}}{M_{HCO_3}} \right) \Big/ \frac{C_{H_2O}}{M_{H_2O}}$							
>1400	Salt/Ion	NaCl	$CaCl_2$	Na	SO_4	K	Mg	Br	HCO_3
	Concentration *C* (mg/l)	14000	57000	1000	800	30	3	300	10
	Formula for total molar concentration x_c	$x_{c5} = \left(\frac{2C_{NaCl}}{M_{NaCl}} + \frac{3C_{CaCl_2}}{M_{CaCl_2}} + \frac{C_{Na}}{M_{Na}} + \frac{C_{SO_4}}{M_{SO_4}} + \frac{C_K}{M_K} + \frac{C_{Mg}}{M_{Mg}} + \frac{C_{Br}}{M_{Br}} + \frac{C_{HCO_3}}{M_{HCO_3}} \right) \Big/ \frac{C_{H_2O}}{M_{H_2O}}$							

References

Laaksoharju M, Smellie J, Tullborg E-L, Gimeno M, Hallbeck L, Molinero J, Waber N, 2008. Bedrock hydrogeochemistry Forsmark. Site descriptive modelling. SDM-Site Forsmark. SKB R-08-47, Svensk Kärnbränslehantering AB.

Lide D R, 1999. CRC Handbook of Chemistry and Physics 1999. D.R. Lide eds. CRC Press: Boca Raton, FL.

Appendix G

Heat generation from the repository

Thomas Wallroth, Bergab

The repository, with a vertical dimension between 450 and 470 m depth, is located within rock domains RFM29 and RFM45, schematically described in Figure G-2. The layout of the repository is shown in Figure G-1. The rock domain RFM45 is not cut by the profile studied in the current work.

Calculations of thermal power resulting from deposition of canisters have been made by (Hökmark and Lönnqvist, pers comm.), using a methodology presented by /Hökmark et al. 2009/. The canister spacing in the two domains RFM045 and RFM029 is 7 m and 6 m, respectively. With a distance between deposition tunnels of 40 m, this will give a heat power per area of 6 W/m^2 and 7.1 W/m^2, respectively. The assumptions made in the calculations are illustrated in Figure G-2. Any loss of canister positions has been neglected, which means that the power per unit area has been exaggerated by about 10%.

The corresponding power per scanline for a 2D representation will be 5.4 W/m and 6.3 W/m, for RFM045 and RFM029, respectively. Such an approach assumes an infinite out-of-plane thermal load. In the permafrost simulations heat power from the repository has been assigned a value of (5.4+6.3)/2 = 5.85 W/m. Since the part of the repository located in RFM45 is much less than the part located in RFM29, the use of this value implies that the thermal power from the repository is underestimated in the permafrost simulations.

Temperature calculations have been made by (Hökmark and Lönnqvist, pers comm.) using average Forsmark values for heat conductivity and heat capacity and a standard decay function for the heat load. These calculations are based on a panel solution, i e the average temperature contributions from each heated panel. Calculated contour plots for at times 50, 100, 500, 1,000 and 4,000 years are shown in Figure G-3.

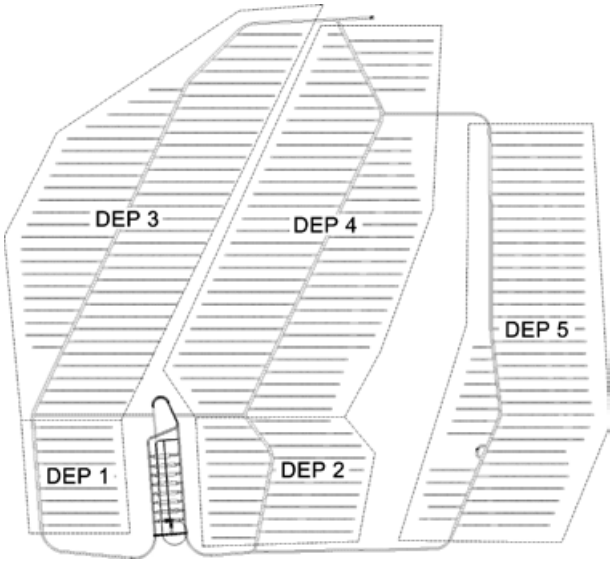

Figure G-1. *Layout D1 with about 6,800 canister positions /Brantberger et al. 2006/.*

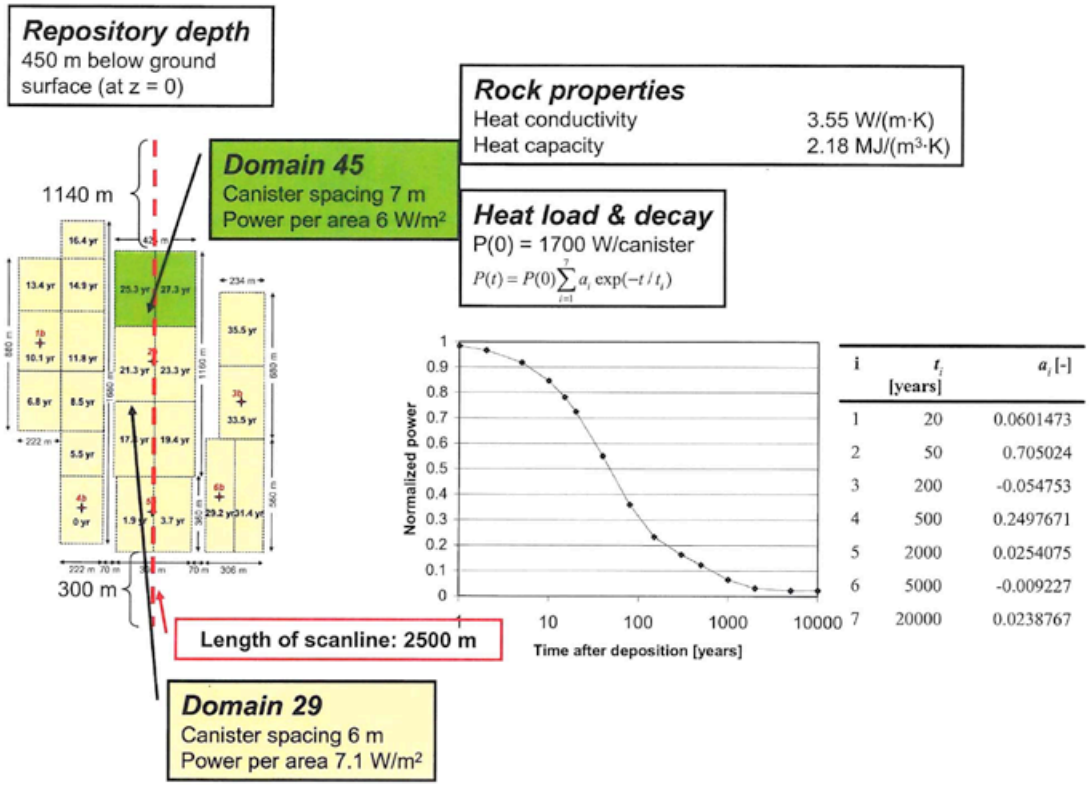

Figure G-2. *Illustration of power and temperature calculations (Hökmark and Lönnqvist, pers comm.).*

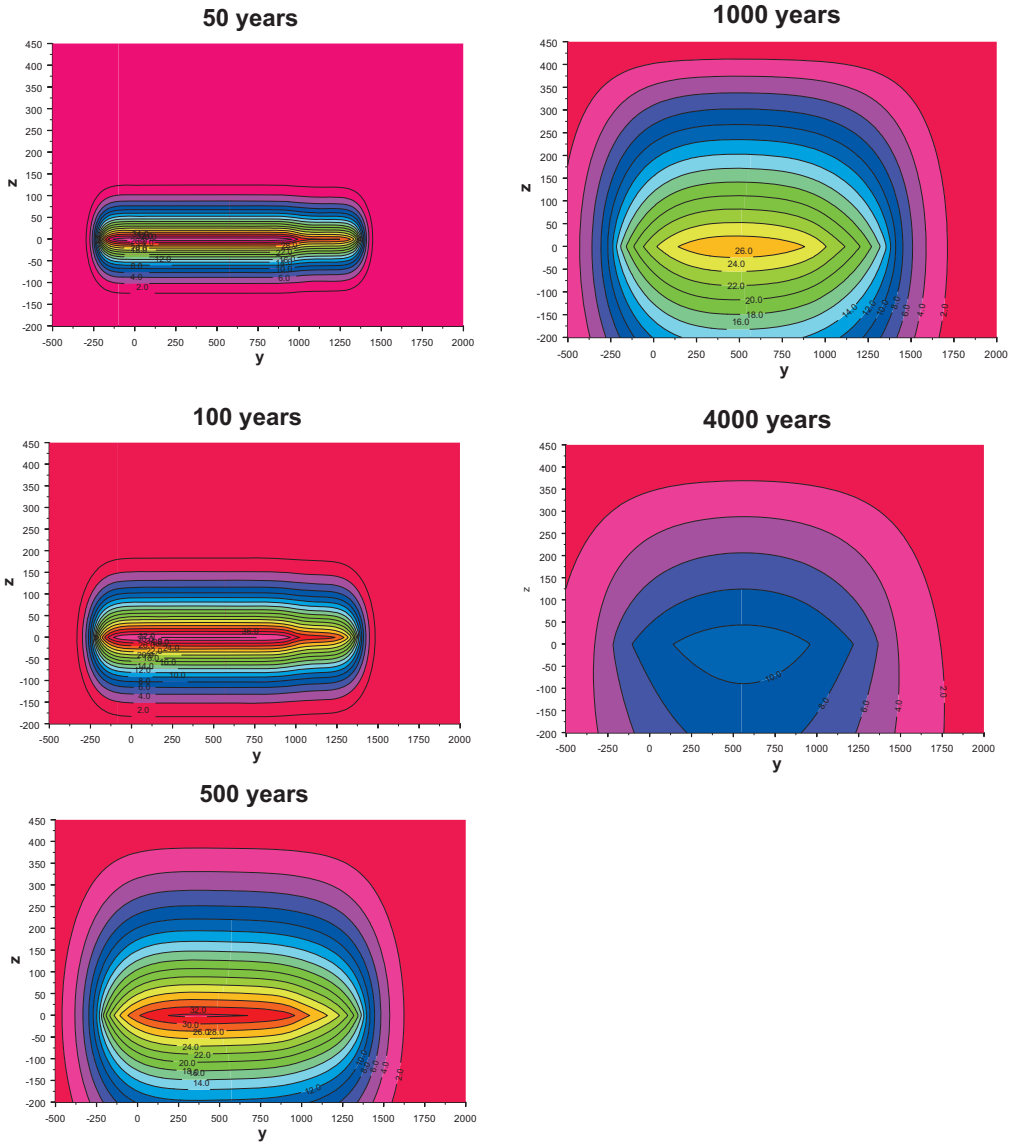

Figure G-3. *Contour plots of the calculated temperature distribution around the repository at times 50, 100, 500, 1,000 and 4,000 years. The undisturbed in-situ temperature has been assumed to be 0°C everywhere, which means that the plots show only the increase in temperature due to the repository (Hökmark and Lönnqvist, pers comm.).*

References

Brantberger M, Zetterqvist A, Arnbjerg-Nielsen T, Olsson T, Outters N, Syrjänen P, 2006. Final repository for spent nuclear fuel. Underground design Forsmark, Layout D1. SKB R-06-34, Svensk Kärnbränslehantering AB.

Hökmark H, Sundberg J, Lönnqvist M, Hellström G, Kristensson O, 2009. Strategy for thermal dimensioning of the final repository for spent nuclear fuel. SKB R-09-04, Svensk Kärnbränslehantering AB.

Appendix H

Reconstructed air temperature curve for the past 120 000 years

Jens-Ove Näslund, SKB

A published reconstruction of last glacial cycle air temperatures /Dansgaard et al. 1993/ have been used together with The University of Maine Ice Sheet Model to extract time series of site-specific ground level air temperatures for the Forsmark area /SKB 2010a/.

The reconstructed air temperature curves for Forsmark for the past 120,000 years are seen in Figure H-1. The figure shows the reconstructed last glacial cycle temperatures for Forsmark (blue line), including two periods when the site is overridden by the Weichselian ice sheet, and two subsequent periods of submerged conditions. For the ice covered periods, the temperature constitute the basal ice temperature calculated with the ice sheet model, while for periods with submerged conditions the temperature is set to +4°C.

Adjustment of air temperature curves to include Eemian conditions. In the reconstruction of temperatures for the past 120 kyrs the likely environmental conditions in the Forsmark region during interglacials and interstadial also need to be considered. Following the deglaciation of the large Saalian ice sheet, it is very likely that the Forsmark site was submerged by the Baltic Sea during a large part of the Eemian interglacial, much in the same way as following the Weichselian glaciation, e.g. /SKB 2010a/. The palaeotemperature curve in was adjusted to reflect this. The description of how this was done is presented in /SKB 2010a, Appendix 1/.

One result of including, the very likely, submerged conditions for the main part of the Eemian interglacial is that not much of the warm Eemian temperatures are seen in the resulting ground temperature curve (Figure H-1, blue line). After 115 kyrs BP, there is a 1,000 year long period of warm Eemian terrestrial conditions before temperatures starts to drop. It should be emphasized that this is a crude reconstruction of Eemian conditions for the Forsmark site, both in terms of timing, length and prevailing conditions. Nevertheless it is very likely that this provides a better estimate of Eemian conditions at the Forsmark site than simply applying an air temperature curve without submerged conditions. In addition, the assumption of a submerged temperature of +4°C for the major part of the Eemian constitutes a pessimistic assumption of thermal conditions for the permafrost simulations; keeping a long period of very warm terrestrial conditions would have heated the bedrock prior to cooling and resulted in less permafrost than with the approach taken here.

Adjustment of air temperature curves to include Mid-Weichselian conditions. In the SR-Site reference glacial cycle /SKB 2010a/, ice sheet modelling resulted in ice-free conditions at Forsmark during marine Isotope Stage 3 between c. 55 and 30 kyrs BP. Given this input, Glacial Isostatic Adjustment (GIA) simulations suggest that the Forsmark site remained submerged for c. 8,000 years during this period /SKB 2010a/. Therefore, a submerged ground surface temperature of +4°C were set for this first ice free period of MIS 3 (Figure H1, blue curve).

Adjustment of air temperature curves to include Holocene conditions. The starting time for the Holocene period is in SR-Site, locally defined as the time of the Weichselian deglaciation of Forsmark, occurring at c. 8,800 BC (10,800 years ago) /Söderbäck 2008/. In line with the method above, the temperature curve has been adjusted to show a submerged temperature of +4°C from that time up to near-present conditions (Figure H-1).

The resulting blue temp curve in Figure H-1 is in the present permafrost study used for the *Repetition of last glacial cycle* case. For a detailed description of how the curve was constructed see the /SKB 2010a, Appendix 1/.

Figure H-1 also shows what the reconstructed temperatures would look like had the site not been covered by an ice sheet or been submerged by the Baltic (red line). For a description of how this curve was constructed, see /SKB 2010a, Appendix A/. This temperature curve is used for the simulation of the *Severe permafrost* case.

Uncertainties in temperature data. The conceptual-, data- and temporal uncertainty of the air temperature curve are discussed in /SKB 2010a,b/. Based on how the air temperature curve has been constructed and a comparison against Weichselian climate proxy data, it is in /SKB 2010a, Appendix 1/ estimated that the uncertainty in the reconstructed temperature curve is

- not larger than 6° C for periods with the largest uncertainties,
- up to c. 4-5° C for the major part of the curve, and
- for some parts of the curve, such as for the Holocene and the Eemian, smaller than 4° C.

Handling of uncertainties in the *Repetition of last glacial cycle* case
Based on the above estimates, and on the nature of the conceptual- and data uncertainty associated with the temperature curve /SKB 2010b/, it is here considered adequate to lower the entire temperature curve by 6°C as a pessimistic case in the sensitivity analysis for examining the effect of the temperature curve uncertainty for the Repetition of last glacial cycle case.

Handling of uncertainties in the *Severe permafrost* case
Mid-latitude ice sheets form essentially as a response to low air temperatures, see /SKB 2010a, Section 2.1 and 3.1/. In line with this there is a strong correlation between cold interstadial periods during glacial cycles and large ice sheet configurations, see /SKB 2010a, Section 3.4.1/. The *Severe permafrost* case, was constructed to handle remaining uncertainties that were not handled in the reference glacial cycle, such as the absence of an ice sheet over the site. Therefore, the main assumption is that the climate is cold but without an ice sheet reaching the Forsmark site. This means that the maximum ice sheet configuration for this hypothetical case does not reach middle central Sweden. This hypothetical ice sheet thus has significantly smaller ice sheet configurations than the Weichselian ice sheet. This in turn implies that that air temperatures during the fictive glacial cycle of the *Severe permafrost* case would be higher than in the *Repetition of last glacial cycle* case that hosts the Weichselian ice sheet (but still significantly colder than for temperate climate conditions). If temperatures would be the same as during the Weichselian, a larger ice sheet would form and cover the Forsmark site for parts of the glacial cycle. It is difficult to estimate what temperatures would correspond to the glacial cycle of the *Severe permafrost* case. The temperature curve used for permafrost simulations for the *Severe permafrost* case should, in line with the above reasoning, be warmer than the one used for the *Repetition of last glacial cycle* case.

On the other hand the temperature curve reconstructed also has a significant uncertainty interval /SKB 2010a, Appendix 1/. The comparison of the reconstructed last glacial cycle temperature curve (Figure H-1) with (the few) existing quantitative proxy data on Weichselian temperatures from the Fennoscandian region seems, however, to indicate that the reconstructed temperature curve is in broad agreement with proxy data /SKB 2010a, Appendix 1/. Furthermore, the comparison suggests that the temperature curve does not overestimate temperatures for the compared last glacial cycle stadials and interstadials. Instead, the general picture from the comparison with Fennoscandian proxy data is that the reconstructed temperature curve gives roughly correct or slightly too low temperatures by a few degrees.

In order to make a reasonable choice of temperature curve for the severe permafrost case, with the above issues in consideration, air temperatures were pessimistically assumed to fall according to the reconstructed temperature curve for the reference glacial cycle, but without a presence of ice sheets and submerged conditions (Figure H-1, red line).

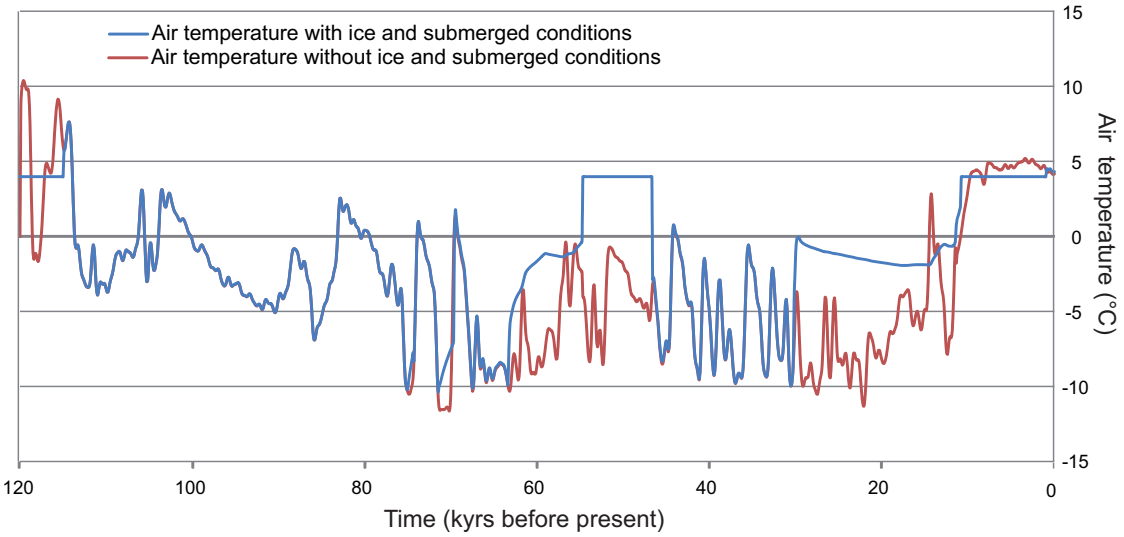

Figure H-1. *Reconstructed air temperature curve for the Forsmark region for the past 120 ka, including estimated submerged periods of the Eemian, Mid-Weichselian and Holocene interglacials. The blue line includes periods of ice sheet coverage, i.e. it shows simulated basal ice temperatures for glaciated periods, air temperatures for ice free periods, and a temp of +4 for submerged periods. The red line shows reconstructed last glacial cycle air temperatures without a presence of an ice sheet and also without submerged periods. The data are from /SKB 2010a, b/. The uncertainty of the temperature curves is discussed in the text and in the /SKB 2010a, b/.*

References

Dansgaard W, Johnsen S J, Clausen H B, Dahl-Jensen D, Gundestrup N S, Hammer C U, Hvidberg C S, Steffensen J P, Sveinbjörnsdottir A E, Jouzel J, Bond G, 1993. Evidence for general instability of past climate from a 250-kyr ice-core record. Nature, 364, pp 218–220.

SKB, 2010a. Climate and climate related issues for the safety assessment SR-Site. SKB TR-10-49, Svensk Kärnbränslehantering AB.

SKB, 2010b. Data report for the safety assessment SR-Site. SKB TR-10-52, Svensk Kärnbränslehantering AB.

Söderbäck B, 2008. Geological evolution, palaeoclimate and historical development of the Forsmark and Laxemar-Simpevarp areas. Site descriptive modelling. SDM-Site. SKB R-08-19, Svensk Kärnbränslehantering AB.

Appendix I

Future lakes developed due to isostatic uplift

Thomas Wallroth, Bergab

The model, which is presented in /Brydsten 2006/ consists of two modules – a marine module and a lake module. The description of the model below is taken from this report.

The marine module runs from model start until lake isolation time and calculates change in bathymetry due to shoreline displacement and accumulation or erosion of post-glacial fine-grained sediments. Inputs to the marine module are a digital elevation model (DEM), a digital map showing the extensions of the objects and a marine Quaternary map. The outputs from the module for each time are water volume, water area and sea level. The time for future lake isolation is calculated using the future lake threshold level and a shoreline displacement equation presented by /Påsse 1997/ including site-specific data from the Forsmark site investigations.

The lake module calculates change in water volume and water area due to sedimentation of inorganic material and colonization of macrophyte vegetation. Input to the lake module is either the DEM from the lake isolation time or a DEM calculated from depth sounding data for an existing lake. The lake module simulates the progress from a newly isolated lake to a wetland considering accumulation of fine-grained sediments and choke-up processes. The outputs from the module are mean water depth, water area, added sediment volume since lake isolation, and area and volume of organic material.

Two future lakes will develop along the studied profile; Lake #18 and Lake #28. The positions of these lakes are illustrated in Figures I-1 and I-2.

Some of the output data from the simulations are shown in Figures I-3–I-4.

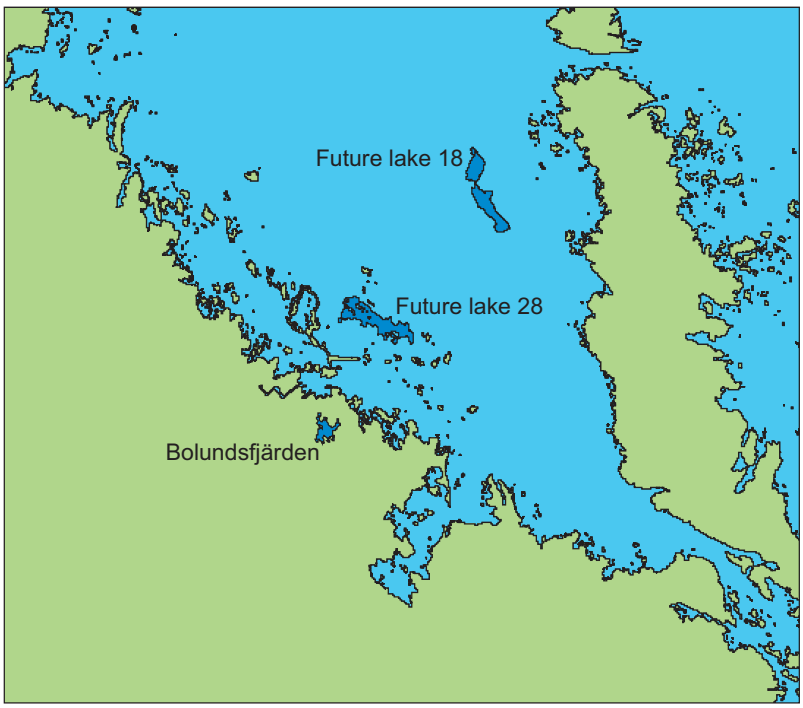

Figure I-1. *Locations of future lakes #18 and #28 developed outside the current shoreline at Forsmark /Brydsten 2009/.*

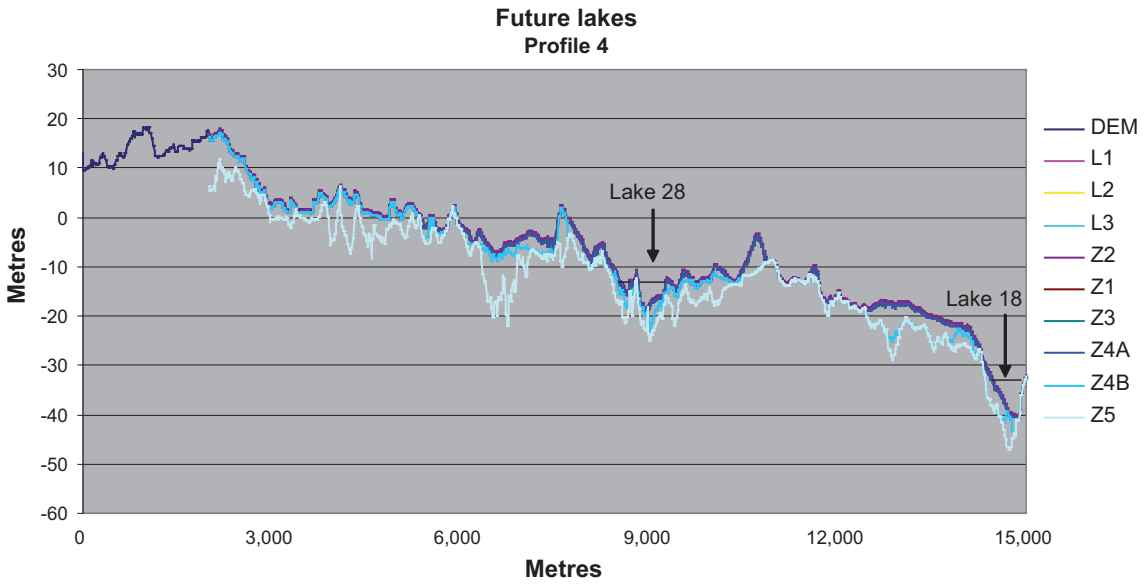

Figure I-2. *Positions of future lakes #18 and #28.*

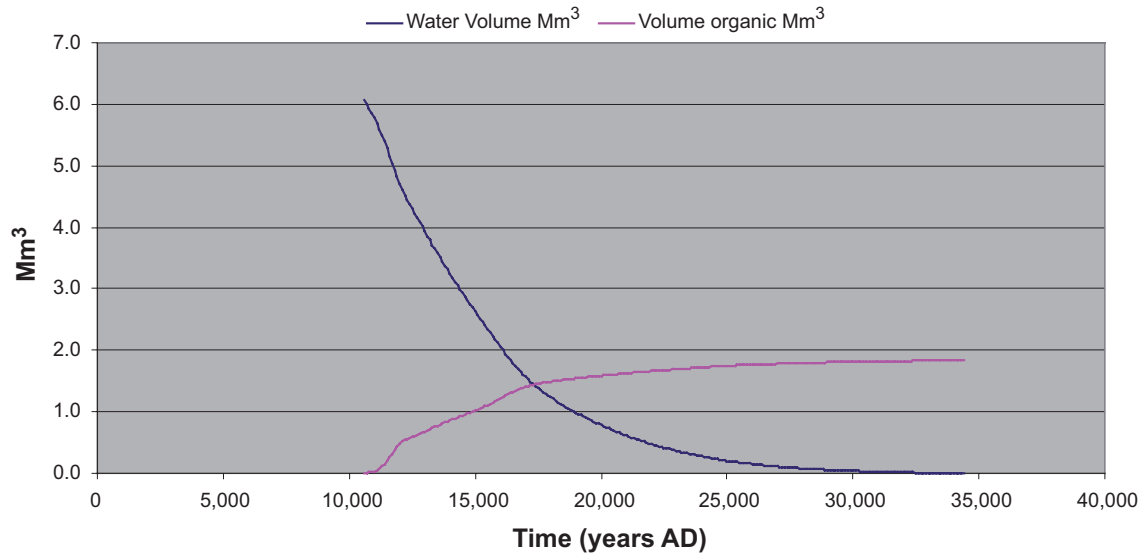

Figure I-3. *Development of future lake #18. The diagram shows that the lake will be completely filled at 34.000 years AD. However, in the part of the lake crossed by Profile 4, this will occur already at 16.500 years AD.*

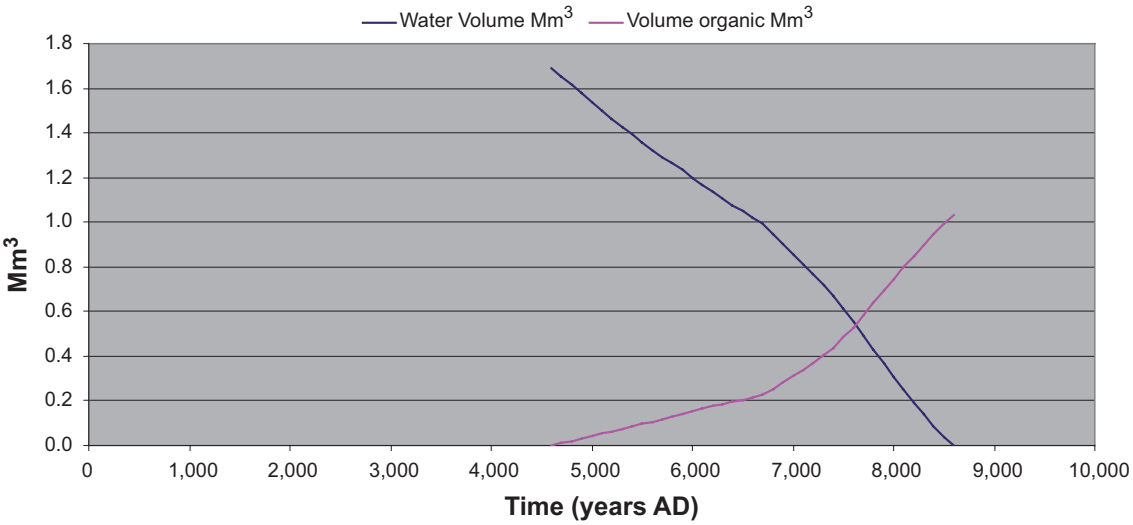

Figure I-4. *Development of future lake #28. The diagram shows that the lake will be completely filled at 8,500 years AD.*

References

Brydsten L, 2006. A model for landscape development in terms of shoreline displacement, sediment dynamics, lake formation, and lake choke-up processes. SKB TR-06-40, Svensk Kärnbränslehantering AB.

Brydsten L, 2009. Sediment dynamics in the coastal areas of Forsmark and Laxemar during an interglacial. SKB TR-09-07, Svensk Kärnbränslehantering AB.

Påsse T, 1997. A mathematical model of past, present and future shore level displacement in Fennoscandia. SKB TR-97-28, Svensk Kärnbränslehantering AB.

Appendix J

Vegetation/surface cover types for three different climate zones at Forsmark

Anders Löfgren, SKB/Stockholm University

Introduction

Regional vegetation patterns are mainly determined by regional climatic factors, soil properties and human land use. However, the local differences are a function of both local site factors and regional climate. The site factors may be soil moisture, fire resistance, temperature, field layer composition and low elevations i.e. along rivers etc. Fire history have been attributed a large impact upon the present spatial pattern of the forest -tundra distribution in Canada /Payette et al. 2001/ and this is most certainly valid for Scandinavia too. Consequently, a number of factors could be used to infer the local distribution of vegetation during different climate regimes.

The two biomes that intersect the tree line is according to Köppen the group D, subgroup subarctic (Dfc), which have a continental/microthermal climate defined as having an average temperature above 10°C in their warmest months (at least one month and at most 3 month), and a coldest month average below −3°C. The vegetation is dominated by evergreen conifers in Fennoscandia. The other biome is the Group E subgroup Tundra (ET), where the warmest month has an average temperature between 0°C and 10°C. The vegetation is dominated by the field and bottom layer. A shrub layer (mainly Betula 0a and Salix sp.) may be dominating in a transition zone between the tree line and the tundra, and are present in the tundra environment under more moist conditions in mires or along rivers. Similarly, sheltered low points (which in most cases also have a deeper soil layer) would be colonised early during an advancing tree-line or will contain the last fragments of trees when the tree-line is regressing. These sheltered areas are less exposed to wind and, have a warmer and moister microclimate. Localities exposed to wind and low temperature under more arctic/alpine conditions are often have very sparse vegetation due to cryoturbation and wind erosion, and may be termed “barrens”.

Topographical wetness index

A Topographical Wetness Index (TWI) can be used to identify and contrast low-laying, moist locations and more dry exposed locations in the landscape. By defining intervals the index could be used to indicate the presence of trees, shrub, tundra grassland and barrens during different climate regimes.

The TWI is used to calculate the likelihood for soil saturation and is defined as follows /Beven and Kirkby 1979/:

$$TWI = \ln\left(\frac{Flowacc}{\tan\beta}\right)$$

where Flowacc is specific catchment area and β is local slope in degrees. High wetness index occurs in places with high flow accumulation values and flat slopes. The flow accumulation grid often shows great differences in values in adjacent cells, and small changes in elevation values can denote great changes in the accumulation grid. Therefore, the resulting TWI-grid is often very patchy. In order to reduce this phenomenon, both the slope grid and the flow accumulation grid were smoothed using a low pass filter with a 3·3 kernel before the calculation of the wetness index. A digital elevation model was used as input data for calculating the TWI for Forsmark /Strömgren and Brydsten 2008/. A large index indicates wet soil conditions and low index dry conditions.

References

Beven K J, Kirkby M, 1979. A physically-based variable contributing area model of basin hydrology. Hydrological Science Bulletins, 24, pp 43–69.

Payette S, Fortin M-J, Gamache I, 2001. The subarctic forets-tundra: the structure of a biome in a changing climate. BioScience, 51, pp 709–718.

Strömgren M, Brydsten L, 2008. Digital elevation models of Forsmark. Site-descriptive modelling. SDM Site Forsmark, SKB R-08-62, Svensk Kärnbränslehantering AB.

Appendix K

Modelling results for the Severe permafrost case

Juha Hartikainen, Aalto University School of Science and Technology

The evolution of maximum permafrost depth and maximum depth of perennially frozen ground over the repository for the Severe permafrost case are presented in Table K-1.

Table K-1. Evolution of maximum permafrost depth and maximum depth of perennially frozen ground over the repository modelled for the Severe permafrost case. The table also shows the prevailing mean annual air temperatures.

Time before present (ka)	Mean annual air temperature (°C)	Maximum permafrost depth (m)		Maximum depth of perennially frozen ground (m)	
		Humid variant	Dry variant	Humid variant	Dry variant
112	–3.4	104	69	97	64
111.5	–0.6	30	0	27	0
110	–3.5	71	46	68	44
108	–1.5	44	0	42	0
106	2.5	0	0	0	0
104	–0.6	33	0	30	0
102	1.6	0	0	0	0
100	–0.3	7	0	5	0
98	–1.9	55	9	52	8
96	–2.9	102	56	97	53
94	–3.9	127	86	122	82
92	–4.8	158	117	151	113
90	–4.1	168	123	161	118
88	–0.9	54	0	49	0
86	–6.4	155	120	149	115
84	–3.1	164	105	156	98
82	2.1	0	0	0	0
80	0.4	0	0	0	0
78	–2.5	88	37	84	35
76	–4.2	147	102	140	98
74	–1.3	256	211	241	198
72	–3.6	130	78	124	74
70	–10.0	319	290	303	277
68	–6.1	178	133	166	126
66	–9.6	290	255	268	239
64	–8.6	325	289	304	272
62	–8.3	343	308	321	290
60	–8.4	334	297	310	277
58	–7.3	315	269	294	253
56	–3.2	212	140	200	130
54	–8.3	231	189	212	178
52	–3.7	282	235	260	217
50	–1.9	114	25	105	21
48	–4.2	194	136	182	129
46	–5.8	213	159	200	151
44	0.3	162	0	132	0
42	–5.1	198	145	185	137
40	–5.3	219	158	201	147
38	–7.7	278	235	252	214
36	–7.3	340	302	313	281
34	–6.6	233	179	214	167

Time before present (ka)	Mean annual air temperature (°C)	Maximum permafrost depth (m)		Maximum depth of perennially frozen ground (m)	
		Humid variant	Dry variant	Humid variant	Dry variant
32	–7.9	268	217	242	196
30	–4.3	323	279	294	253
28	–9.6	355	315	323	288
26	–9.4	350	304	321	278
24	–8.7	354	311	324	284
22	–11.0	385	348	352	320
20	–8.3	370	325	341	302
18	–4.3	340	283	315	263
16	–5.0	284	225	266	211
14	–0.3	10	0	8	0
12	–6.8	262	216	244	202
10	3.2	0	0	0	0
8	3.9	0	0	0	0
6	4.5	0	0	0	0
4	5.0	0	0	0	0
2	4.8	0	0	0	0
0	4.2	0	0	0	0